TARGETING NUTRIENT STRESS AS AN ANTIBIOTIC APPROACH

EXPLOITING BACTERIAL NUTRIENT STRESS IN THE TREATMENT OF ANTIBIOTIC-RESISTANT PATHOGENS

By Lindsey April Carfrae, B.H.Sc.

A thesis submitted to the School of Graduate Studies in partial fulfillment of the requirements for the degree of Doctor of Philosophy

McMaster University DOCTOR OF PHILOSOPHY (2022) Hamilton, Ontario (Biochemistry and Biomedical Sciences)

TITLE: Exploiting bacterial nutrient stress in the treatment of antibiotic-resistant pathogens

AUTHOR: Lindsey A. Carfrae, B.H.Sc.

SUPERVISOR: Eric D. Brown, Ph.D.

NUMBER OF PAGES: XV; 235

Foreword

Abstract

To revitalize the antibiotic pipeline, it is critical to identify and validate new antimicrobial targets. An uncharted area of antibiotic discovery can be explored by inhibiting nutrient biosynthesis. Herein, we investigate the potential of inhibiting biotin biosynthesis in monotherapy and combination therapy approaches to treat multidrug-resistant Gram-negative pathogens. In chapter 2, we validate biotin biosynthesis as a viable target for Gram-negative pathogens. Historically, biotin biosynthesis was overlooked as a target in Gram-negative pathogens as there was no observed fitness cost associated with its inhibition in standard mouse infection models. We discovered traditional mouse models do not accurately represent the biotin levels in humans. We developed an innovative mouse model to account for this discrepancy, validating biotin biosynthesis as an antimicrobial target in the presence of human-mimicking levels of biotin. Exploiting this sensitivity, we show that an inhibitor of biotin biosynthesis, MAC13772, is efficacious against *Acinetobacter baumannii* in a systemic murine infection model. In chapter 3, we continue to investigate the potential of targeting biotin biosynthesis in a combination therapy approach. In this work, we identify the ability of MAC13772 to synergize with colistin exclusively against colistin-resistant pathogens. The first committed step of fatty acid biosynthesis requires biotin as a cofactor; therefore, it is indirectly inhibited through the action of

MAC13772. We propose that the inhibition of fatty acid biosynthesis leads to changes in membrane fluidity and phospholipid composition, restoring colistin sensitivity. The combination of a fatty acid biosynthesis inhibitor and colistin proved superior to either treatment alone against *mcr-1* expressing *Klebsiella pneumoniae* and colistin-resistant *Escherichia coli* murine infection models. Together, these data suggest that biotin biosynthesis is a robust antibiotic target for further development in monotherapy and combination therapy approaches.

Acknowledgements

Dr. Eric Brown – Thank you for the opportunity to conduct research in a supportive and fun environment. You gave me the right balance of independence and guidance, giving me room to grow into a better scientist.

Dr. Brian Coombes – Thank you for your scientific input, pushing me in committee meetings, and sharing all resources relating to animal studies (including Aline for training).

Dr. John Whitney – Thank you for always spending the time to advise on proper experimental controls and sharing your perspective of academia and postdoctoral fellowships.

Dr. Craig MacNair – Thank you for developing my organizational and cleaning skills. You have been an awesome mentor, and I will continue to build my scientific communication abilities thanks to you.

Megan – Thank you for loving science as much as I do and making me look like a good mentor. Keep up the fantastic work so I can keep on taking credit for it.

Rodion – Thank you for always wanting to chat about science or working out with me and trying to teach me basic chemistry.

Brown Lab – Thank you all for always being ready to chat, share your data, knowledge, or time, and making me laugh and enjoy my time in the lab. I won't

ever forget the Brown lab Christmas parties, bowling, lab retreat and all the other times just hanging out with you all.

Dad – Thank you for spending the past five years trying to understand what I do and explaining it to people semi-correctly along the way.

Mom – Thank you for trying to convince me to have a life for my whole Ph.D., even if it was just by hanging out with you.

Johanna – Thank you for convincing all your friends that I am a cold-blooded killer (much cooler than just a nerd who loves science).

Grandpa – Thank you for reading all my papers and probably being the only one who will even try reading this thesis.

Rest of my family and friends (Emily) – Knowing you will all support me is all I ever need.

Deep – Saved the best for last, thank you for reading this thesis one too many times.

Table of Contents

List of figures

Chapter I

Chapter II

List of abbreviations

ACP ..... acyl-carrier protein
ATP ..... adenosine triphosphate
BisMePA ..... bismethyl phosphatidic acid
BLAST ..... basic local alignment search tool
CoA ..... Coenzyme A
CCCP ..... carbonyl cyanide m-chlorophenyl hydrazone
CDP-DAG ..... CDP-diacylglycerol
CFU ..... colony-forming units
CL ..... cardiolipin
CLSI ..... clinical and laboratory standards institute
CRISPR ..... clustered regularly interspaced short palindromic repeats
CTP ..... cytidine triphosphate
DAP ..... diaminopimelate
DAPA ..... diamino-pelargonic acid
DG ..... diacylglycerol
$DiSC_3(5)$ ..... 3,3′-dipropylthiadicarbocyanine iodide
DNA ..... deoxyribonucleic acid
DPH 1,6-diphenyl-1,3,5-hexatriene
EDTA ..... ethylenediaminetetraacetic acid
EUCAST ..... European committee on antimicrobial susceptibility testing
5-FABA ..... 2-amino-5-fluorobenzoic acid
6-FABA ..... 2-amino-6-fluorobenzoic acid
FIC_i ..... fractional inhibitory concentration index
FOR ..... frequency of resistance
GTP ..... guanosine triphosphate
HITS ..... high-throughput insertion tracking by deep sequencing
IFN-γ ..... interferon gamma
IMP ..... inosine monophosphate
INSeq ..... insertion sequencing
3-IPA ..... 3-indolepropionic acid
KAPA ..... (*S*)-keto-amino-pelargonic acid
L-Ara4N 4-amino-4-deoxy-L-arabinose
LB ..... lysogeny broth
LPE ..... lysophosphatidylethanolamine
LPG ..... lysophosphatidylglycerol
LPS ..... lipopolysaccharide
MALDI-TOF ..... matrix-assisted laser desorption/ionization – time of flight
mcr ..... mobilized colistin resistance
MHB ..... mueller hinton broth

MIC ..... minimum inhibitory concentration
MG ..... monoacylglycerol
MGDG ..... glycosyldiacylglycerol
MGMG ..... glycosylmonoacylmonoglycerol
NAD ..... nicotinamide adenine dinucleotide
NO ..... nitric oxide
OD ..... optical density
PA ..... phosphatidic acid
PABA ..... *para*-aminobenzoic acid
PBS ..... phosphate buffered saline
PE ..... phosphatidylethanolamine
PEtN ..... phosphoethanolamine
PG ..... phosphatidylglycerol
PGP phosphatidyl-3-P-glycerol
PLP ..... pyridoxal 5'-phosphate
PRPP ..... phosphoribosyl pyrophosphate
PS ..... phosphatidylserine
Psp ..... phage shock protein
RNA ..... ribonucleic acid
RNA-Seq ..... RNA sequencing
SAM ..... *S*-adenosyl-L-methionine
TG ..... triacylglycerol
TraDIS ..... transposon-directed insertion site sequencing
TnSeq ..... transposon insertion sequencing
UMP ..... uridine-5'-phosphate
UPEC ..... uropathogenic *E. coli*
WHO ..... World Health Organization

Chapter I – Introduction

Preface

Some of the work presented in this chapter is in preparation for submission, as of August 15, 2022:

Carfrae LA and Brown ED, Inhibiting nutrient stress in the development of novel antimicrobials*. In preparation.*

LAC wrote the manuscript with input from EDB.

Drug discovery in a post-antibiotic era

The dissemination of multidrug-resistant bacteria, combined with the decline in antibiotic discovery, is a critical threat to public health. Antibiotics are part of the infrastructure supporting modern medical interventions, including immunosuppression, oncology, and surgery. Unfortunately, the increasing rates of antibiotic resistance threaten the routine use of antibiotics. Overcoming antibiotic resistance will require multifaceted approaches spanning regulatory, economic, and societal (stewardship and global access) changes[1]. Wide-scale policy-based changes are beginning to create an environment preventing the rapid development and spread of resistance[2–5]. In addition to delaying the development of resistance, it is paramount to expand drug discovery efforts. Identifying novel chemical matter with new targets or mechanisms of action is crucial to combating the plight of antibiotic resistance.

Most antibiotic classes in clinical use were discovered in a narrow window between 1940 and 1960, termed the “Golden Era” of antibiotic discovery[6] (Figure 1). The Golden Era was characterized by the discovery of natural products using whole-cell screens[7]. The laboratory of Dr. Selman Waksman pioneered a systematic approach to screening Actinomycetes and other soil-dwelling microorganisms. The technique was used to identify secondary metabolites inhibiting bacterial growth on microbiological media. This strategy became the standard for finding novel antibiotics[8]. Although successful, this standard protocol

was soon plagued with rediscovery. As antibiotic resistance emerged, research turned to medicinal chemistry to optimize chemical scaffolds of existing antibiotics to increase potency, expand the spectrum of activity, and overcome resistance[7]. However, incremental changes to chemical classes of antibiotics are prone to cross-resistance[9]. In the 1980s, pharmaceutical companies began to abandon antibacterial drug discovery as fewer antibiotics were identified and increased levels of resistance threatened profits.

Advancements in computation, robotics, and genomics sparked new hope for antibiotic development. Researchers could now identify and purify large quantities of enzymes unique to bacteria, broadly conserved, and essential for growth[7]. Enzymes of interest were screened against huge compound libraries generating numerous inhibitors. However, the field soon learned that a compound's in vitro activity did not translate to the development of new drugs. These molecules' physical and chemical properties often preclude their entry into whole cells. Advances in genomics and bioinformatics enabled the sequencing of thousands of bacterial genomes, and high-throughput mutagenesis techniques allowed the systematic exploration of gene dispensability. However, despite identifying over 4000 genes in model organisms such as *E. coli,* only a small percentage (7%) were essential for bacterial growth in conventional laboratory conditions[10]. The failure of the genomic era further diminished investment in antibiotic development by pharmaceutical companies.

The burden of novel drug discovery has shifted mainly to academic labs and small biotechnology companies[11]. Current preclinical antibiotic discovery efforts focus on unconventional and innovative techniques to identify novel molecules with unique targets. Strategies include uncovering unexplored antibiotic producers, combination approaches, drug repurposing, anti-virulence targets, immunotherapy, bioinformatic approaches, and computational predictions[11]. Preclinical projects focus on developing small molecules for Gram-negative pathogens, particularly top priority pathogens: *A. baumannii,* carbapenem-resistant Enterobacterales, and *Pseudomonas aeruginosa*[12]*.* There is a strong trend towards molecules representing new classes, new targets, or new mechanisms of action. Research into non-traditional approaches, including anti-virulence molecules, microbiome-modifying strategies, engineered bacteriophages, pathogen-specific compounds, or combination approaches, continues to grow[11]. Regulatory support, a continued supply of molecules, and improvements to the economic models will be integral to long-term success in combatting antibiotic resistance. The critical feature of these discovery programs is their ability to uncover molecules with novel mechanisms of action and unique chemical scaffolds. Promising compounds have begun to enter early development stages, sparking hope for the revitalization of the antibiotic pipeline[9]. However, derivatives of known antibiotic classes still dominate the clinical pipeline[9]. The future of antibiotic development requires more public

investment in antibacterial research and incentives to ensure that new antibiotics can be profitable.

Targeting bacterial nutrient stress

Traditional antibiotics target a narrow spectrum of bacterial processes, including cell envelope biogenesis, DNA replication, protein translation, and transcription. The overexploitation of traditional antibiotic targets has diminished returns in drug discovery efforts[7,13]. Therefore, it is critical to identify, characterize, and validate novel drug targets. Recent efforts have explored genes essential during infection and adopted in vitro conditions mimicking the infection environment to expand the target base for antimicrobial screening[14–16].

Antibiotic discovery has focused on the approximately 300 genes essential for bacterial growth in nutrient-rich laboratory media[2,14]. However, gene essentiality in laboratory media is a poor predictor for genes required during infection[14]. The emergence of transposon insertion sequencing (TnSeq) technologies has systematically identified genes essential exclusively during animal infection models[7]. In addition to canonical virulence factors, bacterial pathogens must adapt their metabolic and biosynthetic processes to colonize and proliferate in the host environment[15,17]. Bacteria must either synthesize or scavenge exogenous nutrients from the environment, such as amino acids, nucleotides, and vitamins. Host defence systems can further exacerbate bacterial

proliferation by limiting key nutrients during infection[18]. Inhibiting vital biosynthetic pathways is an intriguing avenue to uncover new antibiotic targets.

When grown in minimal media, such as M9, nutrient biosynthesis genes become essential for bacterial growth. Targeting nutrient stress is of particular interest as conventional drug discovery assays can be amended by altering the media, lowering the innovation risk associated with the development of inhibitors[7]. By contrast, many conditionally essential targets lack an in vitro phenotype, making them intractable to standard drug discovery assays[7]. Several vulnerable nutrient stress pathways have been identified as potential targets[19]. Many of these pathways are either pathogen or site of infection specific, presenting an opportunity to develop drugs targeting specific pathogenic bacteria or only function at the nutrient deplete site of infection.

Many amino acid and vitamin biosynthesis pathways are well conserved across bacteria with no human homologues (Figure 2)[20]. Glutamine, glycine, proline, serine, nucleotide, and folate pathways are at least partially present in humans. However, the ability to selectively target either the bacterial or human enzymes has been demonstrated in nucleotide[21], amino acid[22], and vitamin biosynthesis[23]. Trimethoprim is the archetypal example of such an inhibitor, exclusively targeting the bacterial folate biosynthesis enzyme, dihydrofolate reductase[23]. Despite identifying viable nutrient biosynthesis targets, the transition

of the field away from nutrient-rich growth media has been slow and largely incomplete.

Screening in nutrient-limited media has successfully identified several promising inhibitors of validated nutrient biosynthesis pathways, including biotin, *para*-aminobenzoic acid (PABA), and tryptophan[16]. To date, only *E. coli* and *Mycobacterium tuberculosis* have been screened in minimal media[16,24,25]. Screens against high-priority pathogens, including *A. baumannii*, *K. pneumoniae,* and *P. aeruginosa,* have the potential to yield further successes. Additionally, because several nutrient biosynthesis pathways are integral for antibiotic-resistant pathogens, targeting them can resensitize resistant pathogens to existing antibiotics, extending their clinical lifespan[26,27]. This chapter first discusses bacterial nutrient biosynthesis and its role during host infection. We then explore screening platforms developed to search for inhibitors of these targets and the successes in this area. Finally, we highlight the connections between bacterial nutrient biosynthesis, antibiotic activity, and resistance.

Bacterial nutrient biosynthesis

In bacteria such as *E. coli*, replication requires a source of carbon, nitrogen, sulphate, inorganic phosphate, salts, and trace metals. Bacteria must acquire nutrients such as nucleotides, amino acids, and vitamins exogenously from the environment or through their biosynthetic capabilities. The biosynthetic

pathways of these nutrients are closely linked and share several key intermediates originating from glycolysis, the tricarboxylic acid cycle, and the pentose phosphate pathway[32]. *E. coli* metabolism is extensively characterized and can be used as a representative species for many metabolic pathways. Although gaps remain in identifying non-canonical pathways, comparative genomic predictions can estimate the biosynthetic capabilities of sequenced bacteria[28].

Nucleotide biosynthesis

Purine and pyrimidines are essential for nucleic acids, energy metabolism, and cell signalling. Accordingly, the de novo biosynthesis pathways for nucleotides are well conserved across all domains of life[29]. Nucleotide biosynthesis requires the precursor phosphoribosyl pyrophosphate (PRPP)[30–32]. Purines contain a six-membered pyrimidine ring fused to a five-membered imidazole ring. De novo biosynthesis of purine begins with the synthesis of inosine monophosphate (IMP), which is then modified to create all other purines. De novo pyrimidine biosynthesis first converts bicarbonate, glutamine, aspartate, and PRPP to uridine-5'-phosphate (UMP)[31]. UMP is the precursor to pyrimidine deoxyribonucleotide and ribonucleotide biosynthesis. The biosynthesis of polysaccharides, glycoproteins, and phospholipids uses pyrimidine's mono and di-phosphorylated forms. In *E. coli* de novo nucleotide biosynthesis is largely conserved with the mammalian pathway. However, bifunctional enzymes

catalyze several reactions in humans, unlike *E. coli*[29]. In addition to de novo biosynthesis, salvage pathways uptake exogenous free bases and nucleosides from the environment that can enter de novo biosynthesis pathways. Accordingly, the nucleotide biosynthesis steps required for the synthesis of UMP and IMP are dispensable in nutrient-rich laboratory conditions.

Amino acid biosynthesis

In contrast to mammals, many bacteria can synthesize all twenty standard amino acids de novo; major pathogens, *A. baumannii, E. coli, K. pneumoniae, M. tuberculosis*, *P. aeruginosa,* and *S.* Typhimurium, are among this list. *S. aureus* is unique as it contains the biosynthetic genes for synthesizing all 20 amino acids; however, phenotypically strains can be auxotrophic to several amino acids, including arginine, cysteine, glycine, leucine, proline, and valine[33,34]. *S. aureus* auxotrophies are caused by complex regulatory circuits, and their impact during infection is unclear[33]. Many amino acid biosynthesis pathways are well conserved across bacterial phyla, and only six pathways show complete overlap with those present in humans (Figure 2).

The biosynthesis of amino acids manipulates six primary precursor metabolites: PRPP, 3-phosphoglycerate, phosphoenolpyruvate, pyruvate, α-ketoglutarate, and oxaloacetate (Figure 3). The precursors are obtained from glycolysis, the tricarboxylic acid cycle, or the pentose phosphate pathway

intermediates[32,35]. Biosynthesis of the various amino acids occurs in sequential reactions, for example, the synthesis of glycine from serine or through interconnected branched pathways, such as aromatic amino acid biosynthesis. Amino acids are integral for protein biosynthesis and play several other vital roles in bacteria. Glutamate or glutamine are generally used as a nitrogen donor to synthesize other amino acids, nucleotides, and glucosamine. Similarly, glycine and serine serve as a source of one-carbon for various compounds, including purines, thymidine, methionine, choline, and lipids. Cysteine is a precursor for methionine, thiamine, and coenzyme A (CoA) and an important source of sulphur in cellular components. The synthesis of amino acids requires significant energy costs. Bacteria generate less energy by diverting intermediates from carbon metabolism, and additional energy is required to convert intermediates to amino acids. Bacterial cells prefer an environmental source of amino acids instead of synthesizing their own.

α-ketoglutarate derived amino acids use glutamate as the precursor for glutamine, arginine and proline[32,35]. *M. tuberculosis* and *S. aureus* have an alternate proline biosynthesis pathway, using ornithine instead of glutamate[36]. In *M. tuberculosis,* both the *E. coli* and alternate pathway are present; however, in *S. aureus* proline biosynthesis can only be synthesized via ornithine[36]. 3-phosphoglycerate-derived amino acids include serine, glycine, and cysteine, with

serine acting as the precursor for glycine and cysteine biosynthesis. Histidine biosynthesis converts PRPP and ATP to histidine in a ten-step process[32,37].

Aspartate is synthesized from the transamination of glutamate with oxaloacetate and acts as the precursor for asparagine, methionine, threonine, and lysine synthesis in *E. coli*[32,38]. Asparagine can be synthesized from aspartate using either glutamine or ammonia as the amino donor. Methionine, threonine, and lysine synthesis in *E. coli* begin with converting aspartate to aspartate 4-semialdehyde[32,38]. At this point, the pathways branch into the synthesis of lysine and homoserine biosynthesis. Homoserine acts as the precursor for threonine and methionine biosynthesis. Lysine synthesis overlaps with cell-wall biosynthesis sharing the precursor diaminopimelate (DAP)[32,38]. Accordingly, the genes involved in the synthesis of DAP are essential, and only the conversion of DAP to lysine is dispensable. Methionine biosynthesis in *E. coli* is non-canonical, and there are diverse biosynthetic enzymes employed by other species, with only the final step in methionine biosynthesis generally well-conserved across bacteria[39]. Methionine is essential both as a proteinogenic amino acid and a component of the cofactor *S*-adenosyl methionine.

The aromatic amino acids are synthesized from D-erythrose 4-phosphate and phosphoenolpyruvate, which first enters the shikimate pathway, followed by the chorismate pathway[32,40]. Phenylalanine, tryptophan, and tyrosine are then synthesized from chorismate. Tyrosine and phenylalanine biosynthesis share

several bifunctional enzymes used in branched-chain amino acids and aspartate synthesis[32,40].

Alanine can be synthesized in three redundant pathways in *E. coli* using pyruvate[32,41]. Accordingly, the biosynthetic enzymes for alanine synthesis are dispensable. The branched-chain amino acid biosynthetic pathways share several enzymes. Valine is synthesized from pyruvate in a 4-step biosynthetic pathway shared with isoleucine biosynthesis[32,41]. Isoleucine is synthesized in a 5-step pathway from threonine, sharing the last four steps of the pathways with valine biosynthesis[32,41]. Leucine biosynthesis begins from the final intermediate in the valine pathway[32,41]. The shared branched-chain amino acid transaminase (IlvE) catalyzes the final step of leucine biosynthesis after the action of several leucine-specific enzymes.

Vitamin biosynthesis

Bacteria can synthesize several vitamins de novo, including biotin, pyridoxal 5'-phosphate (PLP), nicotinamide adenine dinucleotide (NAD), pantothenate, thiamine diphosphate, and tetrahydrofolate. Aside from the late steps of tetrahydrofolate synthesis, these pathways are unique to bacteria and are generally well conserved across pathogens.

De novo biotin biosynthesis is divided into early and late steps. In the first stage of biotin production, a pimeloyl moiety is synthesized from malonyl-CoA

using fatty acid biosynthesis enzymes[42]. The late steps are performed by four conserved enzymes responsible for converting pimeloyl to biotin, creating the bicyclic ring structure[43]. Biotin is an essential cofactor for carboxylation reactions[43]. Specifically, in *E. coli,* it is required for the first committed step of fatty acid biosynthesis[44]. PLP is an essential cofactor primarily for transamination reactions; however, it also can be used in decarboxylation, racemization, Cα-Cβ cleavage, and α-β elimination reactions[45]. Accordingly, it plays a critical role in amino acid biosynthesis. PLP biosynthesis involves two branches stemming from erythrose 4-phosphate and the other 3-phosphoglycerate and pyruvate[45].

In bacteria, NAD is synthesized from aspartate, requiring PRPP and glutamine in the process[46]. By contrast, NAD synthesis in humans begins from tryptophan. NAD and its phosphorylated derivative NADP are essential in redox reactions[46]. Pantothenate is an essential precursor for CoA and acyl carrier protein (ACP)[46]. The biosynthesis of pantothenate is derived from a precursor in valine biosynthesis and aspartate. Thiamine biosynthesis is composed of a pyrimidine and thiazole moiety combined to form thiamine phosphate and phosphorylated[47]. Thiamine is an essential cofactor for dehydrogenases, including several enzymes in carbon metabolism. Tetrahydrofolate and its derivatives, referred to as folates, are used to transfer one-carbon units in amino acid and nucleotide biosynthesis[48]. GTP and chorismate are modified to create the precursors for tetrahydrofolate synthesis. The final enzyme dihydrofolate

reductase, the target of trimethoprim, is present in mammals but distinct from the mammalian enzyme.

Strategies to identify conditionally essential targets during infection

TnSeq techniques such as HITS[49], INSeq[50], TraDIS[51], and TnSeq[52], have proved invaluable in investigating host-pathogen interactions, replacing previous practices, such as microarrays[53] and individual auxotroph survival or competition studies. In vivo TnSeq screens have probed the role of bacterial nutrient biosynthesis during infection and unveiled niche-specific fitness determinants (Figure 4). Further, the versatility of TnSeq technologies expanded studies of in vivo essentiality to various bacterial species, highlighting the species specificity of fitness determinants. Notably, these studies have unveiled that nutrient biosynthesis genes play a role in infection for all top priority pathogens, to varying degrees. Perhaps unsurprisingly, critical nutrient biosynthesis pathways vary between pathogens and sites of infection.

Despite the technique's success, several limitations exist in the application of TnSeq. The efficacy of TnSeq during infection depends on the pathogen and infection site. A substantial number of bacteria are often killed stochastically during the establishment of infection[54]. For example, the establishment of gastrointestinal and urinary tract infections is subject to severe bottlenecks limiting the applicability of TnSeq to conventional mouse models[55,56]. The

population bottleneck should be estimated using a set of neutral insertions and the experimental inoculum designed to align with these results. Using mouse infection models that do not exert significant selection and creating several smaller pools of mutants is essential for effectively evaluating in vivo fitness determinants. Another weakness is the potential for cross-complementation, the sharing of resources between strains. Secreted products such as siderophores are often dispensable in pooled infections. The extent to which cross-complementation affects metabolic precursors is unclear. Despite the limitations, TnSeq datasets provide a wealth of information on the vulnerability of nutrient biosynthesis genes and, accompanied by reconfirmation studies, help to direct future drug discovery efforts.

Viable nutrient stress targets

Nucleotide biosynthesis

De novo purine biosynthesis first emerged as a fitness determinant for *Salmonella* species in the early 1950's[57,58]. Mutations to adenine-specific biosynthesis genes (*purA* and *purB*) result in avirulent strains, and mutants in guanine (*guaA* or guaB) or non-specific genes of purine biosynthesis (*purC, purD, purE, purF, purH, purL,* and *purM*) reduce virulence[8]. It has since been demonstrated in various bacterial pathogens that purine biosynthesis is essential during intracellular replication, including *S.* Typhi, *S.* Typhimurium, and *M.*

tuberculosis[59–61]. Indeed, purine biosynthesis mutants have been applied as live attenuated vaccines in animal models and humans against these pathogens[59,60]. To a lesser extent, pyrimidine biosynthesis is critical for *S.* Typhimurium during infection, showing reduced virulence[62] and colonization[63] capabilities.

Similarly, in *S. aureus,* purine and pyrimidine biosynthesis has been demonstrated as critical to survival in blood, abscesses, osteomyelitis, pneumonia, and bacteremia[19,64]. However, mutants in *S. aureus* are not completely avirulent, suggesting some purines can be scavenged during infection. Furthermore, in *S. aureus,* regulation of nucleotide biosynthesis is linked with virulence. Inactivation of the PurR repressor is associated with increased purine biosynthesis, up-regulation of fibronectin-binding proteins, and hyper-virulence during bacteremia[65].

In *E. coli, K. pneumoniae,* and *P. aeruginosa* de novo nucleotide biosynthesis, genes are critical for replication in human blood, and the corresponding enzymes are putative targets for the treatment of bloodstream infections[66–68]. A *purF* mutant in *P. aeruginosa* was avirulent in a burn wound model[69]. By contrast, nucleotide biosynthesis genes appear to be largely dispensable during urinary tract infection for *E. coli,* except for guanosine biosynthesis genes[70]. Notably, there is some indication that uropathogenic *E. coli* (UPEC) requires purine biosynthesis specifically to replicate in bladder epithelial

cells but not urine[71]. Overall, nucleotide biosynthesis is a viable antimicrobial target for top priority bacterial pathogens in various sites of infection.

Amino acid biosynthesis

Several amino acid biosynthesis pathways have been identified as promising antimicrobial targets with significant diversity in their dispensability across pathogens. Aromatic amino acid biosynthesis is among the earliest successful candidates for live attenuated vaccine trials in *S.* Typhi and *S.* Typhimurium[72], and later used in *M. tuberculosis* vaccines[59]. Similarly, aromatic amino acid biosynthesis has been established as a viable target in *S. aureus*[73]. All three aromatic amino acids are derived from the shared precursor, chorismate[32,40]. Chorismate biosynthesis is essential for aromatic amino acid production and PABA and siderophore creation[32,40]. Notably, in *S. aureus, S.* Typhi, and *S.* Typhimurium, it is predicted that the role of chorismate as a precursor for PABA biosynthesis is exerting the fitness cost[73]. The role of aromatic amino acid biosynthesis for pathogens *A. baumannii* and *P. aeruginosa* is context-dependent. Aromatic amino acids are potentially available to *A. baumannii* during systemic infection, while tryptophan is a limiting metabolite in lung infection models. Only tryptophan biosynthesis was dispensable in *P. aeruginosa* lung infection, burn, and chronic infection models. Similarly, in cystic fibrosis sputum, chorismate and tyrosine are limited for *P. aeruginosa*[74]. By

contrast, all three aromatic amino acids are important for *K. pneumoniae's* fitness during a lung infection[75–77].

Branched-chain amino acids are critical for several pathogens, particularly in lung infection environments. Branched-chain amino acid biosynthesis is a critical fitness determinant for the lung infection in *A. baumannii* and *K. pneumoniae*. Minimal follow-up on the level of attenuation has been performed for *A. baumannii*[76,78]*.* However, an *ilvC* or *ilvD* deletion in *K. pneumoniae* has approximately a 100-fold reduction in bacterial load in the lung for a competitive infection model[76]. Similarly, deletion of *leuA* resulted in a 1000-fold reduction in bacterial load in the lungs of immunocompromised mice[75]. In a TnSeq screen of UPEC, branched-chain amino acid biosynthesis auxotrophs were slightly (2-3 fold) attenuated in a urinary tract infection[55]. In Gram-positive pathogens such as *S. aureus,* branched-chain amino acids provide intermediates for branched-chain fatty acid synthesis, the predominant fatty acids in Gram-positive membranes and effectors of global transcriptional regulators[79]. The regulator CodY binds DNA under branched-chain amino acid limitation, acting primarily to repress virulence genes[79]. The importance of branched-chain amino acid transport during *S. aureus* infection suggests that the pathogen prioritizes the scavenging and utilization of exogenous branched-chain amino acids[79].

Nutritional immunity, the host sequestering nutrients to limit pathogenicity during infection, can impact pathogen biosynthetic requirements. There is

evidence of altered tryptophan, histidine, and arginine concentrations in specific niches during infection. Tryptophan biosynthesis has been an antibacterial target and vaccine candidate of interest for *M. tuberculosis*[80]. Experiments conducted in immunocompromised mice[80] and zebrafish models[24] lacking an adaptive immune response indicate attenuation of tryptophan biosynthesis is independent of the adaptive immune response. However, $CD4^+$ T-cell produced IFN-γ depletes intracellular tryptophan levels by upregulating the tryptophan degrading enzyme indolamine-2,3-dioxygenase[18]. Thus, the presence of the adaptative immune system may enhance the restriction of growth for *M. tuberculosis* tryptophan auxotrophs in the intracellular environment. The importance of $CD4^+$ T cell–produced IFN-γ in depleting host tryptophan has also been demonstrated for intracellular pathogens *Chlamydia*[81], *Coxiella*[82], *Francisella*[83], and *Listeria*[84]. However, the depletion of tryptophan produces kynurenine derivates that dampen the immune response[85,86]. Thus, in parallel to evading tryptophan depletion through tryptophan biosynthesis, it can enable successful colonization through immunomodulation[86–88]. Taking advantage of the restriction of nutrients by the host immune response by targeting nutrient biosynthesis is a promising avenue for antibacterial development.

Recently, it has been demonstrated that the INF-γ response also upregulates histidine catabolizing enzymes, histidine ammonia-lyase and histidine decarboxylase to starve *M. tuberculosis* of histidine[89]. Accordingly, *M.*

tuberculosis histidine auxotrophs are severely attenuated during infection[89]. The role of IFN-γ mediated histidine depletion on other intracellular pathogens remains unexplored. In *M. tuberculosis*-infected mice, histidine depletion begins 15 days post-infection[89]. It is unclear if the response would be effective against rapidly dividing pathogens such as *S.* Typhimurium. The dispensability of histidine biosynthesis for *S.* Typhimurium during infection suggests that histidine is available[90]. Similarly, for extracellular pathogens, *E. coli, P. aeruginosa,* and *S. aureus,* there is sufficient environmental histidine to support growth during infection[74,91,92]. By contrast, histidine auxotrophs are severely attenuated in both *A. baumannii* and *K. pneumoniae* lung infection and thus should be considered a potential target for developing new antimicrobial therapies[75,93].

Arginine is an integral part of the host defence system during infection. The arginine metabolite nitric oxide (NO) is part of the innate immune response and is antimicrobial against pathogens such as *E. coli, K. pneumoniae, M. tuberculosis, S. aureus,* and *S.* Typhimurium[94,95]. Utilization of host arginine by bacteria reduces energy expenditure and the pool of host arginine available for NO production[94]. Auxotrophic mutants of *M. tuberculosis* defective in arginine biosynthesis are avirulent, suggesting that the intracellular environment restricts arginine availability[96]. Arginine auxotrophy depletes thiols and accumulates ROS and DNA damage, leading to rapid death in *M. tuberculosis* in vitro and in vivo[96]. In contrast to *M. tuberculosis,* the intracellular pathogen *S.* Typhimurium uses

exogenous arginine to meet its nutrient requirements. Specifically, *S.* Typhimurium recruits the host cell cationic amino acid transporter to the *Salmonella*-containing vacuole to access the cytosolic arginine reservoir[97]. Subsequently, the pathogen over-expresses its arginine transporter (ArgT) to support its growth[97].

The arginine biosynthesis pathway in *S. aureus* is not functional under laboratory growth conditions. However, *argH* and *argJ* are attenuated during infection and play a role in bacterial persistence[98,99]. However, other arginine biosynthesis genes are dispensable, suggesting that the recycling of intermediates may be necessary during infection[98,99]. Interestingly, for uropathogenic *E. coli* (UPEC), arginine biosynthesis is dispensable in acute infections, but is required for chronic bladder infection[100]. Arginine biosynthesis is essential for *P. aeruginosa* growth in serum and urine, yet was dispensable in a neutropenic mouse infection model[68]. Further investigation revealed arginine biosynthesis was critical for growth in human serum but dispensable in mouse serum[68].

The nutritional requirements of *M. tuberculosis* are the best studied of any pathogen. *M. tuberculosis* relies primarily on de novo biosynthesis to meet most of its amino acid requirements, making nutrient biosynthesis a viable target for this pathogen. Only asparagine biosynthesis is confirmed as dispensable during infection, and there is no data on glycine, phenylalanine, serine, or tyrosine

auxotrophs during infection. Arginine[96], cysteine[101], histidine[89], methionine[102], threonine[103], and tryptophan[18] biosynthesis are top priority pathways as auxotrophic strains are entirely cleared. Arginine, methionine, and threonine auxotrophies are associated with rapid cell death or are bactericidal. Homoserine (methionine and threonine auxotrophies) and sulphate assimilation mutants (cysteine and methionine auxotrophies) have impaired persistence during infection[101,103]. Aspartate, glutamate, glutamine, glycine, alanine, leucine, valine, and isoleucine are imported from the intracellular environment and used as nitrogen sources during infection[104]. However, the biosynthetic pathways for glutamine and branched-chain amino acids are still required to meet the nutrient requirements for replication and auxotrophs are attenuated during infection[105–107].

There is no robust data on the dispensability of the biosynthetic pathways outside of *M. tuberculosis* for several amino acids. TnSeq studies can be used to identify potential pathways for follow-up experiments using single mutants (Figure 4). From TnSeq studies, the importance of many amino acid biosynthetic pathways is primarily pathogen-specific. Glycine biosynthesis is dispensable for most bacterial pathogens during infection except for *S.* Typhimurium. In *S.* Typhimurium, a *glyA* mutant had a reduction in virulence in a competitive murine infection model. The glycine levels available during infection are speculated to be insufficient for the requirement of one-carbon units[90,108]. Notably, serine biosynthesis is dispensable during infection for *S.* Typhimurium, indicating that

serine is available in sufficient concentrations to support one-carbon flux[90,108]. However, this may be serovar dependent as a TnSeq study of *S.* Typhi in humanized mice identified *serC* as a fitness determinant[109]. Serine is also limited in the lungs as serine biosynthesis is a fitness determinant for *A. baumannii*[78] and *K. pneumoniae*[76]. Inactivation of *serA* and *serB* results in a significant reduction of bacterial load in *K. pneumoniae* infection[75]. Validation of serine as an antimicrobial target for *A. baumannii* requires further studies of the level of attenuation. Cysteine and proline biosynthesis are also critical for *S.* Typhimurium. Deleting *cysE* in *S.* Typhimurium results in severe attenuation and has been evaluated as a vaccine candidate in mice[110]. A *proC* mutant in *S.* Typhimurium was severely attenuated in a systemic infection model[111,112]. Interestingly, a *proB* mutant does not show the same level of attenuation, potentially due to accumulation of the precursor[112]. Proline depletion may be detrimental for *S.* Typhimurium, impacting the expression of *mgtCBR* virulence operon[112].

Several amino acids have been identified as fitness determinants during a mouse pneumonia model of *A. baumannii,* including methionine, proline, and threonine[78]. However, further studies are still needed to understand the extent of the attenuation. Threonine biosynthesis is similarly crucial in a *K. pneumoniae* lung infection model[76]. Threonine, methionine, and lysine biosynthesis play an essential role in *S. aureus* bacteremia, with mice infected with auxotrophs for

each amino acid having improved survival compared with wild-type[113]. Methionine is also limiting in the human nose and appears to be a key pathway for *S. aureus* colonization[114]. Similarly, in both *P. aeruginosa* and *E. coli,* methionine auxotrophs have a reduced ability to proliferate in human serum. This suggests validation in bloodstream models of infection should be considered[115].

Vitamin biosynthesis

Sulfonamides and trimethoprim both target folate (vitamin B9) biosynthesis in bacteria. Sulfonamides are of particular interest, as their target, FolP, is dispensable in nutrient-rich media. Following the discovery of the sulfonamides, it has been demonstrated that PABA is limiting during infection. Beyond folate biosynthesis, vitamin biosynthesis during infection is best studied in *M. tuberculosis,* with auxotrophs in biotin[116], pantothenate[117], pyridoxine[118], and thiamine[119] playing a critical role during infection. Pyridoxine and biotin auxotrophies are bactericidal in vitro and during infection. Using conditional knockdown, Park *et al.* demonstrated that biotin is critical for persistence during latent infection in mice[116]. Accordingly, both biotin and pyridoxine are priority targets for antimycobacterial drug development. Vitamin biosynthesis also plays a vital role for *P. aeruginosa* in several infection sites. Pantothenate and pyridoxine are limited in chronic and burn wound environments for *P. aeruginosa*[69]*.* Similarly, in addition to pantothenate and pyridoxine, biotin is predicted to be limited in the cystic fibrosis lung environment[74]. Vitamin biosynthesis is a putative

target for novel antibiotics in *P. aeruginosa,* requiring study to assess the vulnerability of the biosynthetic pathways.

Outside of *M. tuberculosis* and *P. aeruginosa,* vitamin biosynthesis has been overlooked as an antibiotic target. This can be attributed to the lack of attenuation observed for vitamin biosynthesis genes during transposon mutagenesis studies in murine infection models for *A. baumannii, K. pneumoniae, S.* Typhimurium, and *S. aureus* (Figure 4). Although, NAD biosynthesis appears to play a role in *K. pneumoniae* pathogenesis in the lungs[75–77]. In chapter 2, we find that previous studies did not consider the 40-fold higher concentration of biotin in mouse plasma compared with human plasma. We developed a murine model mimicking human biotin levels. In our model, biotin biosynthesis is essential during infection and a valid antimicrobial target for *A. baumannii, K. pneumoniae,* and *P. aeruginosa*. Literature indicates that mouse plasma levels of several vitamins, including pantothenate, pyridoxine, and thiamine, are elevated compared with human plasma[120–122]. Pantothenate biosynthesis is critical for the growth of *K. pneumoniae* in human serum[67]. However, in murine infection models pantothenate biosynthesis is dispensable[76,77]. Testing in human mimicking environments will be essential for evaluating vitamin biosynthesis genes and candidate antimicrobial targets.

Strategies to uncover inhibitors of nutrient stress

Mimicking the trajectory of the antibiotic discovery field, initial efforts to develop inhibitors of nutrient biosynthesis were primarily focused on enzyme inhibition, yielding little success. Pairing enzymatic screens with simultaneous whole-cell assays and medicinal chemistry has only identified a few scaffolds active against bacteria[123]. For instance, the pairing of an enzymatic screen of *M. tuberculosis* BioA inhibitors with a secondary assay for whole-cell activity identified a whole-cell-active inhibitor of biotin biosynthesis[123]. Further improvements to potency were achievable through medicinal chemistry efforts. However, activity in murine models of infection has not been demonstrated[124]. Overall, in vitro screens have proved inefficient and largely unsuccessful at achieving whole-cell activity[7,20]. That said, finding enzyme inhibitors of many nutrient biosynthesis enzymes suggests the targets are druggable and tractable.

Screening in nutrient-limited media, excluding amino acids, nucleotides, and vitamins, has led to the rapid identification of whole-cell active inhibitors of nutrient stress[16,25]. Target identification is a significant limitation of most whole-cell screens. Metabolic suppression arrays are an effective tool for target identification unique to nutrient stress targets. This technique uses an array of mostly primary metabolites that can be screened for suppressors of inhibitory molecules to quickly identify the targeted biosynthetic pathway[16]. This assay can complement conventional target identification techniques such as the generation

of resistant mutants, knockdown libraries, enzyme assays, or multicopy-suppression[125,126].

The application of growth media closely mimicking physiologic conditions can identify inhibitors of nutrient stress processes. Screens of ordered genomic libraries and TnSeq studies have identified critical nutrient biosynthesis pathways for the replication of pathogens in biological fluids, including urine, serum, and sputum[66–68,74]. Additionally, in media replicating the intracellular environment, *S.* Typhimurium requires several nutrient biosynthesis pathways to replicate efficiently[61]. Promisingly, in *P. aeruginosa,* biological fluids could predict bacterial fitness in the corresponding site of infection[68]. Small-molecule screens in serum[67] and macrophages[61] have successfully identified the nucleoside analogs, 5-fluorouracil and carmofur. Both antimetabolites are anti-cancer agents unlikely to be used clinically to treat an infection; however, their identification highlights the ability of host mimicking environments to identify inhibitors of nucleotide biosynthesis[67].

Nutrient biosynthesis inhibitors

Prontosil is the first antibiotic used to treat human infections and the only inhibitor of nutrient biosynthesis in clinical use[48]. It was discovered in unique conditions prior to the widespread practice of systematic screening techniques in nutrient-rich laboratory media. In the early 1930s, physician Dr. Gerhard Dogmak

was working on testing compounds related to synthetic dyes for their effectiveness against disease[127]. Dogmak believed that a drug's role was to support the immune system to overcome infection[127]. With this unique perspective, he evaluated a compound's effectiveness in curing an infection in mice even if the compound had failed against cultured bacteria. The group identified an azo dye with a sulfonamide group that was inactive in vitro, yet had weak activity against *Streptococcus* in mice[127]. After several alterations to the structure to improve potency, the compound was patented as Prontosil, becoming the first sulfonamide in clinical use[127].

Sulfonamides target dihydropteroate synthase, which converts dihydropteroate diphosphate and PABA into dihydropteroic acid[48]. Excess PABA in laboratory media outcompetes the sulfonamides for access to dihydropteroate synthases and suppresses any inhibitory activity[48]. Sulfonamides are the only inhibitors of nutrient biosynthesis in clinical application and would remain undiscovered with conventional antibiotic discovery techniques. Despite the nominal change required of screening protocols, only a handful of initiatives have employed nutrient limiting conditions, with varying levels of success.

In the literature, successful screening campaigns have combined innovative small-molecule screens with target validation. The research by Pethe *et al.,* discovering the pyrimidine-imidazoles, highlights the limitations of not combining screening with careful target validation[128]. The molecules were

identified in a whole-cell screen against *M. tuberculosis* conducted in the common culture media, Middlebrook 7H9, lacking amino acids and nucleotides, supplemented with 0.2% glycerol as the carbon source[128]. The compounds targeted GlpK, glycerol kinase, had bactericidal activity against *M. tuberculosis* and a good cytotoxicity profile. However, the lead compounds lacked in vivo activity, and further research revealed that *glpK* is dispensable during lung infection.

In contrast, screening for inhibitors of *M. tuberculosis* growth in minimal media identified BRD4592, a synthetic azetidine derivative[24]. Mechanistic studies revealed that BRD4592 allosterically inhibits tryptophan synthase (TrpAB)[24]. Tryptophan biosynthesis has been validated as essential for the survival of *M. tuberculosis* and the related *M. marinum* during infection[24]. BDR4592 demonstrated moderate success in macrophage and zebrafish models of infection[24]. However, poor pharmacokinetic properties limited testing in more complex animal models. Improving the scaffolds' pharmacokinetics is a promising direction for future development efforts, given the substantial target validation for tryptophan biosynthesis.

Tryptophan biosynthesis has proved to be a druggable target. Previous efforts in targeting tryptophan biosynthesis evaluated halogenated anthranilate analogs, 2-amino-5-fluorobenzoic acid (5-FABA) and 6-FABA, against *M. tuberculosis*[18]. Tryptophan biosynthesis enzymes modify the antimetabolites to

produce toxic fluorinated tryptophan[129]. The efficacy of 6-FABA and an ester analog given daily at 200 mg/kg were evaluated against an *M. tuberculosis* infection in mice. Both were able to reduce the bacterial load by 1.0-$\log_{10}$ in the spleen and only 2-fold in the lungs[18]. However, mice were unable to tolerate 6-FABA beyond 2-weeks. With weak in vivo activity and toxicity, further efforts with the antimetabolites were abandoned. More recently, a screen of 50,000 compounds against pools of strains with depleted essential targets identified BRD-7721, a 3-indolepropionic acid (3-IPA) ester[130]. A TrpG hypomorph showed increased sensitivity to 3-IPA, and the compound's activity was suppressed by tryptophan supplementation[130]. Notably, 3-IPA was also identified in a fragment-based screen and targets TrpE[131]. However, the compound demonstrated limited in vivo activity[131].

A screen against *E. coli* in M9 minimal media with glucose as the carbon source identified a plethora of compounds inhibiting nutrient biosynthesis. A metabolic suppression profile was developed for 71 inhibitors, and the mechanism of action was characterized for three molecules[132]. MAC168425 interferes with glycine metabolism, MAC173979 is a time-dependent inhibitor of PABA biosynthesis, and MAC13772 inhibits biotin biosynthesis. Again, the application of the lead molecules is contingent on target validation. Sulfamethoxazole exemplifies the therapeutic utility for inhibitors of PABA biosynthesis. However, no data on the efficacy of MAC173979 in animal infection

models has been reported. Targeting biotin biosynthesis has been widely explored in *M. tuberculosis* subsequent to its validation as essential during infection[116]. MAC13772 is active against *M. tuberculosis* and has shown potential as a combination therapy with rifampicin. Chapter 2 validates biotin biosynthesis as a promising target for *A. baumannii, K. pneumoniae,* and *P. aeruginosa* in human mimicking infection conditions. MAC13772 reduced the bacterial load during a systemic *A. baumannii* infection[133], making it the first biotin biosynthesis inhibitor to demonstrate any in vivo activity. The natural products amiclenomycin and acidomycin are other known inhibitors of biotin biosynthesis[134,135]. Recently, amiclenomycin-producing strains were identified in a screen against *E. coli* lacking its high-affinity biotin transporter, BioP and the biosynthetic gene cluster for amiclenomycin reported[136]. Acidomycin has potent activity against *M. tuberculosis*, is inactive against Gram-positive pathogens, and has limited activity against Gram-negative pathogens with a permeabilized outer membrane[134]. Acidomycin lacks in vivo activity owing to its poor pharmacokinetic properties. However, a synthesis scheme for acidomycin was recently developed, supporting future efforts to develop analogs with improved pharmacokinetic properties[134]. Additional exploration of amiclenomycin, acidomycin and future analogs in humans mimicking infection conditions is warranted.

In a similar experimental setup, Wallace *et al.* screened *E. coli* in M9 minimal media[25]. The screen focused on pathways related to tetrahydrofolate by

counter screening specifically for molecules suppressed by the presence of methionine or PABA[25]. This yielded the discovery of N-(phenyl) thioacetamide-linked 1,2,3-triazoles, a group of antimetabolites disrupting the cysteine biosynthesis[25]. The scaffold acts on CysK, resulting in false product formation. Despite the potent inhibition of CysK, further validation of the target is still required to explore the clinical viability of the molecules. Cysteine biosynthesis is a viable target in both *M. tuberculosis* and *S.* Typhimurium[101,110]. Testing against *S.* Typhimurium may hold promise for further development of the scaffold. Tailoring secondary screening to focus on targets validated in vivo can counter the need to design culture media to largely unknown in vivo conditions.

Small molecule screening approaches for nutrient biosynthesis inhibitors have primarily focused on synthetic chemical libraries. However, several known natural product antimetabolites interfere with diverse metabolic pathways. Antimetabolites are compounds with a similar chemical structure to essential metabolites that disrupt metabolic processes by acting as a competitive substrate or binding key enzymes. Incorporating an antimetabolite can often have downstream impacts on other metabolic pathways. One major limitation of antimetabolites is the potential for toxicity if similar metabolites are used in mammals. For example, nucleotide antimetabolites such as 5-fluorouracil and mercaptopurine have antineoplastic activity. Antimetabolites targeting glutamine synthetase (GlnA), threonine synthase (ThrC), pantothenate kinase (CoaA), and

N-acetyl glutamate synthase (ArgA) have been identified and demonstrated antibacterial activity[137]. The spectrum of activity, toxicity, and efficacy in animal infection models are critical next steps for these antimetabolites.

The potential for inhibitors of nutrient biosynthesis in combination therapy approaches is also of interest. Sulfonamides and trimethoprim, inhibitors of folate biosynthesis, show potent synergy in combination. The synergistic activity of the sulfonamide-trimethoprim combination is driven by mutual potentiation resulting from a complex metabolic feedback loop connecting tetrahydrofolate to glycine, methionine, and nucleotide biosynthesis[138]. Biotin biosynthesis has been prioritized as a frontline target in *M. tuberculosis* due to its synergistic activity with rifampicin and ethambutol[139]. Synergistic interactions between 45 probes of bacterial nutrient biosynthesis and known antimicrobials show several synergistic interactions highlighting the potential for combination therapies[140]. Several auxotrophs have exhibited increased susceptibility to antimicrobials. For example, deletion of *glyA* is associated with loss of resistance to trimethoprim in *E. coli*[141]. Deletion of *cysK* is also associated with increased susceptibility to trimethoprim, sulfamethoxazole and an inhibitor of PABA biosynthesis[25]. There are significant prospects for applying nutrient biosynthesis inhibitors in combination therapies.

The connection between nutrient stress and antibiotic resistance

Antibiotic resistance is a resource-intensive process, often associated with a fitness cost, characterized by an attenuation of growth, morphology, or virulence. Beyond the direct impact on antimicrobial susceptibility, the expression of resistance elements can alter gene essentiality and expression. Accordingly, there is the potential for interactions between bacterial nutrient biosynthesis and antimicrobial resistance. Bacteria can undergo fitness trade-offs that lead to system-level changes in metabolic phenotypes and growth dynamics[142]. Understanding the relationships between bacterial metabolism and antibiotic resistance can be used to develop novel adjuvants targeting metabolic pathways integral to antibiotic resistance.

The connection between bacterial tolerance or persistence and the development of antibiotic resistance is well established[27,143]. Antibiotic tolerance is a state of reduced metabolism and replication. Several groups have demonstrated the ability of specific nutrients to stimulate metabolism, reviving tolerant populations and restoring antibacterial susceptibility[144–146]. For example, arginine and lysine can sensitize tolerant pathogens to aminoglycoside antibiotics by enhancing the proton motive force[147]. Likewise, defects in nutrient biosynthesis have been shown to suppress antibiotic persistence, thus representing a strategy to enhance antibiotic activity. Specifically, nucleotide biosynthesis genes and regulators of nucleotide metabolism have been identified

as contributors to bacterial tolerance. In antibiotic-tolerant *E. coli* strains, deletions in nucleotide biosynthesis genes were sensitized to ciprofloxacin killing[26]. Similarly, in *S. aureus,* purine auxotrophs are defective for persistence to rifampicin[148]. The mechanism behind this interaction is predicted to relate to the role of purines in alarmones, activating the stringent response leading to antibacterial tolerance[149]. Accordingly, there may be a role for purine biosynthesis inhibitors as anti-persistence or anti-tolerance molecules in treating chronic infections.

Beyond tolerant populations, antibiotic resistance has been demonstrated to alter metabolic pathways. In *P. aeruginosa,* populations with evolved resistance to piperacillin experienced a loss of leucine utilization, while tobramycin-evolved lineages have improved growth using *N*-acetyl-D-glucosamine as the carbon source[142]. By analyzing changes in metabolite abundances, gene expression and growth dynamics, it has been demonstrated that strains with evolved resistance to ß-lactams and aminoglycosides undergo significant changes in metabolism[142,145]. Nutrient biosynthesis pathways may be particularly sensitive to the expression of antibiotic resistance elements. The relationship between evolved antibiotic resistance and bacterial metabolism has been investigated; however, the impact of plasmid-mediated resistance mechanisms on bacterial metabolism has not been comprehensively explored. Plasmid-mediated resistance may result in a more homogenous transcriptomic

and metabolic response compared to chromosomal mutations. There is interest in exploiting essential pathways specific to antibiotic-resistant populations. Chapter 3 identifies that biotin and fatty acid biosynthesis are critical for colistin resistance. Inhibitors of biotin and fatty acid biosynthesis can resensitize *mcr-1* expressing bacteria to colistin in vitro and in vivo. The interaction is specific to colistin-resistant bacteria highlighting metabolic changes required to support *mcr-1* expression.

Systems-level analysis of the impact of antibiotic resistance on bacterial growth, gene expression and metabolism can be evaluated through TnSeq, RNA-Seq, and metabolomics analysis, respectively. TnSeq or synthetic-genetic arrays can be used to explore targets specific to antibiotic-resistant pathogens beyond the scope of nutrient biosynthesis[150]. Both RNA-Seq and metabolomic analysis have been applied to understand changes in antibiotic-resistant pathogens. For example, comprehensive proteomic and metabolic profiling of *mcr-1* expressing *E. coli* revealed changes in phospholipid, thiamine, and lipopolysaccharide metabolism[151]. In chapter 3, we find that *mcr-1* expression induces a cell envelope stress transcriptomic profile. Correspondingly, lipidomic analysis uncovered changes in phospholipid composition. We were able to exploit these changes using a combination therapy approach. Transcriptomic signatures of *E. coli* populations with evolved resistance to several antibiotics found tetracycline-resistant populations overexpressed histidine and leucine biosynthesis

pathways[152]. Careful investigations of the impact of resistance on nutrient biosynthesis using transcriptomics or specific nutrient requirements are of interest to explore. Future studies should examine the effect of inhibition of upregulated pathways on antibiotic resistance.

Purpose and goals of this thesis

My thesis work has focused on the potential to target biotin biosynthesis in monotherapy and combination therapy approaches. Chapter 2 describes the validation of biotin biosynthesis as an overlooked target for *A. baumannii*, *K. pneumoniae*, and *P. aeruginosa* by developing an innovative murine model of infection mimicking human biotin levels. Biotin biosynthesis is a viable and druggable pathway for future antibiotic development. I next sought to address the possibility of combination therapy approaches targeting biotin biosynthesis. Chapter 3 comprises our work on the interaction between biotin biosynthesis and colistin resistance, in which inhibitors of biotin biosynthesis synergize with colistin exclusively against colistin-resistant pathogens. Inhibiting biotin biosynthesis sensitizes pathogens to colistin by indirectly impeding fatty acid metabolism, altering membrane phospholipid composition and fluidity. In chapter 4, I integrate the results of chapters 2 & 3 with recent advances and progress in the development of inhibitors of nutrient stress. Further, I review our current understanding of *mcr-1* mediated colistin resistance and the interconnected nature of bacterial nutrient biosynthesis with outer membrane biogenesis. Finally,

I provide suggestions on how to further expand our understanding of colistin resistance and the impact of modifications to membrane properties on the activity of antibiotics.

Figures and Legends

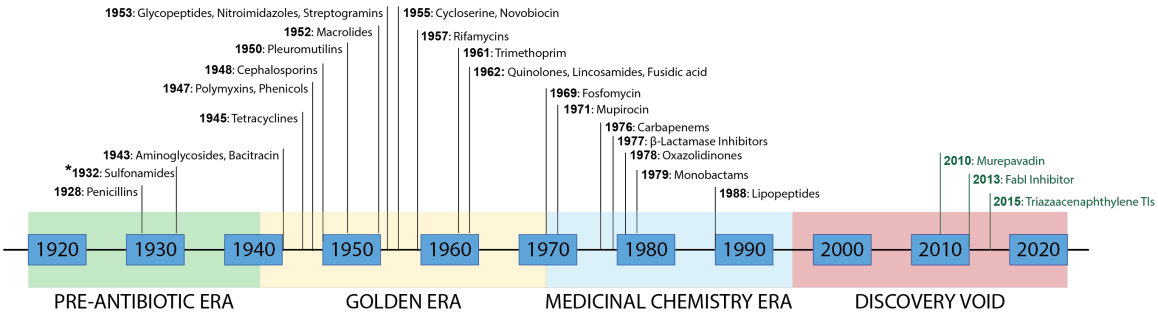

Figure 1. Timeline of antibiotic discovery. The year of discovery of the first member of each antibiotic class is in bold. Antibiotics currently in clinical trials are in green, including murepavidin, Debio1452 (FabI inhibitor), and the new class triaacenaphthylene topoisomerase II inhibitors (TIs; including Geptotidacin and Zoliflodacin). The * denotes an antibiotic class discovered using unconventional conditions.

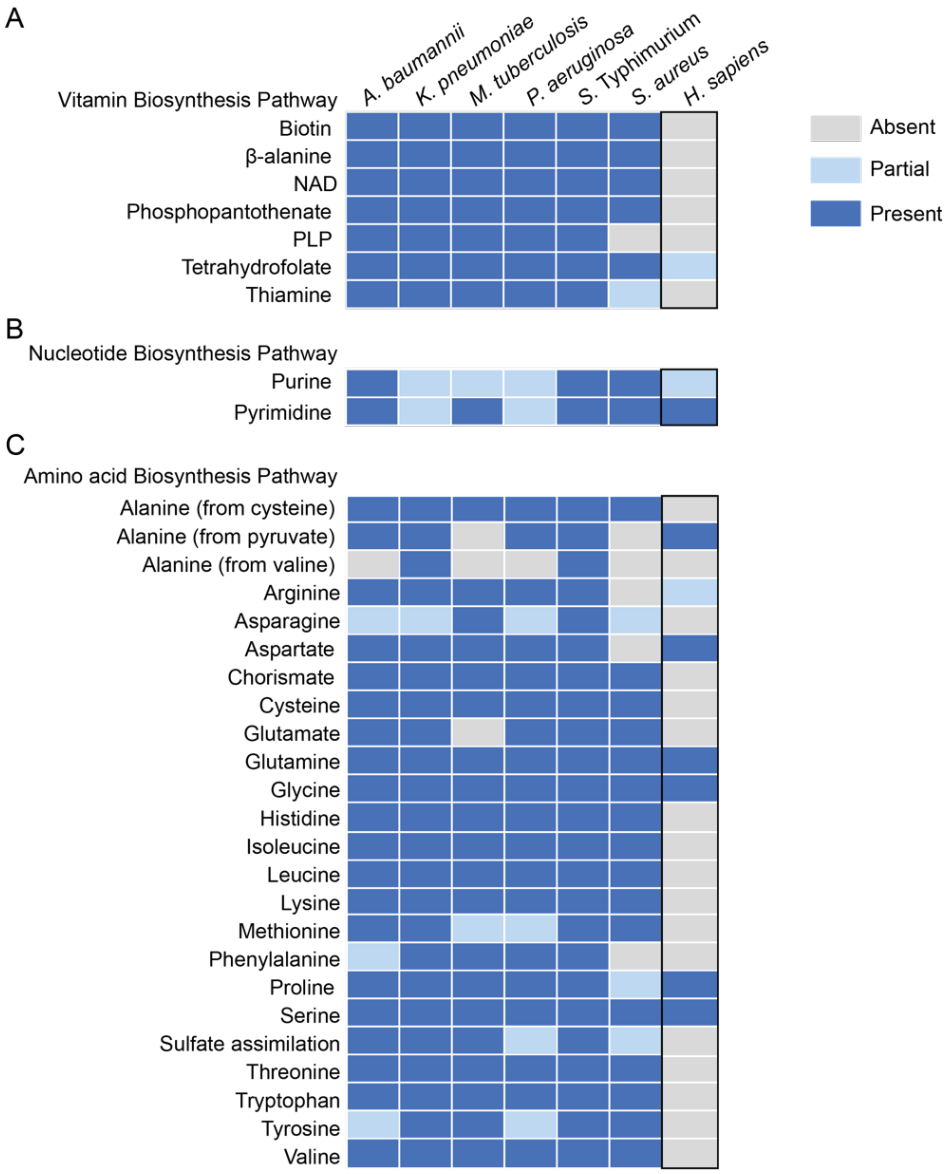

Figure 2. Conservation of amino acid, nucleotide, and vitamin biosynthesis pathways across bacterial pathogens and humans. Presence of an orthologous biosynthetic pathway to *E. coli* for a) vitamins, b) nucleotides, and c) amino acids across pathogens, *A. baumannii, K. pneumoniae, M. tuberculosis, P. aeruginosa, S.* Typhimurium, and *S. aureus* and humans. Blue indicates an orthologous pathway is present, light blue indicates at least one orthologous enzyme is present, and grey indicates the pathway is absent or shares no homology with the pathway in *E. coli.* The overlap with human nutrient biosynthesis is outlined in black.

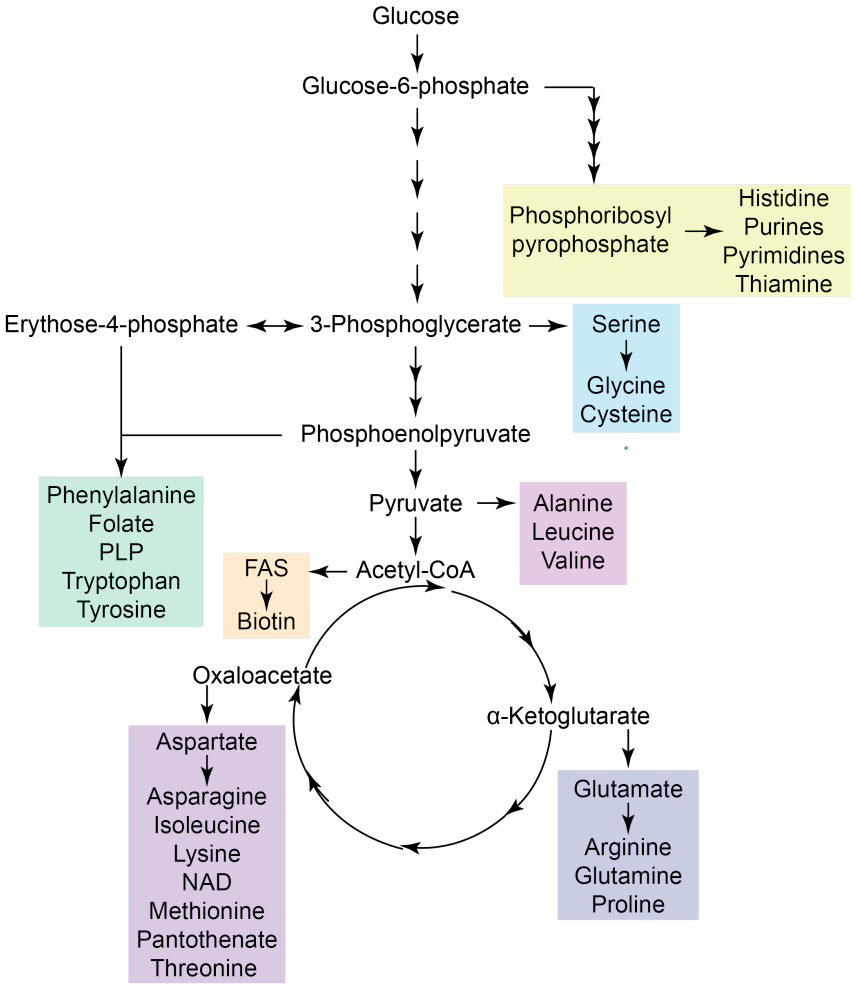

Figure 3. Overview of amino acid, nucleotide, and vitamin biosynthesis pathways in *E. coli.* Precursors from glycolysis, the tricarboxylic acid cycle, and the pentose phosphate pathway required for the nutrient biosynthetic pathways are shown in black. Amino acids, nucleotides, and vitamins are grouped by similar precursors.

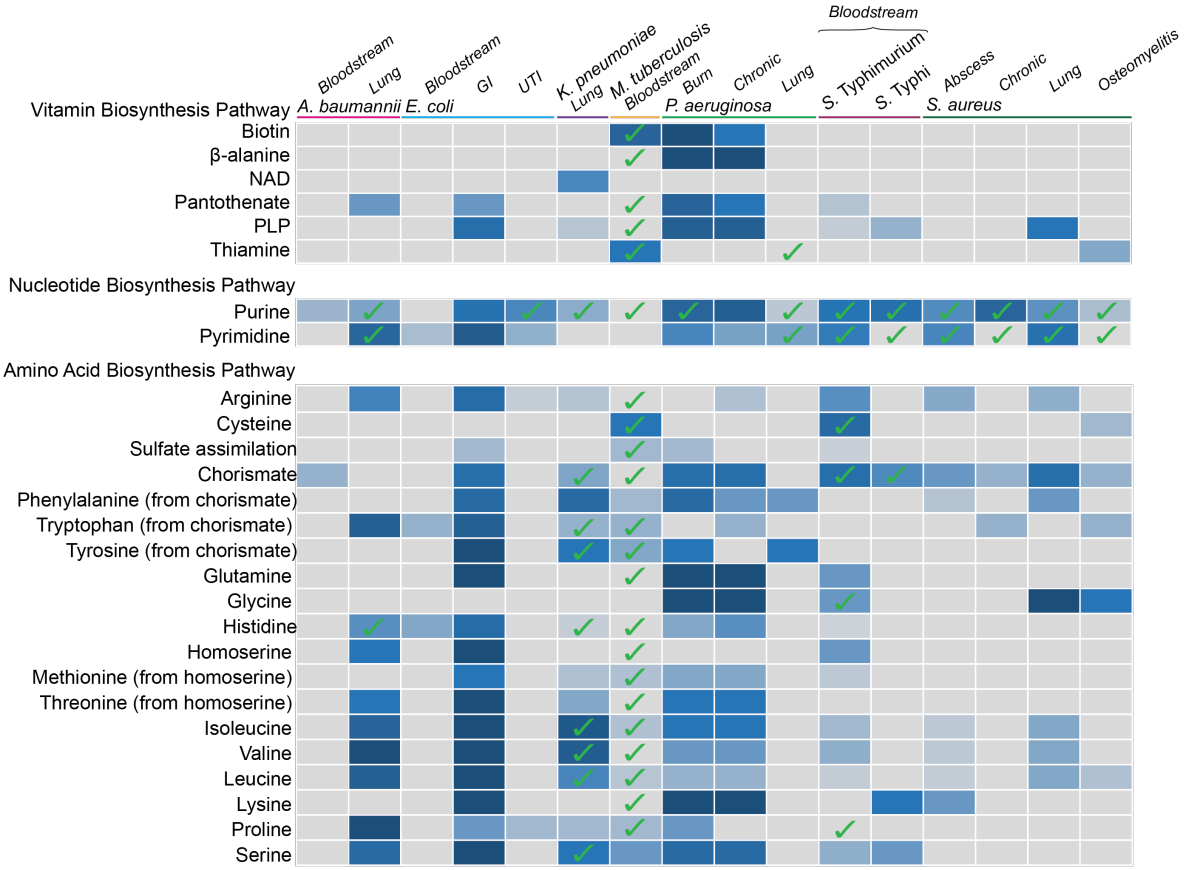

Figure 4. Summary of putative nutrient stress targets during infection. Heatmap demonstrates conditionally essential genes identified in TnSeq screens of pathogens, *A. baumannii*[59,60], *E. coli*[56,58,61,62], *K. pneumoniae*[63,64], *M. tuberculosis*[18,65], *P. aeruginosa*[66,67], *S.* Typhimurium[68–70], *S.* Typhi[71], and *S. aureus*[72–75], in various animal infection models. Dark blue indicates the entirety of the pathway is essential, and grey indicates the pathway is dispensable. Green checkmarks denote pathways that have been validated in single-mutant or survival analysis.

References

1. Årdal, C. *et al.* Antibiotic development — economic, regulatory and societal challenges. *Nat. Rev. Microbiol.* **18**, 267-274 (2020).

2. Noyes, N. R., Slizovskiy, I. B. & Singer, R. S. Beyond antimicrobial use: a framework for prioritizing antimicrobial resistance interventions. *Annu. Rev. Anim. Biosci.* **9**, 313-332 (2021).

3. Van Katwyk, S. R. *et al.* Government policy interventions to reduce human antimicrobial use: a systematic review and evidence map. *PLoS Med.* **16**, e1002819 (2019).

4. Gotham, D. *et al.* Reimbursement models to tackle market failures for antimicrobials: approaches taken in France, Germany, Sweden, the United Kingdom, and the United States. *Health Policy.* **125**, 296-306 (2021).

5. Léger, A. *et al.* AMR-Intervene: A social-ecological framework to capture the diversity of actions to tackle antimicrobial resistance from a One Health perspective. *Journal of Antimicrobial Chemotherapy* **76**, 1-21 (2021).

6. Aminov, R. I. A brief history of the antibiotic era: lessons learned and challenges for the future. *Front. Microbiol.* **1**, (2010).

7. Brown, E. D. & Wright, G. D. Antibacterial drug discovery in the resistance era. *Nature* **529**, 336–343 (2016).

8. Lewis, K. The science of antibiotic discovery. *Cell.* **181**, 29–45 (2020).

9. Theuretzbacher, U. *et al.* Critical analysis of antibacterial agents in clinical development. *Nat. Rev. Microbiol.* **18**, 286–298 (2020).

10. Baba, T. *et al.* Construction of *Escherichia coli* K-12 in-frame, single-gene knockout mutants: the Keio collection. *Mol. Syst. Biol.* **2**, 1–11 (2006).

11. Theuretzbacher, U., Outterson, K., Engel, A. & Karlén, A. The global preclinical antibacterial pipeline. *Nat. Rev. Microbiol.* **18**, 275-285 (2020)

12. WHO. *2020 Antibacterial Agents in Clinical and Preclinical Development*. *World Health Organization* (2021).

13. Coates, A. R., Halls, G. & Hu, Y. Novel classes of antibiotics or more of the same? *Br. J. Pharmacol.* **163**, 184–194 (2011).

14. D'elia, M. A., Pereira, M. P. & Brown, E. D. Are essential genes really essential? *Trends Microbiol.* **17**, 433–438 (2009).

15. Murima, P., McKinney, J. D. & Pethe, K. Targeting bacterial central metabolism for drug development. *Chem. Biol.* **21**, 1423–1432 (2014).

16. Zlitni, S., Ferruccio, L. F. & Brown, E. D. Metabolic suppression identifies new antibacterial inhibitors under nutrient limitation. *Nat. Chem. Biol.* **9**, 796–804 (2013).

17. Brown, S. A., Palmer, K. L. & Whiteley, M. Revisiting the host as a growth medium. *Nat. Rev. Microbiol.* **6**, 657–666 (2008).

18. Zhang, Y. J. *et al.* Tryptophan biosynthesis protects mycobacteria from CD4 T-cell-mediated killing. *Cell* **155**, 1296–1308 (2013).

19. Goncheva, M. I., Chin, D. & Heinrichs, D. E. Nucleotide biosynthesis: the base of bacterial pathogenesis. *Trends Microbiol.* (2022)

20. Silver, L. L. Challenges of antibacterial discovery. *Clin. Microbiol. Rev.* **24**, 71–109 (2011).

21. Marcinkeviciene, J. *et al.* Selective inhibition of bacterial dihydroorotate dehydrogenases by thiadiazolidinediones. *Biochem. Pharmacol.* **60**, 339-342 (2000).

22. Amorim Franco, T. M. & Blanchard, J. S. Bacterial branched-chain amino acid biosynthesis: structures, mechanisms, and drugability. *Biochemistry*. **56**, 5849-5865 (2017).

23. Wróbel, A., Arciszewska, K., Maliszewski, D. & Drozdowska, D. Trimethoprim and other nonclassical antifolates an excellent template for searching modifications of dihydrofolate reductase enzyme inhibitors. *J. Antibiot*. **73**, 5-27 (2020).

24. Wellington, S. *et al.* A small-molecule allosteric inhibitor of *Mycobacterium tuberculosis* tryptophan synthase. *Nat. Chem. Biol.* **13**, 943–950 (2017).

25. Wallace, M. J. *et al.* Discovery and characterization of the antimetabolite action of thioacetamide-linked 1,2,3-triazoles as disruptors of cysteine biosynthesis in Gram-Negative bacteria. *ACS Infect. Dis.* **6**, 467–478 (2020).

26. Stokes, J. M. *et al.* A multiplexable assay for screening antibiotic lethality against drug-tolerant bacteria. *Nat. Methods.* **16,** 303-306 (2019).

27. Stokes, J. M., Lopatkin, A. J., Lobritz, M. A. & Collins, J. J. Bacterial metabolism and antibiotic efficacy. *Cell Metab.* **30**, 251-259 (2019).

28. Price, M. N. *et al.* Filling gaps in bacterial amino acid biosynthesis pathways with high-throughput genetics. *PLoS Genet.* **14**, e1007147 (2018).

29. Chua, S. M. H. & Fraser, J. A. Surveying purine biosynthesis across the domains of life unveils promising drug targets in pathogens. *Immunol. Cell Biol*. **98**, 819-831 (2020).

30. Zalkin, H. & Dixon, J. E. De novo purine nucleotide biosynthesis. *Prog. Nucleic Acid Res. Mol. Biol.* **42**, 259–287 (1992).

31. Cohen, G. N. The biosynthesis of nucleotides. in *Microbial Biochemistry* (2014).

32. Shimizu, K. & Matsuoka, Y. Feedback regulation and coordination of the main metabolism for bacterial growth and metabolic engineering for amino acid fermentation. *Biotechnol. Adv*. **55**, (2022).

33. Audretsch, C., Gratani, F., Wolz, C. & Dandekar, T. Modeling of stringent-response reflects nutrient stress induced growth impairment and essential amino acids in different *Staphylococcus aureus* mutants. *Sci. Rep.* **11**, 9651 (2021).

34. Lee, D. S. *et al.* Comparative genome-scale metabolic reconstruction and flux balance analysis of multiple *Staphylococcus aureus* genomes identify novel antimicrobial drug targets. *J. Bacteriol.* **191**, 4015-4024 (2009).

35. Cohen, G. N. Biosynthesis of the amino acids of the glutamic acid family and its regulation. in *Microbial Biochemistry* (2014).

36. Christgen, S. L. & Becker, D. F. Role of proline in pathogen and host interactions. *Antioxidants and Redox Signaling*. **30**, (2019).

37. Cohen, G. N. The biosynthesis of histidine and its regulation. in *Microbial Biochemistry* (2014).

38. Cohen, G. N. The Aspartic Acid Family of Amino Acids: Biosynthesis. in *Microbial Biochemistry* (2014).

39. Ferla, M. P. & Patrick, W. M. Bacterial methionine biosynthesis. *Microbiology*. **160**, 1571-1584 (2014).

40. Cohen, G. N. Biosynthesis of aromatic amino acids and its regulation. in *Microbial Biochemistry* (2014).

41. Cohen, G. N. Biosynthesis of amino acids derived from phosphoglyceric acid and pyruvic acid. in *Microbial Biochemistry* (2014).

42. Lin, S., Hanson, R. E. & Cronan, J. E. Biotin synthesis begins by hijacking the fatty acid synthetic pathway. *Nat. Chem. Biol.* **6**, 682–688 (2010).

43. Streit, W. R. & Entcheva, P. Biotin in microbes, the genes involved in its biosynthesis, its biochemical role and perspectives for biotechnological production. *Appl. Microbiol. Biotechnol.* **61**, 21–31 (2003).

44. Heath, R. J. & Rock, C. O. Fatty acid biosynthesis as a target for novel antibacterials. *Curr. Opin. Investig. Drugs* **5**, 146–53 (2004).

45. Parra, M., Stahl, S. & Hellmann, H. Vitamin B6 and its role in cell metabolism and physiology. *Cells*. **7**, (2018).

46. Begley, T. P., Kinsland, C., Mehl, R. A., Osterman, A. & Dorrestein, P. The biosynthesis of nicotinamide adenine dinucleotides in bacteria. *Vitam. Horm*. **61**, 103-119 (2001).

47. Leonardi, R. & Roach, P. L. Thiamine biosynthesis in *Escherichia coli*: in vitro reconstitution of the thiazole synthase activity. *J. Biol. Chem.* **279**, 17054-17062 (2004).

48. Bourne, C. R. Utility of the biosynthetic folate pathway for targets in antimicrobial discovery. *Antibiotics*. **3**, 1-28 (2014).

49. Gawronski, J. D., Wong, S. M. S., Giannoukos, G., Ward, D. V. & Akerley, B. J. Tracking insertion mutants within libraries by deep sequencing and a genome-wide screen for Haemophilus genes required in the lung. *Proc. Natl. Acad. Sci. U. S. A.* **106**, 16422-16427 (2009).

50. Goodman, A. L. *et al.* Identifying genetic determinants needed to establish a human gut symbiont in its habitat. *Cell Host Microbe.* **6**, 279-289 (2009).

51. Langridge, G. C. *et al.* Simultaneous assay of every *Salmonella* Typhi gene using one million transposon mutants. *Genome Res.* **19**, 2308–2316 (2009).

52. Van Opijnen, T., Bodi, K. L. & Camilli, A. Tn-seq: high-throughput parallel sequencing for fitness and genetic interaction studies in microorganisms. *Nat. Methods* **6**, 767–772 (2009).

53. Hensel, M. *et al.* Simultaneous identification of bacterial virulence genes by negative selection. *Science.* **269**, 400-403 (1995).

54. Van Opijnen, T. & Camilli, A. Transposon insertion sequencing: A new tool for systems-level analysis of microorganisms. *Nat. Rev. Microbiol.* **11**, 435-442 (2013).

55. Shea, A. E. *et al. Escherichia coli* CFT073 fitness factors during urinary tract infection: Identification using an ordered transposon library. *Appl. Environ. Microbiol.* **86**, e00691-20 (2020).

56. Warr, A. R. *et al.* Transposon-insertion sequencing screens unveil requirements for EHEC growth and intestinal colonization. *PLOS Pathog.* **15**, e1007652 (2019).

57. Bacon, G. A., Burrows, T. W. & Yates, M. The effects of biochemical mutation on the virulence of Bacterium typhosum; the virulence of certain mutants. *Br. J. Exp. Pathol.* **31**, 714-724 (1950).

58. Bacon, G. A., Burrows, T. W. & Yates, M. The effects of biochemical mutation on the virulence of Bacterium typhosum; the loss of virulence of certain mutants. *Br. J. Exp. Pathol.* **32**, 85-96 (1951).

59. Jackson, M. *et al.* Persistence and protective efficacy of a *Mycobacterium tuberculosis* auxotroph vaccine. *Infect. Immun.* **67**, 2867-2873 (1999).

60. Stocker, B. A. D. Auxotrophic *Salmonella* Typhi as live vaccine. *Vaccine* **6**, 141-145 (1988).

61. Ellis, M. J. *et al.* A macrophage-based screen identifies antibacterial compounds selective for intracellular *Salmonella* Typhimurium. *Nat. Commun.* **10**, 197 (2019).

62. Chaudhuri, R. R. *et al.* Comprehensive identification of *Salmonella enterica* serovar Typhimurium genes required for infection of BALB/c mice. *PLoS Pathog.* **5**, e1000529 (2009).

63. Yang, H. J., Bogomolnaya, L., McClelland, M. & Andrews-Polymenis, H. De novo pyrimidine synthesis is necessary for intestinal colonization of *Salmonella* Typhimurium in chicks. *PLoS One* **12**, e0183751 (2017).

64. Kumari, S. & Tripathi, P. Nucleotide metabolism pathway: the achilles' heel for bacterial pathogens. *Curr. Sci.* **120**, 1458-1463 (2021).

65. Goncheva, M. I. *et al.* Stress-induced inactivation of the *Staphylococcus aureus* purine biosynthesis repressor leads to hypervirulence. *Nat. Commun.* **10**, 775 (2019).

66. Samant, S. *et al.* Nucleotide biosynthesis is critical for growth of bacteria in human blood. *PLoS Pathog.* **4**, e37 (2008).

67. Weber, B. S. *et al.* Genetic and chemical screening in human blood serum reveals unique antibacterial targets and compounds against *Klebsiella pneumoniae*. *Cell Rep.* **32**, (2020).

68. Poulsen, B. E. *et al.* Defining the core essential genome of *Pseudomonas aeruginosa*. *Proc. Natl. Acad. Sci. U. S. A.* **116,** 10072-10080 (2019)

69. Turner, K. H., Everett, J., Trivedi, U., Rumbaugh, K. P. & Whiteley, M. Requirements for *Pseudomonas aeruginosa* acute burn and chronic surgical wound infection. *PLoS Genet.* **10**, e1004518 (2014).

70. García, V. *et al.* Genome-wide analysis of fitness-factors in uropathogenic *Escherichia coli* during growth in laboratory media and during urinary tract infections. *Microb. Genom.* **7**, (2021).

71. Shaffer, C. L. *et al.* Purine biosynthesis metabolically constrains intracellular survival of uropathogenic *Escherichia coli*. *Infect. Immun.* **85**, e00471-16 (2017).

72. Hoiseth, S. K. & Stocker, B. A. D. Aromatic-dependent *Salmonella* Typhimurium are non-virulent and effective as live vaccines. *Nature.* **291**, 238-239 (1981).

73. O'Connell, C., Pattee, P. A. & Foster, T. J. Sequence and mapping of the *aroA* gene of *Staphylococcus aureus* 8325-4. *J. Gen. Microbiol.* **139**, 1449-1460 (1993).

74. Turner, K. H., Wessel, A. K., Palmer, G. C., Murray, J. L. & Whiteley, M. Essential genome of *Pseudomonas aeruginosa* in cystic fibrosis sputum. *Proc. Natl. Acad. Sci. U. S. A.* **112**, 4110–4115 (2015).

75. Silver, R. J. *et al.* Amino acid biosynthetic pathways are required for *Klebsiella pneumoniae* growth in immunocompromised lungs and are druggable targets during infection. *Antimicrob. Agents Chemother.* **63**, e02674-18 (2019).

76. Bachman, M. A. *et al.* Genome-wide identification of *Klebsiella pneumoniae* fitness genes during lung infection. *mBio* **6**, e00775-15 (2015).

77. Paczosa, M. K. *et al.* Transposon mutagenesis screen of *Klebsiella pneumoniae* identifies multiple genes important for resisting antimicrobial activities of neutrophils in mice. *Infect. Immun.* **88**, e00034-20 (2020).

78. Wang, N., Ozer, E. A., Mandel, M. J. & Hauser, A. R. Genome-wide identification of *Acinetobacter baumannii* genes necessary for persistence in the lung. *mBio* **5**, e01163-14 (2014).

79. Kaiser, J. C. & Heinrichs, D. E. Branching out: alterations in bacterial physiology and virulence due to branched-chain amino acid deprivation. *mBio* **9**, e01188-18 (2018).

80. Smith, D. A., Parish, T., Stoker, N. G. & Bancroft, G. J. Characterization of auxotrophic mutants of *Mycobacterium tuberculosis* and their potential as vaccine candidates. *Infect. Immun.* **69**, 1142–1150 (2001).

81. Leonhardt, R. M., Lee, S.-J., Kavathas, P. B. & Cresswell, P. Severe tryptophan starvation blocks onset of conventional persistence and reduces reactivation of *Chlamydia trachomatis*. *Infect. Immun.* **75**, 5105–5117 (2007).

82. Ganesan, S. & Roy, C. R. Host cell depletion of tryptophan by IFNγ-induced indoleamine 2,3-dioxygenase 1 (IDO1) inhibits lysosomal replication of *Coxiella burnetii*. *PLoS Pathog.* **15**, e1007955 (2019).

83. Peng, K. & Monack, D. M. Indoleamine 2,3-dioxygenase 1 is a lung-specific innate immune defense mechanism that inhibits growth of *Francisella tularensis* tryptophan auxotrophs. *Infect. Immun.* **78**, 2723–2733 (2010).

84. Niño-Castro, A. *et al.* The IDO1-induced kynurenines play a major role in the antimicrobial effect of human myeloid cells against *Listeria monocytogenes*. *Innate Immun.* **20**, 401–411 (2014).

85. Schmidt, S. V. & Schultze, J. L. New insights into IDO biology in bacterial and viral infections. *Front. Immunol.* **5**, (2014).

86. Costantini, C. *et al.* Tryptophan co-metabolism at the host-pathogen interface. *Front. Immunol.* **11**, (2020).

87. Gautam, U. S. *et al.* In vivo inhibition of tryptophan catabolism reorganizes the tuberculoma and augments immune-mediated control of *Mycobacterium tuberculosis*. *Proc. Natl. Acad. Sci. U. S. A.* **115**, 62–71 (2018).

88. Loughman, J. A. & Hunstad, D. A. Induction of indoleamine 2,3-dioxygenase by uropathogenic bacteria attenuates innate responses to epithelial infection. *J. Infect. Dis.* **205**, 1830–1839 (2012).

89. Dwivedy, A. *et al.* De novo histidine biosynthesis protects *Mycobacterium tuberculosis* from host IFN-γ mediated histidine starvation. *Commun. Biol.* **4**, 410 (2021).

90. Jelsbak, L. *et al.* Identification of metabolic pathways essential for fitness of *Salmonella* Typhimurium in vivo. *PLoS One* **9**, e101869 (2014).

91. Subashchandrabose, S., Smith, S. N., Spurbeck, R. R., Kole, M. M. & Mobley, H. L. T. Genome-wide detection of fitness genes in uropathogenic *Escherichia coli* during systemic infection. *PLoS Pathog.* **9**, e1003788 (2013).

92. Valentino, M. D. *et al.* Genes contributing to *Staphylococcus aureus* fitness in abscess- and infection-related ecologies. *mBio* **5**, e01729-14 (2014).

93. Martínez-Guitián, M. *et al.* Involvement of *hisF* in the persistence of *Acinetobacter baumannii* during a pneumonia infection. *Front. Cell. Infect. Microbiol.* **9**, (2019).

94. Gogoi, M., Datey, A., Wilson, K. T. & Chakravortty, D. Dual role of arginine metabolism in establishing pathogenesis. *Curr. Opin. Microbiol.* **29**, 43-48 (2016).

95. Chen, X., Qin, S., Zhao, X. & Zhou, S. L-Proline protects mice challenged by *Klebsiella pneumoniae* bacteremia. *J. Microbiol. Immunol. Infect.* **54**, 213-220 (2021).

96. Tiwari, S. *et al.* Arginine-deprivation-induced oxidative damage sterilizes *Mycobacterium tuberculosis*. *Proc. Natl. Acad. Sci. U. S. A.* **115**, 9779-9784 (2018).

97. Das, P. *et al.* Cationic amino acid transporters and *Salmonella* Typhimurium *argT* collectively regulate arginine availability towards intracellular *Salmonella* growth. *PLoS One* **5**, e15466 (2010).

98. Yee, R. *et al.* Identification of a novel gene *argJ* involved in arginine biosynthesis critical for persister formation in *Staphylococcus aureus. Discov. Med.* **29**, 65-77 (2020).

99. Nuxoll, A. S. *et al.* CcpA regulates arginine biosynthesis in *Staphylococcus aureus* through repression of proline catabolism. *PLoS Pathog.* **8**, e1003033 (2012).

100. Hibbing, M. E., Dodson, K. W., Kalas, V., Chen, S. L. & Hultgren, S. J. Adaptation of arginine synthesis among uropathogenic branches of the *Escherichia coli* phylogeny reveals adjustment to the urinary tract habitat. *mBio* **11**, e02318-20 (2020).

101. Senaratne, R. H. *et al.* 5′-Adenosinephosphosulphate reductase (CysH) protects *Mycobacterium tuberculosis* against free radicals during chronic infection phase in mice. *Mol. Microbiol.* **59**, 1744-1753 (2006).

102. Berney, M. *et al.* Essential roles of methionine and *S*-adenosylmethionine in the autarkic lifestyle of *Mycobacterium tuberculosis*. *Proc. Natl. Acad. Sci. U. S. A.* **112**, 10008-10013 (2015).

103. Hasenoehrl, E. J. *et al.* Derailing the aspartate pathway of *Mycobacterium tuberculosis* to eradicate persistent infection. *Nat. Commun.* **10**, 4215 (2019).

104. Borah, K. *et al.* Intracellular *Mycobacterium tuberculosis* exploits multiple host nitrogen sources during growth in human macrophages. *Cell Rep.* **29**, 3580-3591 (2019).

105. Awasthy, D. *et al.* Inactivation of the *ilvB1* gene in *Mycobacterium tuberculosis* leads to branched-chain amino acid auxotrophy and attenuation of virulence in mice. *Microbiology* **155**, 2978-2987 (2009).

106. Singh, V., Chandra, D., Srivastava, B. S. & Srivastava, R. Downregulation of Rv0189c, encoding a dihydroxyacid dehydratase, affects growth of *Mycobacterium tuberculosis* in vitro and in mice. *Microbiology* **157**, 38-46 (2011).

107. Hondalus, M. K. *et al.* Attenuation of and protection induced by a leucine auxotroph of *Mycobacterium tuberculosis*. *Infect. Immun.* **68**, 2888-2898 (2000).

108. Jelsbak, L., Mortensen, M. I. B., Kilstrup, M. & Olsen, J. E. The in vitro redundant enzymes PurN and PurT are both essential for systemic infection of mice in *Salmonella enterica* serovar Typhimurium. *Infect. Immun.* **84**, 2076-2085 (2016).

109. Karlinsey, J. E. *et al.* Genome-wide analysis of *Salmonella enterica* serovar Typhi in humanized mice reveals key virulence features. *Cell Host Microbe* **26**, 426-434 (2019).

110. Grant, A. J. *et al.* Genes required for the fitness of *Salmonella enterica* serovar Typhimurium during infection of immunodeficient *gp91 $^{-/-}$ phox* mice. *Infect. Immun.* **84**, 989–997 (2016).

111. Steeb, B. *et al.* Parallel exploitation of diverse host nutrients enhances *Salmonella* virulence. *PLoS Pathog.* **9**, e1003301 (2013).

112. Lee, E. J., Choi, J. & Groisman, E. A. Control of a *Salmonella* virulence operon by proline-charged tRNA Pro. *Proc. Natl. Acad. Sci. U. S. A.* **111**, 3140-3145 (2014).

113. Oogai, Y. *et al.* Lysine and threonine biosynthesis from aspartate contributes to *Staphylococcus aureus* growth in calf serum. *Appl. Environ. Microbiol.* **82**, 6150-6157 (2016).

114. Krismer, B. *et al.* Nutrient limitation governs *Staphylococcus aureus* metabolism and niche adaptation in the human nose. *PLoS Pathog.* **10**, e1003862 (2014).

115. Jochim, A. *et al.* Methionine limitation impairs pathogen expansion and biofilm formation capacity. *Appl. Environ. Microbiol.* **85**, e00177-19 (2019).

116. Park, S. W. *et al.* Evaluating the sensitivity of *Mycobacterium tuberculosis* to biotin deprivation using regulated gene expression. *PLoS Pathog.* **7**, e1002264 (2011).

117. Sambandamurthy, V. K. *et al.* A pantothenate auxotroph of *Mycobacterium tuberculosis* is highly attenuated and protects mice against tuberculosis. *Nat. Med.* **8**, 1171–1174 (2002).

118. Dick, T., Manjunatha, U., Kappes, B. & Gengenbacher, M. Vitamin B6 biosynthesis is essential for survival and virulence of *Mycobacterium tuberculosis*. *Mol. Microbiol.* **78**, 980-988 (2010).

119. Sassetti, C. M., Boyd, D. H., Rubin, E. J. & Collier, R. J. Comprehensive identification of conditionally essential genes in mycobacteria. *Proc. Natl. Acad. Sci. U. S. A.* **98**, 12712-12717 (2001).

120. Wishart, D. S. *et al.* HMDB 4.0: the human metabolome database for 2018. *Nucleic Acids Res.* **46**, 608–617 (2018).

121. Takach, E., O'Shea, T. & Liu, H. High-throughput quantitation of amino acids in rat and mouse biological matrices using stable isotope labeling and UPLC–MS/MS analysis. *J. Chromatogr. B* **964**, 180–190 (2014).

122. Scheller, K., Röckl, T., Scheller, C. & Schubert, J. Lower concentrations of B-vitamin subgroups in the serum and amniotic fluid correlate to cleft lip and palate appearance in the offspring of A/WySn mice. *J. Oral Maxillofac. Surg.* **71**, 1601–1607 (2013).

123. Park, S. W. *et al.* Target-based identification of whole-cell active inhibitors of biotin biosynthesis in *Mycobacterium tuberculosis*. *Chem. Biol.* **22**, 76–86 (2015).

124. Liu, F. *et al.* Structure-based optimization of pyridoxal 5′-phosphate-dependent transaminase enzyme (BioA) inhibitors that target biotin biosynthesis in *Mycobacterium tuberculosis*. *J. Med. Chem.* **60**, 5507–5520 (2017).

125. Farha, M. A., French, S. & Brown, E. D. Systems-level chemical biology to accelerate antibiotic drug discovery. *Acc. Chem. Res.* **54**, 1909-1920 (2021).

126. Farha, M. A. & Brown, E. D. Strategies for target identification of antimicrobial natural products. *Nat. Prod. Rep*. **33,** 668-680 (2016).

127. Bentley, R. Different roads to discovery: prontosil (hence sulfa drugs) and penicillin (hence β-lactams). *J. Ind. Microbiol. Biotechnol.* **36**, 775-786 (2009).

128. Pethe, K. *et al.* A chemical genetic screen in *Mycobacterium tuberculosis* identifies carbon-source-dependent growth inhibitors devoid of in vivo efficacy. *Nat. Commun.* **1**, 1–8 (2010).

129. Nurul Islam, M. *et al.* Mechanism of fluorinated anthranilate-induced growth inhibition in *Mycobacterium tuberculosis*. *ACS Infect. Dis.* **5**, 55–62 (2019).

130. Johnson, E. O. *et al.* Large-scale chemical–genetics yields new *M. tuberculosis* inhibitor classes. *Nature* **571**, 72–78 (2019).

131. Negatu, D. A. *et al.* Whole-cell screen of fragment library identifies gut microbiota metabolite indole propionic acid as antitubercular. *Antimicrob. Agents Chemother.* **62**, e01571-17 (2018).

132. Zlitni, S., Ferruccio, L. F. & Brown, E. D. Metabolic suppression identifies new antibacterial inhibitors under nutrient limitation. *Nat. Chem. Biol.* **9**, 796–804 (2013).

133. Carfrae, L. A. *et al.* Mimicking the human environment in mice reveals that inhibiting biotin biosynthesis is effective against antibiotic-resistant pathogens. *Nat. Microbiol.* **5**, 93–101 (2020).

134. Bockman, M. R. *et al.* Investigation of (S)-(-)-acidomycin: A selective antimycobacterial natural product that inhibits biotin synthase. *ACS Infect. Dis.* **5**, 598–617 (2019).

135. Okami, Y. *et al.* Studies on a new amino acid antibiotic, amiclenomycin. *J. Antibiot.* **27**, 656–664 (1974).

136. Gehrke, S. S. *et al.* Exploiting the sensitivity of nutrient transporter deletion strains in discovery of natural product antimetabolites. *ACS Infect. Dis.* **3**, 955–965 (2017).

137. Wencewicz, T. A. New antibiotics from nature's chemical inventory. *Bioorg. Med Chem.* **24**, 6227-6252 (2016).

138. Minato, Y. *et al.* Mutual potentiation drives synergy between trimethoprim and sulfamethoxazole. *Nat. Commun.* **9**, 1003 (2018).

139. Tiwari, D. *et al.* Targeting protein biotinylation enhances tuberculosis chemotherapy. *Sci. Transl. Med.* **10**, (2018).

140. El Zahed, S. S. & Brown, E. D. Chemical-chemical combinations map uncharted interactions in *Escherichia coli* under nutrient stress. *iScience* **2**, 168–181 (2018).

141. Bhosle, A. *et al.* A strategic target rescues trimethoprim sensitivity in *Escherichia coli*. *iScience* **23**, (2020).

142. Dunphy, L. J., Yen, P. & Papin, J. A. Integrated experimental and computational analyses reveal differential metabolic functionality in antibiotic-resistant *Pseudomonas aeruginosa*. *Cell Syst.* **8**, 3–14 (2019).

143. Balaban, N. Q. *et al.* Antibiotic tolerance facilitates the evolution of resistance. *Science.* **355**, 826–830 (2017).

144. Allison, K. R., Brynildsen, M. P. & Collins, J. J. Metabolite-enabled eradication of bacterial persisters by aminoglycosides. *Nature* **473**, 216-220 (2011).

145. Peng, B. *et al.* Exogenous alanine and/or glucose plus kanamycin kills antibiotic-resistant bacteria. *Cell Metab.* **21**, 249-262 (2015).

146. Liu, Y., Li, R., Xiao, X. & Wang, Z. Bacterial metabolism-inspired molecules to modulate antibiotic efficacy. *J. Antimicrob. Chemother.* **11**, 3409-3417 (2019)

147. Liu, Y., Yang, K., Zhang, H., Jia, Y. & Wang, Z. Combating antibiotic tolerance through activating bacterial metabolism. *Frontiers in Microbiology* **11**, (2020).

148. Yee, R., Cui, P., Shi, W., Feng, J. & Zhang, Y. Genetic screen reveals the role of purine metabolism in *Staphylococcus aureus* persistence to rifampicin. *Antibiotics* **4**, 627-642 (2015).

149. Lopatkin, A. J. & Yang, J. H. Digital insights into nucleotide metabolism and antibiotic treatment failure. *Front. Digit. Heal.* **3**, (2021).

150. Rasouly, A. *et al.* Analysing the fitness cost of antibiotic resistance to identify targets for combination antimicrobials. *Nat. Microbiol.* **6**, 1410-1423 (2021).

151. Li, H. *et al.* Comprehensive proteomic and metabolomic profiling of *mcr-1*-mediated colistin resistance in *Escherichia coli*. *Int. J. Antimicrob. Agents* **53**, 795-804 (2019).

152. Erickson, K. E., Otoupal, P. B. & Chatterjee, A. Transcriptome-level signatures in gene expression and gene expression variability during bacterial adaptive evolution. *mSphere* **2**, e0009-17 (2017).

Chapter II – Mimicking the human environment in mice reveals that inhibiting biotin biosynthesis is effective against antibiotic-resistant pathogens

Preface

The work presented in this chapter was previously published in:

Carfrae, L.A., MacNair, C.R., Brown, C.M., Tsai C.N., Weber B.S., Zlitni S., Rao V.N., Chun J., Junop M.S., Coombes B.K., and Brown E.D. Mimicking the human environment in mice reveals that inhibiting biotin biosynthesis is effective against antibiotic-resistant pathogens. *Nat Microbiol* **5,** 93–101 (2020). https://doi.org/10.1038/s41564-019-0595-2

LAC wrote the manuscript with editing from EDB. LAC designed and conducted main experiments with input from all authors except for the crystallization experiments and analysis conducted by CMB, SZ, JC, and MSJ.

Abstract

To revitalize the antibiotic pipeline, it is critical to identify and validate new antimicrobial targets[1]. In *Mycobacteria tuberculosis* and *Francisella tularensis*, biotin biosynthesis is a key fitness determinant during infection[2-5], making it a high-priority target. However, biotin biosynthesis has been overlooked for priority pathogens such as *Acinetobacter baumannii*, *Klebsiella pneumoniae* and *Pseudomonas aeruginosa*. This can be attributed to the lack of attenuation observed for biotin biosynthesis genes during transposon mutagenesis studies in mouse infection models[6-9]. Previous studies did not consider the 40-fold higher concentration of biotin in mouse plasma compared to human plasma. Here, we leveraged the unique affinity of streptavidin to develop a mouse infection model with human levels of biotin. Our model suggests that biotin biosynthesis is essential during infection with *A. baumannii*, *K. pneumoniae* and *P. aeruginosa*. Encouragingly, we establish the capacity of our model to uncover in vivo activity for the biotin biosynthesis inhibitor MAC13772. Our model addresses the disconnect in biotin levels between humans and mice, and explains the failure of potent biotin biosynthesis inhibitors in standard mouse infection models.

Main

Biotin biosynthesis genes are upregulated during enterotoxigenic *Escherichia coli* gastrointestinal infections[10] and *Salmonella enterica* sv. Typhi bloodstream infections in humans[11]. To investigate the discrepancy between human infection expression data[10.11] and mouse transposon mutagenesis infection studies[6-9,12-14], we first quantified the minimum concentration of biotin required to restore the growth of biotin auxotrophic mutants. De novo biosynthesis is performed by four conserved enzymes, BioF, BioA, BioD, and BioB, which are responsible for the conversion of pimeloyl to biotin[15-16] (Figure 1a). We selected the antepenultimate step in biotin biosynthesis (BioA) for target validation due to the diversity of available inhibitors[17-21] (Figure 1a and Supplemental Table 1).

Auxotrophic strains of *A. baumannii, E. coli, K. pneumoniae, P. aeruginosa, S.* Typhimurium, and uropathogenic *E. coli* (UPEC) were grown in M9 minimal media supplemented with varying biotin concentrations. The pathogens can be separated into two distinct groups based on their biotin requirement (Figure 1b). *E. coli* Δ*bioA*, *K. pneumoniae* Δ*bioA*, *S*. Typhimurium Δ*bioA* and UPEC Δ*bioA* require low biotin concentrations (0.2-0.4 ng/mL) to restore growth to 50% of the maximum. By contrast, biotin concentrations of 4.7 ng/mL and 5.5 ng/mL were necessary for *A. baumannii* and *P. aeruginosa* biotin auxotrophs, respectively. Biotin requirements were similar (less than a twofold

difference) for *A. baumannii* deficient in BioC, D, or F or *E. coli* Δ*bioB, C, D,* or *F,* irrespective of which biotin biosynthesis gene is inactivated, suggesting that these findings can be broadly applied to the entire pathway (Extended Data Figure 1a, b).

The essentiality of biotin biosynthesis during *M. tuberculosis* and *F. tularensis* infection has been attributed to the absence of a high-affinity biotin transporter (BioP or BioY) in their genomes[22]. We hypothesized the presence of a biotin transporter accounts for the observed pathogen-specific variation in biotin requirements and could be used to prioritize pathogens for evaluation of biotin essentiality. Here, we used the BioA inhibitor MAC13772 at four times its minimal inhibitory concentration (MIC) as a chemical probe to determine the exogenous biotin requirement of *E. coli* with and without a biotin transporter. Notably, the biotin concentration required to rescue the growth of *E. coli* Δ*bioA* phenocopied the concentration required to abrogate MAC13772 activity with wild-type *E. coli*, validating its use as a chemical probe in this assay. Indeed, removal of the *E. coli* biotin transporter BioP increased the biotin requirement approximately 200-fold in the presence of MAC13772 to 38.25 ng/mL, a concentration well above human biotin levels of 0.1-1.2 ng/mL[23-27] (Figure 1c). Accordingly, we predicted that pathogens lacking biotin transporters would require biotin biosynthesis in physiological conditions.

Pathogenic bacterial species containing BioA but lacking orthologues to the known biotin transporters, BioY and BioP, were identified through OrthologueDB[28] using *Staphylococcus aureus* BioY and *E. coli* BioP as reference sequences (Extended Data Figure 1c and Supplemental Table 2). BioP is found mainly in Gammaproteobacteria and Epsilonproteobacteria species. By contrast, BioY is found across diverse bacterial phyla. We predicted *Acinetobacter, Burkholderia, Coxiella, Legionella,* and *Neisseria* species lack a high-affinity biotin transporter, they would require high levels of exogenous biotin compared with species with a transporter. Fifteen pathogens predicted to have a high-affinity transporter required lower biotin concentrations for growth than those without a transporter (Figure 1d and Supplemental Table 3). The exception to this is *P. aeruginosa,* which was found to have an orthologue to *E. coli* BioP but its biotin requirement was 34 times that of *E. coli.* These results suggest that the presence or absence of a biotin transporter is a preliminary indicator of a pathogen's biotin requirement.

We found biotin levels in human plasma (0.25 ± 0.06 ng/mL) were 40 times lower than in mouse plasma (9.82 ± 0.79 ng/mL; Extended Data Figure 2a). Investigating this discrepancy, we measured bacterial growth in 50% pooled human plasma. After 24 h of growth in human plasma, BioA-deficient *A. baumannii, K. pneumoniae,* and *P. aeruginosa* had significantly (unpaired *t*-test, $P<0.01$) fewer viable cells compared with wild-type strains (Figure 2a). The

addition of exogenous biotin (10 μg/mL) abrogated the attenuation in growth (Extended Data Figure 2c). Notably, there was no significant difference between the growth of a biotin auxotroph and wild-type strain in 50% mouse plasma, irrespective of bacterial species (Figure 2b). This aligns with the biotin concentration in mouse plasma being in excess of the biotin requirements of all auxotrophs assayed. The differential growth of *A. baumannii, K. pneumoniae,* and *P. aeruginosa* in human and mouse plasma indicates the importance of determining the essentiality of biotin biosynthesis in an environment mimicking human conditions.

The growth of *A. baumannii, K. pneumoniae, P. aeruginosa,* and *S.* Typhimurium in mouse plasma suggests that biotin biosynthesis is dispensable during murine infection. To confirm this, we evaluated the essentiality of biotin biosynthesis using standard murine co-infection models for *A. baumannii, K. pneumoniae, P. aeruginosa, S. aureus,* and *S.* Typhimurium at several infection sites.

Regardless of the pathogen, wild-type and auxotrophic strains had equivalent fitness in the blood, spleen, kidney, liver, and lungs following systemic infection (Figure 2c,g and Extended Data Figure 3 a-e). Similarly, in a *K. pneumoniae* lung infection model, Δ*bioA* conferred no fitness defect when compared to wild-type (Figure 2d and Extended Data Figure 3f). Following infection in the thigh, an identical ratio of wild-type and mutant strains were

enumerated for *A. baumannii, K. pneumoniae, P. aeruginosa,* and *S. aureus* (Figure 3e and Extended Data Figure 3g). Together, these results support previous studies[6-9,12-14] indicating sufficient exogenous biotin is present throughout the murine host for biotin biosynthesis to be dispensable during infection.

The biotin concentration in the plasma from three conventional strains of mice (BALB/c, CD-1, C57BL/6) were measured at 11.8 ± 2.9 ng/mL, 11.9 ± 1.8 ng/mL, and 10.1 ± 2.4 ng/mL, respectively (Extended Data Figure 2b). The biotin concentration in these strains is predicted to be sufficient to rescue all biotin auxotrophs tested in vitro and is far in excess of the normal biotin levels in humans. Therefore, we sought to develop a murine model that mimicked human biotin levels using the high-affinity interaction of streptavidin with biotin.

As human biotin concentrations can vary up to 100% daily[24], we expanded the range of acceptable concentrations in our model to 0.05-2.4 ng/mL. Streptavidin administered intraperitoneally at 2 mg/kg resulted in a suitable range of biotin availability (Figure 2f and Extended Data Figure 4a,b). Initial biotin levels decreased from 11.9 ± 1.8 ng/ml to 0.07 ± 0.02 ng/mL 1 h after administration and increased to 2.16 ± 0.68 ng/mL over 12 h (Figure 2f).

Using the developed model, we assessed the requirement for biotin biosynthesis in *A. baumannii, K. pneumoniae, P. aeruginosa,* and *S. aureus*. We

infected mice 1 h after streptavidin treatment to generate a systemic infection in an environment mimicking human biotin levels. The ability of wild-type strains to establish an acute systemic infection was unimpeded by streptavidin pretreatment (Extended Data Figure 4c). Following streptavidin pretreatment, BioA-deficient *A. baumannii, K. pneumoniae* and *P. aeruginosa* had 99.8%, 97.5%, and 90% lower bacterial burdens, respectively, in the spleen compared with standard infection models (Figure 2g and Extended Data Figure 5 and 6). By contrast, BioA was dispensable during systemic *S. aureus* infection, indicating exogenous biotin levels were adequate for growth, probably due to the presence of the BioY transporter.

To distinguish whether the attenuation of the BioA-deficient strains was produced by an inability to colonize or replicate during infection, we measured the competitive index 1 h after infection. We observed an equal ratio of wild-type to BioA-deficient *A. baumannii, K. pneumoniae,* and *P. aeruginosa* 1 h after infection in mice pretreated with streptavidin (Extended Data Figure 7). These results indicate biotin biosynthesis is critical for bacterial proliferation during infection, but not colonization. Having demonstrated that biotin biosynthesis is required for *A. baumannii, K. pneumoniae,* and *P. aeruginosa* infection in streptavidin-treated mice, we sought to characterize the consequences of chemically inactivating BioA. Previous work identified MAC13772 as an inhibitor of *E. coli* BioA[29] with a reported MIC of 8 μg/mL. We characterized the spectrum

of MAC13772 activity in biotin-depleted medium, finding MAC13772 was active (MIC ≤ 64 μg/mL) against 11 of the 30 bacterial species tested, including *Acinetobacter* spp.*, N. gonorrhoeae,* and *Mycobacterium* spp. and had intermediate activity (MIC ≤ 128-512 μg/mL) against 10 of 30 species (Figure 3c and Supplemental Table 4). MAC13772 was inactive against species that had BioA with low levels of similarity (less than 50%) to *E. coli* BioA, suggesting that BioA structure is the dominant driver of potency against bacterial cells (Supplemental Table 5).

To further investigate the species specificity of MAC13772, we evaluated the interaction of the compound with *E. coli* BioA. Previous studies suggested MAC13772 covalently binds to pyridoxal-5-phosphate (PLP), forming a tightly bound adduct of inhibitor and cofactor in the active site[29]. This was confirmed by the crystal structure of *E. coli* BioA in complex with MAC13772 solved to 2.4 Å (Protein Data Bank ID 6ED7), which further uncovered several key interactions between residues in the active site of BioA with the inhibitor-PLP covalent adduct (Figure 3a and Supplemental Table 6). Hydrophobic interactions with Trp52, Tyr144, Phe393 and hydrogen bonding with Lys274 and Tyr398 are predicted to occur with MAC13772 (Figure 3b).

Notably, Phe393, Tyr144, Trp52, Tyr398, and Lys274 are conserved in all species sensitive (MIC ≤ 512 μg/mL) to MAC13772. At least one amino acid is substituted in intrinsically resistant species (Figure 3c and Supplemental Table

5). We predicted the activity of MAC13772 against a list of 100 pathogens using the conservation of Phe393, Tyr144, Trp52, Tyr398, and Lys274 (Supplemental Table 7). All five residues are present in 44 of the 77 (57%) species with BioA (Supplemental Table 7). The susceptibility predictions demonstrate the broad applicability of MAC13772 as a biotin biosynthesis inhibitor for Gram-negative bacteria and *Mycobacterium* spp. Encouragingly, there is no predicted biotin transporter in 15 of the 44 species, including *Acinetobacter* spp., *Mycobacteria* spp., and *Neisseria* spp., meaning that these pathogens are probably susceptible to biotin starvation by MAC13772 (Supplemental Table 7).

The necessity of Phe393, Tyr144, Trp52, Tyr398, and Lys274 for MAC13772 activity could provide a means for bacteria to develop resistance. Mutants to MAC13772 (at 8×MIC) were generated in *A. baumannii* and *E. coli* with a frequency of resistance of 2×10^{-9} and 4×10^{-9}, respectively. However, MAC13772-resistant clones did not carry mutations in *bioA,* suggesting that there is a fitness cost with modification to Phe393, Tyr144, Trp52, Tyr398, and Lys274. To investigate further, we made four BioA constructs, replacing Trp52, Lys274, Phe393, and Tyr398 with alanine. The removal of functionality at Trp52 and Lys274 completely abolished BioA activity (Figure 3d). F393A and Y398A mutations had a modest effect on MAC13772 binding affinity (Figure 3e). However, F393A and Y398A mutations display a reduced affinity and a reduced

turnover rate for (*S*)-keto-amino-pelargonic acid (KAPA) and *S*-adenosyl-L-methionine (SAM) (Figure 3d and Extended Data Figure 8a, b).

An alternative method to develop resistance to a biotin biosynthesis inhibitor could be by reducing the minimal concentration of biotin required for growth. To test if a pathogen could adapt to require lower levels of biotin, BioA-deficient *A. baumannii* was passaged daily in the minimal biotin concentration able to support growth for 14 d–no change in biotin requirement was observed (Extended Data Figure 8c and Supplemental Table 8).

The use of antibiotic combinations has shown promise in *M. tuberculosis* with biotin biosynthesis inhibition[30]. We evaluated the potential of MAC13772 in combination with diverse antibiotics against *A. baumannii.* In the presence of MAC13772 (0.25×MIC) the clinical classification of resistant to susceptible was not changed for any combination tested, in agreement with previously described work in *E. coli*[31] (Supplemental Table 9). Overall, the spectrum of activity and relatively low rate of resistance to MAC13772 is promising for the future development of this compound.

We investigated the in vivo activity of MAC13772 against an *A. baumannii* systemic infection. Mice typically succumb to acute systemic *A. baumannii* infection within 12 h with high bacterial burdens in the blood, spleen, liver, kidney, and lungs. In a standard systemic murine infection model, MAC13772 (15 mg/kg)

had no significant effect on bacterial load (Figure 4a and Extended Data Figure 9a). However, by using our model to mimic human biotin levels, the administration of MAC13772 (15 mg/kg) reduced the bacterial load by 97.5% in the blood compared with the vehicle (Figure 4a and Extended Data Figure 9b). We propose that MAC13772 is not completely inhibiting biotin biosynthesis throughout the infection, as BioA-deficient *A. baumannii* showed a 99.9% reduction in bacterial load compared with wild-type in our model (Figure 4b). When treated with MAC13772, 14% (1 of 7 mice) of mice survived an *A. baumannii* systemic infection following streptavidin pretreatment, with a prolonged median survival of 12 h compared with the vehicle (Figure 4c). By contrast, 86% (6 of 7 mice) of mice survived after 7 d of infection with BioA-deficient *A. baumannii* in mice pretreated with streptavidin. We hypothesized that the pharmacokinetic properties of MAC13772 may account for the reduced efficacy compared with BioA-deficient *A. baumannii*.

Pharmacokinetic testing of MAC13772 revealed that it had poor bioavailability. Following intravenous administration of MAC13772 (5 mg/kg (body weight)) in rats, blood levels peaked after 5 minutes at 3,220 ± 690 ng/mL. However, MAC13772 cleared rapidly (4680 mL/hr/kg), resulting in a brief half-life of 0.3 h (Extended Data Figure 9c). To circumvent the pharmacokinetic limitations of MAC13772, we investigated its activity in a standard *A. baumannii* skin infection model. Animals were treated with MAC13772 (3%) over a 36 h

period, resulting in a 83.3% reduction in colony-forming units (CFU) (Figure 4d). To improve this efficacy we exploited streptavidin, predicting it would remove any exogenous biotin available at the wound, increasing the potency of MAC13772. During skin infection, the bacterial load was unchanged with streptavidin (0.5%) treatment. However, the combination of streptavidin (0.5%) and MAC13772 (3%) proved efficacious, resulting in a 99.9% reduction (P<0.01) in CFU when compared with the vehicle control 36 h after infection (Figure 4d).

Here we reveal the potential for targeting biotin biosynthesis in priority pathogens. We propose the 40-times higher biotin levels found in mouse plasma accounts for the discordance between the requirement for biotin biosynthesis during human and mouse infections. Despite the widespread application of murine models in biomedical research, differences between human and mouse infections have been largely overlooked, contributing to the preclinical failure of drug leads[32]. While progress has been made towards humanizing the mouse immune system[32], considerations for the nutritional environment have been overlooked. This study highlights the importance of predictive in vitro and in vivo conditions in both target identification and testing antimicrobial leads.

We developed a mouse model mimicking human biotin conditions that can be broadly leveraged in testing both genetic and chemical perturbation of biotin biosynthesis. Applying this model, we show biotin biosynthesis is essential during systemic infection for *A. baumannii, K. pneumoniae,* and *P. aeruginosa*. We

demonstrated the efficacy of MAC13772 against *A. baumannii* in a systemic infection mimicking human biotin levels, showing that BioA is susceptible to inhibition by a drug-like compound in vivo.

Whereas MAC13772 is a capable probe of biotin biosynthesis, it is restricted in its efficacy due to pharmacokinetic limitations. Nevertheless, we demonstrate complete inhibition of BioA has the potential to cure a systemic *A. baumannii* infection. The success of MAC13772 justifies revisiting previously dismissed biotin biosynthesis inhibitors in our model. We highlight nine biotin biosynthesis inhibitors with reported in vitro activity, of which five have whole cell activity against at least one bacterial species[17-21,29,33-38] (Supplemental Table 1). Additionally, biotin biosynthesis has been prioritized as a frontline target in *M. tuberculosis* following its classification as in vivo essential[2,5] with synergistic activity with rifampicin and ethambutol[30]. Accordingly, many groups have initiated screening platforms to identify inhibitors of both biotin biosynthesis and biotin protein ligase[19,20,29,39]. Expanding testing of these molecules to Gram-negative pathogens presents the prospect for a broad-spectrum application of biotin-biosynthesis targeting antibiotics. The ability to treat bacterial infections in the post-antibiotic era will depend on the identification and exploitation of conditionally essential targets such as biotin biosynthesis in the development of treatments.

Methods

Reagents

MAC13772 was purchased from MayBridge (DSHS 00862) and characterized by ^{1}H NMR, ^{13}C NMR, and HR-MS. KAPA was supplied from Santa Cruz Biotechnology, diamino-pelargonic acid (DAPA) from Caymen Chemicals, and streptavidin was obtained from IBA Lifesciences. All other chemicals and reagents were purchased from Sigma.

Bacterial Strains

A complete list of bacterial strains and plasmids used in the study can be found in Supplemental Table 10. To study the essentiality of BioA, we generated biotin auxotrophic strains *E. coli* Δ*bioA, K. pneumoniae* Δ*bioA, S.* Typhimurium Δ*bioA*, and UPEC Δ*bioA* by homologous recombination using a λ-Red system. Preparation of competent cells, electroporation, and mutant construction were performed as previously described[40-42]. In brief, *E. coli, S.* Typhimurium, and UPEC were first transformed with the plasmid pSim6 (Supplemental Table 10), containing *exo*, *beta*, and *gam* genes from phage λ[40]. Bacteria were grown at 30℃ to mid-log phase (optical density at 600 nm (OD_{600}) 0.6-0.8) and expression of recombination genes was induced by a 20 min heat shock at 42℃. The cells were made electrocompetent and transformed with PCR products of 50-bp

regions of homology to *bioA* flanking a kanamycin- or chloramphenicol-resistance cassette. Cells were then plated on the appropriate selection medium and single colonies were picked for verification. Recombinants were confirmed using primers homologous to regions upstream and downstream from *bioA* and primers inside the resistance cassette.

Similarly, *K. pneumoniae* Δ*bioA* was created using the pACBSR-Hyg plasmid containing the same λ-Red system used to construct knockouts in *E. coli* under the control of an arabinose-inducible promoter[42] (Supplemental Table 10). Bacteria were grown at 30℃ to mid-log phase (OD_{600} 0.6-0.8) in the presence of 0.1 M arabinose. The cells were made electrocompetent and transformed with PCR products of 100-bp regions of homology to *bioA* flanking a kanamycin resistance cassette. Cells were then plated on the appropriate selection and single colonies picked for verification.

Biotin auxotrophs had no growth defect in LB media (Supplemental Figure 1), however, were unable to grow in M9 minimal media or LB media supplemented with the biotin-binding protein avidin (0.1 U/mL). Transposon mutants *A. baumannii bioA*169::T26[43], *P. aeruginosa bioA*G04::ISphoA/hah[44], and *S. aureus bioA*::Tn (NE1090)[45] were obtained from ordered libraries of transposon insertion mutants. Effective inactivation of *bioA* was confirmed in all auxotrophic strains used in the study by resupplementation of intermediates in

the biotin biosynthesis pathway (10 µg/mL of KAPA, DAPA, or biotin; Supplemental Figure 2 and 3).

Overnight cultures of bacteria were inoculated with a single colony and routinely cultured in LB medium (10 g/L NaCl, 10 g/L Tryptone, 5 g/L yeast extract) supplemented with antibiotics as appropriate (kanamycin, 50 µg/mL; chloramphenicol, 20 µg/mL; ampicillin, 100 µg/mL; tetracycline, 10 µg/mL; erythromycin, 10 µg/mL; hygromycin B, 100 µg/mL). M9 with 0.4% glucose was used as minimal medium. Concentrations for amino acid supplementation are in Supplemental Table 11. *M. tuberculosis* mc2 6020 (BSL-2) was cultured in modified Middlebrook 7H9 media containing all components except for biotin.

In vitro biotin requirement of biotin auxotrophs

BioA-deficient *A. baumannii, E. coli, K. pneumoniae, P. aeruginosa, S.* Typhimurium, and UPEC strains were grown overnight in LB medium. The bacterial culture was prepared by washing 1 mL of overnight culture in PBS (×3), resuspending to OD 0.1, then diluting 1:200 into M9 minimal media supplemented with amino acids. Biotin was added to each well in twofold serial dilutions. The plates were incubated at 37°C for 18 h before the absorbance at OD_{600} was measured. A four-parameter logistic curve was used to determine the biotin concentration required to restore 50% growth.

Abrogation of MAC13772 activity with biotin

The bacterial culture was prepared by washing 1 mL of overnight culture in PBS (in triplicate), resuspending to OD 0.1, then diluting 1:200 into M9 minimal media supplemented with amino acids. MAC13772 was added to the media at four times MIC. Biotin was added to each well in twofold serial dilutions. The plates were incubated at 37°C for 18 h before the absorbance at OD_{600} was measured. A four-parameter logistic curve was fit for each strain to determine the biotin concentration required to restore 50% growth.

Plasma Growth Assays

BioA-deficient *A. baumannii, K. pneumoniae, P. aeruginosa,* and *S.* Typhimurium, strains and the corresponding wild-type strains were grown overnight in LB medium. The cells were resuspended into fresh M9 minimal media and cultures incubated at 37 ℃ for 2-3 h. The cells were washed with PBS and BioA-deficient or wild-type strains were separately inoculated into 50% plasma at the following cell densities: *A. baumannii* and *K. pneumoniae*: ~5×10^5 CFU/ml; *P. aeruginosa,* and *S.* Typhimurium: ~10^7 CFU/ml. The inability of *S. aureus* to replicate in 50% human or mouse plasma precluded the species from evaluation. Cultures were incubated at 37 ℃. At 0 and 24 h, cultures were serially diluted and plated on LB agar plates to determine the viable cell counts.

Fold change was calculated by dividing the viable cell count at 24 h by the viable cell count at 0 h. Biotin-rescue experiments were conducted identically,

except plasma was supplemented with biotin (10 µg/mL). Pooled normal human male AB plasma and CD-1 (collected in Li heparin tubes) mouse plasma was purchased from Innovative Research. Pooled normal human male AB plasma or CD-1 mouse plasma were diluted with M9 salts and 25 mM of sodium bicarbonate.

Animal studies

All animal studies were conducted according to guidelines set by the Canadian Council on Animal Care using protocols approved by the Animal Review Ethics Board at McMaster University under Animal Use Protocol #17-03-10. All animal studies were performed with 6-10-week-old female mice from Charles River (for C57BL/6 and BALB/c) or Envigo (for CD-1). Female mice were used in accordance with previously established models, as well as ease of housing, and randomization. Before infection, mice were relocated at random from a housing cage to treatment or control cages. No animals were excluded from analyses and blinding was considered unnecessary. No assumptions regarding sample or effect size were made. Sample sizes were selected based on results from pilot experiments. All animal experiments were performed a minimum of two independent times and with a minimum of two mice included per group.

Mouse systemic infection model

Systemic infection was established with *A. baumannii, K. pneumoniae, P. aeruginosa,* or *S. aureus* in an immunocompetent model. For competitive infections, mice were inoculated with a 1:1 mixture of BioA-deficient and wild-type bacteria. CD-1 (*K. pneumoniae* and *P. aeruginosa*) or C57BL/6 (*A. baumannii* and *S. aureus*) mice were infected intraperitoneally with the following: *A. baumannii:* ~1×10^6 CFU; *K. pneumoniae*: ~5×10^4 CFU; *P. aeruginosa*: ~1×10^7 CFU; *S. aureus:* ~1×10^8 CFU suspended in 5% porcine mucin PBS solution. The experimental endpoint was defined as 10 h after infection. The blood (collected in Li heparin tubes by facial bleed), spleen, kidney, liver, and lungs were collected, homogenized, diluted, and plated on to solid LB and LB supplemented with a selective antibiotic to enumerate the bacterial load.

Mouse systemic *S.* Typhimurium infection model

A competitive infection was established with wild-type and *S.* Typhimurium *ΔbioA* in an immunocompetent systemic infection model. C57BL/6 mice were infected intraperitoneally with ~5×10^4 CFU of bacteria in PBS. Experimental endpoint was defined as 72 h after infection. The blood (collected in Li heparin tubes by facial bleed), spleen, kidney, liver, and lungs were collected, homogenized, and plated on to solid LB and LB supplemented with chloramphenicol (20 μg/mL) to enumerate the bacterial load. *S.* Typhimurium was not evaluated in a systemic murine model with human biotin levels due to the

challenges of controlling biotin levels over the duration of systemic infection (72 h).

Mouse lung infection model

A lung infection was established in neutropenic CD-1 mice by intranasal co-infection of wild-type and *K. pneumoniae* Δ*bioA* in a 1:1 ratio. CD-1 mice were pretreated with 150 mg/kg (Day -4) and 100 mg/kg (Day -1) of cyclophosphamide to render mice neutropenic. The lung infection was established by intranasal administration of 30 µL of inoculum to each nostril with a total of ~2×10^7 CFU of *K. pneumoniae.* Mice were euthanized at the experimental endpoint of 36 h and the bacterial load in the lung was determined by plating on to solid LB and LB media supplemented with kanamycin (50 µg/mL) to enumerate the bacterial load.

Mouse thigh infection model

A neutropenic mouse thigh infection was established with BioA-deficient and wild-type *A. baumannii, K. pneumoniae, P. aeruginosa,* and *S. aureus*. CD-1 mice were rendered neutropenic using cyclophosphamide, dosed at 150 and 100 mg/kg delivered on days -4 and -1 prior to infection. The wild-type and BioA-deficient bacteria were suspended in sterile saline and diluted to a concentration of ~5×10^5 CFU (*K. pneumoniae* and *S. aureus*) or ~5×10^6 CFU (*A. baumannii* and *P. aeruginosa*) per infection site and injected into the right and left thighs of mice. Mice were euthanized 12 h (*A. baumannii* and *P. aeruginosa*) or 16 h (*K.*

pneumoniae and *S. aureus*) after infection, thigh tissue was aseptically collected, weighed, homogenized, serially diluted in PBS and plated onto solid LB and LB supplemented with a selective antibiotic. Plates were incubated overnight at 37°C and colonies were enumerated to determine bacterial load.

Competitive index calculation

CIs were calculated as follows, where the BioA-deficient strain is CFU_m and that of the wild-type strain is CFU_w.

$CI = (\frac{CFUm}{CFUw}, recovered)/(\frac{CFUm}{CFUw}, present)$.

Quantification of plasma biotin

Plasma biotin was determined using a commercially available biotin ELISA kit (K8140; Immundiagnostik) according to the manufacturer's procedure. In brief, each plasma sample (50 µL) was added to individual wells. Plasma samples and standard biotin solutions were incubated with 50 µL streptavidin-enzyme conjugate solution for 30 min at room temperature. The enzyme substrate TMB was added and the samples incubated for 15 minutes in the dark. After stopping the reaction by adding 100 µL 0.12 M hydrochloric acid to each well, absorbance at 450nm and 620nm was measured. Absorbance was calculated by subtracting the reference absorbance at 620 nm from that at 450 nm. The range of the assay is 0.048-1.10ng/mL, when biotin was higher than 1.10 ng/mL, the sample was diluted to a suitable concentration with a dilution solution included in the kit. The

average of three replicates was used as the biotin concentration in the plasma of each mouse.

Expression of recombinant BioA

E. coli BioA was isolated using the AG1-pCA24N-*bioA* (JW0757) from the ASKA library for crystallization. BioA, BioA(W52A), BioA(K274A), BioA(F393A), and BioA(Y398A) were expressed from the pCA24N-*bioA* plasmid in *E. coli* Δ*bioA*. The mutations were introduced into the plasmid with the QuikChange II Site-Directed Mutagenesis kit (Agilent Technologies). The entire insert was sequenced to ensure the absence of other mutations. Overexpression of BioA was induced with 0.1 mM isopropyl-β-D-thiogalactoside when the culture reached an OD_{600} of 0.6. Cells were harvested by centrifugation 3 h after induction. The cell pellet was resuspended in 0.85% saline solution and stored at -20°C.

The cell pellet was resuspended in 25 mL of lysis buffer (50 mM HEPES pH=8, 500 mM NaCl, 100 μM PLP, 50 mM imidazole, 0.5 mg DNase, 0.5 mg RNase, protease inhibitor cocktail). Cells were lysed by passage through a cell disrupter with continuous flow at 30,000 psi and clarified by centrifugation at 40,000*g* for 1 h.

Purification of recombinant BioA

Recombinant BioA for protein crystallization was purified by nickel chromatography using a 1 mL HiTrap affinity column. The column was washed

with buffer A (50 mM HEPES pH=8, 500 mM NaCl, 100 μM PLP, 50 mM imidazole) and eluted with a linear gradient of 50-400 mM of imidazole. Fractions were analyzed by SDS-PAGE, and those containing pure His-tagged protein were pooled and desalted through a HiPrep 26/10 desalting column (GE Healthcare) against the final storage buffer (50 mM HEPES pH 8 and 10% glycerol). Recombinant BioA for enzyme kinetics was purified by nickel chromatography using His-Select Nickel Affinity Gel. The column was washed with 50 mM HEPES PH=8, 500 mM NaCl, 100 μM PLP, 50 mM imidazole and eluted with 200 mM imidazole. Fractions were analyzed by SDS-PAGE, and those containing pure His-tagged protein were concentrated and desalted through a 30 kDa ultra centrifugal filter against the final storage buffer (50 mM HEPES pH 8 and 10% glycerol).

Protein Crystallization

Purified protein was concentrated to a final concentration of 10 mg/ml in a buffer containing 25 mM HEPES, pH 7.5, 50 mM NaCl, 1 mM DTT, 1 mM EDTA, 10% glycerol and a final concentration of 1mM of inhibitor. This solution (3.5 μL) was mixed with 1 μL of the crystallization condition (0.05 M ammonium citrate dibasic, 5% (w/v) PEG3350) and 0.45 μL of 1 M spermidine as an additive. Hanging drops were dehydrated over 1 M ammonium sulfate. Crystals were flash frozen in a nitrogen bath prior to data collection.

Data Collection

Diffraction data were collected at the National Synchroton Light Source X25 Beamline at Brookhaven National Laboratory (NY, USA). The dataset was processed and scaled to 2.45 using HKL2000 (Otwinowski). The structure was solved by molecular replacement with Phenix-Auto MR using the apo structure of BioA (Protein Data Bank 1QJ5) as a search model[46]. The inhibitor-PLP adduct was built manually into the structure using Coot and structure refinement was carried out via successive iterations of automated refinement with Phenix-Auto MR until the geometry statistics reached an appropriate range and R and R_{free} values converged[47].

Standard enzymatic reaction

The reaction catalyzed by BioA was carried out as described previously[48], with slight modifications. The enzymatic reaction mixture was composed of 100 mM HEPES pH 8.5, 1 mM dithiothreitol, and varying concentrations of KAPA and SAM. The KAPA and SAM concentrations were 25 μM and 0.5 mM, respectively, while the other substrate was varied. The reaction was initiated by the addition of 100 nM BioA after 2 minutes of preincubation of the substrate mixture at 37℃. To stop the reaction, two times the reaction volume of derivatizing solution composed of o-phthaldialdehyde/2-mercaptoethanol reagent, 0.26 M sodium borate buffer pH 9.4, and ethanol were added. The reaction was incubated at

room temperature for 2 h and the fluorescent signal was measured at 470 nm with excitation at 410 nm. The concentrations of DAPA were calculated from a standard curve of DAPA derivatized in the enzymatic assay conditions without BioA. The initial rates for the steady-state reactions were determined by linear fits of plots of the quantity of DAPA produced versus time. These initial rates were then plotted against substrate concentration and fit to the Michaelis−Menten equation to determine apparent K_m and k_{cat}.

Inhibition of BioA by MAC13772

For the determination of the half-maximal inhibitory concentration (IC_{50}) of MAC13772, the BioA enzyme assay was conducted as described above with 1–20,000 nM of MAC13772. The reactions were quenched after 15 minutes and DAPA production determined using a standard curve. For each inhibitor concentration, the amount of DAPA formed was expressed as a percentage of the DMSO control, and a four-parameter logistic curve was used to determine the IC_{50}.

Antibacterial susceptibility testing

Thirty-four bacterial isolates were investigated for susceptibility to MAC13772. The MIC was determined in LB media supplemented with avidin (0.1 U/mL) and in M9 minimal media supplemented with amino acids (for species capable of growing in M9). The bacterial culture was prepared by washing 1 mL

of overnight culture in PBS (in triplicate), resuspending to OD_{600} 0.1, then diluting 1:200 into media. The plates were incubated at 37°C without shaking overnight before the absorbance at OD_{600} was measured. The MIC was defined as the lowest concentration inhibiting visible growth. MAC13772 was considered active if the MIC ≤ 64 μg/mL and had intermediate activity if the MIC ≤ 128-512 μg/mL. Susceptibility assays were performed three independent times.

Prediction of BioY or BioP Transporter

OrtholugeDB[28] searches using the *E. coli* K-12 MG1655 BioP transporter and the *S. aureus* 71193 BioY transporter were conducted. The presence of an orthologue was shown against 98 bacterial species with a 1:1 orthologue of *E. coli* BioA.

Treatment of systemic *A. baumannii* infection

Systemic *A. baumannii* infections were established as described above. Infections were established 1 h prior to intraperitoneal administration of MAC13772 or the vehicle (1.65% DMSO, 20% PEG 300, 78.35% H_2O). When determining bacterial load, experimental endpoint was defined as 6 h. For survival experiments MAC13772 or the vehicle were administered at 1, 4, and 8 h after infection. Clinical endpoint was determined using a five-point body-condition score analyzing weight loss, decrease in body temperature, respiratory distress,

hampered mobility, and hunched posture. Experimental endpoint was defined as 7 d after infection for mice not reaching clinical endpoint.

Treatment of murine skin infection with streptavidin and MAC13772

BALB/c mice were pretreated with 150 mg/kg (Day -4) and 100 mg/kg (Day -1) of cyclophosphamide to render mice neutropenic. Mice were anesthetized using isofluorane and administered the analgesic buprenorphine (0.1 mg/kg) intraperitoneally. A 2-cm^2 abrasion on the dorsal surface section of the mouse was inflicted through tape-stripping to the basal layer of epidermis using approximately 25-30 pieces of autoclave tape. Mice were infected with ~5×10^5 CFU of *A. baumannii* 17098 directly pipetted on the wounded skin. The infection was established 2 h before treatment with a cream (Glaxal Base) containing the vehicle, streptavidin (0.5%), MAC13772 (3%), or both streptavidin and MAC13772. Groups of mice were treated six times over the course of the experiment, 2, 8, 14, 22, 28, and 34 h after infection. Mice were euthanized at the experimental endpoint of 36 h and the wounded tissue collected, homogenized, and plated on LB to enumerate the bacterial load.

Data availability

The crystal structure of *E. coli* BioA in complex with MAC13772 solved to 2.4 Å has been deposited to the Protein Data Bank with accession code 6ED7. The source data underlying Figures. 1d and 4a-c, are provided as Supplementary

Data Tables 2-9. The data supporting the findings of this study are available from the corresponding author on reasonable request.

Acknowledgements

We would like to thank S. McCusker from the Centre for Microbial Chemical Biology and G. Wright for bacterial strains from the Institute for Infectious Disease Research clinical collection, A. Fiebig-Comyn for amendments to the animal use protocol, National Institute of Allergy and Infectious Diseases preclinical services for pharmacokinetic testing, A. Eakin for advice and guidance (contract HHSN272201100022I awarded to SRI, International) and R. Melano at Public Health Ontario for bacterial strains GB687 and C0064. This research was supported by a Foundation grant from the Canadian Institutes for Health Research (FDN-143215), a donation from the Boris Family Foundation and by funding from the Ontario Research Fund Research Excellence program (RE07-048). E.D.B. was supported by a salary award from the Canada Research Chairs program. L.A.C. was supported by an Ontario Graduate Scholarship Award and a Canadian Institutes for Health Research scholarship.

Author contributions

L.A.C. conceived the research, designed, and carried out experiments and data analysis, and wrote the manuscript. C.R.M. assisted with data acquisition and interpretation and manuscript editing. L.A.C designed and conducted the in

vitro assays to determine biotin requirement and in vitro enzyme assays. C.N.T. performed the orthologue search and phylogenetic analysis. L.A.C. and B.S.W. designed and performed the plasma growth assays. C.M.B., S.Z. and J.C. designed and performed crystallization experiments and C.M.B performed the analysis with input from M.S.J. L.A.C. and V.N.R. performed susceptibility testing. L.A.C and C.R.M. designed and performed in vivo infection model experiments. B.S.W., M.S.J. and B.K.C. assisted with data interpretation. E.D.B. conceived the research and assisted with data interpretation and manuscript editing.

Figures and Legends

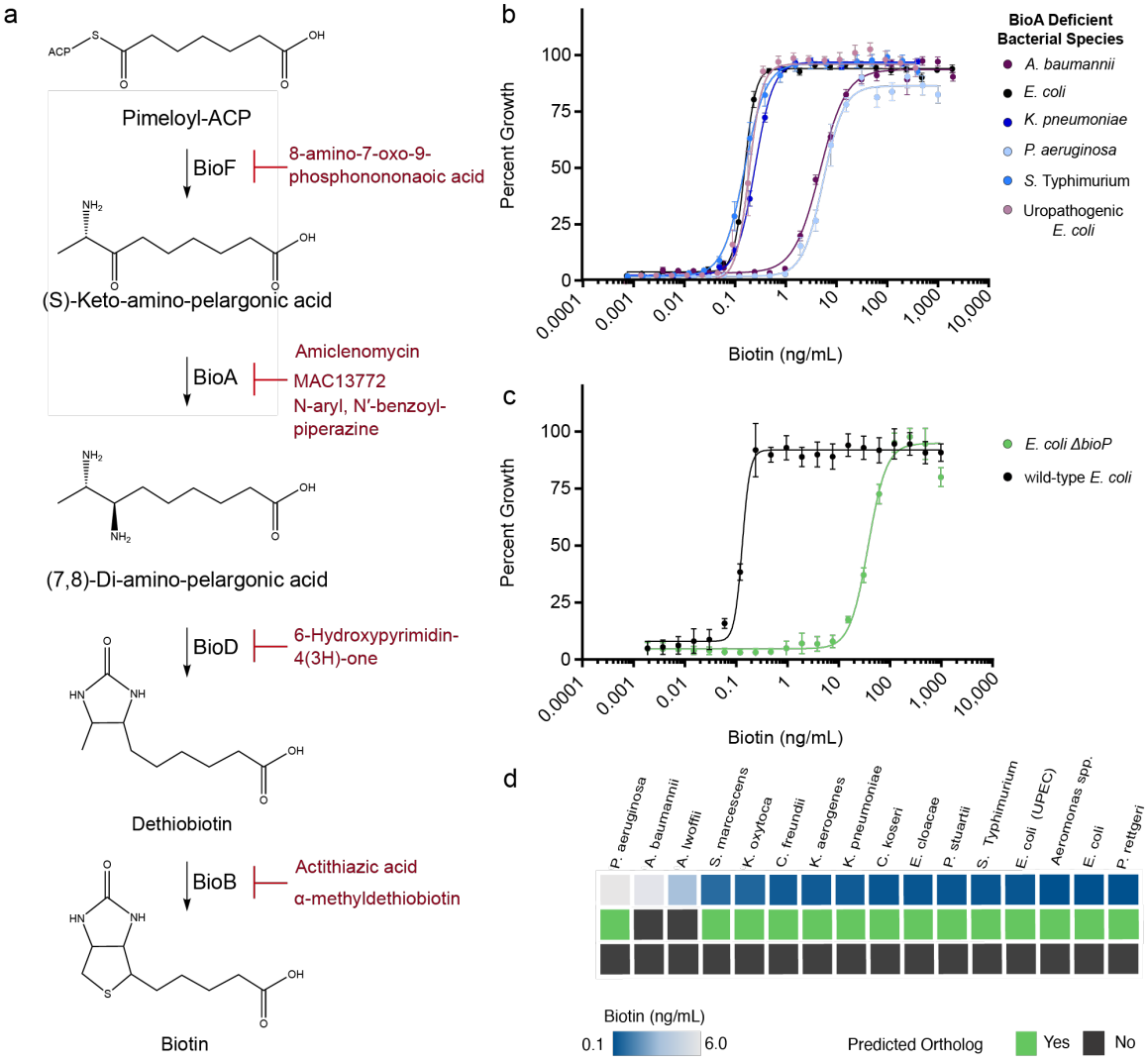

Figure 1. Presence of a high-affinity biotin transporter in pathogens accounts for variation in biotin requirements. (a) The conserved late steps of biotin biosynthesis, responsible for forming the heterocyclic ring of biotin. A subset of the known inhibitors for each enzymatic reaction is listed (red). ACP, acyl-carrier protein **(b)** Analysis of the biotin concentrations required to restore the growth of BioA-deficient *A. baumannii, E. coli, K. pneumoniae, P. aeruginosa, S.* Typhimurium, and UPEC. Data are mean ± s.d. (n=12) and the solid lines show a four-parameter dose-response curve. **(c)** Analysis of the biotin

concentrations required to abrogate MAC13772 activity at four times MIC in wild-type *E. coli* (black) and biotin transporter-deficient (Δ*bioP*) *E. coli* (green. Data are mean ± s.d. (n=8) and the solid lines show a four-parameter dose-response curve. **(d)** Heat map depicting the exogenous biotin requirement to restore 50% growth and presence of a predicted high-affinity biotin transporter for 16 bacteria (*P. aeruginosa, A. baumannii, Acinetobacter lwoffii, Serratia marcescens, Klebsiella oxytoca, Citrobacter freundii, Klebsiella aerogenes, K. pneumoniae, Citrobacter koseri, Enterobacter cloacae, Providencia stuartii, S.* Typhimurium, *E. coli* (UPEC), *Aeromonas* spp., *E. coli,* and *Providencia rettgeri*). The biotin requirement was calculated from the EC_{50} of a four-parameter dose response curve.

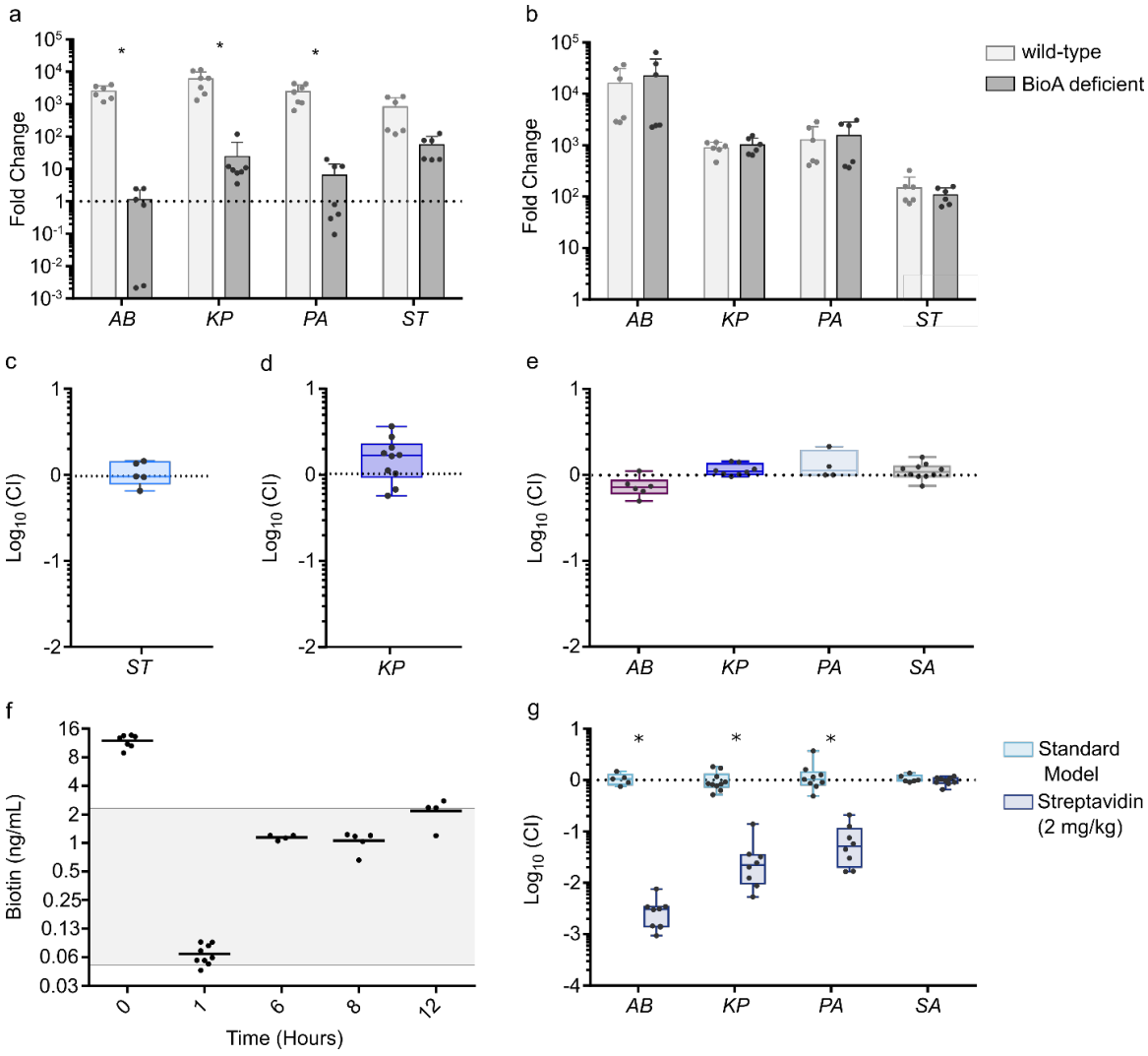

Figure 2. Biotin biosynthesis is essential for *A. baumannii, K. pneumoniae*, and *P. aeruginosa* during an infection mimicking human biotin levels. (a,b) Fold change in viable cell counts of BioA-deficient (light grey) and wild-type (dark grey) *A. baumannii* (*AB; n=6*), *K. pneumoniae* (*KP; n=7*), *P. aeruginosa* (*PA; n=7*), and *S.* Typhimurium (*ST; n=6*) growth in 50% human plasma **(a)** or 50% mouse plasma **(b)**. The dashed line indicates a fold change of 1, bars indicate the mean ± s.d., * $P < 0.01$ for each mutant relative to wild-type using an unpaired two-tailed *t*-test with Holm-Sidak's multiple comparisons test. **(c)** Competitive index (CI) for the co-infection of Δ*bioA* and wild-type *S.* Typhimurium in the spleen following a standard systemic infection (*n*=5). **(d)** CI for the co-infection of mice (*n*=10) with wild-type *K. pneumoniae* and Δ*bioA* in a lung infection. **(e)** CI for

the co-infection of BioA-deficient and wild-type *A. baumannii* (*n=6*)*, K. pneumoniae* (*n=8*)*, P. aeruginosa* (*n=4*)*,* and *S. aureus* (*SA; n=10*) in the thigh muscle. **(f)** Quantification of biotin by enzyme-linked immunosorbent assay in the plasma of mice 0 h (n=7), 1 h (*n*=9), 6 h (*n*=4), 8 h (*n*=5), and 12 h (*n*=4) following intraperitoneally administered streptavidin (2 mg/kg). Each point represents the biotin levels of a single mouse and the line shows the mean. The grey area indicates the range of biotin concentration in human plasma accounting for fluctuations (0.05-2.4 ng/mL)[34-38]. **(g)** CI for the co-infection of BioA-deficient and wild-type *A. baumannii* (*n*=5 and 8, respectively)*, K. pneumoniae* (*n*=10 and 8, respectively)*, P. aeruginosa* (*n*=9 and 8, respectively)*,* and *S. aureus* (*n*=6 and 9, respectively) in the spleen in a standard systemic infection model (light blue) or systemic infection in mice pretreated with streptavidin (2 mg/kg; blue) The dotted line represents a CI of 1. Groups were analyzed with an unpaired two-tailed *t*-test with Holm-Sidak's multiple comparisons test, * $P<0.01$. In all instances, box plot whiskers show the minimum to maximum values, the box denotes the interquartile range, and the line in the box shows the median.

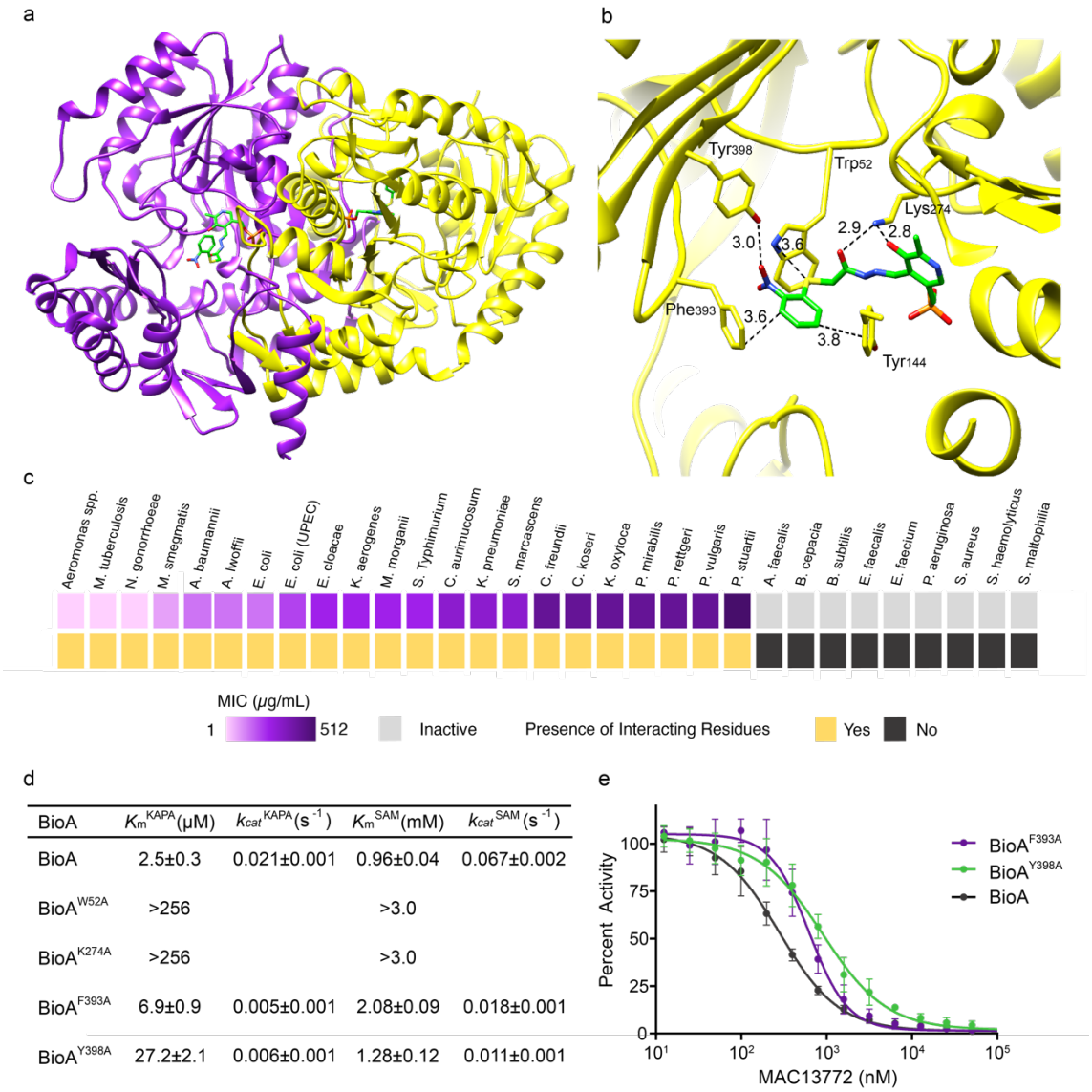

BioA	K_m^{KAPA}(μM)	k_{cat}^{KAPA}(s^{-1})	K_m^{SAM}(mM)	k_{cat}^{SAM}(s^{-1})
BioA	2.5±0.3	0.021±0.001	0.96±0.04	0.067±0.002
$BioA^{W52A}$	>256		>3.0	
$BioA^{K274A}$	>256		>3.0	
$BioA^{F393A}$	6.9±0.9	0.005±0.001	2.08±0.09	0.018±0.001
$BioA^{Y398A}$	27.2±2.1	0.006±0.001	1.28±0.12	0.011±0.001

Figure 3. Crystal structure of *E. coli* BioA in complex with MAC13772. (a) Structure of *E. coli* BioA bound to MAC13772 (2.4 Å resolution). Ribbon diagram illustrating the BioA dimer formed by two identical monomers is shown in yellow and purple. The MAC13772-PLP adduct is shown as sticks in both monomers. **(b)** Shown is the structure of the BioA active-site region surrounding the MAC13772-PLP adduct (green stick). Residues within ~4 Å radius are shown as yellow sticks and their interactions with the inhibitor-PLP adduct are indicated by dashed lines. **(c)** Conservation of Phe393, Tyr144, Trp52, Tyr398, and Lys274 in BioA correlates with MAC13772 activity. Heat map showing the MIC of MAC13772 against 30 bacterial species (purple) and the presence of Phe393, Tyr144, Trp52, Tyr398, and Lys274 in the species' BioA (yellow). As well as

those listed in Figure 1d, species compared include *M. tuberculosis, Neisseria gonorrhoeae, mycobacterium smegmatis, Morganella morganii, Corynebacterium aurimucosum, Proteus mirabilis, Proteus vulgaris, Alcaligenes faecalis, Burkholderia cepacian, Bacillus subtilis, Enterococcus faecalis, enterococcus faecium, S. aureus, Staphylococcus haemolyticus,* and *Stenotrophomonas maltophilia.* **(d)** Michaelis-Menten parameters for the steady-state reactions of BioA, BioA(W52A), BioA(K274A), BioA(F393A), and BioA(Y398A). Data are mean ± s.d. n=4 (KAPA half-saturation value (K_m)), n=4 (KAPA turnover number (k_{cat})), n=6 (SAM K_m), and n=6 (SAM k_{cat}). **(e)** Dose-response curve of MAC13772 against recombinant BioA, BioA(F393A), and BioA(Y398A). Data are mean ± s.d. of 12 replicates and are fitted to a four-parameter dose response curve.

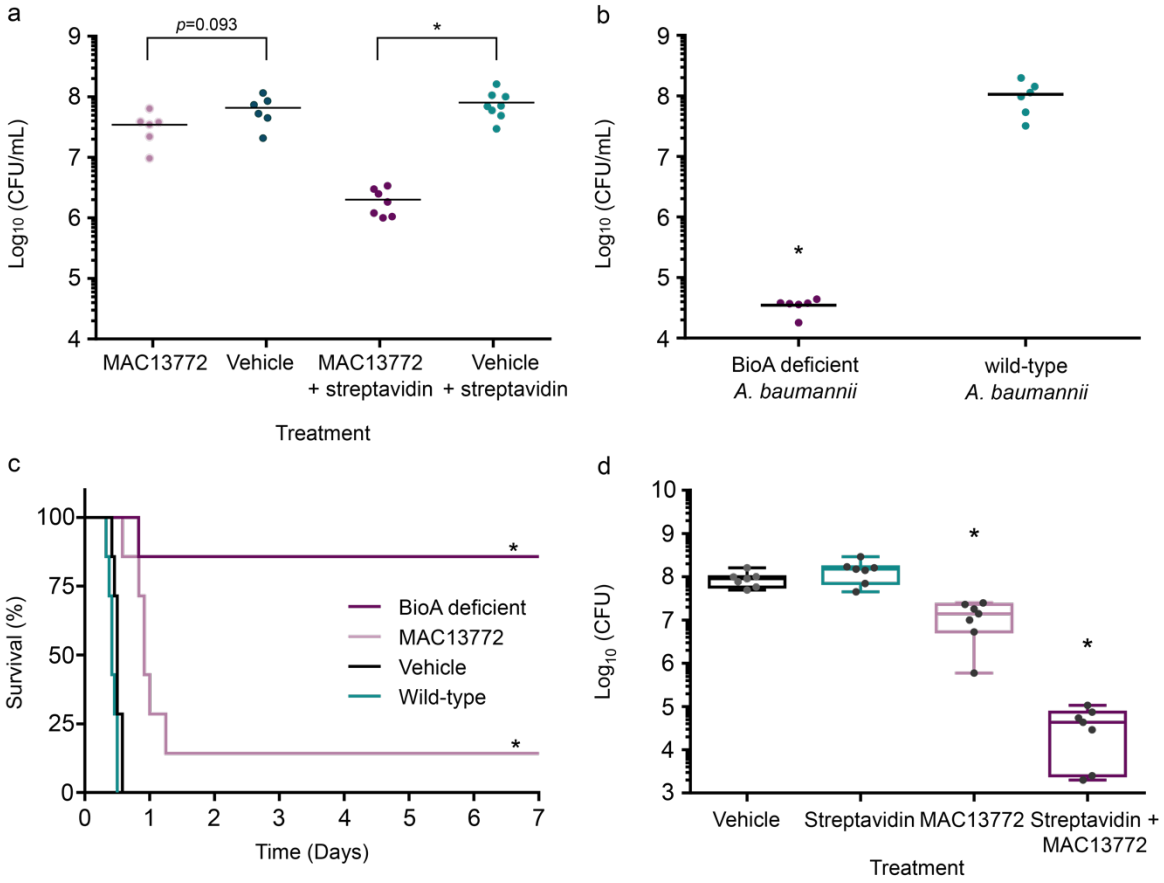

Figure 4. In vivo efficacy of biotin biosynthesis inhibition. (a) Bacterial load in the blood following MAC13772 treatment of an *A. baumannii* systemic infection in the standard and humanized biotin level models. Before infection, mice were treated with streptavidin (2 mg/kg) or water. Groups of mice were treated by intraperitoneal injection 1 h after infection with MAC13772 (15 mg/kg; purple; *n*=6 (water), 7 (streptavidin)) or vehicle (blue; *n*=6 (water), 8 (streptavidin)). MAC13772 lowered the bacterial load in the blood 97.5% (*P*<0.01, two-sided Mann-Whitney test) compared to the vehicle 6 h after infection in the model with human biotin levels. Each point represents an individual mouse and the line indicates the mean. **(b)** *A. baumannii* bacterial load in the blood following infection with the BioA-deficient (purple) or wild-type (blue) strain. Groups of mice (*n*=6) were administered streptavidin (2 mg/kg) 1 h after infection. Each point represents an individual mouse and the line indicates the mean; **P*<0.01, two-sided Mann-Whitney test. **(c)** Survival curve of an *A. baumannii* systemic infection following a single streptavidin treatment (2 mg/kg) 1 h before infection. Four groups of mice (*n*=7) were evaluated: mice infected with wild-type *A. baumannii* (blue), mice infected with wild-type *A. baumannii* and treated with MAC13772 at 1, 4, and 8 h after infection (15 mg/kg, pink), mice infected with

wild-type *A. baumannii* and treated with a vehicle at 1, 4, and 8 h after infection (black), and mice infected with BioA-deficient *A. baumannii* (purple). Mouse survival as determined by a two-sided Mantel–Cox test; **P*<0.01, with Bonferroni's multiple comparisons test. **(d)** Treatment of *A. baumannii* skin infection with a cream containing the vehicle (black), 0.5% streptavidin (blue), 3% MAC13372 (pink), or the combination of streptavidin and MAC13772 (purple). Groups of mice (*n*=7) were treated at 2, 8, 14, 22, 28, and 34 h after infection. The combination of streptavidin and MAC13772 resulted in a 99.9% reduction (*P*<0.01, two-sided Mann-Whitney test) in CFU when compared with the vehicle. Box plot whiskers show the minimum to maximum values, the box denotes the interquartile range, and the line in the box shows the median.

Extended Data and Legends

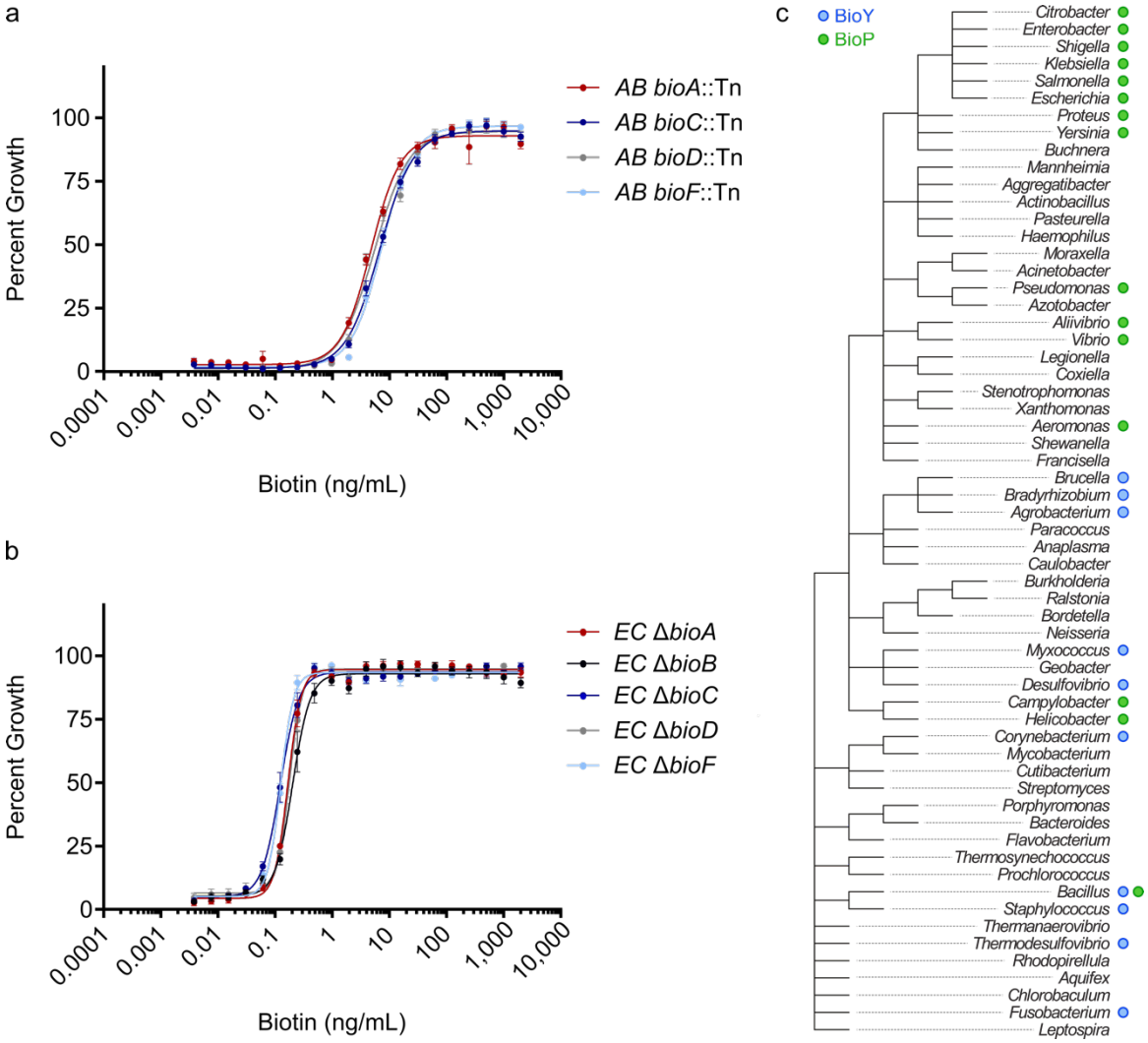

Extended Data Fig. 1 Biotin requirements of BioA-deficient strains represent the entirety of the biosynthetic pathway. Analysis of the biotin concentrations required to restore the growth of (a) *A. baumannii* transposon mutants in *bioACDF* and (b) *E. coli* Δ*bioABCDF* in M9 minimal media supplemented with amino acids after 18 h. Points show the mean of 8 replicates ± s.d. and the solid lines show a four-parameter dose response curve. (c) Presence or absence of a high-affinity biotin transporter in a phylogenetic tree of pathogenic bacteria with an orthologue to *E. coli* BioA. The presence of an orthologue to biotin transporters, *E. coli* BioP and *S. aureus* BioY

was determined using OrtholugeDB. Species with a predicted orthologue to *E. coli* BioP (green) or *S. aureus* BioY (blue) transporters are demarked by a circle.

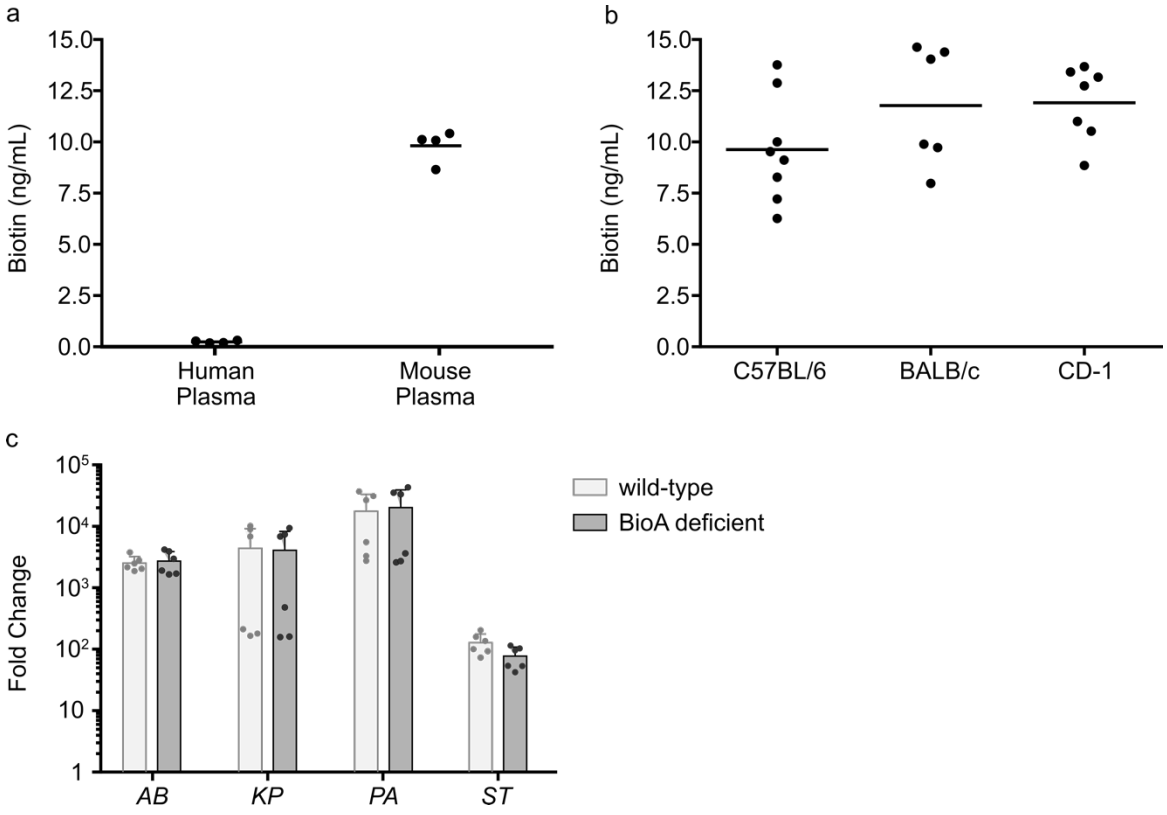

Extended Data Fig. 2 Biotin levels are comparable among three common mouse strains. (a) Quantification of biotin levels in purchased human and mouse plasma from Innovative Research. Each point represents a technical replicate (n = 4) and the line is the mean. (b) Quantification of biotin in the plasma of BALB/c (n = 6), CD-1 (n = 7), and C57Bl/6 (n = 8) mice. Each point represents the biotin levels of a single mouse and the line is the mean. (c) Fold change in viable cell counts of BioA-deficient (grey) and wild-type (black) *A. baumannii* (*AB*), *K. pneumoniae* (*KP*), *P. aeruginosa* (*PA*), and *S*. Typhimurium (*ST*) growth after 24 h in 50% human plasma supplemented with biotin (10 µg/mL). BioA-deficient or wild-type strains were separately inoculated into plasma diluted with M9 salts supplemented with 25 mM of sodium bicarbonate. Viable cell counts were calculated at time 0 and 24 h. Fold change was calculated by dividing the viable cell count at 24 h by the viable cell count at time 0. The bars indicate the mean of 6 replicates ± s.d.

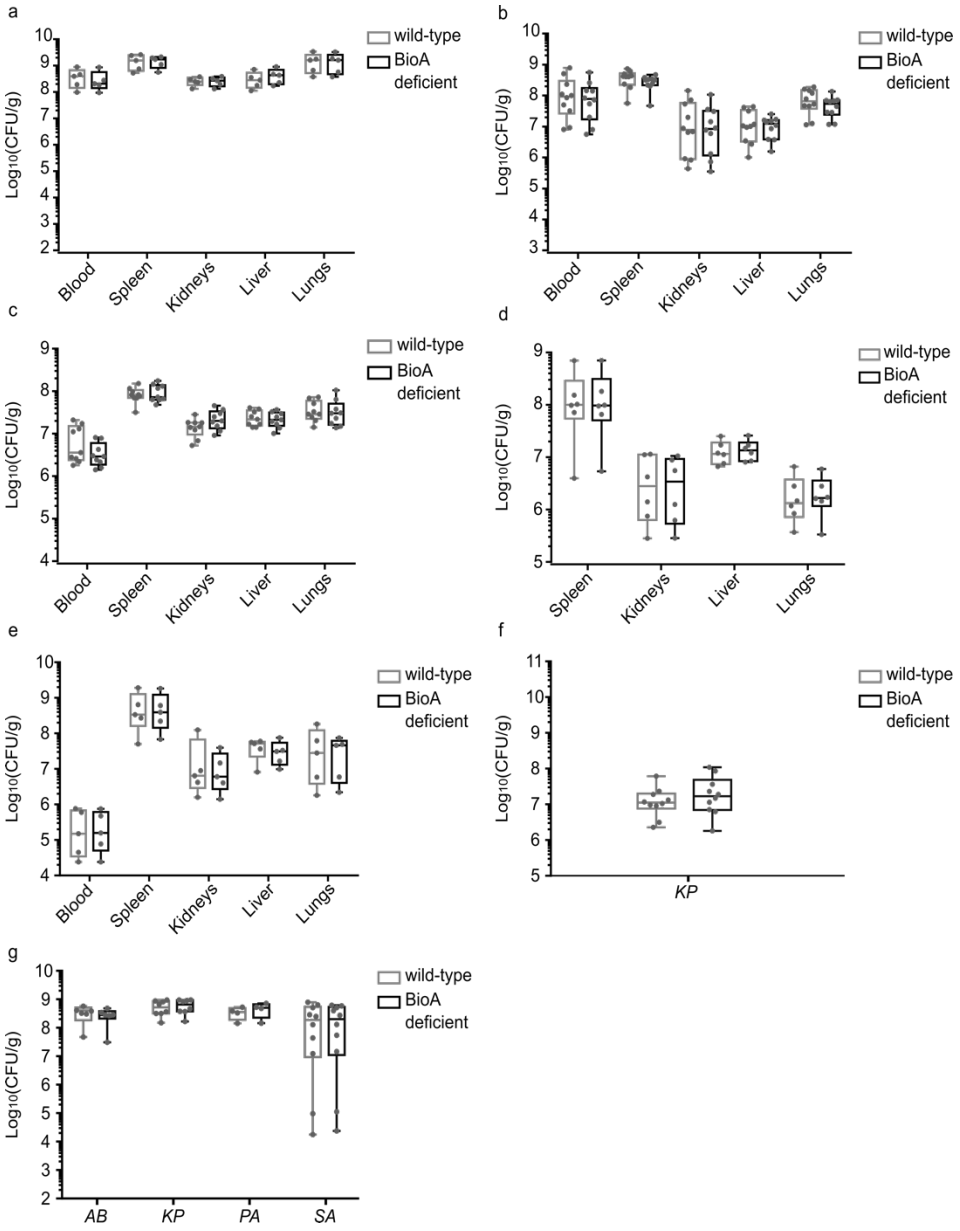

Extended Data Fig. 3 Biotin biosynthesis is dispensable for *A. baumannii, K. pneumoniae, P. aeruginosa, S. aureus*, and *S*. Typhimurium during standard infection models. Bacterial load in the blood, spleen, kidneys, liver, and lungs following a systemic infection with (a) *A. baumannii (AB; n = 5)*, (b) *K. pneumoniae (KP; n=10)*, (c) *P. aeruginosa (PA; n=9)*, (d) *S. aureus (SA; n=6)*, and (e) *S*. Typhimurium (*ST; n=5)*. Mice were co-infected with a mixed inoculum of wild- type (grey) and BioA-deficient (black) bacteria inoculated by intraperitoneal injection. (f) Bacterial load in the lungs of mice co-infected with a

mixed inoculum of wild-type (grey) and Δ*bioA* (black) bacteria. Infection was established by intranasal administration of 2×10^7 CFU by micropipette and mice (n=10) euthanized 36 h later. (g) Bacterial load in the thighs of mice co-infected with a mixed inoculum of wild-type (grey) and BioA-deficient (black) *A. baumannii* (*AB; n=6*), *K. pneumoniae* (*KP; n=8*), *P. aeruginosa* (*PA; n=4*), and *S. aureus* (*SA; n=10*). 5×10^5 (*KP* and *SA*) or 5×10^6 (*AB* and PA) CFU were injected into the thighs of mice. In all instances box plot whiskers show the minimum to maximum values, the box denotes the interquartile range, and the line in the box shows the median.

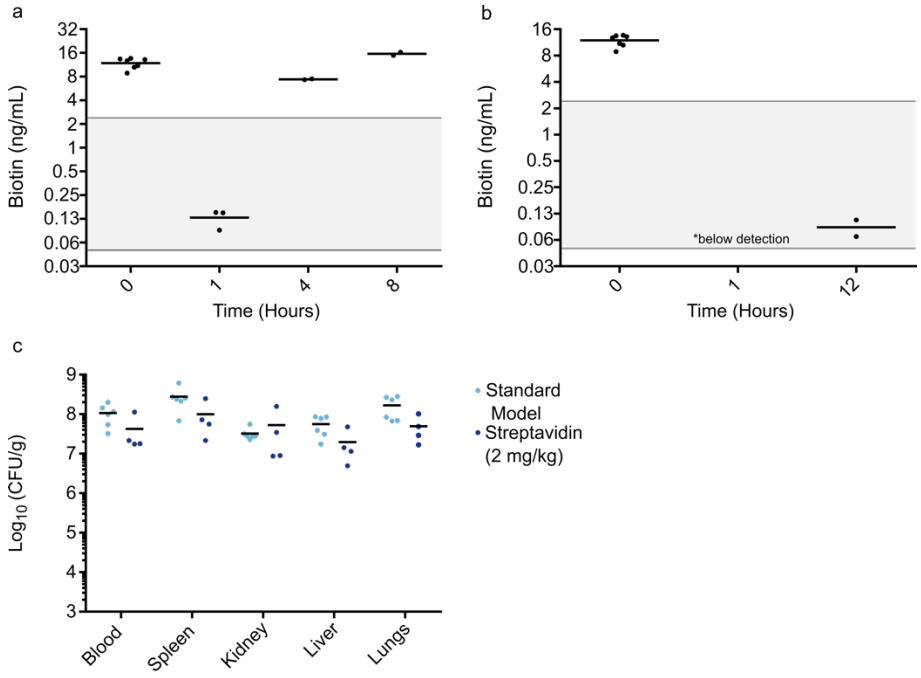

Extended Data Fig. 4 Determination of an optimal dose of streptavidin to mimic human biotin levels. Quantification of biotin in the plasma of CD-1 mice following intraperitoneal administration of (a) streptavidin (1 mg/kg) or (b) streptavidin (4 mg/kg) treatment. Each point represents the biotin levels of a single mouse (n = 2–7) and the line indicates the mean. The grey area indicates the typical range of human biotin concentration in plasma accounting for daily fluctuations. (c) Streptavidin pretreatment has no effect on the ability of wild-type bacteria to cause infection. *A. baumannii* bacterial load in the blood, spleen, kidney, liver, and lungs in a standard infection model (n=6) or mice pretreated with streptavidin (2 mg/kg; n=4). Mice were infected by intraperitoneal injection and euthanized 10 h post-infection. Each point represents the bacterial load from an individual mouse and the line indicates the mean.

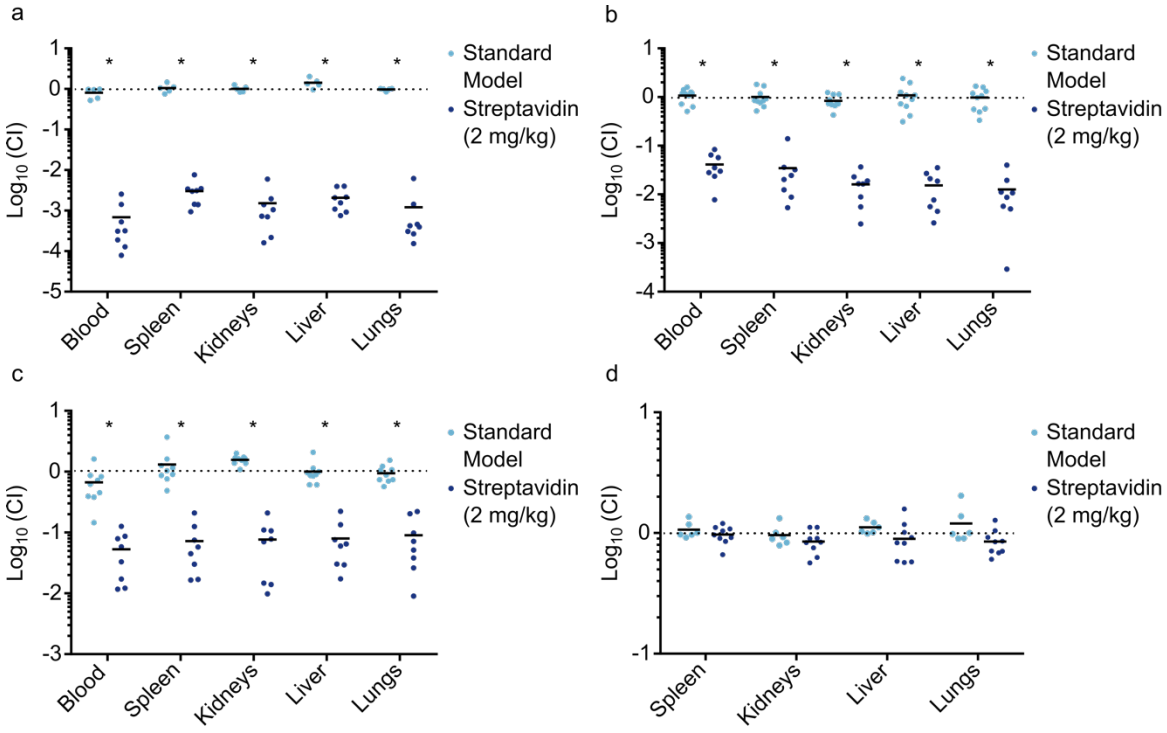

Extended Data Fig. 5 Biotin biosynthesis is a critical fitness determinant for *A. baumannii, K. pneumoniae*, and *P. aeruginosa* during a systemic infection with human biotin levels. Competitive index (CI) for the co-infection of BioA-deficient and wild-type strains of (a) *A. baumannii* (n=5, 8), (b) *K. pneumoniae* (n=10, 8), (c) *P. aeruginosa* (n=9, 8), and (d) *S. aureus* (n=6, 9) in the blood, spleen, kidneys, liver, and lungs in a standard systemic infection model (light blue) or systemic infection in mice pretreated with streptavidin (2 mg/kg; blue) 1 h prior to inoculation. CI is calculated by dividing the bacterial load of the query strain (BioA-deficient) by the bacterial load of the wild-type strain. Each point represents the CI from an individual mouse and the line indicates the mean. The dotted line represents a CI of 1 indicating the two strains are proliferating equally in vivo. Groups were analyzed with an unpaired two-tailed *t*-test and corrected for multiple comparisons with a Holm-Sidak test, * indicates a $p<0.01$.

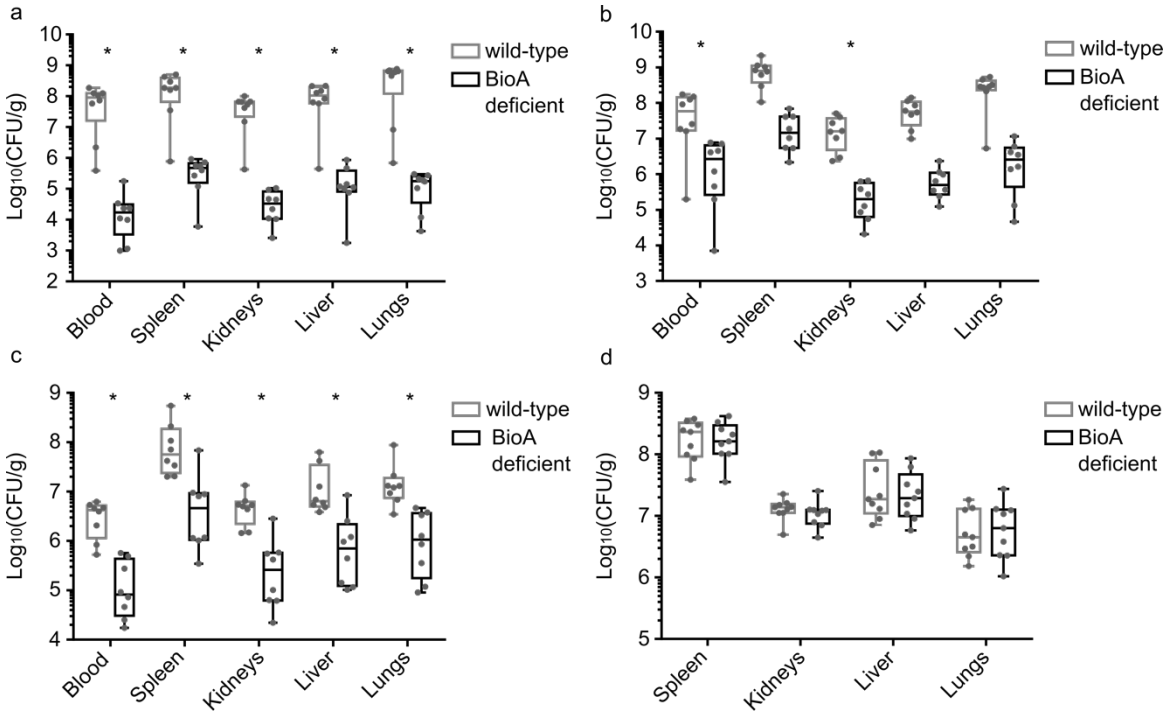

Extended Data Fig. 6 Biotin biosynthesis is a critical fitness determinant for *A. baumannii, K. pneumoniae*, and *P. aeruginosa* during a systemic infection with human biotin levels. Bacterial load in the blood, spleen, kidneys, liver, and lungs following a systemic infection with human biotin levels with (a) *A. baumannii* (n=8), (b) *K. pneumoniae* (n=8), (c) *P. aeruginosa* (n=8), and (d) *S. aureus* (n=9). Mice were pretreated with streptavidin (2 mg/kg) 1 h prior to co-infection with a mixed inoculum of wild-type (grey) and BioA-deficient (black) bacteria. Box plot whiskers show the minimum to maximum values, the box denotes the interquartile range, and the line in the box shows the median of each group. Groups were analyzed with an unpaired two-tailed *t*-test and corrected for multiple comparisons with a Holm-Sidak test, * indicates a $p<0.01$.

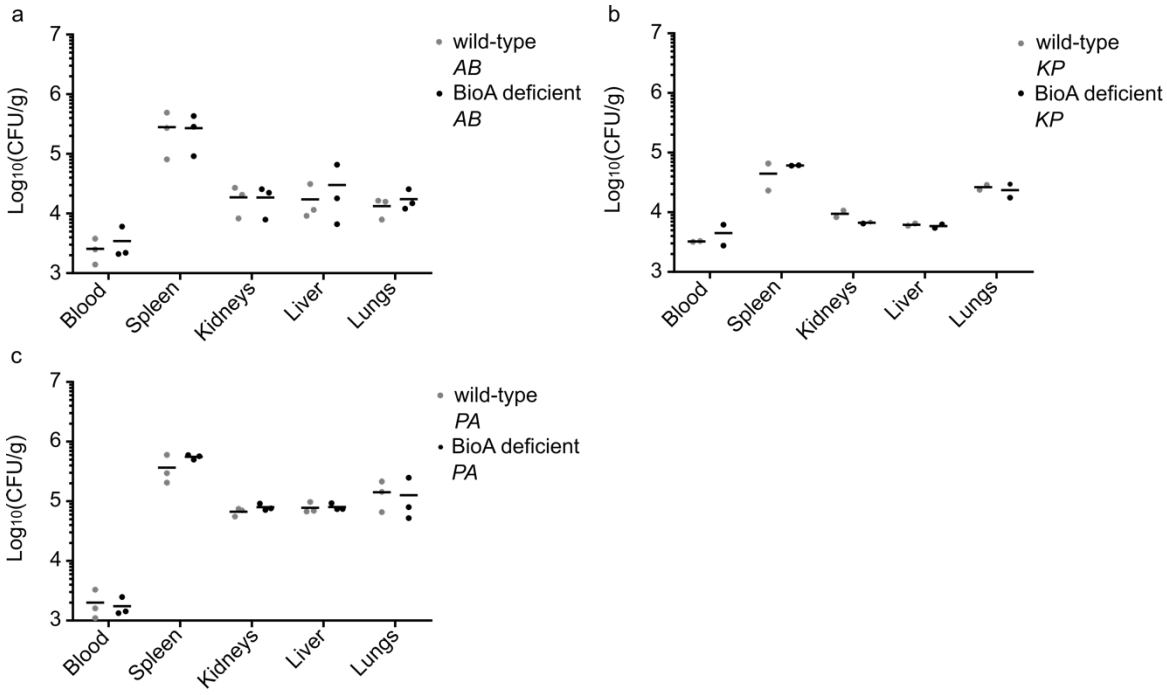

Extended Data Fig. 7 Biotin biosynthesis is dispensable during colonization of a systemic murine infection mimicking human biotin levels. Bacterial load in the blood, spleen, kidneys, liver, and lungs 1- h after infection following a systemic infection with human biotin levels with (a) *A. baumannii* (*AB;* n=3), (b) *K. pneumoniae* (*KP;* n=2), and (c) *P. aeruginosa* (*PA;* n=3). Mice were pretreated with streptavidin (2 mg/kg) 1 h prior to co-infection with a mixed inoculum of wild-type (grey) and BioA-deficient (black) bacteria. Each point represents the bacterial load from an individual mouse and the line indicates the mean.

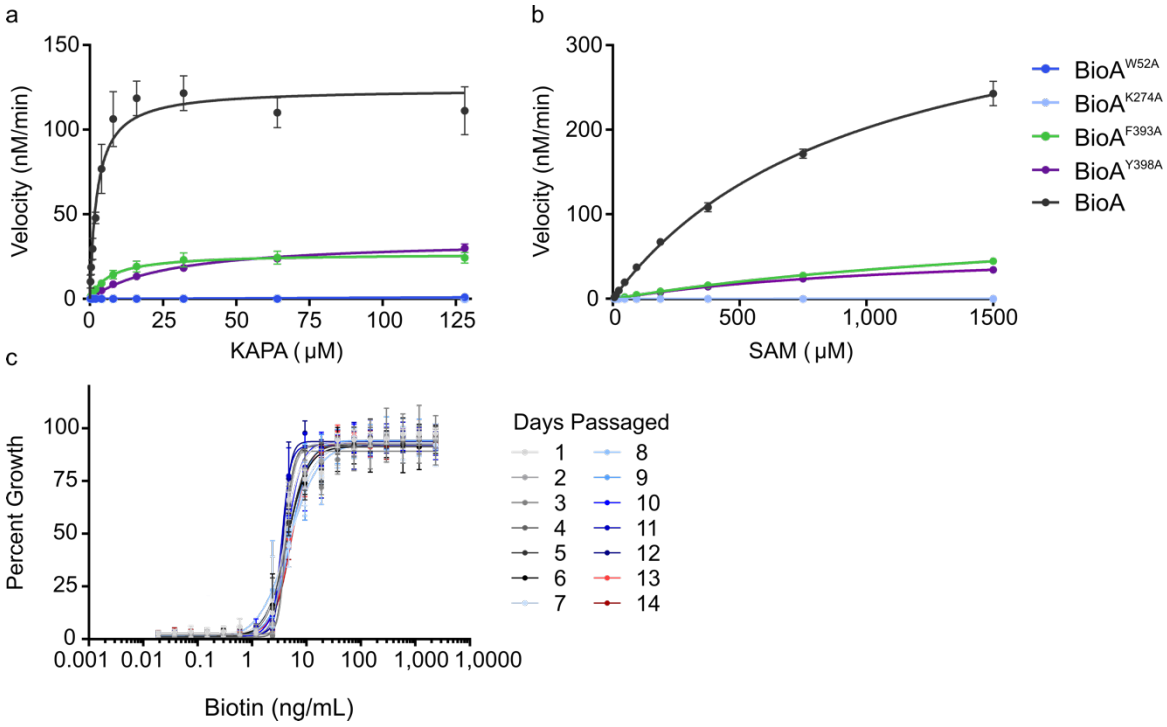

Extended Data Fig. 8 Resistance to inhibition of biotin biosynthesis imparts a fitness cost. Kinetics of (7,8)-di-amino-pelargonic acid production. Initial velocities of (7,8)-di-amino-pelargonic acid production with BioA, BioA^{W52A}, BioA^{K274A}, BioA^{F393A}, and BioA^{Y398A} were determined at various (a) (S)-keto-amino-pelargonic acid (KAPA; n=4) and (b) *S*-adenosyl-L-methionine (SAM; n=6) concentrations. Points show the mean of replicates ± s.d. and the solid lines show a Michaelis-Menten curve. (c) Analysis of the biotin concentrations required to restore the growth of BioA-deficient *A. baumannii* passaged into the lowest biotin concentration supporting growth for 14 days. Points show the mean of 8 replicates ± s.d. and the solid lines show a four-parameter dose response curve.

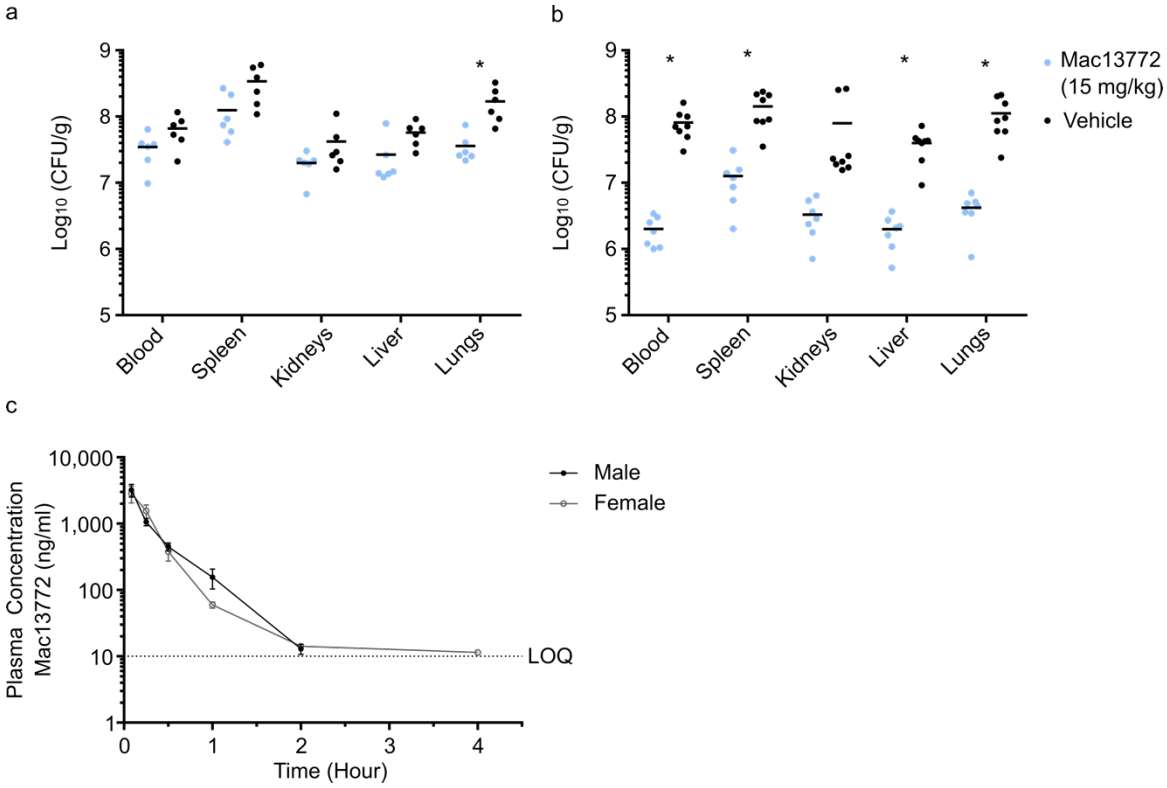

Extended Data Fig. 9 MAC13772 is efficacious against *A. baumannii* in a systemic infection with human biotin levels. Bacterial load of *A. baumannii* in the blood, spleen, kidneys, liver, and lungs following a systemic infection with (a) standard biotin levels and (b) human biotin levels, treated with MAC13772 (15 mg/kg). Mice were pretreated with streptavidin (2 mg/kg) 1 h prior to infection and treated with MAC13772 (15 mg/kg) 1 h following infection. Groups were analyzed with an unpaired two-tailed *t*-test and corrected for multiple comparisons with a Holm-Sidak test, * indicates a $p<0.01$. (c) Time course of plasma concentrations of MAC13772 in male (black) and female (grey) Sprague Dawley rats, after intravenous administration. Each data point represents the mean ± s.d. concentration from n=3 rats, the dotted line indicates the limit of quantification (LOQ).

Supplementary Information

For Supplementary Tables 2–11, Supplementary Figures 1–3, Supplementary References, and Reporting Summary see: https://doi.org/10.1038/s41564-019-0595-2

References

1. Brown, E. D. & Wright, G. D. Antibacterial drug discovery in the resistance era. *Nature* **529**, 336–343 (2016).

2. Sassetti, C. M. & Rubin, E. J. Genetic requirements for mycobacterial survival during infection. *Proc. Natl. Acad. Sci. U. S. A.* **100**, 12989–12994 (2003).

3. Weiss, D. S. *et al.* In vivo negative selection screen identifies genes required for *Francisella* virulence. *Proc. Natl. Acad. Sci. U. S. A.* **104**, 6037–6042 (2007).

4. Napier, B. A. *et al.* Link between intraphagosomal biotin and rapid phagosomal escape in *Francisella*. *Proc. Natl. Acad. Sci. U. S. A.* **109**, 18084–18089 (2012).

5. Park, S. W. *et al.* Evaluating the sensitivity of *Mycobacterium tuberculosis* to biotin deprivation using regulated gene expression. *PLoS Pathog.* **7**, e1002264 (2011).

6. Wang, N., Ozer, E. A., Mandel, M. J. & Hauser, A. R. Genome-wide identification of *Acinetobacter baumannii* genes necessary for persistence in the lung. *mBio* **5**, e01163-14 (2014).

7. Subashchandrabose, S. *et al. Acinetobacter baumannii* genes required for bacterial survival during bloodstream infection. *mSphere* **1**, e00013-15 (2016).

8. Bachman, M. A. *et al.* Genome-wide identification of *Klebsiella pneumoniae* fitness genes during lung infection. *mBio* **6**, e00775-15 (2015).

9. Skurnik, D. *et al.* A comprehensive analysis of in vitro and in vivo genetic fitness of *Pseudomonas aeruginosa* using high-throughput sequencing of transposon libraries. *PLoS Pathog.* **9**, e1003582 (2013).

10. Crofts, A. A. *et al.* Enterotoxigenic *E. coli* virulence gene regulation in human infections. *Proc. Natl. Acad. Sci. U. S. A.* **115**, 8968–8976 (2018).

11. Sheikh, A. *et al.* In vivo expression of *Salmonella enterica* serotype Typhi genes in the blood of patients with typhoid fever in Bangladesh. *PLoS Negl. Trop. Dis.* **5**, e1419 (2011).

12. Subashchandrabose, S., Smith, S. N., Spurbeck, R. R., Kole, M. M. & Mobley, H. L. T. Genome-wide detection of fitness genes in uropathogenic *Escherichia coli* during systemic infection. *PLoS Pathog.* **9**, e1003788 (2013).

13. Silva-Valenzuela, C. A. *et al.* Analysis of two complementary single-gene deletion mutant libraries of *Salmonella* Typhimurium in intraperitoneal infection of BALB/c mice. *Front. Microbiol.* **6**, 1–9 (2016).

14. Valentino, M. D. *et al.* Genes contributing to *Staphylococcus aureus* fitness in abscess- and infection-related ecologies. *mBio* **5**, e01729-14 (2014).

15. Streit, W. R. & Entcheva, P. Biotin in microbes, the genes involved in its biosynthesis, its biochemical role and perspectives for biotechnological production. *Appl. Microbiol. Biotechnol.* **61**, 21–31 (2003).

16. Lin, S., Hanson, R. E. & Cronan, J. E. Biotin synthesis begins by hijacking the fatty acid synthetic pathway. *Nat. Chem. Biol.* **6**, 682–688 (2010).

17. Okami, Y. *et al.* Studies on a new amino acid antibiotic, amiclenomycin. *J. Antibiot. (Tokyo).* **27**, 656–664 (1974).

18. Kitahara, T., Hotta, K., Yoshida, M. & Okami, Y. Biological studies on amiclenomycin. *J. Antibiot.* **28**, 215–222 (1975).

19. Dai, R., Wilson, D. J., Geders, T. W., Aldrich, C. C. & Finzel, B. C. Inhibition of *Mycobacterium tuberculosis* transaminase BioA by aryl hydrazines and hydrazides. *Chembiochem* **15**, 575–586 (2014).

20. Park, S. W. *et al.* Target-based identification of whole-cell active inhibitors of biotin biosynthesis in *Mycobacterium tuberculosis*. *Chem. Biol.* **22**, 76–86 (2015).

21. Liu, F. *et al.* Structure-based optimization of pyridoxal 5′-phosphate-dependent transaminase enzyme (BioA) inhibitors that target biotin biosynthesis in *Mycobacterium tuberculosis*. *J. Med. Chem.* **60**, 5507–5520 (2017).

22. Salaemae, W., Booker, G. W. & Polyak, S. W. The role of biotin in bacterial physiology and virulence: a novel antibiotic target for *Mycobacterium tuberculosis*. *Microbiol. Spectr.* **4**, VMBF-0008-2015 (2016).

23. Mock, D. M. & Malik, M. I. Distribution of biotin in human plasma: most of the biotin is not bound to protein. *Am. J. Clin. Nutr.* **56**, 427–432 (1992).

24. Trüeb, R. M. Serum biotin levels in women complaining of hair loss. *Int. J. Trichology* **8**, 73–77 (2016).

25. Harthe, C. & Claustrat, B. A sensitive and practical competitive radioassay for plasma biotin. *Ann. Clin. Biochem.* **40**, 259–263 (2003).

26. Perry, C. A. *et al.* Pregnancy and lactation alter biomarkers of biotin metabolism in women consuming a controlled diet. *J. Nutr.* **144**, 1977–1984 (2014).

27. Wakabayashi, K. *et al.* Serum biotin in Japanese children: enzyme-linked immunosorbent assay measurement. *Pediatr. Int.* **58**, 872–876 (2016).

28. Whiteside, M. D., Winsor, G. L., Laird, M. R. & Brinkman, F. S. L. OrthologueDB: a bacterial and archaeal orthology resource for improved comparative genomic analysis. *Nucleic Acids Res.* **41**, 366–376 (2013).

29. Zlitni, S., Ferruccio, L. F. & Brown, E. D. Metabolic suppression identifies new antibacterial inhibitors under nutrient limitation. *Nat. Chem. Biol.* **9**, 796–804 (2013).

30. Tiwari, D. *et al.* Targeting protein biotinylation enhances tuberculosis chemotherapy. *Sci. Transl. Med.* **10**, eaal1803 (2018).

31. El Zahed, S. S. & Brown, E. D. Chemical-chemical combinations map uncharted interactions in *Escherichia coli* under nutrient stress. *iScience* **2**, 168–181 (2018).

32. Legrand, N. *et al.* Humanized mice for modeling human infectious disease: challenges, progress, and outlook. *Cell Host Microbe* **6**, 5–9 (2009).

33. Lin, S. & Cronan, J. E. The BioC O-methyltransferase catalyzes methyl esterification of malonyl-acyl carrier protein, an essential step in biotin synthesis. *J. Biol. Chem.* **287**, 37010–37020 (2012).

34. Ploux, O., Breyne, O., Carillon, S. & Marquet, A. Slow-binding and competitive inhibition of 8-amino-7-oxopelargonate synthase, a pyridoxal-5′-phosphate-dependent enzyme involved in biotin biosynthesis, by substrate and intermediate analogs. *Eur. J. Biochem.* **259**, 63–70 (1999).

35. Hanka, L. J., Martin, D. G. & Reineke, L. M. Two new antimetabolites of biotin: α-methyldethiobiotin and α-methylbiotin. *Antimicrob. Agents Chemother.* **1**, 135–138 (1972).

36. Eisenberg, M. A. & Hsiung, S. C. Mode of action of the biotin antimetabolites actithiazic acid and α-methyldethiobiotin. *Antimicrob. Agents Chemother.* **21**, 5–10 (1982).

37. Alexeev, D. *et al.* Rational design of an inhibitor of dethiobiotin synthetase; interaction of 6-hydroxypyrimindin-4(3H)-one with the adenine base binding site. *Tetrahedron* **54**, 15891–15898 (1998).

38. Bockman, M. R. *et al.* Investigation of (S)-(−)-acidomycin: a selective antimycobacterial natural product that inhibits biotin synthase. *ACS Infect. Dis.* **5**, 598–617 (2019).

39. Taira, J. *et al.* Identification of a novel class of small compounds with anti-tuberculosis activity by in silico structure-based drug screening. *J. Antibiot. (Tokyo).* **70**, 1057–1064 (2017).

40. Datta, S., Costantino, N. & Court, D. L. A set of recombineering plasmids for Gram-negative bacteria. *Gene* **379**, 109–115 (2006).

41. Datsenko, K. a & Wanner, B. L. One-step inactivation of chromosomal genes in *Escherichia coli* K-12 using PCR products. *Proc. Natl. Acad. Sci. U. S. A.* **97**, 6640–6645 (2000).

42. Huang, T.W. *et al.* Capsule deletion via a λ-Red knockout system perturbs biofilm formation and fimbriae expression in *Klebsiella pneumoniae* MGH 78578. *BMC Res. Notes* **7**, 13 (2014).

43. Gallagher, L. A. *et al.* Resources for genetic and genomic analysis of emerging pathogen *Acinetobacter baumannii*. *J. Bacteriol.* **197**, 2027–2035 (2015).

44. Held, K., Ramage, E., Jacobs, M., Gallagher, L. & Manoil, C. Sequence-verified two-allele transposon mutant library for *Pseudomonas aeruginosa* PAO1. *J. Bacteriol.* **194**, 6387–6389 (2012).

45. Fey, P. D. *et al.* A genetic resource for rapid and comprehensive phenotype screening of nonessential *Staphylococcus aureus* genes. *mBio* **4**, e00537-12 (2013).

46. Adams, P. D. *et al.* PHENIX : a comprehensive Python-based system for macromolecular structure solution. *Acta Crystallogr. Sect. D Biol. Crystallogr.* **66**, 213–221 (2010).

47. Emsley, P. & Cowtan, K. Coot: Model-building tools for molecular graphics. *Acta Crystallogr. Sect. D Biol. Crystallogr.* **60**, 2126–2132 (2004).

48. Mann, S., Eveleigh, L., Lequin, O. & Ploux, O. A microplate fluorescence assay for DAPA aminotransferase by detection of the vicinal diamine 7,8-diaminopelargonic acid. *Anal. Biochem.* **432**, 90–96 (2013).

Chapter III – Inhibiting fatty acid biosynthesis overcomes colistin resistance

Preface

The work presented in this chapter is in review, as of May 4, 2022:

Carfrae, L.A., Rachwalski, K., French, S., Seidel, L., Tsai, C.N., Tu, M.M., MacNair, C.R., Ovchinnikova, O.G., Whitfield, C., and Brown, E.D., Inhibiting fatty acid biosynthesis overcomes colistin resistance. *Under review at Nature Microbiology.* Manuscript #: NMICROBIOL-22051089. (2022).

LAC performed all experiments, LAC and EDB wrote the manuscript.

Abstract

The treatment of multidrug-resistant infections has become increasingly reliant on last-resort antibiotics, including the cationic antimicrobial peptides, colistin (polymyxin E) and polymyxin B. Unfortunately, with more routine use, the prevalence of polymyxin resistance is on the rise and increases mortality rates, for example, in patients with bloodstream infections. Restoring sensitivity to polymyxins using combination therapy is a promising approach to reviving its clinical utility. Herein, we describe the ability of the biotin biosynthesis inhibitor, MAC13772, to synergize with colistin exclusively against colistin-resistant Enterobacteriaceae. MAC13772 indirectly disrupts fatty acid biosynthesis and restores sensitivity to the last-resort antibiotic, colistin. Accordingly, we found combinations of colistin and other fatty acid biosynthesis inhibitors, cerulenin, triclosan and Debio1452-NH_3, had broad potential against both chromosomal and plasmid-mediated colistin resistance. Furthermore, combining a subinhibitory concentration of a fatty acid biosynthesis inhibitor with colistin reduced the rate of spontaneous resistance development. Combination therapy with colistin and the clinically relevant FabI inhibitor, Debio1452-NH_3, showed efficacy against *mcr-1* positive *Klebsiella pneumoniae* and colistin-resistant *Escherichia coli* systemic infections in mice. We propose that inhibiting fatty acid biosynthesis restores colistin sensitivity through changes to membrane fluidity and phospholipid

composition. In all, this work reveals a surprising link between fatty acid biosynthesis and colistin resistance.

Introduction

The rise of antibiotic-resistant Gram-negative pathogens forces clinicians to rely on last-resort antibiotics, including polymyxins (polymyxin B and polymyxin E/colistin). Unfortunately, resistance to last-resort antibiotics is limiting to their clinical utility[1]. In 2015, the first plasmid-mediated colistin resistance gene (*mcr-1*) was identified in an agricultural *E. coli* isolate[2]. Since its initial discovery, colistin-resistant isolates carrying *mcr-1* and orthologues (*mcr-2-10*) have been detected globally and found in multidrug-resistant bacterial isolates[2,3]. Multidrug-resistant strains containing *mcr-1* alongside extended-spectrum β-lactamase and carbapenemase resistance genes are particularly concerning[4,5]. In addition to pre-existing chromosomally mediated colistin resistance, the emergence of *mcr-1* threatens to diminish the therapeutic utility of polymyxins from an already shrinking antibiotic arsenal. Furthermore, colistin resistance is linked to increased mortality rates in bloodstream infections[6,7]. Accordingly, the World Health Organization has prioritized the development of novel antimicrobials against multidrug-resistant Gram-negative pathogens, including *Acinetobacter baumannii,* Enterobacteriaceae*,* and *Pseudomonas aeruginosa.*

Gram-negative bacteria are particularly challenging to antibiotic discovery, due in large part to the permeability barrier of the outer membrane[8]. The outer membrane is a unique asymmetric bilayer composed of an outer leaflet of lipopolysaccharides (LPS) and an inner membrane of phospholipids. LPS is

composed of a negatively charged, hydrophobic lipid A anchor linked to an oligosaccharide core[9]. Adjacent LPS molecules are stabilized in the outer membrane by bridging with divalent cations (Ca^{2+} and Mg^{2+})[10]. Polymyxins lyse Gram-negative bacteria through their interaction with the lipid A component of LPS, resulting in outer membrane destabilization followed by leakage of cytoplasmic contents[11–13]. Despite the clinical use of colistin, its precise mechanism of lysis remains unknown. Recent work has implicated LPS in the outer leaflet of the cytoplasmic membrane as colistin's ultimate target[14], consistent with the widely recognized mechanism where colistin disrupts the physical integrity of the cytoplasmic membrane, causing leakage of intracellular contents[11].

Resistance to polymyxin antibiotics is predominantly mediated through modifications to the lipid A component of LPS[15]. LPS is typically modified in response to environmental signals, including the presence of cationic peptides, or fluctuations in ions such as Al^{3+}, Fe^{3+}, Mg^{2+}, and PO_4^{3-} [16–18]. The PhoPQ and PmrAB two-component signal transduction systems mediate modifications to lipid A in Enterobacteriaceae species through the regulation of 4-amino-4-deoxy-arabinose (L-Ara4N) or phosphoethanolamine (PEtN) transferases (*arnT* and *eptA,* respectively)[15,16]. The addition of L-Ara4N or PEtN to the 1' and/or 4' phosphates of lipid A reduces the net anionic charge of the cell surface, conferring resistance to polymyxins[19]. Chromosomal mutations activating the

PhoPQ and PmrAB two-component systems are commonly associated with polymyxin resistance[20]. Similarly, *mcr-1* is an orthologue of *eptA,* conferring resistance through PEtN modification of lipid A[2]. Modification of lipid A has a limited impact on polymyxin's ability to permeabilize the outer membrane; yet inhibits polymyxin's lytic activity[14,21]. Recent evidence suggests the modification of LPS molecules in the outer leaflet of the cytoplasmic membrane facilitates this protection[14].

Efforts to identify and modify novel colistin congeners have recently succeeded in overcoming colistin resistance[22,23]. Another promising approach to prolong the clinical utility of polymyxins is applying combination therapy approaches. Polymyxin has proven to be a synergistic partner with compounds: (i) targeting enzymes responsible for the modification of lipid A, (ii) disrupting the cytoplasmic membrane or proton motive force to exacerbate polymyxin lysis, (iii) targeting two-component systems controlling lipid A modification, or (iv) functioning as antimicrobials that require polymyxins for entry[15]. There is renewed interest in polymyxins' ability to potentiate antibiotic entry in both polymyxin susceptible and resistant isolates[3,21,24]. The combination of colistin with other antibiotics, including rifampicin[25], carbapenems[26], macrolides[27], tigecycline[28], and glycopeptides[29], have been applied in dose-sparing regimes with varying degrees of success. Antibiotic adjuvants inhibiting the expression of the two-component systems PmrAB or PhoPQ controlled genes have been identified but are not

effective against plasmid-mediated resistance[30–32]. Undirected compound screening approaches for synergistic combinations have further identified bioactive compounds where the mechanism of synergy remains unidentified[33,34]. Despite a resurgence of effort in this area, there is still a need for novel combinations with efficacy against colistin-resistant pathogens. Antibiotic resistance is a resource-intensive process that often exerts a fitness cost requiring bacteria to undergo changes in their metabolic pathways[35]. Exploiting altered metabolic pathways may represent an untapped target space for developing innovative therapies specifically against drug-resistant bacteria.

Here, we show that the inhibition of fatty acid biosynthesis can overcome polymyxin resistance and prevent the development of spontaneous resistance. We demonstrate that colistin synergizes with both indirect inhibition of fatty acid biosynthesis through the biotin biosynthesis inhibitor, MAC13772, or direct inhibition with cerulenin, triclosan and Debio1452-NH_3, exclusively against colistin-resistant bacteria. Combining these molecules with colistin is effective against plasmid-mediated and chromosomal resistance mechanisms. Inhibiting fatty acid biosynthesis resensitizes *mcr-1* expressing bacteria to the bactericidal activity of colistin without altering PEtN lipid A modification. We propose that MAC13772 restores colistin sensitivity through an indirect mechanism, where the reliance of fatty acid biosynthesis on biotin leads to changes in membrane fluidity and phospholipid composition, revealing an exploitable link between fatty acid

biosynthesis and colistin resistance. The combination of colistin and a fatty acid biosynthesis inhibitor was efficacious in mouse infection models using *mcr-1*-positive hypervirulent *K. pneumoniae* and colistin-resistant *E. coli*.

Results

Colistin synergizes with MAC13772 against *mcr-1* expressing Enterobacteriaceae

Biotin biosynthesis genes in *E. coli*[36] and *A. baumannii*[37] are upregulated in response to colistin treatment, implicating biotin in the response to colistin-mediated membrane damage. Therefore, we probed the combinatory potential of the biotin biosynthesis inhibitor, MAC13772, with colistin against colistin-resistant and colistin-sensitive *E. coli*. In a chequerboard assay, combining subinhibitory concentrations of MAC13772 and colistin, the two drugs were synergistic (fractional inhibitory concentration index (FIC_i) =0.15; Figure 1a) against *mcr-1* expressing *E. coli*. In contrast, the synergy was lost (FIC_i=0.70) when evaluated against *E. coli* expressing the empty vector (pGDP2-*empty*; Figure 1b). The combination was also synergistic against a wide variety of clinically important *mcr-1* expressing Enterobacteriaceae, including *Enterobacter cloacae, Klebsiella aerogenes, K. pneumoniae,* and *Salmonella enterica* sv. Typhimurium (Figure 1c; Table S1). The synergistic combination persisted against two foodborne *E. coli* isolates harbouring the *mcr-1* gene on natural plasmids (FIC_i=0.14, Figure S1).

Notably, in all combinations, the presence of MAC13772 decreased the colistin MIC to below 2 μg/mL (Table S1), which represents a concentration obtainable during standard therapeutic colistin dosing[38].

To ensure colistin was disrupting outer-membrane integrity through its association with LPS, we tested the effect of adding exogenous LPS into the growth medium. Adding purified *E. coli* LPS (1 mg/mL) to the growth medium abolished synergy (FIC_i=1; Figure S2a; Table S1). Synergy was also abolished in media with high Mg^{2+} levels (20 mM; FIC_i= 1; Figure S2b; Table S1), consistent with Mg^{2+} stabilizing electrostatic interactions between adjacent LPS molecules[39]. MAC13772 was similarly acting on target, with the addition of biotin (10 μg/mL) to the media or overexpression of *bioA* abolishing the synergy (FIC_i=0.85 & FIC_i =0.68; Figure S3a-c; Table S1). We also elicited increased colistin susceptibility (32-fold) using a CRISPR knockdown of *bioA*, demonstrating that both genetic and chemical manipulation result in similar phenotypes (Figure S3d-e).

High levels of *mcr-1* expression result in severe morphology, virulence, and growth defects caused by both the embedding of the protein in the *E. coli* cytoplasmic membrane and the PEtN modification of LPS[40]. To distinguish if the synergy between colistin and MAC13772 results from MCR-1's catalytic activity or incorporation of the protein in the inner membrane, we evaluated the synergy in *E. coli* expressing the catalytically inactive *mcr-1* (E246A)[40,41]. The pairing of colistin with MAC13772 was not synergistic against *E. coli* pGDP2-*mcr-*

*1::*E246A, demonstrating that LPS modification is required for synergy (FIC_i=0.80; Figure S4; Table S1).

Combinations of fatty acid biosynthesis inhibitors and colistin are synergistic against *mcr-1* expressing Enterobacteriaceae

MAC13772 inhibits biotin biosynthesis, an essential cofactor for bacterial growth[42,43]. In *E. coli,* a single biotin-dependent enzyme, acetyl-CoA carboxylase, is responsible for catalyzing the first committed step of fatty acid biosynthesis (Figure 1f), the conversion of acetyl-CoA to malonyl-CoA[44,45]. We posited that inhibiting fatty acid biosynthesis would elicit a similar synergy with colistin against resistant bacteria. The natural product cerulenin, an inhibitor of β-ketoacyl-ACP synthases (FabB) in *E. coli* [46,47]*,* exhibited synergy with colistin against *mcr-1* expressing *E. coli* (FIC_i=0.11; Figure 1d; Table S1). The combination was efficacious against *mcr-1* expressing *E. aerogenes, E. cloacae, K. pneumoniae,* and *S.* Typhimurium, with FIC_i values ranging from 0.13-0.24 (Figure 1c; Table S1). In contrast, there were minimal changes in susceptibility (FIC_i 0.58-0.72) against wild-type bacterial isolates (Figure 1c; Table S1). Similarly, the FabI inhibitor, triclosan[48], synergized with colistin against *E. coli* expressing *mcr-1* (FIC_i=0.11; Figure 1e) and increased colistin susceptibility in all *mcr-1* expressing isolates (FIC_i 0.07-0.15; Figure 1c; Table S1). Subinhibitory triclosan had minimal effects (FIC_i 0.38-0.58) against wild-type bacteria (Figure 1c; Table S1). Combinations of cerulenin and triclosan with colistin were effective against two

foodborne *E. coli* isolates (N15-02865 and N15-02866) harbouring the *mcr-1* gene on natural plasmids (FIC_i =0.11 and FIC_i=0.09, respectively; Figure S1; Table S1).

The combination of MAC13772 and colistin is effective against a wide variety of colistin-resistant pathogens

Given the efficacy of the combinations against plasmid-mediated colistin resistance, we looked to evaluate their spectrum of coverage. We examined the efficacy of the combinations against colistin-resistant clinical isolates of *E. coli* and *K. pneumoniae*, intrinsically colistin-resistant *Serratia marcescens* and *Staphylococcus aureus,* and a pan-drug resistant strain of *A. baumannii*. Subinhibitory concentrations (¼ MIC) of cerulenin, MAC13772, and triclosan, increased susceptibility to colistin 32-fold against the colistin-resistant isolates: *E. coli* C0244, and *K. pneumoniae* C0106, C0298, and C0373 (Table S2, S3). Notably, against 10 colistin-sensitive *E. coli* and 6 colistin-sensitive *K. pneumoniae* clinical isolates, there was no more than a 2-fold change in colistin susceptibility (Table S2, S3). *S. marcescens* is extremely colistin-resistant (MIC=10 mg/mL); however, the presence of subinhibitory concentrations of cerulenin, MAC13772, or triclosan reduced the colistin MIC 64-128-fold (FIC_i 0.12-0.17; Figure S5a; Table S1). Similarly, all three inhibitors increased the susceptibility of *A. baumannii* CDC 288 (MIC=1 mg/mL) to colistin up to 64-fold (FIC_i 0.14-0.18; Figure S5b; Table S1). When tested against the Gram-positive

pathogen *S. aureus*, no synergy was observed with either cerulenin (FIC_i=0.75) or triclosan (FIC_i=0.63), confirming the importance of LPS in the synergistic interaction (Figure S5c; Table S1). Overall, the combinations of cerulenin, MAC13772, and triclosan with colistin are broadly applicable to colistin-resistant Gram-negative pathogens.

Inhibition of fatty acid biosynthesis induces synergy in colistin resistance mediated by L-Ara4N modification of lipid A

In many of the tested clinical isolates, the mechanism of colistin resistance has not been characterized. Chromosomally mediated colistin resistance commonly induces the overexpression of L-Ara4N and PEtN modifications of LPS[49]. Given the applicability of combinations of colistin and fatty acid biosynthesis inhibitors against *mcr-1* expressing bacteria, we were interested in determining if the synergy was specific to PEtN decorated LPS. We implemented a chemical genomics approach with a transposon library in the colistin-resistant strain, *K. pneumoniae* MKP103 (colistin MIC=400 µg/mL; Table S1). *K. pneumoniae* MKP103 was susceptible to combinations of cerulenin, MAC13772, and triclosan paired with colistin (Figure S6). To understand the genetic determinants of colistin resistance, we screened the transposon library against a subinhibitory concentration of colistin (⅛ MIC). We looked for any mutant with increased sensitivity to colistin alone, excluding all strains with a fitness defect in M9 minimal media (<50% growth). In total, 133 independent mutants in the library

fit this criterion, representing 96 different genes (Figure S7a; Table S4). A diverse range of bacterial pathways were enriched among these mutants, including genes involved in lipid A modification (*arnA, arnB, arnC, arnD, arnT, phoPQ*), cell division (*envC, ftsK, ftsN, ftsX, nlpD, pal, tolA, tolB, tolQ, tolR*), and enterobactin biosynthesis (*entA, entD, entE, fes*) (Figure S7a; Table S4). The inactivation of genes involved in L-Ara4N biosynthesis and transfer to lipid A increased colistin sensitivity by 800-fold, while the predicted PEtN transferase (KPNIH1_25195) had no impact on colistin susceptibility. We predict that colistin resistance in *K. pneumoniae* MKP103 is mediated primarily by L-Ara4N decoration, not PEtN decoration. Importantly, this demonstrated that combinations of colistin with cerulenin, MAC13772, and triclosan are also efficacious against colistin resistance mediated by L-Ara4N decoration of lipid A. The screen also revealed a non-inactivating transposon insertion (at 95 base pairs into the gene) in the essential biotin ligase, *birA*, was sensitized to colistin, further highlighting the importance of biotin biosynthesis to colistin resistance. Several mutants with increased sensitivity to colistin, including *arnA*, *arnB*, *arnC*, *arnD*, *arnT*, *birA, entA, entD, entE, fes*, *ftsX*, *pal*, *phoP*, *phoQ*, *tolQ*, and *tolR* were not further potentiated for colistin sensitivity in the presence of MAC13772 or triclosan, demonstrating that the synergy is specific to colistin-resistant pathogens (Figure S7b; Table S5).

Cerulenin, MAC13772, and triclosan do not synergize with outer membrane permeabilizing agents

Having confirmed the potential of pairing colistin with fatty acid biosynthesis inhibitors against colistin-resistant pathogens, we looked to explore the mechanism of synergy. Previous work has demonstrated the ability of polymyxins to potentiate the activity of large-scaffold hydrophobic antibiotics through the disruption of the outer membrane[50]. To determine if the synergy between fatty acid biosynthesis inhibitors and colistin resulted from colistin permeabilizing the outer membrane, we evaluated the synergy between cerulenin, MAC13772, and triclosan and known outer membrane potentiating compounds, ethylenediaminetetraacetic acid (EDTA) and pentamidine. Pentamidine perturbs the outer membrane through its interaction with lipid A[51], while EDTA is a metal chelator that induces outer-membrane disruption through the destabilization of Mg^{2+} bridging between LPS molecules[52]. Notably, combinations of fatty acid biosynthesis inhibitors with either pentamidine or EDTA did not demonstrate any synergy against *mcr-1* expressing *E. coli* (FIC_i=0.60-0.92; Figure 2a-b; Figure S8). To further verify that colistin does not increase the intracellular accumulation of cerulenin, MAC13772, or triclosan, we assessed the ability of colistin to enhance the cytoplasmic accumulation of the inhibitors using liquid chromatography with tandem mass spectrometry (LC-MS/MS)[53]. There was no significant difference in intracellular accumulation of MAC13772 (1.0-fold;

p=0.82), cerulenin (1.2-fold; *p*=0.20), or triclosan (1.4-fold; *p*=0.56) in *mcr-1* expressing *E. coli* in the presence of colistin (6 μM; Figure 2c, Figure S9a,b). Importantly, in the presence of colistin the intracellular rifampicin concentration increased 6.1-fold (*p*=0.01) (Figure S9c). These findings suggest that increased intracellular accumulation of fatty acid biosynthesis inhibitors is not responsible for the synergy, supporting an alternative mechanism.

Cerulenin, MAC13772, and triclosan do not target the bacterial inner membrane

We next screened nine additional antibiotics, including DNA-damaging molecules, macrolides, translation inhibitors, and β-lactams, for changes in their minimal inhibitory concentration (MIC) in the presence of MAC13772 to ensure that MAC13772 synergizes selectively with polymyxin antibiotics. We observed no potentiation in any of the combinations and did not see synergy with any antibiotics typically restricted to Gram-positive bacteria, indicating MAC13772 was not potentiating the activity of colistin by disrupting the outer membrane (Figure S10; Table S6). Chemicals that target the bacterial inner membrane are known to synergize with polymyxin antibiotics[54], as well as with other inner membrane disruptors[55]. To exclude disruption of the proton motive force as a potential mechanism of action, we examined the impact of cerulenin, MAC13772, and triclosan on the inner membrane. We determined that cerulenin, MAC13772, and triclosan did not significantly alter fluorescence produced by 3,3'-

dipropylthiadicarbo-cyanine iodide ($DiSC_3(5)$; Figure S11a), a probe that accumulates in the inner membrane in a manner dependent on the proton motive force[56]. Moreover, cerulenin, MAC13772, and triclosan did not exhibit synergy with carbonyl cyanide m-chlorophenyl hydrazone (CCCP), an ionophore that dissipates the proton gradient across the inner membrane (Figure 3d, S11b-c). Taken together, these data suggest that inhibition of fatty acid biosynthesis does not lead to disruption of the bacterial inner membrane or membrane potential.

The combination of MAC13772 and colistin is lytic against *mcr-1* expressing *E. coli*

We then sought to determine the directionality of potentiation between MAC13772 and colistin. MCR-1 mediated lipid A modification provides resistance to colistin-induced lysis but not outer-membrane perturbation[21]. We hypothesized that if MAC13772 is resensitizing *mcr-1* expressing *E. coli* to colistin, then the combinations would be bactericidal. We assessed the efficacy of MAC13772 and colistin in a bacterial cell-killing assay. The presence of colistin (2 μg/mL; ⅛ MIC) or MAC13772 (32 μg/mL; ¼ MIC) alone are unable to inhibit the growth of *mcr-1* expressing *E. coli* (Figure 2e). The combination of colistin (2 μg/mL) and MAC13772 (32 μg/mL) led to a 3.01-$\log_{10}$ decrease in bacterial load over 24-hours (Figure 2e). The in vitro killing kinetics were relatively slow, with only a 0.66-$\log_{10}$ reduction after 8 hours. Notably, MAC13772 (4×MIC) is bacteriostatic (Figure S12). The bactericidal nature of the interaction suggests that colistin was

the lysing agent while MAC13772 resensitized resistant bacteria to colistin. Similarly, combinations of cerulenin and triclosan with colistin were bactericidal (Figure S13).

We speculated that changes to lipid A decoration could resensitize *mcr-1* expressing bacteria to colistin. We evaluated the levels of MCR-1 protein in *E. coli* treated with cerulenin (½ MIC), MAC13772 (½ MIC), or triclosan (½ MIC). There were no changes in the abundance of MCR-1 protein following treatment with an inhibitor of fatty acid biosynthesis (Figure S14). We next looked to isolate lipid A from *E. coli* expressing *mcr-1* grown in the presence of cerulenin (½ MIC), MAC13772 (½ MIC) or triclosan (½ MIC) and compared the extent of lipid A modification to untreated *E. coli* by MALDI-TOF mass spectrometry. As expected, analysis of lipid A from *mcr-1* expressing *E. coli* produced a major molecular ion at 1919.5 *m/z* corresponding to PEtN modified lipid A that was absent in *E. coli* expressing the empty vector (Figure 2f, Figure S15). Cerulenin, MAC13772 or triclosan had no impact on lipid A decoration with PEtN (Figure 2g; Figure S16).

mcr-1 expression and MAC13772 treatment induce cell envelope stress responses

To understand the physiologic response of *E. coli* to both *mcr-1* expression and MAC13772 treatment, we conducted RNA sequencing. To investigate the impact of *mcr-1* expression, we sequenced total RNA from *E. coli*

expressing either *mcr-1* or containing the empty vector. A total of 99 genes were differentially regulated (p_{adj}<0.05) in *mcr-1* expressing *E. coli*, with 23 upregulated and 76 downregulated. We observed the downregulation of genes involved in cell motility, flagella biosynthesis, and chemotaxis, as well as the upregulation of genes required for colanic acid biosynthesis (Figure 3a, Figure S17a,c; Tables S7). Interestingly, previous work has shown that the Rcs phosphorelay system mediates the expression of motility genes and colanic acid biosynthesis in response to cell envelope stress. Specifically, truncations to LPS inner core[57,58], low temperature[59] and osmotic stress[60] are associated with a decrease in flagellar biosynthesis and increases in colanic acid biosynthesis (Figure 3c). Similar transcriptional profiles are also associated with perturbation of the cell envelope with polymyxins and inhibitors of lipoprotein transport[61].

To examine the impact of MAC13772 treatment, *E. coli* expressing *mcr-1* was grown to mid-log phase in the presence of MAC13772 (½ MIC), and whole-transcriptome sequencing was performed. MAC13772 treatment of *mcr-1* expressing *E. coli* led to the differential expression of 196 genes (p_{adj}<0.05; $\log_2$>2) compared to *mcr-1* expressing *E. coli*, with 53 genes upregulated and 143 genes downregulated. Similar to *mcr-1* expression, treatment with MAC13772 repressed motility genes and upregulated colanic acid biosynthesis genes (Figure 3b; Figure S17b,d; Table S7). In addition to genes under the control of the Rcs phosphorelay system, genes in the Cpx regulon, and phage

shock proteins (Psp) had altered expression specific to MAC13772 treatment (Figure 3b,d; Figure S17b,d; Table S7). The Cpx two-component signal transduction pathway and the Psp stress-response system mediate adaptation to envelope protein misfolding and stabilize the cell membrane, respectively[62,63]. Notably, a subset of genes involved in fatty acid biosynthesis and biotin biosynthesis were also upregulated in response to treatment with MAC13772 (Figure 3b, Table S7).

We were interested if the changes to the transcription of motility genes led to a detectable motility phenotype. Indeed, *mcr-1* expression reduced motility by 2-fold compared to the vector control (Figure S18a). Further, MAC13772 treatment of *E. coli* expressing *mcr-1* had a dose-dependent decrease in bacterial motility (Figure S18b). Bacterial motility plays an important role in biofilm formation; deletions in motility genes are associated with impaired biofilm formation[64,65]. Expression of *mcr-1* was associated with a 1.96-fold reduction in biofilm formation after 48 hours of growth (Figure S18c). Similarly, it has been demonstrated that chromosomally mediated colistin resistance is associated with reduced biofilm formation[66]. Genes in colanic acid biosynthesis play an important role in the late stages of biofilm formation[67]. However, their overexpression does not overcome the impact of motility defects. We suggest that even though this level of *mcr-1* expression does not alter bacterial cell viability, it modifies bacterial physiology inducing cell envelope stress.

Inhibition of fatty acid biosynthesis alters membrane fluidity and phospholipid profile in *mcr-1* expressing *E. coli*

To determine if the observed membrane stress response was related to the outer membrane or the cytoplasmic membrane, we evaluated the synergy between MAC13772 and colistin in an *E. coli* strain engineered with a chromosomally encoded open pore (Pore) with a 2.4 nm internal diameter to allow for the easy influx of molecules across the outer membrane[68]. Interestingly, the *E. coli*-Pore background did not alter the effect of *mcr-1* expression on colistin resistance, supporting the recent assertion that PEtN modified LPS in the inner membrane is a mediator of colistin resistance[14]. Furthermore, the synergy between MAC13772 and colistin was maintained against *E. coli*-Pore expressing *mcr-1* (FIC_i=0.13; Figure 4a).

To further explore how inhibiting fatty acid biosynthesis alters colistin susceptibility in *mcr-1* expressing *E. coli*, we examined the impact of inhibition on the downstream pathways: phospholipid and LPS biosynthesis (Figure S19)[69]. *E. coli* can uptake exogenous fatty acids, and FadD generates acyl-CoA for incorporation into phospholipid biosynthesis[70]. However, exogenous *R*-3-hydroxymyristoyl-ACP, required for lipid A biosynthesis, cannot be synthesized from exogenous fatty acids[69,71,72]. Accordingly, we looked to distinguish the importance of inhibiting phospholipid biosynthesis from LPS biosynthesis through the supplementation of exogenous fatty acids. We found that adding 2-

hexadecenoic acid (40 μg/mL) or oleic acid (50 μg/mL) impacts colistin's growth inhibitory effects with a 4-fold decrease and 2-fold increase in MIC, respectively. Interestingly, the addition of both 2-hexadecenoic acid and oleic acid completely abolished the synergy between colistin and MAC13772 against *E. coli* expressing *mcr-1* (FIC_i=0.63 and 1, respectively; Figure S19b,c). The suppression of synergy with fatty acid supplementation suggested that the impact of MAC13772 on phospholipid biosynthesis mediates the synergy with colistin.

We hypothesized that MAC13772 induced changes that alter colistin's interaction with the inner membrane. To investigate, we looked at the impact of fatty acid biosynthesis inhibitors on membrane fluidity. *E. coli* expressing *mcr-1* or the empty vector were grown in subinhibitory concentrations (½ MIC) of cerulenin or MAC13772, and membrane fluidity was evaluated by monitoring fluorescence polarization using the probe 1,6-diphenyl-1,3,5-hexatriene (DPH). Membrane fluidity was unaffected by *mcr-1* expression, however, treatment with cerulenin or MAC13772 increased fluorescence polarization (decreased fluidity) compared to untreated cells in *E. coli* expressing *mcr-1* or the empty vector (p<0.05; Figure 4b). We applied untargeted lipidomic analysis to understand the factors mediating the decrease in membrane fluidity following MAC13772 treatment (Figure S20-22). MAC13772 treatment caused a 10% and 17% reduction in phosphatidylethanolamine (PE) in *E. coli* expressing the empty vector or *mcr-1*, respectively (Figure 4c-d). The average chain length and unsaturation of PE

remained unchanged, and the major PE species was PE 17:1/16:0 in all cultures (Table S8). Notably, in *mcr-1* expressing cells, an increase in phosphatidylglycerol (PG), lyso-PG, and diacylglycerols (DG) accompanied the decrease in PE (Figure 4c-d). Although there were no changes to PE unsaturation following MAC13772 treatment, there was an overall enrichment for fatty acids with no chain unsaturation and this trend was maintained in PG (Figure S22).

To understand the importance of PE to colistin resistance, we constructed CRISPR knockdowns using an anhydrotetracycline inducible promotor, targeting phospholipid biosynthesis genes *pssA, psd, pgsA,* and *cdsA* (Figure 4e, Figure S23). Induction of knockdown with *pssA*, *psd*, and *cdsA* sensitized *mcr-1* expressing *E. coli* strains to colistin but did not affect *E. coli* expressing the empty vector. In contrast, knockdown of *pgsA,* upstream of PG biosynthesis, had no impact on colistin sensitivity (Figure S23). Genetic perturbation of PE biosynthesis mimicked the phenotypes observed with MAC13772 perturbation. However, we acknowledge additional subtle changes to membrane composition may mediate the synergy.

The combination of colistin and triclosan is efficacious in treating an *mcr-1* expressing *K. pneumoniae* murine infection

Given the therapeutic potential of combination therapy, we investigated using a fatty acid biosynthesis inhibitor alongside colistin in a murine model of *mcr-1*-positive *K. pneumoniae* infection. Recognizing the potential for dose-sparing during drug combination therapies and noting concerns of colistin toxicity, we tested the efficacy of colistin at approximately one-fifth of the human equivalent dose[73,74]. We sought to test the efficacy with a clinically relevant fatty acid biosynthesis inhibitor. Debio1452 (also called AFN1252) is an inhibitor of FabI identified at GlaxoSmithKline that is currently in Phase II clinical trials. Although the activity of Debio1452 is limited to Gram-positive bacteria, an analogue, Debio1452-NH_3, is well-tolerated in vivo and has potent activity against Gram-negative pathogens[75]. We found that Debio1452-NH_3 synergized with colistin against *K. pneumoniae* expressing *mcr-1* (FIC_i=0.08) and a colistin-resistant clinical isolate of *E. coli* (FIC_i=0.11; Figure S24).

Hypervirulent *K. pneumoniae* bloodstream infections cause a high level of patient mortality and are prototypical cases for last-resort therapeutic options[76,77]. Mice were inoculated with *mcr-1* expressing hypervirulent *K. pneumoniae* at a dose leading to systemic infection with 100% lethality within 12 hours. Monotherapy treatments of colistin (5 mg/kg) or Debio1452-NH_3 (17.5 mg/kg), administered 1-hour post-infection, did not demonstrate a significant decrease in bacterial load in the blood beyond that of the untreated mice (Figure 5a). However, the combination of Debio-1452-NH_3 and colistin was efficacious,

resulting in a 3.5-$\log_{10}$ reduction in bacterial load in the blood compared to the vehicle (p<0.01; Figure 5a). Similarly, against a systemic infection of colistin-resistant *E. coli,* Debio-1452-NH_3 and colistin led to a 3.9-$\log_{10}$ reduction of the bacterial load in the blood compared to the vehicle control (p<0.05, Figure 5b).

Subinhibitory concentrations of cerulenin, MAC13772, and triclosan reduce the emergence of colistin resistance

Traditionally, combinations of antibiotics require the efficacy of both components to inhibit bacterial growth[35,78]. As such, resistance may develop more rapidly than in monotherapy approaches. However, in the scenario where a pair of drugs is only synergistic following the development of resistance, it may be possible to invert the selective pressure to favour sensitivity[35]. Given the ability of MAC13772 to reverse colistin resistance, we hypothesized that the presence of subinhibitory MAC13772 would also be able to limit the development of resistance to colistin. We examined the development of resistance by serial passaging *E. coli* in colistin either alone or with cerulenin (¼ MIC), MAC13772 (¼ MIC), or triclosan (¼ MIC). In the control condition, *E. coli* rapidly gained resistance to colistin, with a 64-fold increase in MIC observed within an average of 10 days (Figure 5c). However, passage in the presence of MAC13772 increased the time to acquire resistance to 19 days, and passages with cerulenin or triclosan showed only a two- and four-fold increase in MIC, respectively, after

21 days (Figure 5c). For passages with cerulenin and triclosan, the MIC of colistin remained below breakpoint throughout the experiment.

We isolated the *E. coli* mutants resistant to the combinations of MAC13772 and colistin. Combining colistin with cerulenin or triclosan revealed that resistance was specific to the MAC13772-colistin combination (Figure S25). The isolated resistance mutants reveal cultures must develop resistance to both colistin and the partner drug. Consequently, the substitution of the antibiotic partner could renew treatment efficacy.

Discussion

The increasing incidence of spontaneous colistin resistance and the acquisition of mobile colistin resistance in multidrug-resistant Enterobacteriaceae are resulting in potentially untreatable infections[79–81]. Colistin resistance is implicated in increased mortality rates and treatment failure[6,7]. Combating resistance through combination therapy is a promising approach and has the potential to spare the dose of colistin, a drug with notorious toxicity problems. Finding compounds capable of reversing colistin resistance is integral to maintaining colistin's efficacy as an agent of last resort. This study demonstrates the potential of using biotin and fatty acid biosynthesis inhibitors in combination with colistin to overcome plasmid-mediated and chromosomal colistin resistance. Notably, the efficacy of these combination therapies is maintained against a

plethora of Gram-negative pathogens, including colistin-resistant *A. baumannii, E. cloacae, E. coli, K. aerogenes, K. pneumoniae,* and *S.* Typhimurium. Importantly, against all Enterobacteriaceae species tested, the combinations reduce susceptibility to therapeutically relevant concentrations (<2 μg/mL)[82].

Combinations of colistin with known antibiotics and adjuvants have been used experimentally with varying degrees of success. Previously studied lead molecules have been limited by their spectrum of activity[32,83], unknown mechanism of action[31,34], potential resistance to the partnering drugs[21], and toxicity concerns[33]. Several established mechanisms for synergistic pairings with colistin include increasing intracellular accumulation of the partner antibiotic, synergy with compounds targeting the inner membrane, and reducing PEtN decoration. Based on both direct measurement and pairings with outer membrane permeabilizing compounds (EDTA and pentamidine), it is unlikely that the activity of colistin led to increased intracellular accumulation of fatty acid biosynthesis inhibitors. Mass spectrometry of purified lipid A revealed no changes to PEtN decoration of LPS. In addition, biotin and fatty acid biosynthesis inhibitors did not directly disrupt the proton motive force, as demonstrated by the lack of synergy with CCCP or $DiSC_3(5)$ activity. However, subinhibitory concentrations of biotin and fatty acid biosynthesis inhibitors enhanced colistin's lytic capabilities.

The transcriptomic signature of MAC13772 revealed expression of the Cpx, Psp, and Rsc regulons, indicative of cell envelope stress. Cpx and Rsc

transcriptional responses have been observed in response to polymyxin treatment[36,61], osmotic stress[60], inhibition of lipoprotein transport[61], low temperature[59], and LPS truncation[57,58]. Using a hyperporinated strain of *E. coli* expressing *mcr-1,* we identified the inner membrane as the source of the membrane stress. The addition of a pore across the outer membrane had no impact on colistin resistance. Similarly, in *B. cepacia* with L-Ara4N modified lipid A, no changes in polymyxin susceptibility were observed with the addition of a pore[84]. These findings support the assertion that modified LPS in the inner membrane is protective against polymyxin lysis[14].

We found that biotin and fatty acid biosynthesis inhibitors increased membrane rigidity. Membrane fluidity is directly influenced by lipid head group packing and fatty acid disorder in the membrane. Lipid saturation, chain length, and charge can alter lipid packing and, accordingly fluidity[85]. The addition of exogenous fatty acids to the media suppressed the synergy between pairings of colistin with cerulenin, MAC13772, or triclosan. Lipidomic analysis revealed that MAC13772 treatment led to a 17% decrease in PE in *E. coli* expressing *mcr-1*. Mimicking the decrease in PE using CRISPR knockdowns in *pssA, psd,* and *cdsA,* we induced colistin sensitivity exclusively in *mcr-1* expressing *E. coli*. Although knockdown of PE phenocopies the changes to colistin sensitivity following MAC13772 treatment, it remains possible that sensitivity is mediated by a loss of substrate for *mcr-1* modification of lipid A specific to the cytoplasmic

membrane. Increases to DG, LPG and PG occurred following MAC13772 treatment. The accumulation of DG has been associated with colistin sensitivity through indirect inhibition of lipid A modification[86]. We did not observe detectable changes to LPS decoration due potentially to lower levels of DG accumulation. Interestingly, it is hypothesized that in response to cytoplasmic stress, PspA preferentially binds to anionic lipids, PG and PS, to stabilize the membrane and maintain the proton motive force[87]. MAC13772 treated *E. coli* expressing *mcr-1* was enriched for saturated fatty acids, likely resulting in higher packing density and the observed decrease in fluidity. Changes to fatty acid saturation could also be playing a role in mediating colistin sensitivity. Similarly, cerulenin inhibits unsaturated fatty acid synthesis, completely altering the saturation of membrane lipids[88].

A better understanding of colistin's interaction with the inner membrane and the impact of modification to lipid composition on colistin sensitivity is needed. Molecular dynamics simulations show that colistin does not permeabilize the inner membrane but stiffens it by filling the lipid packing defect, increasing lipid tail order, and restricting lipid diffusion[89]. However, changes to membrane composition have not been thoroughly explored in molecular dynamics simulations and in vitro assays are needed to confirm these findings. We propose inhibition of biotin or fatty acid biosynthesis induces cell envelope stress by increasing the rigidity of the inner membrane and altering phospholipid

composition, thereby altering colistin's interaction with the inner membrane to allow lysis (Figure 6). How changes to phospholipid composition and membrane fluidity alter colistin's interaction with modified LPS in the inner membrane remains unclear.

Encouragingly, we found the combination of colistin and the FabI inhibitor, Debio1452-NH_3, is effective against a systemic *mcr-1* expressing hypervirulent *K. pneumoniae* and colistin-resistant *E. coli* infection in mice. The efficacy of Debio1452-NH_3 justifies further efforts toward the preclinical development of the scaffold[75]. Furthermore, this work supports the assertion that biotin and fatty acid biosynthesis are viable targets for future antibiotic development against Enterobacteriaceae. We were also able to prevent the development of colistin resistance in the presence of subinhibitory concentrations of biotin or fatty acid biosynthesis inhibitors. The ability of biotin and fatty acid biosynthesis inhibitors to prevent the development of colistin resistance in vitro raises prospects for the use of such a combination prophylactically in colistin-sensitive infections. We posit that the exploitation of fatty acid biosynthesis inhibitors currently in clinical development can address the emerging threat of colistin-resistant Gram-negative infections.

Methods

Bacterial strains and culture conditions.

A complete list of bacterial strains and plasmids used in the study can be found in Table S9. Overnight cultures of bacteria were inoculated with a single colony and routinely cultured in MHB or M9 minimal medium supplemented with antibiotics as appropriate (ampicillin, 100 µg/mL; chloramphenicol, 20 µg/mL; kanamycin, 50 µg/mL; spectinomycin, 100 µg/mL). M9 medium with 0.4% glucose was used as minimal medium. Unless otherwise specified M9 was supplemented with amino acids; concentrations for amino acid supplementation are shown in Supplementary Table S10.

Plasmids, site-directed mutagenesis.

Bacterial strains were transformed with the pGDP2 backbone constitutively expressing *mcr-1*[90]. The E246A mutation was introduced to the pGDP2-*mcr-1* plasmid using the QuikChange II Site-Directed Mutagenesis Kit [Agilent Technologies], according to kit instructions, using the following primers: *mcr-1* E246A (forward: 5'-CGCGTGCCGTCGCACCGACGACG-3'; reverse: 5'-CGTCGTCGGTGCGACGGCACGCG-3'). Mutations were confirmed by Sanger sequencing using primers outside the promotor (5'- GGACACCATCGAATGGC -3') and terminator (5'-ACATTTCCCCGAAAAGTG-3').

Antibacterial susceptibility testing.

Bacterial isolates were investigated for susceptibility to cerulenin, colistin, Debio1452-NH3, MAC13772, or triclosan. The MIC was determined in M9

minimal medium supplemented with amino acids. Bacterial cultures were prepared by washing an overnight culture in PBS (x 3), resuspending to OD600 0.1, then diluting 1:200 into media. The plates were incubated at 37 °C without shaking overnight (~18 hrs) before the absorbance at OD_{600} was measured. The MIC was defined as the lowest concentration inhibiting visible growth. Susceptibility assays were performed three independent times and the mean of the three reported. Bacteria were considered colistin-resistant with an MIC $\geq$ 2, in accordance with EUCAST[38] and CLSI guidelines[82]. Fold reduction of MIC was determined by dividing the MIC of the antibiotic alone by its MIC in the treatment condition (the presence of ¼ MIC cerulenin, ¼ MIC MAC13772, or ¼ MIC triclosan).

Chequerboard broth microdilution assays.

Overnight cultures (~18 h) of the appropriate strain of bacteria were grown in M9 minimal media supplemented with amino acids. Bacteria were washed 3 times in PBS and diluted to an OD_{600} 0.1, then diluted 1:200 into media (including $MgCl_2$ (20 mM) or LPS (1 mg/mL) from *E. coli* O127:B8 [Sigma-Aldrich] at the indicated concentrations, where appropriate). Chequerboard analyses were conducted with a clear, flat-bottom 96-well assay plate containing 2-fold dilutions of each compound in an 8 x 8 dose-point matrix. The plates were incubated at 37 °C without shaking overnight (~18 h) then the absorbance at OD_{600} was

measured using a Tecan Infinite M1000 Pro plate reader. Heat maps were generated by converting OD_{600} to percent growth.

At least three biological replicates were completed for each combination. The FIC for each drug was calculated by dividing the concentration for the drug in the presence of codrug in combination for a well showing <10% growth, by the MIC for that drug alone. The FIC indices (FIC_Is) are the sum of the FICs for the two compounds being tested and the reported FIC_Is are the mean of the replicates[91]. FIC_I values of ≤ 0.5 were considered synergistic.

Genetic screening.

The *K. pneumoniae* transposon mutant library was pinned from frozen stocks at 384-colony density onto MHB agar medium containing 150 µg/mL chloramphenicol using a Singer RoTar HAD [Singer Instruments] and grown for 18 hours at 37°C. The library was then grown overnight in 384-well clear flat-bottom plates [Corning] in M9 minimal medium supplemented with amino acids and chloramphenicol (150 µg/mL). The Singer RoTar HAD was used to inoculate assay plates containing 50 µL/well of M9 minimal media alone or supplemented with MAC13772 (32 µg/mL) or colistin (50 µg/mL). Optical density at 600 nm (OD_{600}) was measured with a Tecan M1000 Infinite Pro plate reader at the time of inoculation (T_0) and after 18 hours (T_{18}) of incubation at 37°C. Growth was calculated by subtracting reads at T_0 from those at T_{18} and interquartile-mean

normalization for the plate was performed as previously described[92]. Mutants that exhibited growth lower than two standard deviations from the mean in MAC13772 or colistin, but not M9, were considered as exclusively defective for growth in that condition. Additional annotations of gene names and function for genes of interest were performed by extracting annotation data for *K. pneumoniae* KPNIH1 and BLAST homology searches[93]. The pathways and gene ontology terms that these genes of interest were associated with were compared to *E. coli* homologs using EcoCyc[94].

$DiSC_3(5)$ assay for inner membrane depolarization.

Effects of MAC13772, cerulenin, and triclosan on the bioenergetics of the cytoplasmic membrane of *E. coli Pore* expressing *mcr-1* (hyperpermeable strain of *E. coli* to allow for dye uptake) were determined using the membrane potential-sensitive cyanine dye $DiSC_3(5)$ by modification of the method of[54]. Briefly, cultures of *E. coli* were grown to exponential phase, washed three times, and resuspended in a buffer containing 5 mM HEPES and 20 mM glucose (pH 7.2). Pellets were resuspended in buffer to OD_{600} = 0.085, loaded with 1 μM $DiSC_3(5)$ and allowed to equilibrate for 1 hour. Cells were then added to a black, flat-bottomed 96-well assay plate containing 2-fold serial dilutions of compound and fluorescence was read using a Tecan Infinite M1000 Pro plate reader using 620 nm excitation and 685 emission wavelengths.

Bacterial lysis assay.

Stationary-phase bacteria were washed in PBS (x 3) and inoculated at $5x10^7$ CFU/mL into 3 mL of M9 supplemented with amino acids containing colistin and/or cerulenin, MAC13772, or triclosan. Cultures were incubated at 37°C, shaking (220 rpm) for 24 hours. Bacteria survival was determined after 0, 2, 4, 8, and 24 hours of incubation by serially diluting in 10-fold steps in PBS, and plating onto MHB agar plates for enumeration.

Accumulation assay.

The accumulation assay was performed in *E. coli* BW25113 pGDP2:*mcr-1* in batches of 12 samples per biological replication, with each biological replicate containing rifampicin as a positive control, as described by[53]. For each replicate, 2.5 ml of an overnight culture of *E. coli* was diluted into 250 ml of fresh M9 minimal media supplemented with amino acids. Cultures were grown at 37 °C with shaking to an optical density at a wavelength of 600 nm (OD_{600}) of 0.5. The bacteria were pelleted at 4,000 rpm for 10 min at 4 °C, and the supernatant was discarded. The pellets were resuspended in 40 ml phosphate buffered saline (PBS) and pelleted as before, and the supernatant was discarded. The pellets were resuspended in 10.8 ml fresh PBS and aliquoted into 12 1.7-ml Eppendorf tubes (890 µl each). The number of colony-forming units (CFU) was determined by 10-fold serial dilutions in PBS plated on LB media and enumerated. The

samples were equilibrated at 37 °C with shaking for 5 min, then compound was added (final concentration = 50 μM) and samples were incubated at 37 °C with shaking for 10 min. Assays measuring permeabilization by colistin were performed as above, with the addition of 6.0 μM colistin sulfate immediately before the compound of interest was added. Colistin concentration was selected to ensure no lysis occurred during incubation. After incubation, 800 μl of the cultures were carefully layered on 700 μl of silicone oil (9:1 AR20 (catalogue number: 174665000)/Sigma High Temperature (Sigma–Aldrich; catalogue number: 175633), cooled to −78 °C). Bacteria were pelleted through the oil by centrifuging at max speed for 2 min at room temperature (with the supernatant remaining above the oil). The supernatant and oil were then removed by pipetting. To lyse the samples, each pellet was resuspended in 200 μl water, and then they were subjected to three freeze–thaw cycle of 3 min in liquid nitrogen followed by 3 min in a water bath at 65 °C. The lysates were pelleted at 13,000 RCF for 2 min at room temperature and the supernatant was collected (180 μl). The debris was resuspended in 100 μl methanol and pelleted as before. The supernatants were removed and combined with the previous supernatants collected. Finally, the remaining debris were removed by centrifuging at 20,000 RCF for 10 min at room temperature.

Supernatants were analyzed with the 6495C Triple Quadrupole LC/MS/MS system (Agilent) in the Centre for Microbial Chemical Biology, McMaster

University. The liquid chromatography separation was performed on an Eclipse Plus C18 column (2.1 x 100mm, 1.8um) with mobile phase A (0.1% formic acid in water) and mobile phase B (0.1% formic acid in acetonitrile). The flow rate was 0.3 ml min^{-1} for rifampicin and triclosan and 0.4 ml min^{-1} for cerulenin and MAC13772 and the injection volume was 5 µl. Mass spectra were acquired under positive electrospray ionization. All compounds reached nM concentrations above the limit of quantitation.

Western blot assay.

Whole-cell lysates were extracted from cultures in mid-log phase of growth (OD_{600} ~0.5) treated with vehicle (DMSO), cerulenin (16 µg/mL), MAC13772 (6 µg/mL), triclosan (0.05 µg/mL) or colistin (4 µg/mL) and were then run on 10% Mini-PROTEAN TGX gels [Bio-Rad]. Samples were transferred onto a nitrocellulose membrane using the Trans Blot Turbo system [Bio-Rad] and were probed with polyclonal mouse MCR-1 (1:10,000; [LS-C501086; LSBio]) or monoclonal mouse α-RNA polymerase (1:15,000; [Cat. No. 663104; BioLegend]) as a control. Membranes were then washed and probed with HRP-conjugated anti-mouse IgG rabbit polyclonal antibody (1:10,000; [AB97046; Abcam]). After incubation of the membrane with a chemiluminescent substrate reagent [Ambersham ECL; Cytiva], bands were visualized using the Chemidoc MP Imager [Bio-Rad].

Lipid A isolation and determination of LPS modification by mass spectrometry.

Lipid A was directly isolated from cultures of *E. coli* expressing *mcr-1* treated with cerulenin, triclosan, or DMSO as previously described[95], and isolated using phenol-chloroform-petroleum (PCP) extraction for *E. coli* expressing *mcr-1* treated with MAC13772 as previously described[96]. Briefly, for direct isolation of lipid A cultures were grown in MHB supplemented with the appropriate antibiotic (16 μg/mL cerulenin or 0.05 μg/mL triclosan) until late-log, cells harvested by centrifugation and washed in PBS. Each cell pellet was extracted with a single phase Bligh/Dyer mixture[97]. After 20 min at room temperature, the mixture was subjected to centrifugation and the resulting cell debris pellet was extracted again with single phase Bligh/Dyer mixture. The final insoluble residue, which contains lipopolysaccharide, was subjected to hydrolysis at 100°C in 12.5 mm sodium acetate buffer, pH 4.5, in the presence of 1% SDS to cleave the Kdo-lipid A linkage[98].The released lipid A molecular species were extracted with a two-phase Bligh/Dyer system consisting of chloroform and methanol (1:1 v/v). The lower phase was extracted, and the upper phase was washed once with a pre-equilibrated acidic lower phase. The pooled lower phases were dried under a stream of N_2 adding chloroform/methanol (4:1, v/v) in the drying process. The isolated lipid A was washed in acidified ethanol, then twice in 95% ethanol, and dried under N_2 to remove any contaminating SDS.

For PCP extraction 3 L cultures of *E. coli* expressing *mcr-1* were grown in M9 supplemented with amino acids and MAC13772 (6 µg/mL), pelleted by centrifugation then frozen and lyophilized. LPS was extracted from dried and finely ground cells by phenol–chloroform–petroleum ether (PCP) extraction[96]. After removal of the chloroform and petroleum ether, the LPS was precipitated by the dropwise addition of water. The precipitated LPS was collected by low-speed centrifugation and washed once with 80% phenol and several times with acetone mixture to remove any phenol. Finally, the phenol-free LPS was suspended in deionized water and collected by centrifugation. This centrifugation step was repeated, and the final precipitate was suspended in water and lyophilized. To isolate lipid A, the sample was resuspended in 0.01 M TEA-citrate (1:1 molar ratio, pH 3.6) and heated to 100°C for 1 hour and the resulting mixture lyophilized. The pellet washed with methanol to remove excess salts and the lipid A extracted with a mixture of chloroform:methanol:water (3:1.5:0.25 v/v).

Lipid A samples were subjected to MALDI-TOF mass spectroscopy analysis, using a Bruker Autoflex Speed MALDI system [Bruker] in reflectron negative ion mode. Equal parts of the lipid sample and the matrix (2,5-Dihydroybenzoic acid [Bruker] saturated in 50% ACN:50% 0.1% TFA) were mixed and applied to the target plate.

RNA isolation and RNA sequencing.

Total RNA was extracted from cultures grown to mid-log phase of growth (OD_{600} ~0.5) using the hot acid phenol method[99], followed by purification with the Monarch Total RNA Miniprep Kit [New England Biolabs]. In brief, *E. coli* pGDP2-*mcr-1* and pGDP2-*empty* were grown overnight in M9 minimal media supplemented with amino acids, then subcultured 1:200 into M9 minimal media and grown in the presence of DMSO, cerulenin (¼ MIC), or MAC13772 (¼ MIC) until an absorbance of OD_{600} ~0.5 was reached (~4 hours). Cultures were stored on ice and growth was stopped through the addition of a 1:10 (phenol:ethanol) solution. Cells were then pelleted (3,500 x g, 10 minutes, 4°C) and stored at -80°C prior to RNA extraction. The cell pellets were resuspended in lysis solution (20 mM NaOAc, 1 mM EDTA, 0.5% SDS) and mixed in a 1:1 ratio with hot acid phenol (65°C) for 10 minutes with gentle mixing. Following centrifugation (16,000 x g, 10 minutes, 4°C), the aqueous phase was extracted once with acid phenol (pH=4.3), and once with phenol:chloroform, then precipitated with ethanol, and loaded onto the RNA purification column of the Monarch total RNA miniprep kit. RNA purification when then conducted according to kit protocol.

Purified RNA was analyzed with BioAnalyzer chip and treated with Ribo-Zero [Illumina] for rRNA depletion, cDNA was barcoded for each sample. cDNA was sequenced on an Illumina HiSeq 2000 platform with single-end reads. Raw reads were processed with FastQC and trimmed with Cutadapt[100] to remove Truseq adapter sequences. Sequencing data was aligned against the reference

genome for *E. coli* K-12 using BWA (mem algorithm)[101] and analyzed using featureCounts[102] and the R package DESeq2[103].

Pathway-tools software[104] was used to test enrichment in biological processes and transcriptional regulation (Fisher exact test; Benjamini-Hochberg Correction), using the EcoCyc databases[94]. Revigo[105] was used to summarize gene ontology terms.

Determination of bacterial motility.

E. coli expressing pGDP2-*empty* or pGDP2-*mcr1* were grown overnight at 37°C in M9 minimal media supplemented with amino acids. Cultures were normalized to an OD_{600} of 0.1 and 10 µL were spotted onto the center of M9 minimal media agarose plates (0.125% w/v) containing various concentrations of MAC13772 or DMSO and incubated at 30°C for 24 hours.

Biofilm formation assays.

Biofilm formation if *E. coli* expressing *mcr-1* or the empty vector was determined in polystyrene 96-well plates as previously described[64], with small modifications. Briefly, bacterial were inoculated 1/500 from an overnight culture and incubated at 30°C for 48 hours. The absorbance at OD_{600} was prior to washing, drying plates at 37°C for 30 minutes, and adding crystal violet to evaluate biofilm formation. After 30 minutes of incubation at room temperature, excess crystal violet was washed away, and the residual was solubilized with

30% acetic acid. Crystal violet was quantified by measuring the absorbance at OD_{570} and the relative amount of biofilm produced calculated by crystal violet (OD_{570})/growth (OD_{600}).

Determination of membrane fluidity.

Membrane fluidity was measured as previous described[106]. In brief, *E. coli* expressing *mcr-1* or the empty vector were subcultured in M9 minimal media with subinhibitory concentrations of MAC13772, cerulenin, triclosan, ethanol (fluidity control), or benzyl alcohol (stabilizing control). Cells were collected by centrifugation (4000 x g) at room temperature and washed 3 times in 20 mM HEPES (pH 7). Cells were resuspended at an OD_{600} of 0.15 and the fluorescent membrane probe 1,6-diphenyl-1,3,5-hexatriene (DPH) was added to a final concentration of 4.3 μM. After incubation at room temperature in the darkness, the samples were analyzed for fluorescence polarization, using excitation and emission wavelengths of 495 and 530 nm, respectively. Florescence polarization was calculated as follows: $P = \frac{I_v - GI_h}{I_v + GI_h}$, where P is fluorescence polarization, G is the instrument grating factor, I_v is the intensity of the emitted beam in the vertical direction, and I_h is the intensity of the emitted beam in the horizontal direction.

Untargeted lipidomic analysis

Sample Preparation: *E. coli* expressing *mcr-1* or the empty vector were cultured in M9 minimal media supplemented with amino acids containing

MAC13772 (¼ MIC) or DMSO. The cell pellets (50-100 mg) were collected at mid-log (OD_{600} 0.4-0.6) and flash frozen. Samples were thawed on ice and suspended in 1.5 mL chloroform:MEOH (2:1, v/v) and 0.5 mL of ultrapure water, mixed and centrifuged at 3,000 rpm. The bottom phase was collected, dried under nitrogen and resuspended in isopropyl alcohol: MeOH (1:1, v/v). LPC (12:0) was then added to each sample as an internal standard. The samples were then centrifuged for 10 minutes (12,000 rpm, 4°C) and the supernatant analyzed using LC-MS.

LS-MS: Separation is performed by Ultimate 3000 LC combined with Q Exactive MS (Thermo) and screened with ESI-MS in positive and negative mode. The LC system is comprised of ACQUITY UPLC BEH C_{18} (100×2.1mm×1.7μm) with Ultimate 3000 LC. The mobile phase is composed of solvent A (60% ACN + 40% H2O + 10 mM HCOONH4). And solvent B (10% CAN+90% isopropyl alcohol-10mM HCOONH4) with a gradient elution (0-10.5 min, 30%-100% B; 10.5 -12.5 minutes, 100% B, 12.5-12.51 min 100%-30% B, 12.51-16.0 min, 30% B). The flow rate of the mobile phase is 0.3 mL/min. The column temperature is maintained at 40 °C, and the sample manager temperature is set at 4°C.

Analysis: Lipids were identified and quantified by Creative Proteomics (Shirley NY, USA). Lipids were filtered by CV% of the QC values, excluding any lipids with a CV% > 30%. Lipid group enrichment and significant changes to lipid molecules were determined using the R package lipidr (version 2.8.1)[107].

CRISPR knockdown assay.

20 bp guide RNAs targeting *E. coli bioA* (sgRNA*bioA* – 5' GGGAGGTCA TGGATGTGTAT 3'), *cdsA* (sgRNA*cdsA* – 5' GTTACAATGGCGAACCCCAC 3'), *pgsA* (sgRNA*pgsA* – 5' AAAAGACCAATACAAAGAAT 3'), *psd* (sgRNA*psd* – 5' CATTCGGATCGGTATCGATT 3'), and *pssA* (sgRNA*pssA* – 5' TTGAGAA ATCTTGGGTAGTT 3') were designed and introduced into pFD152 (Addgene plasmid # 125546; a gift from David Bikard) using a single step golden gate assembly reaction as described[108,109]. sgRNA sequences were verified using Sanger sequencing and the five constructs along with the pFD152 empty vector were transformed in *E. coli* harbouring either *mcr-1* or the corresponding empty vector.

E. coli expressing *mcr-1* or the empty vector and CRISPR knockdown plasmids *pfD152-bioA, pfD152-cdsA, pfD152-pgsA, pfD152-psd, pfd152-pssA,* or *pfD152-empty* were grown overnight in M9 minimal media. The bacterial culture was prepared by washing subculture (OD_{600} 0.3-0.5) in PBS (3 times), resuspending to OD_{600} 0.1, then diluting 1:200 into fresh M9 minimal media supplemented with amino acids. Chequerboard assays analyses were conducted as stated above, with 2-fold dilutions of the inducer anhydrous tetracycline (aTc) and colistin in an 8 x 8 dose-point matrix. The plates were incubated at 37 °C without shaking overnight (~18 h) then the absorbance at OD_{600} was measured

using a Tecan Infinite M1000 Pro plate reader. Heat maps were generated by converting OD_{600} to percent growth.

Animal studies.

All animal studies were conducted according to guidelines set by the Canadian Council on Animal Care using protocols approved by the Animal Review Ethics Board at McMaster University under Animal Use Protocol #20-12-43. All animal studies were performed with 6–10-week-old female CD-1 mice from Envigo. Female mice were used in accordance with previously established models, as well as ease of housing, and randomization. Before infection, mice were relocated at random from a housing cage to treatment or control cages. No animals were excluded from analyses and blinding was considered unnecessary. No assumptions regarding sample or effect size were made. Sample sizes were selected based on results from pilot experiments. All animal experiments were performed a minimum of three independent times and with a minimum of 2 mice included per group.

Mouse systemic infection model.

The combination of colistin and Debio1452-NH_3 was tested against *E. coli* C0244 and *K. pneumoniae* ATCC 43816 transformed with pGDP2:*mcr-1* in an immunocompetent systemic infection model. Female CD-1 mice were infected intraperitoneally with the ~1×10^6 CFU of bacteria suspended in 5% porcine

mucin [Sigma-Aldrich] PBS solution. Infections were established for 1 hour prior to treatment with colistin (1 mg/kg or 5 mg/kg, i.p.), Debio1452-NH_3 (17.5 mg/kg, i.p.), or the combination (colistin and Debio1452-NH_3). The experimental end point was defined as 7 hours after infection. The blood (collected in Li heparin tubes by facial bleed), spleen, kidney, liver and lungs were collected, homogenized, diluted and plated on solid LB or LB supplemented with a kanamycin to enumerate the bacterial load.

Statistical analyses.

Experiments were performed on at least two independent occasions, and the resulting data are presented as the arithmetic mean of these biological repeats, unless stated otherwise. GraphPad Prism 9.3.0 was used for data analysis and figure generation. Data are shown as means ± sem. $P < 0.05$ was considered statistically significant. In this study, no statistical methods were used to predetermine the sample size. The investigators were not blinded to allocation during the experiments and outcome assessments.

Data Availability

RNA sequencing data is available at the NCBI Sequence Read Archive under accession PRJNA824525. The source data underlying Figures 1c, 3a,b, and 4c,d and are provided as Data Tables S1, S7, and S8. The data supporting

the findings of this study are available from the corresponding author on reasonable request.

Acknowledgements

We would like to thank G. Wright for bacterial strains from the Institute for Infectious Disease Research clinical collection, E. Parker and P. Hergenrother for providing ample Debio1452-NH_3 for animal studies, M. Mulvey from the University of Manitoba for providing the environmental *mcr-1*-positive *E. coli* isolates, R. Melano at Public Health Ontario for bacterial strains GB687 and C0064, and D. Bikard for the plasmid, pFD152. The authors also thank the McMaster Centre for Microbial Chemical Biology, specifically, N. Henriquez for LC/MS/MS and S. McCusker for providing bacterial strains. This research was supported by a Tier 1 Canada Research Chair award, a Foundation grant from the Canadian Institutes of Health Research (CHIR; FRN 143215), and a grant from the Ontario Research Fund (RE09-047) to EDB. LAC was supported by a scholarship from the CIHR Canada Graduate Scholarships (CGS-D).

Author contributions

L.A.C. and E.D.B. conceived and designed the research. L.A.C. performed experiments and analyzed data. K.R., S.F., L.S., M.T, C.R.M., O.G.O., and C.W. performed experiments. C.T. analyzed data. C.R.M. and E.D.B. wrote the manuscript.

Figures and Legends

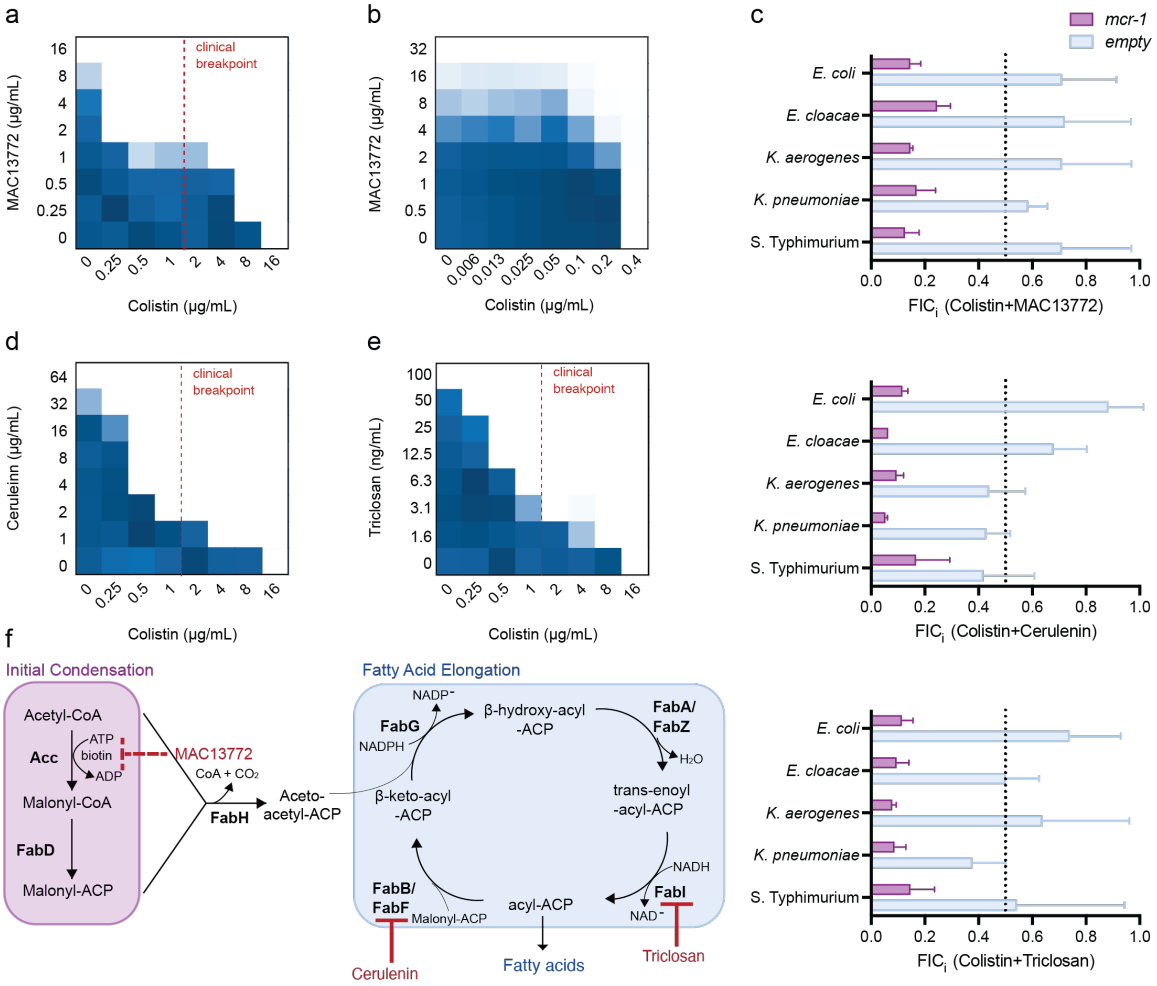

Figure 1. Biotin and fatty acid biosynthesis inhibitors reverse colistin resistance against *mcr-1* expressing Enterobacteriaceae. (a, b) Chequerboard broth microdilution assays of MAC13772 and colistin against **(a)** *mcr-1* expressing *E. coli* or **(b)** *E. coli* expressing the empty vector. **(c)** Fractional inhibitory concentration index (FIC$_i$) for colistin in combination with MAC17322, cerulenin, or triclosan against *mcr-1* expressing and wild-type strains of Enterobacteriaceae. To the left of the dotted line indicates synergy. **(d, e)** Chequerboard broth microdilution assays of **(d)** cerulenin or **(e)** triclosan and colistin against *mcr-1* expressing *E. coli*. **(a-e)** Dark regions represent higher cell density. Colistin's clinical breakpoint (2 μg/mL) is denoted by the dashed red line. Chequerboard and FIC$_i$ data are representative of at least 3 biological replicates.

(f) Fatty acid biosynthetic pathway in *E. coli.* Acetyl-CoA is converted to malonyl-CoA in a biotin-dependent reaction catalyzed by acetyl-CoA carboxylase (Acc) and subsequently modified to malonyl-ACP by FabD. Fatty acid elongation reactions are then carried out by FabH, FabG, FabA, FabZ, FabI, FabB, and FabF until the fatty acid chain is released. Direct inhibitors cerulenin and triclosan are shown in red, and the indirect inhibitor, MAC13772 is shown with a dashed red line.

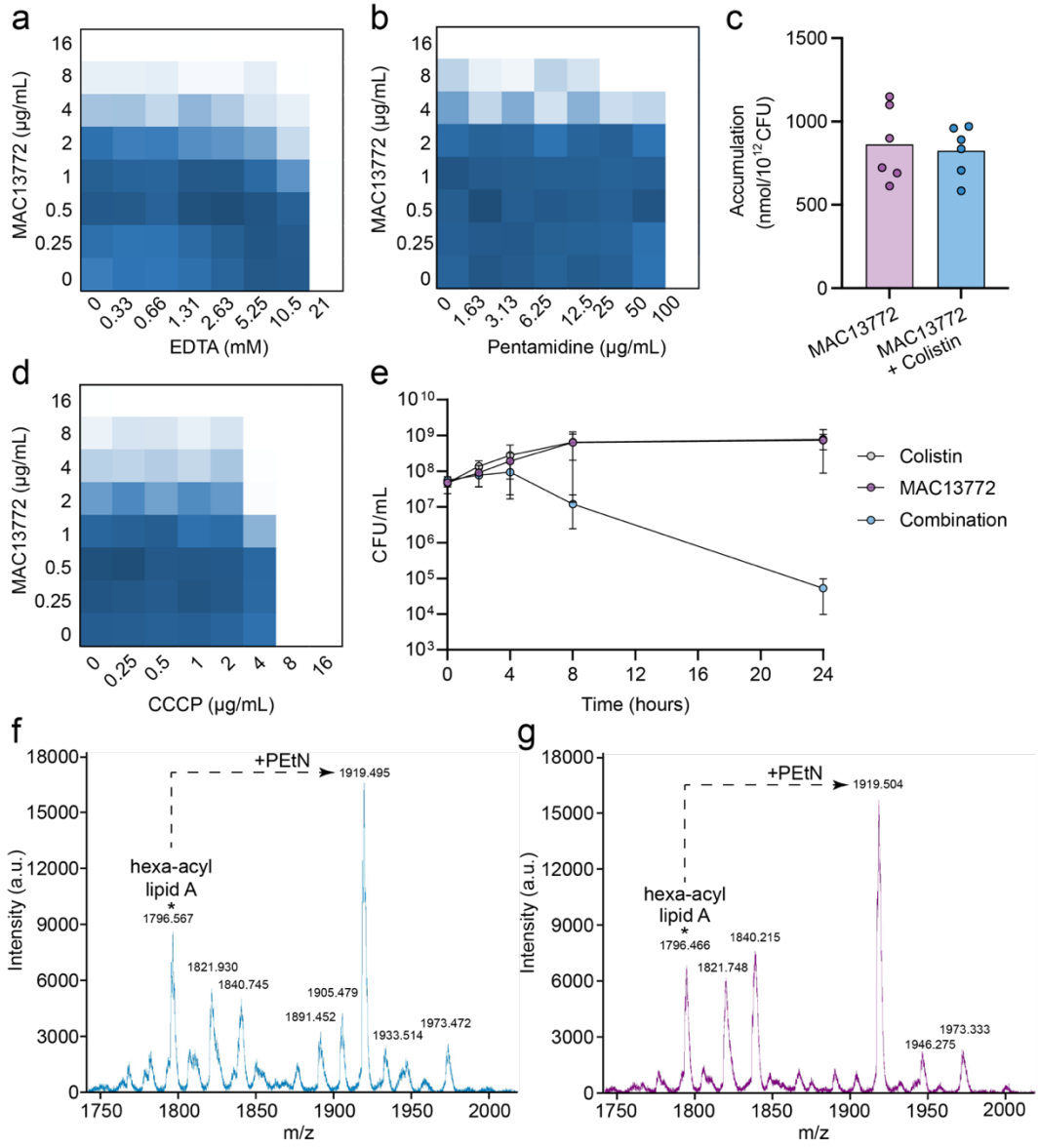

Figure 2. Established mechanisms do not explain the synergy between colistin and MAC13772. (a-c) Chequerboard broth microdilution assays between MAC13772 and **(a)** EDTA, **(b)** pentamidine, or **(d)** carbonyl cyanide m-chlorophenyl hydrazone (CCCP) against *E. coli* expressing *mcr-1*. Higher growth is indicated by dark blue, no detectable growth indicated in white, and results are representative of at least three independent experiments. **(c)** Accumulation of MAC13772 (50 μM treatment) in *mcr-1* expressing *E. coli* in the absence

(purple, *n* = 6) and presence of colistin (6 μM; blue, *n* = 6). Statistical significance was determined using a Mann-Whitney U test, no significant difference between samples was observed (*p*=0.82). **(e)** The combination of MAC13772 and colistin is bactericidal against *mcr-1* expressing *E. coli.* The rate of in vitro bacterial killing for *mcr-1* expressing *E. coli* exposed to colistin (2 μg/ml), MAC13772 (32 μg/mL), or the combination. Each point represents the mean and standard error of at least 4 biological replicates. **(f,g)** Negative-ion MALDI-TOF mass spectra of purified lipid A from *mcr-1* expressing *E. coli* in the **(f)** absence (blue) and **(g)** presence of MAC13772 (6 μg/mL; purple). The star indicates the peak corresponding to hexa-acylated, bis-phosphorylated lipid A species, and the major peak corresponds to lipid A decorated with one PEtN group.

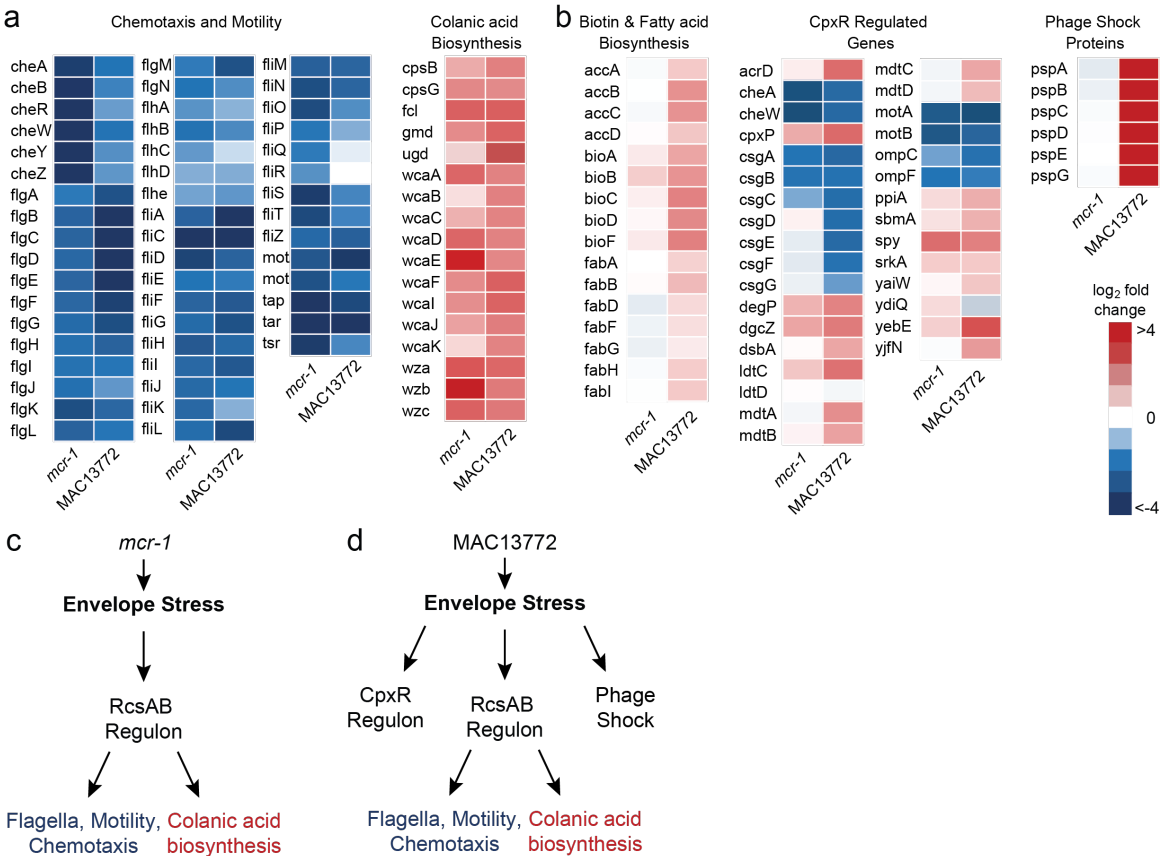

Figure 3. *mcr-1* expression and MAC13772 treatment induce cell envelope stress. (a-b) Heatmap of $\log_2$ fold change in gene expression after RNA sequencing of **(a)** *mcr-1* expressing *E. coli* relative to the empty vector control cells or **(b)** *mcr-1* expressing *E. coli* treated with MAC13772 relative to DMSO treated *mcr-1* expressing *E. coli*. Blue, downregulated; red, upregulated; white, no change in expression. **(c-d)** Proposed pathways involved in the response to **(c)** *mcr-1* expression or **(d)** MAC13772 treatment.

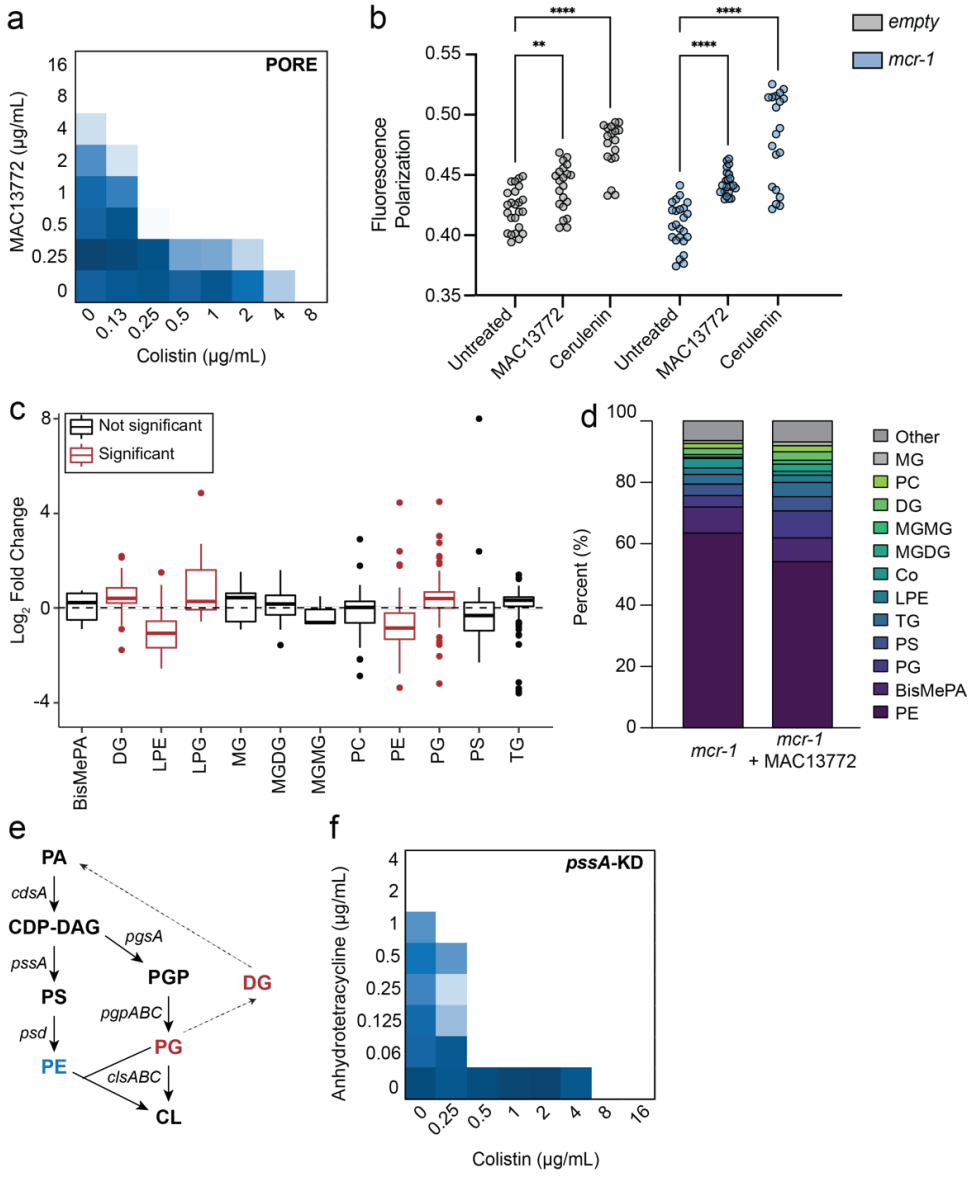

Figure 4. Inhibition of biotin or fatty acid biosynthesis alters membrane fluidity and lipidomic profile in colistin-resistant bacteria. (a) Chequerboard analysis of MAC13772 and colistin against *E. coli*-Pore expressing *mcr-1*. **(b)** Fluorescence polarization of *E. coli* expressing *mcr-1* or empty vector after cultivation in DMSO, MAC13772, or cerulenin. Groups were compared using a two-way ANOVA and corrected for multiple comparisons using the Holm-Sidak method, $^{**}p < 0.01$, $^{****}p < 0.0001$. **(c)** Lipid class enrichment for *E. coli*

expressing *mcr-1* treated with MAC13772. Boxplot shows the mean and quartiles for each class, individual points represent lipid species within the class. Lipid classes significantly enriched are in red. **(d)** Lipid composition of *E. coli* expressing *mcr-1* treated with DMSO or MAC13772. Coloured areas represent the relative contribution of different lipid classes (as indicated) to the overall lipidome. Percentages are the mean of two biological replicates. **(e)** Phospholipid biosynthesis in *E. coli*. Genes associated with each biosynthetic step are listed next to the arrows. **(c-e)** Lipid abbreviations are as follows: BisMePA, bismethyl phosphatidic acid; CL, cardiolipin; DG, diacylglycerol; LPE, lysophosphatidylethanolamine; LPG, lysophosphatidylglycerol; MG, monoacylglycerol; MGDG, glycosyldiacylglycerol; MGMG, glycosylmonoacylglycerol; PC, phosphatidylcholine; PE, phosphatidylethanolamine; PG, phosphatidylglycerol; PS, phosphatidylserine; TG, triacylglycerol. **(f)** Chequerboard assay of colistin and anhydrotetracycline, an inducer of dCas9 expression, against an *E. coli mcr-1* CRISPR knockdown of *pssA*. Dark regions represent higher cell density. Chequerboard data are representative of at least three biological replicates.

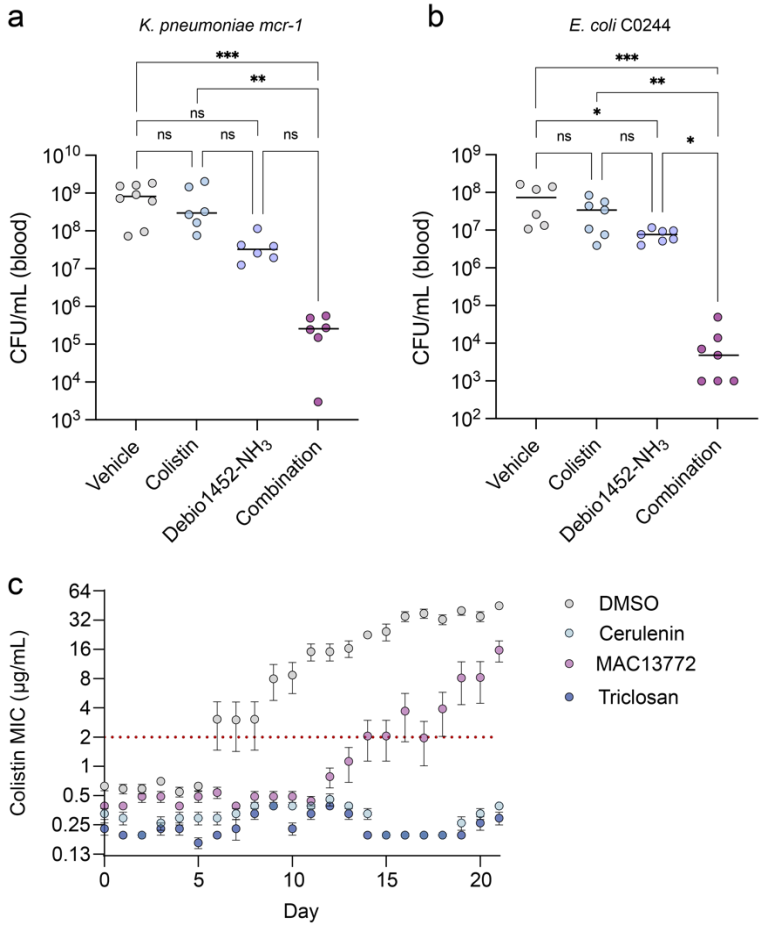

Figure 5. In vivo efficacy of Debio1452-NH_3 and colistin in a murine infection model. (a-b) Colistin and Debio1452-NH_3 combination therapy is efficacious against **(a)** *mcr-1* expressing *K. pneumoniae* systemic infection and **(b)** colistin-resistant *E. coli* systemic infection. Mice were treated with a single dose of vehicle, colistin (5 mg/kg), Debio1452-NH_3 (17.5 mg/kg), or the combination one hour after infection and euthanized at the experimental endpoint (7 hours post-infection). Each point represents an individual mouse, lines indicate geometric means for each group. **p*<0.05, ***p*<0.01 (Holm-Sidak's multiple comparisons test). **(c)** The inhibition of biotin biosynthesis or fatty acid biosynthesis reduces the development of colistin resistance. Colistin MIC during serial passage of *E. coli* with DMSO, cerulenin, MAC13772, or triclosan (¼ MIC). Each point shows the mean and SEM and is representative of at least four biological replicates. The dashed red line shows the clinical breakpoint of colistin.

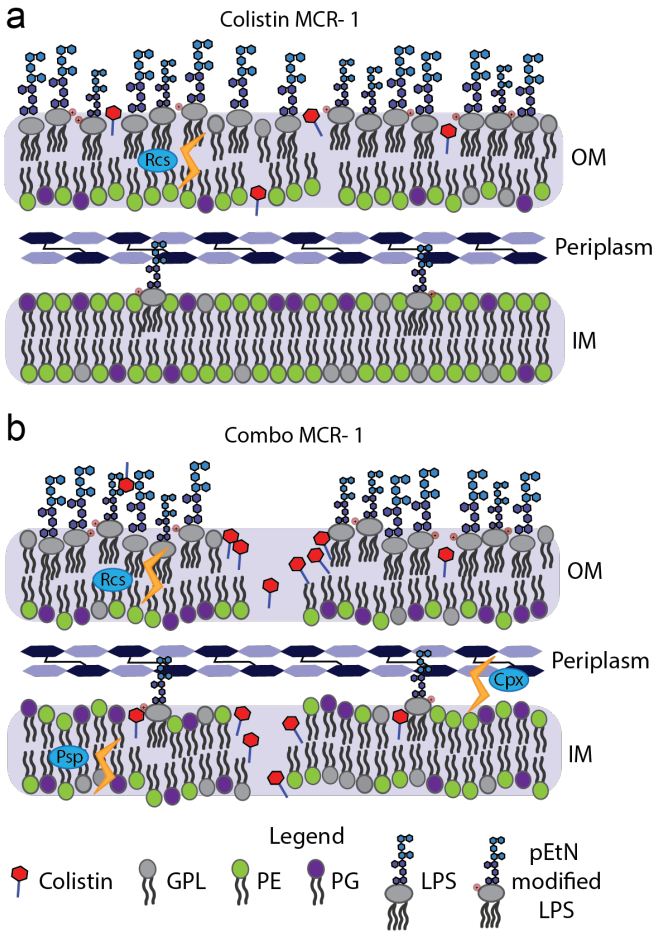

Figure 6. MAC13772 modifies the lipidome to increase membrane fluidity overcoming colistin resistance in *mcr-1* expressing *E. coli.* Diagram of the membrane of *mcr-1* expressing *E. coli* in response to **(a)** colistin treatment or **(b)** treatment with colistin and MAC13772. **(a)** Colistin interacts and disturbs the outer membrane (OM) but is unable to cause inner membrane disruption. Expressing *mcr-1* induces the outer membrane stress response, mediated by RcsAB. **(b)** Treatment with MAC13772 and colistin disrupts both the inner membrane (IM) and outer membrane lysing *E. coli*. MAC13772 treatment decreases phosphatidylethanolamine (PE) and increases phosphatidylglycerol (PG), decreasing membrane fluidity. The changes to membrane composition induce envelope stress responses (indicated by the lightning bolt), including RcsAB, CpxR, and PspF. Lipid abbreviations are as follows: GPL,

glycerophospholipid; PE, phosphatidylethanolamine; PG, phosphatidylglycerol; LPS, lipopolysaccharide.

Supplementary Figures and Legends

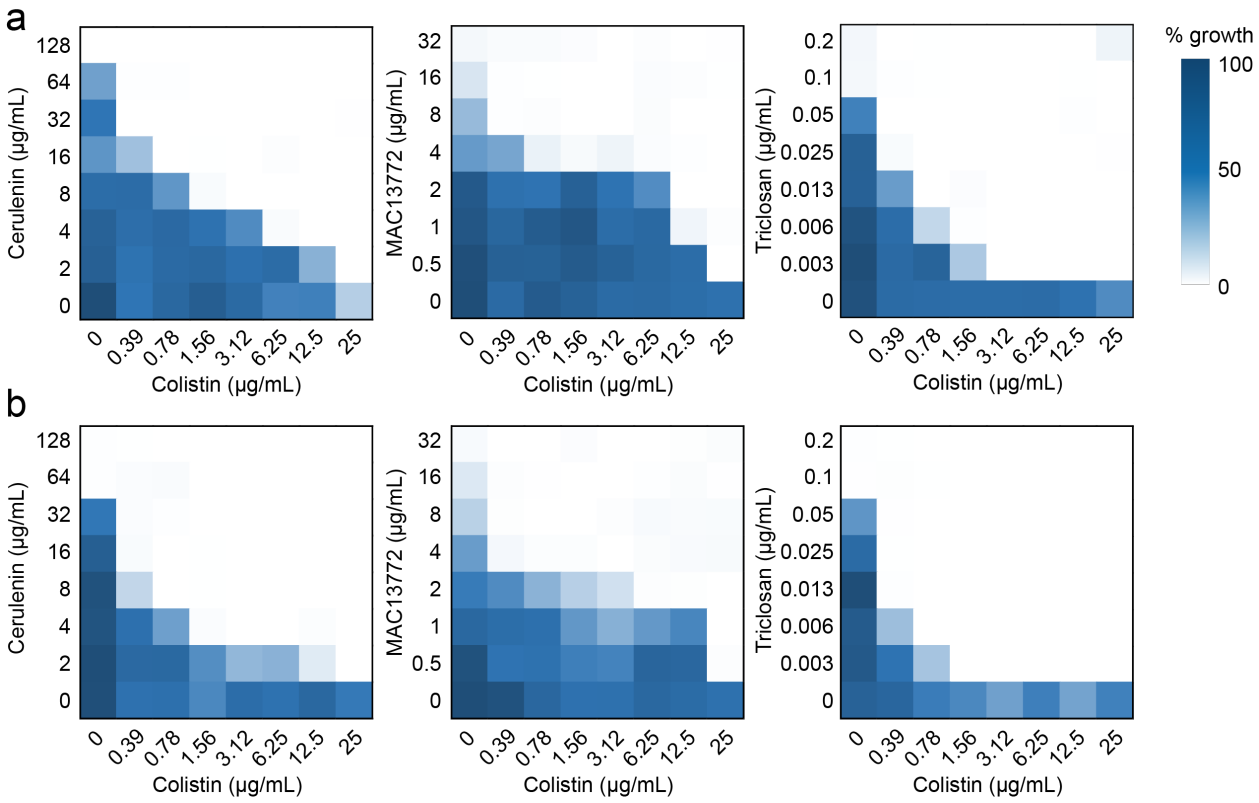

Figure S1. Colistin synergizes with biotin and fatty acid biosynthesis inhibitors against *E. coli* strains harbouring *mcr-1* on natural plasmids. (a-b) Chequerboard broth microdilution assays showing dose-dependent colistin potentiation by cerulenin, MAC13772, and triclosan against *mcr-1* positive *E. coli* strains **(a)** N15-02865 and **(b)** N15-02866. Dark regions represent higher cell density. Chequerboard data are representative of at least three biological replicates.

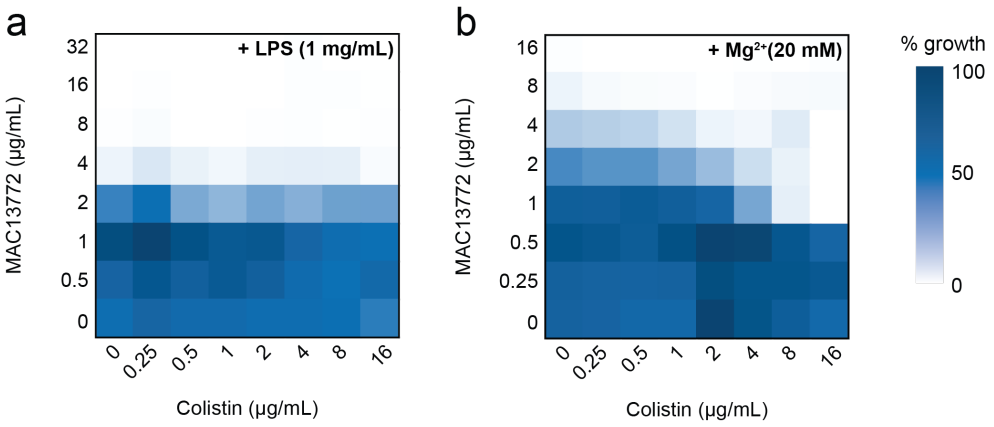

Figure S2. Exogenous LPS or Mg^{2+} abolishes synergy between MAC13772 and colistin against *mcr-1* expressing *E. coli.* Chequerboard broth microdilution assays between MAC13772 and colistin in M9 minimal media supplemented with **(a)** purified *E. coli* LPS (1 mg/mL) or **(b)** Mg^{2+} (20 mM). Dark regions represent higher cell density. Chequerboard data are representative of at least 2 biological replicates.

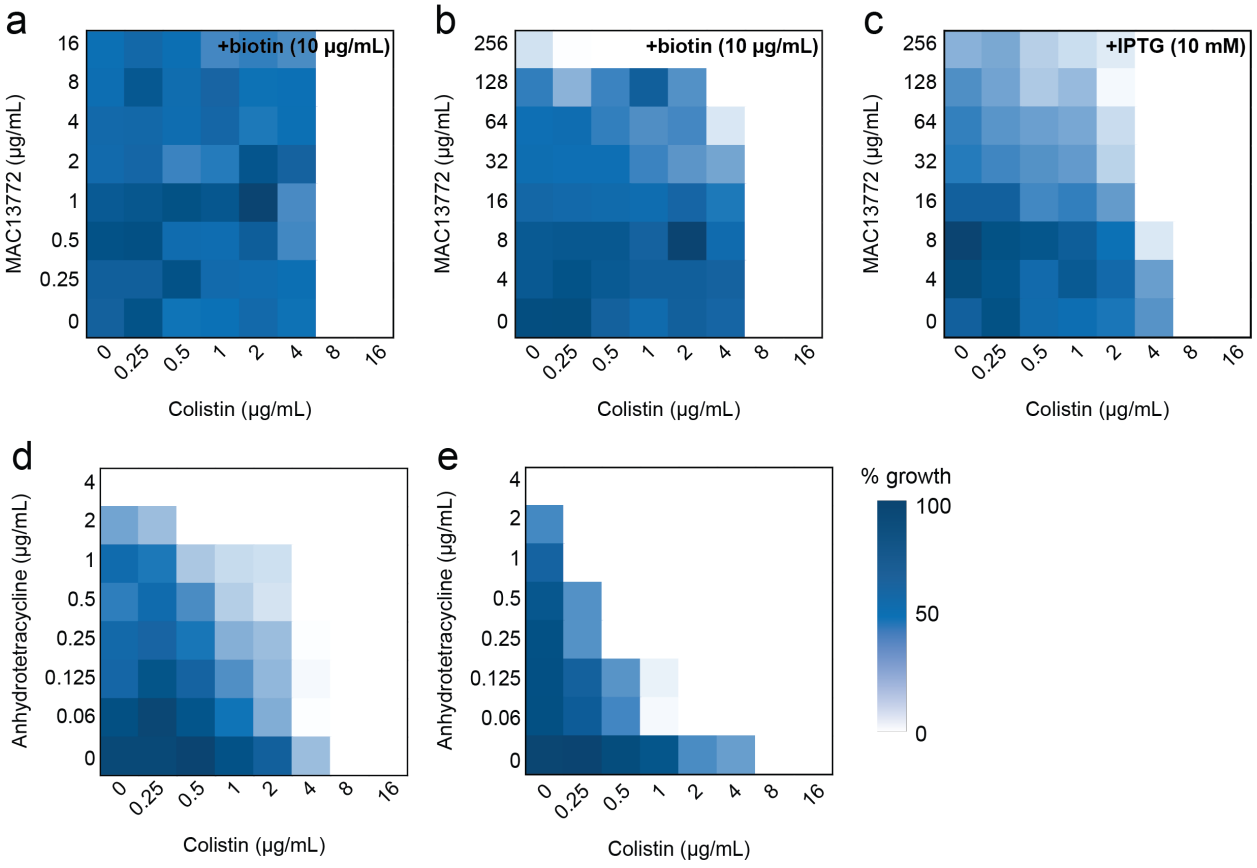

Figure S3. MAC13772 synergizes with colistin against *E. coli* expressing *mcr-1* by inhibiting BioA. (a-b) Chequerboard broth microdilution assays between MAC13772 and colistin M9 minimal media supplemented with biotin (10 µg/mL). **(c)** Expression of *bioA* suppresses MAC13772's potentiation of colistin against *mcr-1* positive *E. coli*. Expression of *bioA* induced by the addition of IPTG (10 mM). **(d-e)** Chequerboard assay of colistin and anhydrotetracycline against *E. coli* expressing **(d)** pfD152 *empty* or **(e)** pfD152 *bioA.* Dark regions represent higher cell density. Chequerboard data are representative of at least 2 biological replicates.

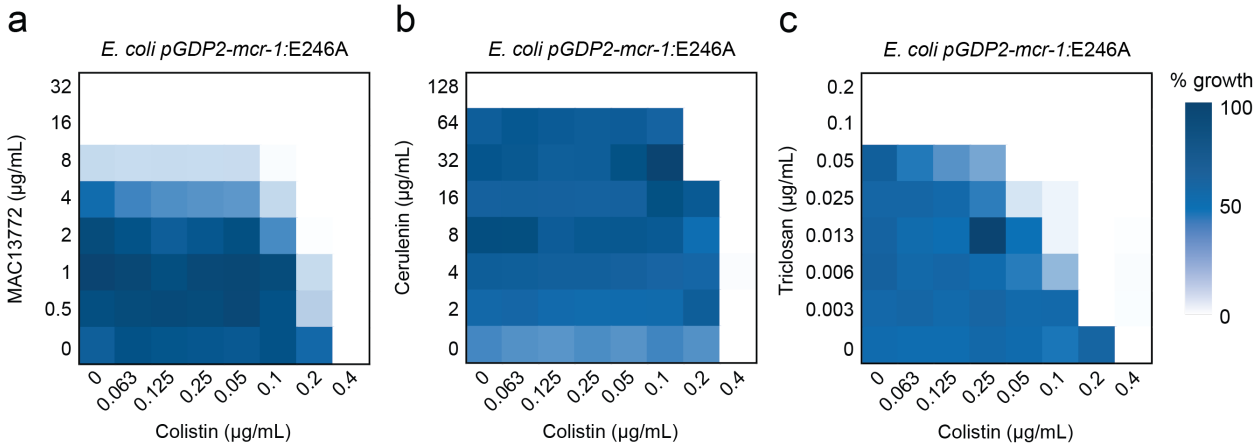

Figure S4. Synergy between MAC13772 and colistin is dependent on PEtN modification of lipid A. Chequerboard broth microdilution assays between colistin and **(a)** MAC13772, **(b)** cerulenin, or **(c)** triclosan against *E. coli* expressing *mcr-1::*E246A. Dark regions represent higher cell density. Chequerboard data are representative of at least 3 biological replicates.

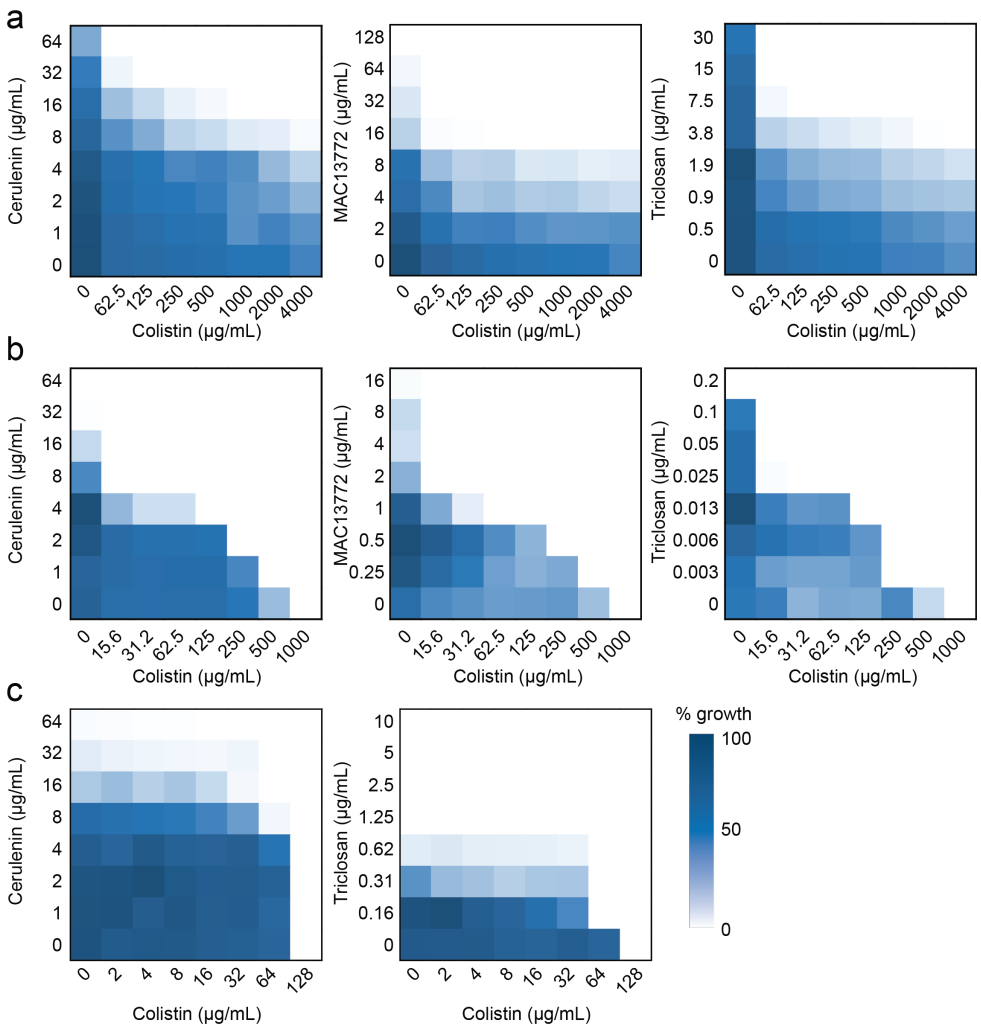

Figure S5. Combinations of cerulenin, MAC13772, or triclosan with colistin are broadly applicable to colistin-resistant Gram-negative pathogens. Chequerboard broth microdilution assays between colistin and MAC13772, cerulenin, or triclosan against **(a)** *S. marcescens,* **(b)** *A. baumannii,* and **(c)** *S. aureus*. Dark regions represent higher cell density. Chequerboard data are representative of at least 3 biological replicates.

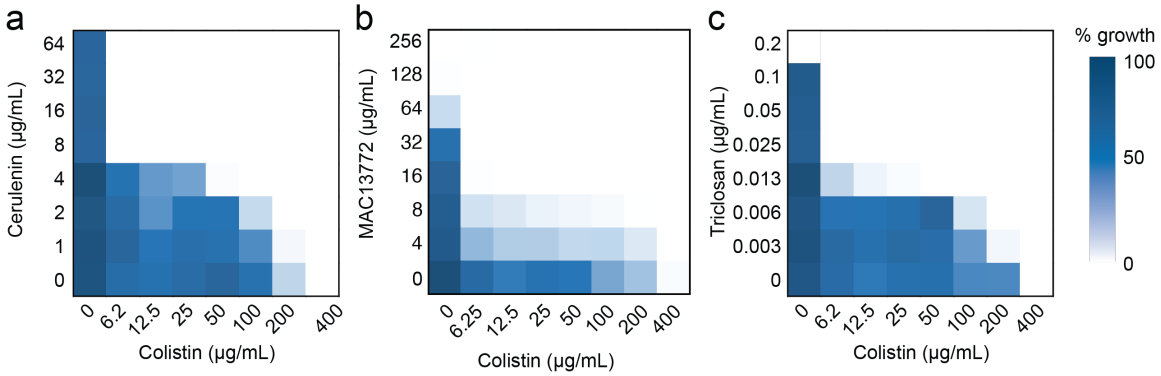

Figure S6. Cerulenin, MAC13772, and triclosan synergize with colistin against colistin-resistant *K. pneumoniae*. Chequerboard broth microdilution assays between **(a)** cerulenin, **(b)** MAC13772, and **(c)** triclosan paired with colistin against *K. pneumoniae* MKP103. Dark regions represent higher cell density. Chequerboard data are representative of at least 3 biological replicates.

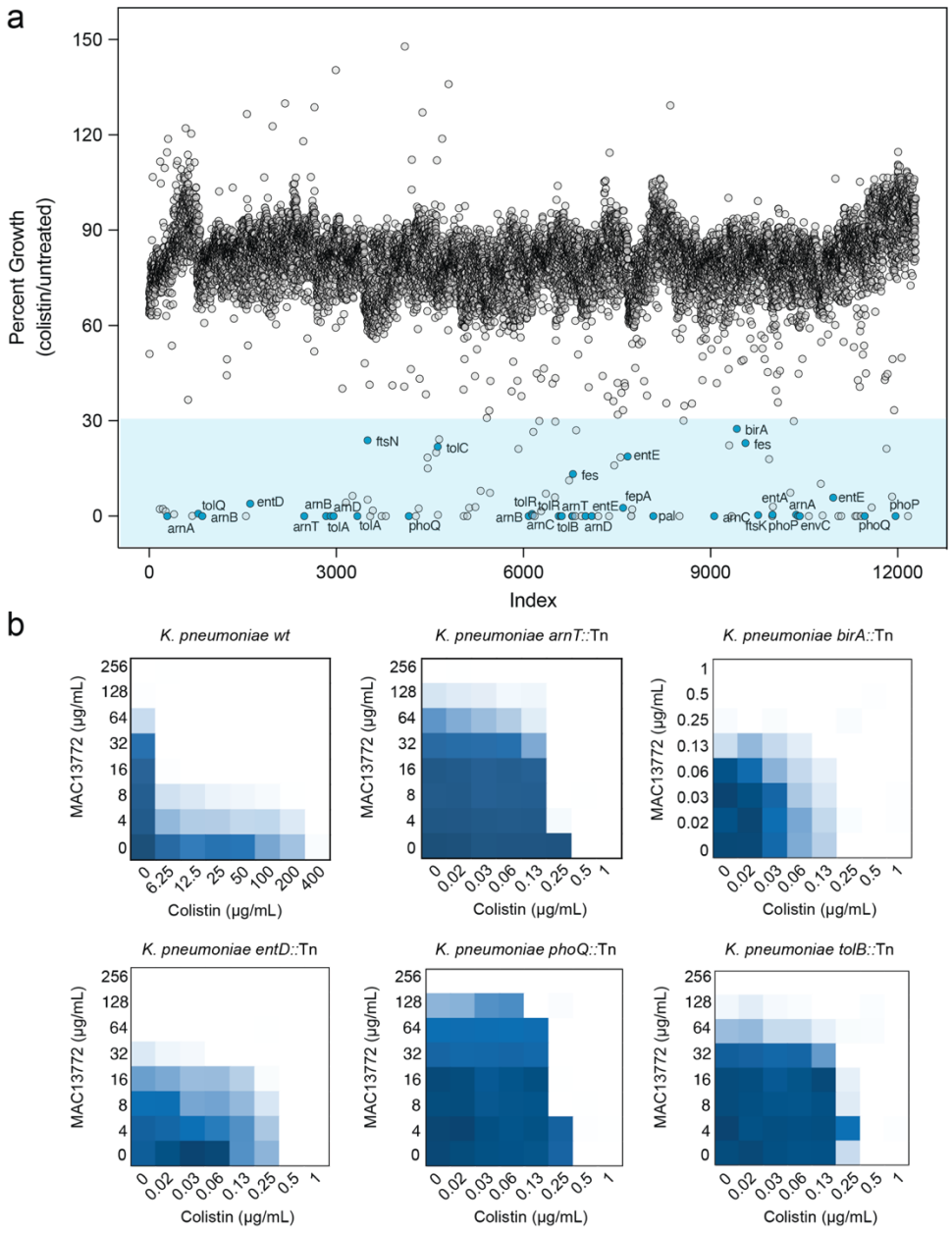

Figure S7. Synergy between MAC13772 and colistin requires L-Ara4N decoration of lipid A. (a) Screening of the *K. pneumoniae* transposon mutant library for sensitivity to colistin. Percent growth was calculated based on growth in the presence of colistin relative to its respective control (untreated strain) growing in M9 minimal media. The blue region indicates genes 3 standard deviations from the mean. **(b)** Chequerboard assays of MAC13772 and colistin against wild-type

and colistin-sensitive transposon mutants. Higher growth is indicated in dark blue, no detectable growth is indicated in white, and results are representative of at least two independent experiments.

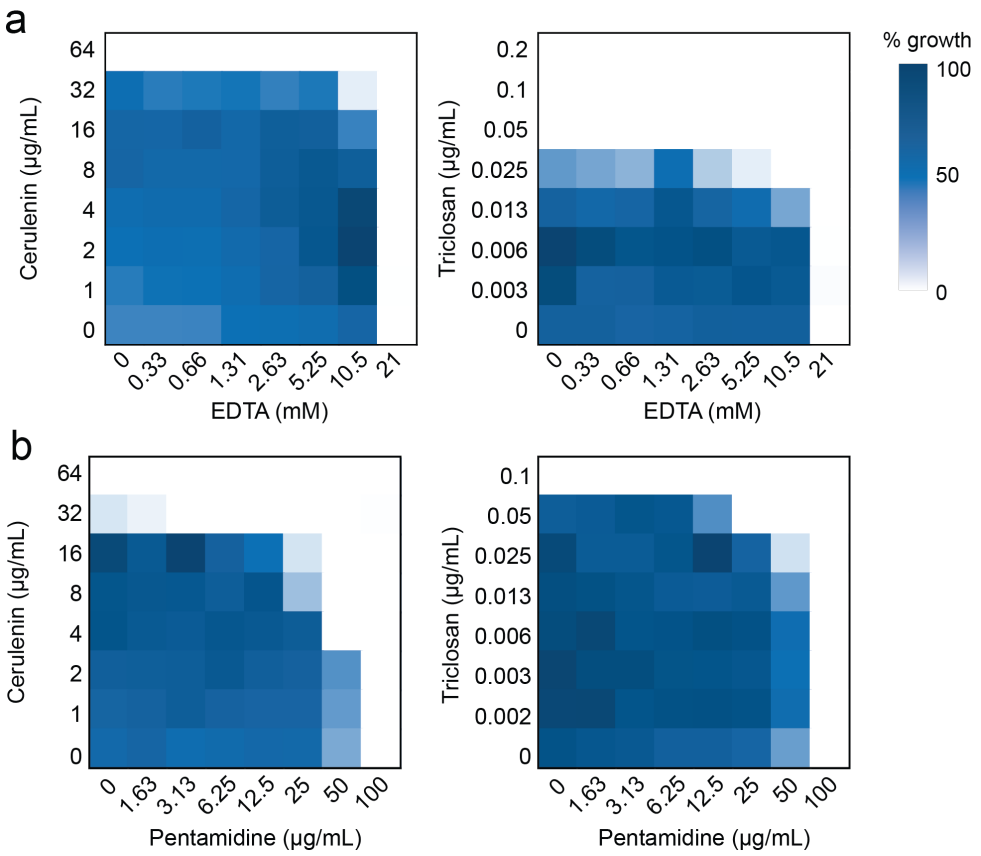

Figure S8. Cerulenin and triclosan do not synergize with pentamidine or EDTA against *mcr-1* expressing *E. coli.* (a,b) Chequerboard broth microdilution assays between cerulenin or triclosan and **(a)** EDTA or **(b)** pentamidine against *mcr-1* expressing *E. coli.* Dark regions represent higher cell density. Chequerboard data are representative of at least 2 biological replicates.

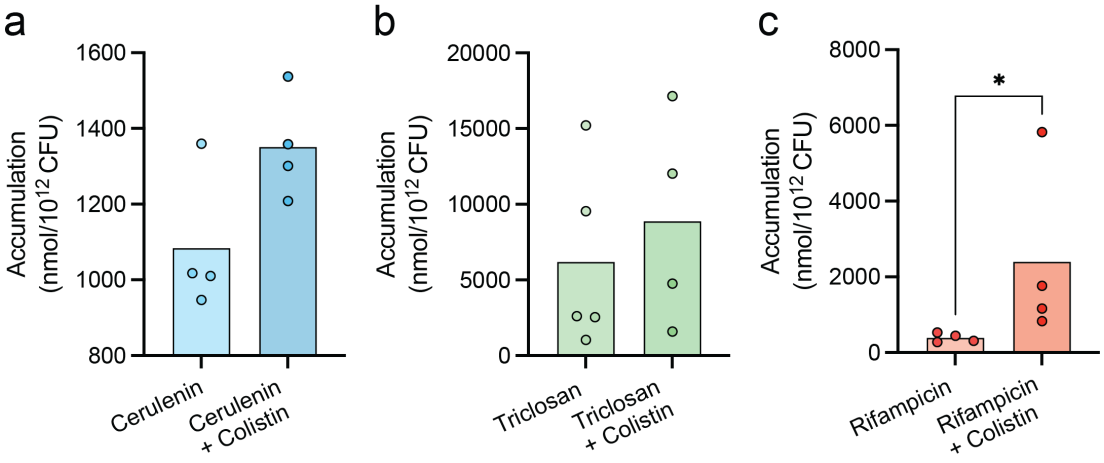

Figure S9. Colistin does not increase the intracellular accumulation of cerulenin and triclosan. (a-c) Accumulation of **(a)** cerulenin (50 μM; blue, *n* = 4), **(b)** triclosan (50 μM; green, *n* = 4-5), and **(c)** rifampicin (50 μM; red, *n* = 4) in *mcr-1* expressing *E. coli* in the absence and presence of colistin (6 μM). Statistical significance was determined using a Mann-Whitney U test relative to the no colistin control, **p* < 0.05.

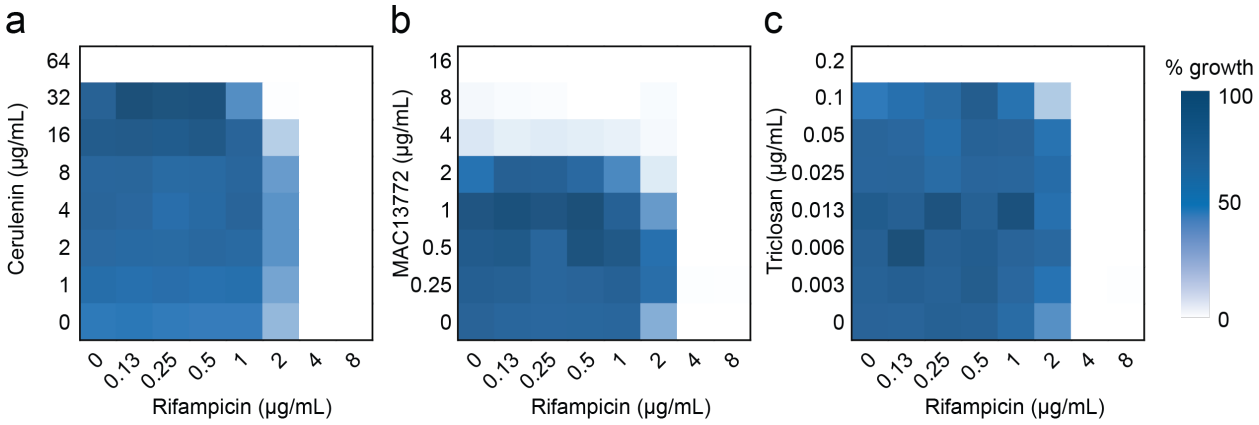

Figure S10. MAC13772, cerulenin, and triclosan do not synergize with rifampicin against *E. coli* expressing *mcr-1*. (a-c) Chequerboard broth microdilution assays between rifampicin and **(a)** MAC13772, **(b)** cerulenin, or **(c)** triclosan. Higher growth is indicated in dark blue, no detectable growth is indicated in white, and results are representative of at least two independent experiments.

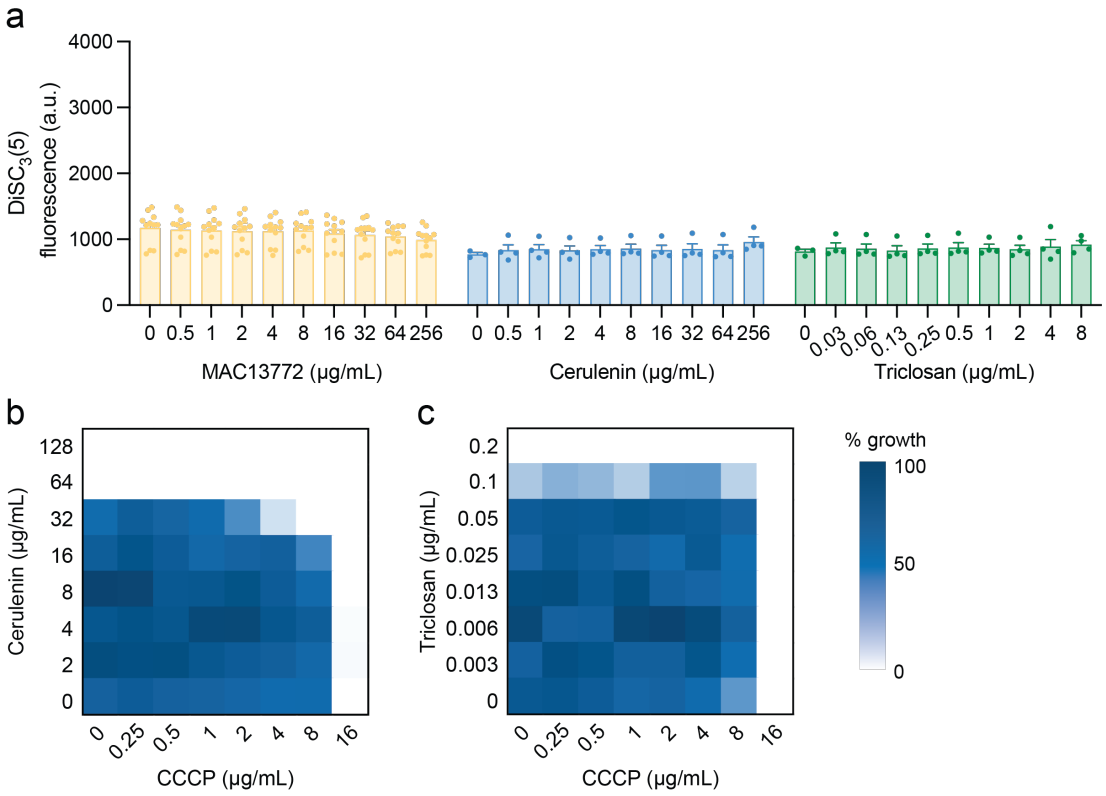

Figure S11. Inhibiting biotin or fatty acid biosynthesis does not disrupt the proton motive force. (a) DiSC3(5) assay, bar plots depict the mean of three biological replicates, error bars indicate standard error. **(b,c)** Chequerboard broth microdilution assays for **(b)** cerulenin or **(c)** triclosan and carbonyl cyanide m-chlorophenyl hydrazone (CCCP). Higher growth is indicated in dark blue; no detectable growth is indicated in white, and the results are representative of at least two independent experiments.

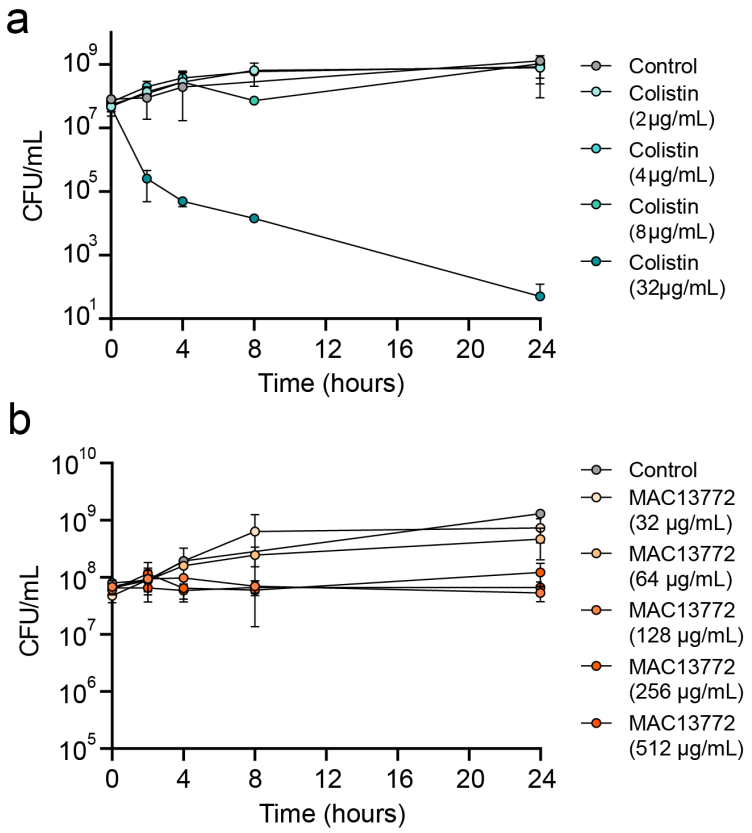

Figure S12. Time-kill assays with colistin and MAC13772 against *mcr-1* expressing *E. coli.* (a,b) The killing of *mcr-1* expressing *E. coli* in the presence of varying concentrations of **(a)** colistin or **(b)** MAC13772. The initial cell density is ~5×10^7 CFU/mL. Shown is the mean of a minimum of three biological replicates. Bars denote standard error.

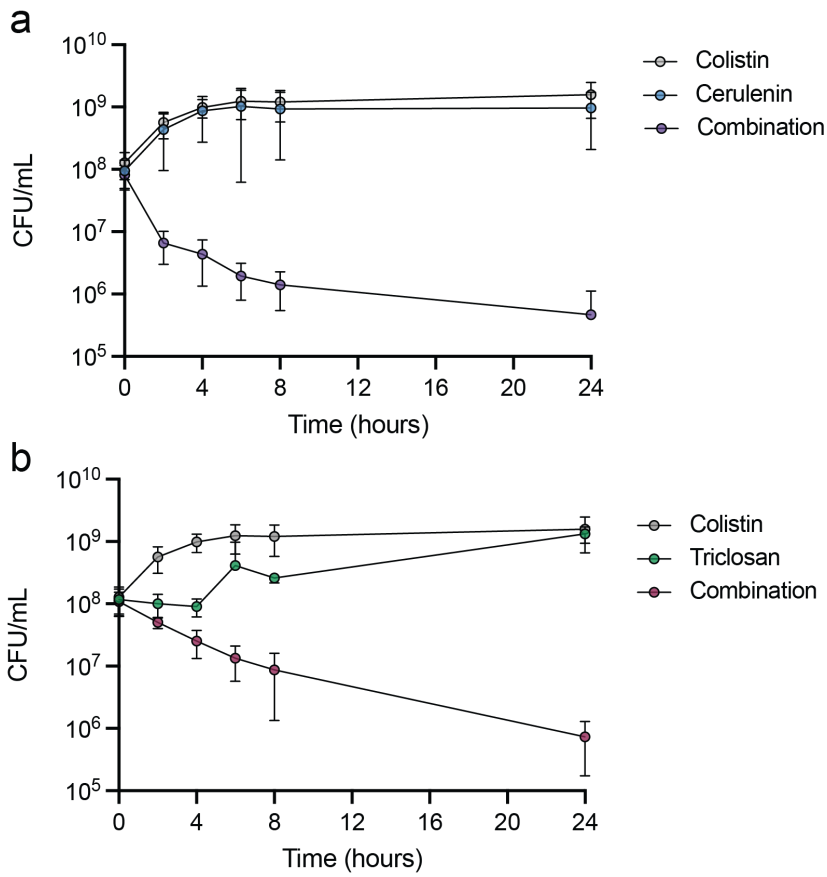

Figure S13. The combinations of cerulenin and triclosan with colistin are lytic against *mcr-1* expressing *E. coli.* (a) The rate of in vitro bacterial killing for *mcr-1* expressing *E. coli* exposed to colistin (2 μg/ml), cerulenin (16 μg/mL), or the combinations thereof. **(b)** The rate of in vitro bacterial killing for *mcr-1* expressing *E. coli* exposed to colistin (2 μg/ml), triclosan (0.1 μg/mL), or the combinations thereof. The initial cell density is ~5×10^7 CFU/mL. Shown is the mean of a minimum of three biological replicates. Bars denote standard error.

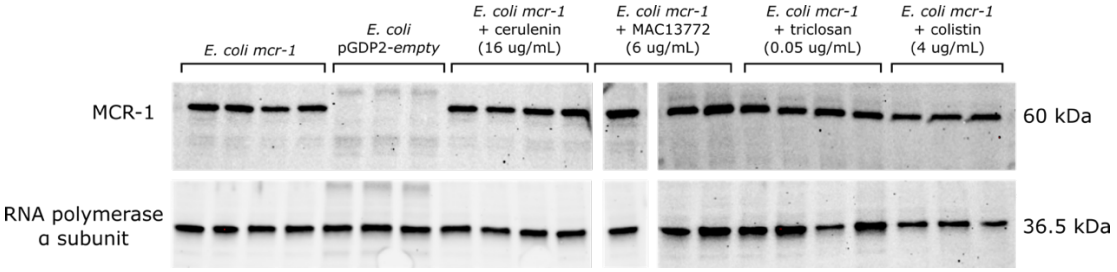

Figure S14. MCR-1 protein levels are unaffected by growth in cerulenin, MAC13772, triclosan or colistin. Western blots analysis of MCR-1 and reference protein RNA polymerase α subunit. Whole-cell lysates were extracted from cultures supplemented with DMSO, cerulenin, MAC13772, triclosan or colistin in mid-log phase of growth.

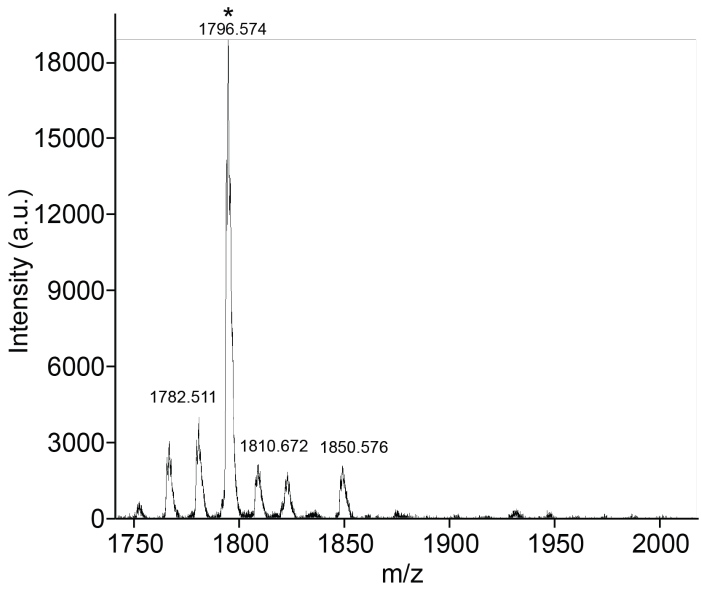

Figure S15. Negative-ion MALDI-TOF mass spectrum of purified lipid A from *E. coli* expressing the empty vector extracted using phenol-chloroform-petroleum (PCP). The star indicates the peak corresponding to hexa-acylated bis-phosphorylated lipid A species.

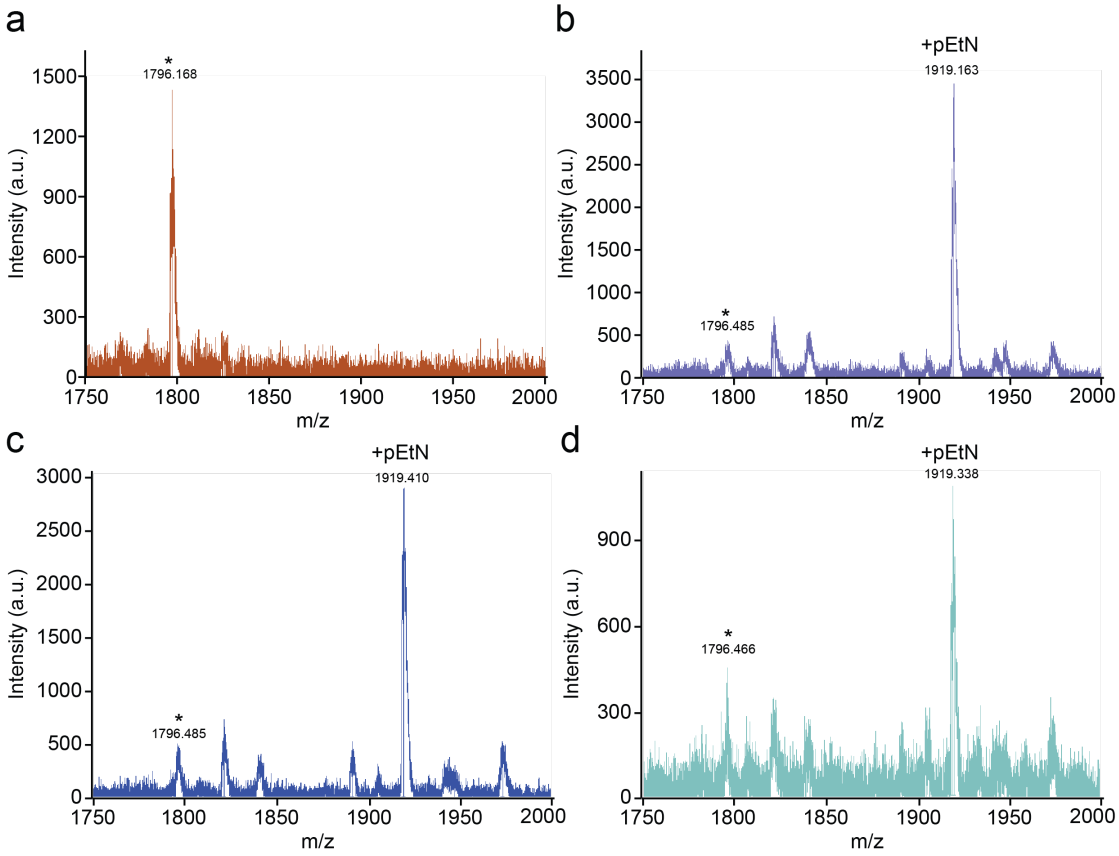

Figure S16. Inhibiting fatty acid biosynthesis has no impact on PEtN decoration of lipid A in *mcr-1* expressing *E. coli.* (a-d) Negative-ion MALDI-TOF mass spectra of purified lipid A from **(a)** *E. coli* expressing the empty vector (orange) or *mcr-1* expressing *E. coli* in the **(b)** absence (purple) and presence of **(c)** cerulenin (blue) or **(d)** triclosan (light blue). The star indicates the peak corresponding to hexa-acylated bis-phosphorylated lipid A species, and the second peak corresponds to lipid A decorated with one PEtN group.

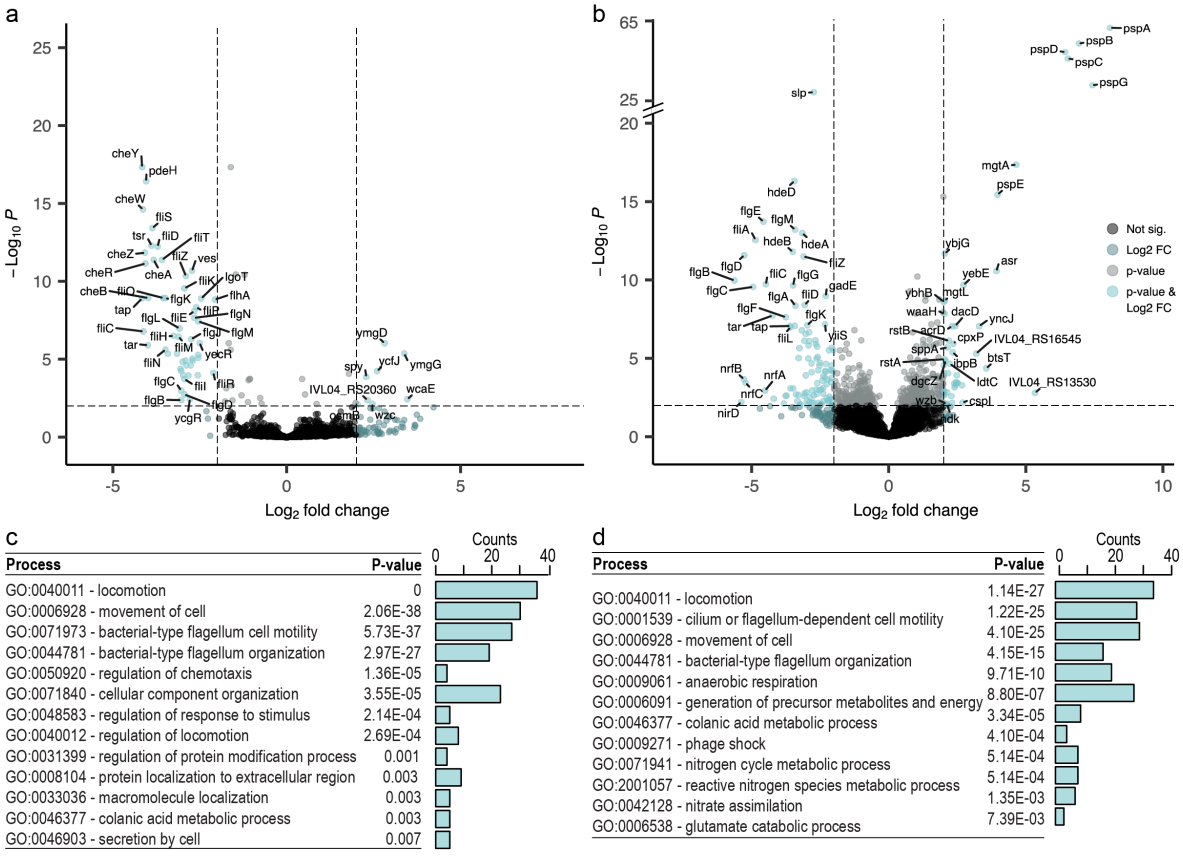

c		d	
Process	**P-value**	**Process**	**P-value**
GO:0040011 - locomotion	0	GO:0040011 - locomotion	1.14E-27
GO:0006928 - movement of cell	2.06E-38	GO:0001539 - cilium or flagellum-dependent cell motility	1.22E-25
GO:0071973 - bacterial-type flagellum cell motility	5.73E-37	GO:0006928 - movement of cell	4.10E-25
GO:0044781 - bacterial-type flagellum organization	2.97E-27	GO:0044781 - bacterial-type flagellum organization	4.15E-15
GO:0050920 - regulation of chemotaxis	1.36E-05	GO:0009061 - anaerobic respiration	9.71E-10
GO:0071840 - cellular component organization	3.55E-05	GO:0006091 - generation of precursor metabolites and energy	8.80E-07
GO:0048583 - regulation of response to stimulus	2.14E-04	GO:0046377 - colanic acid metabolic process	3.34E-05
GO:0040012 - regulation of locomotion	2.69E-04	GO:0009271 - phage shock	4.10E-04
GO:0031399 - regulation of protein modification process	0.001	GO:0071941 - nitrogen cycle metabolic process	5.14E-04
GO:0008104 - protein localization to extracellular region	0.003	GO:2001057 - reactive nitrogen species metabolic process	5.14E-04
GO:0033036 - macromolecule localization	0.003	GO:0042128 - nitrate assimilation	1.35E-03
GO:0046377 - colanic acid metabolic process	0.003	GO:0006538 - glutamate catabolic process	7.39E-03
GO:0046903 - secretion by cell	0.007		

Figure S17. Transcriptional response to *mcr-1* expression and MAC13772 treatment. (a,b) Volcano plot comparing the *p-values* and fold change of **(a)** *mcr-1* expression to the empty vector control or **(b)** MAC13772 treatment of *E. coli* expressing *mcr-1* to an untreated sample. The horizontal dashed line indicates a $p = 0.01$ and the vertical dashed line a $\log_2$ fold-change = 2. **(c, d)** Gene ontology (GO) analysis of genes associated with **(c)** *mcr-1* expression or **(d)** treatment with MAC13772. Tables depict the top unique GO terms enriched by biological function. Bar chart depicts the count of genes associated with each GO term. Enrichment was tested using pathway-tools software (Fisher exact test with the Benjamini-Hochberg Correction).

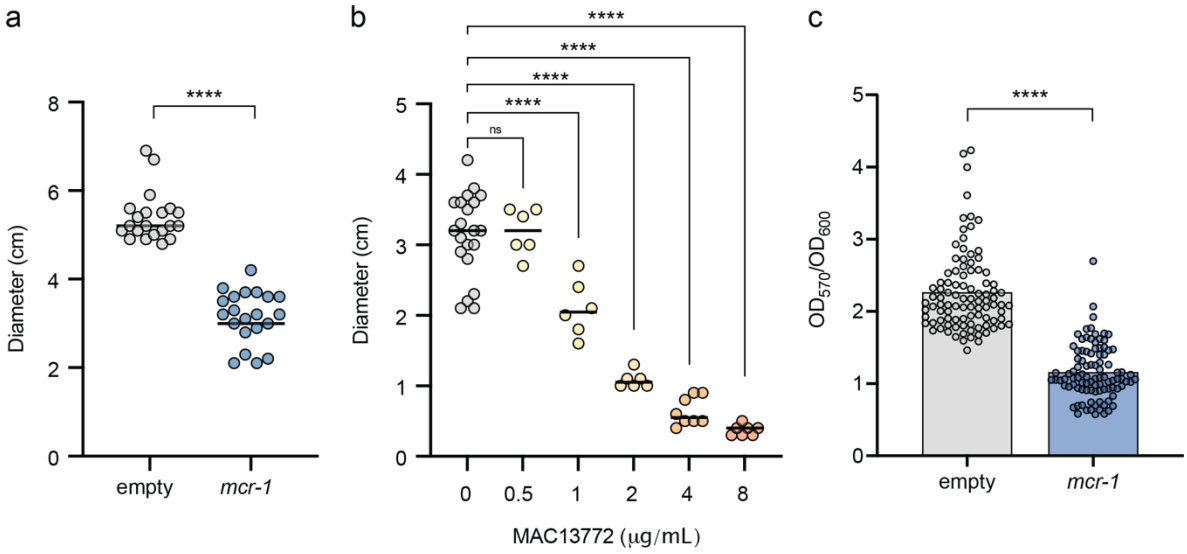

Figure S18. *mcr-1* expression induces cell envelope stress leading to reduced motility and biofilm formation. (a,b) Quantification of motility zones from swimming motility plates of *E. coli* expressing **(a)** empty (grey) or *mcr-1* (blue) or **(b)** *mcr-1* expressing *E. coli* exposed to varying concentrations of MAC13772. The solid line represents the mean for each group. Groups were compared using **(a)** two-sample Student's *t* test or **(b)** one-way ANOVA with Dunnett's test for multiple comparisons, ****p<0.0001. **(c)** Crystal violet biofilm assay for *E. coli* expressing *mcr-1* or the empty vector. Absorbance is calculated by crystal violet (OD_{570})/growth (OD_{600}). All data are shown with the bar representing the mean and representative of at least three biological replicates. Groups were compared using two-sample Student's *t* test, ****p < 0.0001.

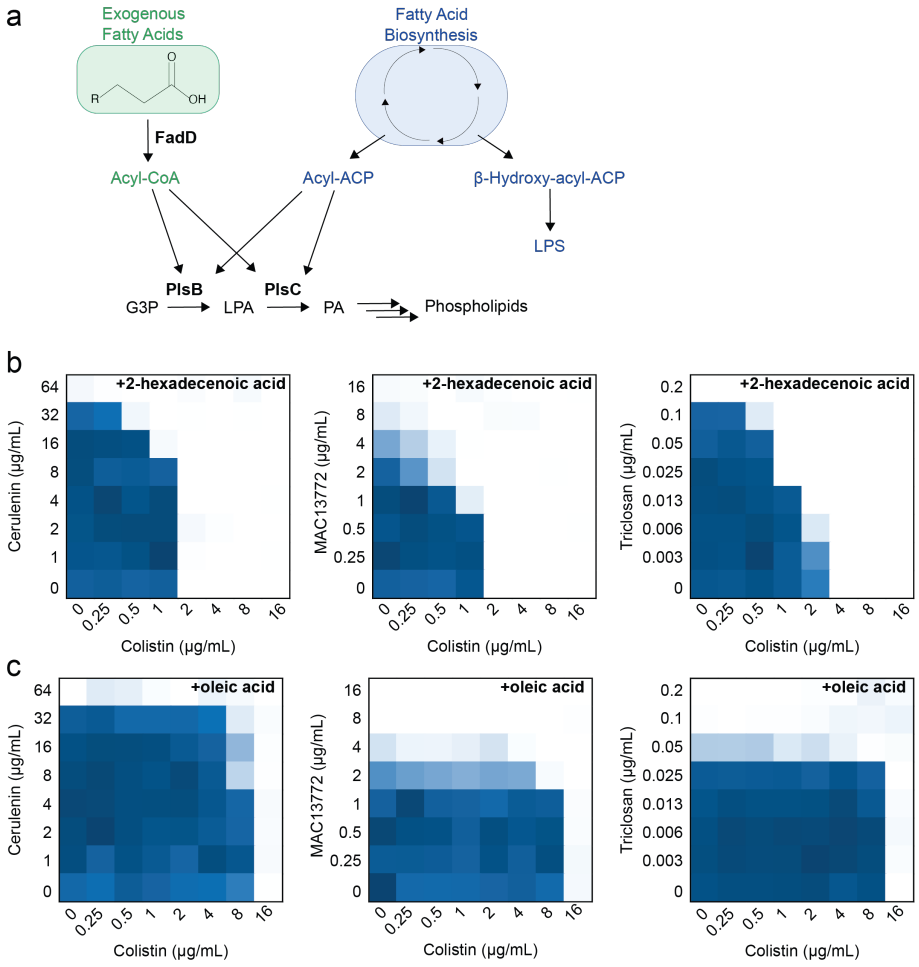

Figure S19. The addition of fatty acids 2-hexadecenoic acid or oleic acid suppresses synergy between colistin and cerulenin or triclosan. (a) Diagram depicting the path for the incorporation of exogenous and endogenous fatty acids in LPS and phospholipids. *E. coli* synthesizes phosphatidic acid (PA), the major precursor to all phospholipid species, through two acylation reactions. First glycerol-3-phosphate (G3P) is acylated to lysophosphatidic acid (LPA) by PlsB, which is subsequently acylated by PlsC to form phosphatidic acid. The acyltransferases (PlsB and PlsC) can use both acyl-CoA, from exogenous fatty acids, and acyl-ACP from fatty acid biosynthesis as acyl donors in the synthesis of phosphatidic acid. Lipopolysaccharide (LPS) biosynthesis requires endogenous β-hydroxyacyl-ACP for acylation reactions as there is not a pathway in *E. coli* to generate β-hydroxyacyl-ACP from exogenous fatty acids. **(b-c)** Chequerboard broth microdilution assays between cerulenin, MAC13772, and triclosan with colistin in media supplemented with **(b)** 2-hexadecenoic acid or **(c)**

oleic acid. Higher growth is indicated in dark blue, no detectable growth is indicated in white, and results are representative of at least two independent experiments.

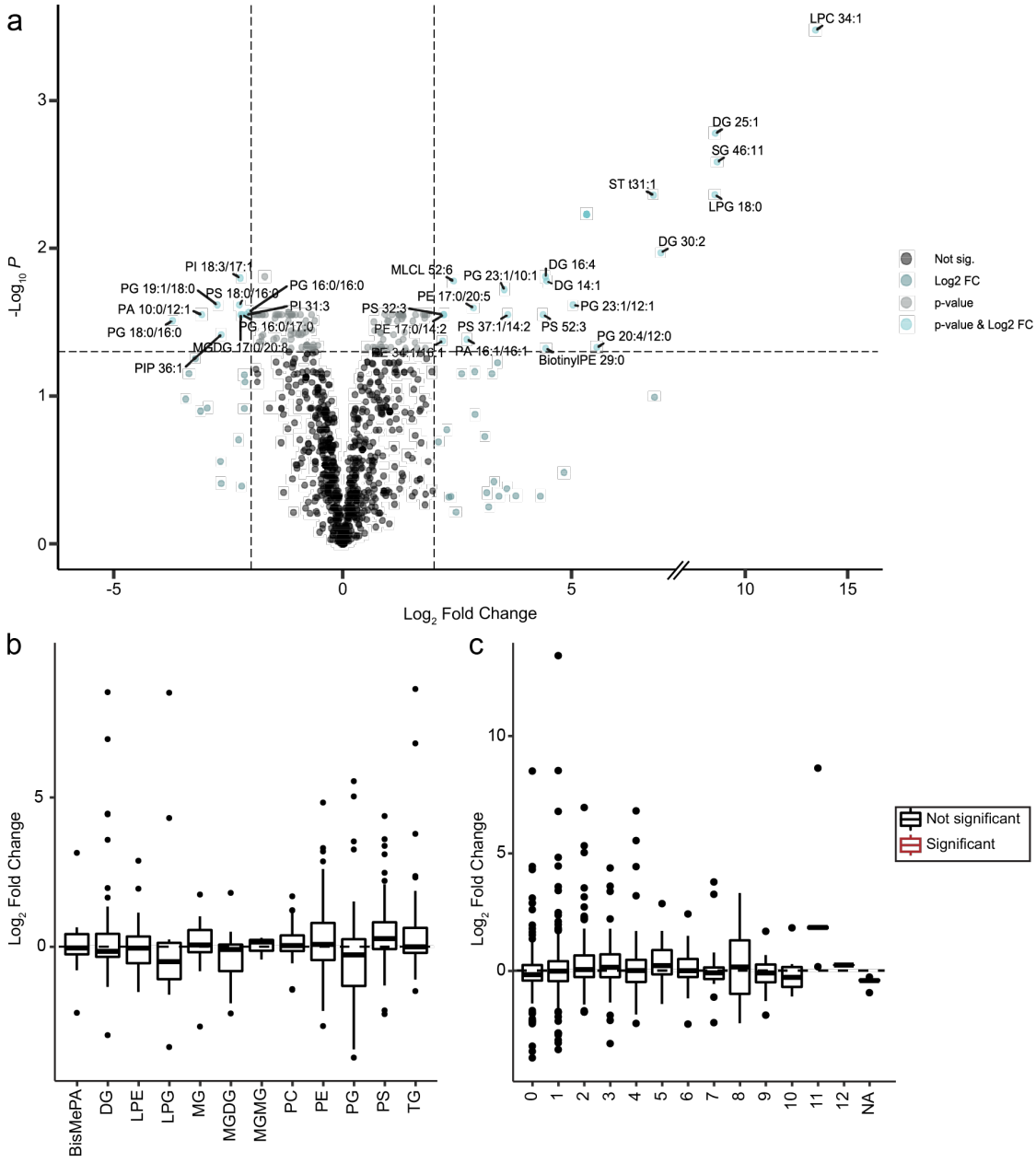

Figure S20. Lipid perturbations in response to *mcr-1* expression. (a) Volcano plot comparing the *p-values* and fold change of *mcr-1* expression to the empty vector control. The horizontal dashed line indicates a $p = 0.05$ and the vertical dashed line a $\log_2$ fold-change = 2. **(b)** Lipid class or **(c)** unsaturation enrichment for *E. coli* expressing *mcr-1*. Boxplot shows the mean and quartiles for each class. Lipid classes significantly enriched are in red. Lipid abbreviations

are as follows: BisMePA, bismethyl phosphatidic acid; CL, cardiolipin; DG, diacylglycerol; LPE, lysophosphatidylethanolamine; LPG, lysophosphatidylglycerol; MG, monoacylglyderol; MGDG, glycosyldiacylglycerol; MGMG, glycosylmonoacylglycerol; PC, phosphatidylcholine; PE, phosphatidylethanolamine; PG, phosphatidylglycerol; PS, phosphatidylserine; TG, triacylglycerol.

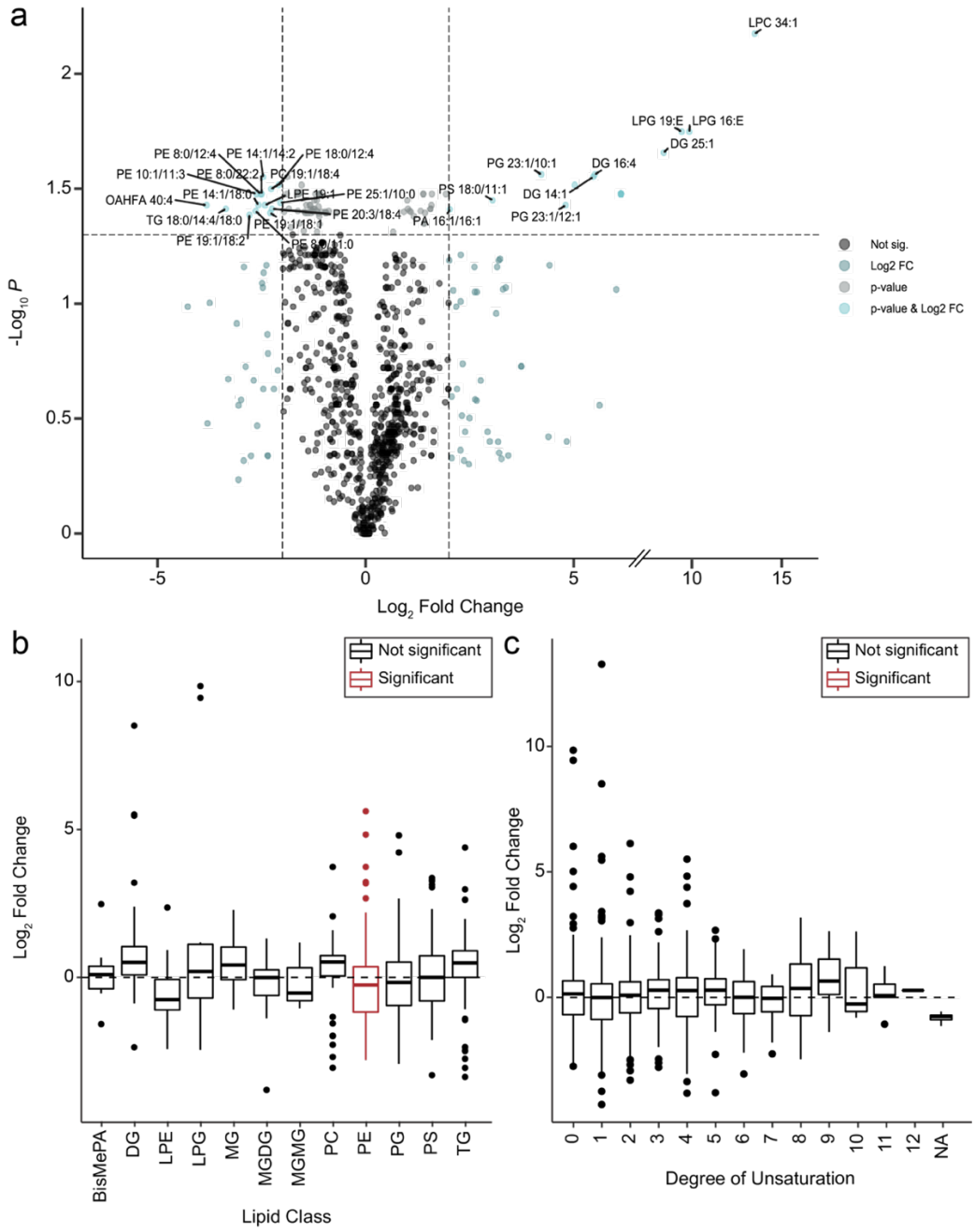

Figure S21. Lipid perturbations in response to MAC13772 treatment. (a) Volcano plot comparing the *p-values* and fold change of MAC13772 treatment to the untreated control in *E. coli* expressing the empty vector. The horizontal dashed line indicates a $p = 0.05$ and the vertical dashed line a $\log_2$ fold-change =

2. **(b)** Lipid class or **(c)** unsaturation enrichment for *E. coli* treated with MAC13772. Boxplot shows the mean and quartiles for each class. Lipid classes significantly enriched are in red. Lipid abbreviations are as follows: BisMePA, bismethyl phosphatidic acid; CL, cardiolipin; DG, diacylglycerol; LPE, lysophosphatidylethanolamine; LPG, lysophosphatidylglycerol; MG, monoacylglyderol; MGDG, glycosyldiacylglycerol; MGMG, glycosylmonoacylglycerol; PC, phosphatidylcholine; PE, phosphatidylethanolamine; PG, phosphatidylglycerol; PS, phosphatidylserine; TG, triacylglycerol.

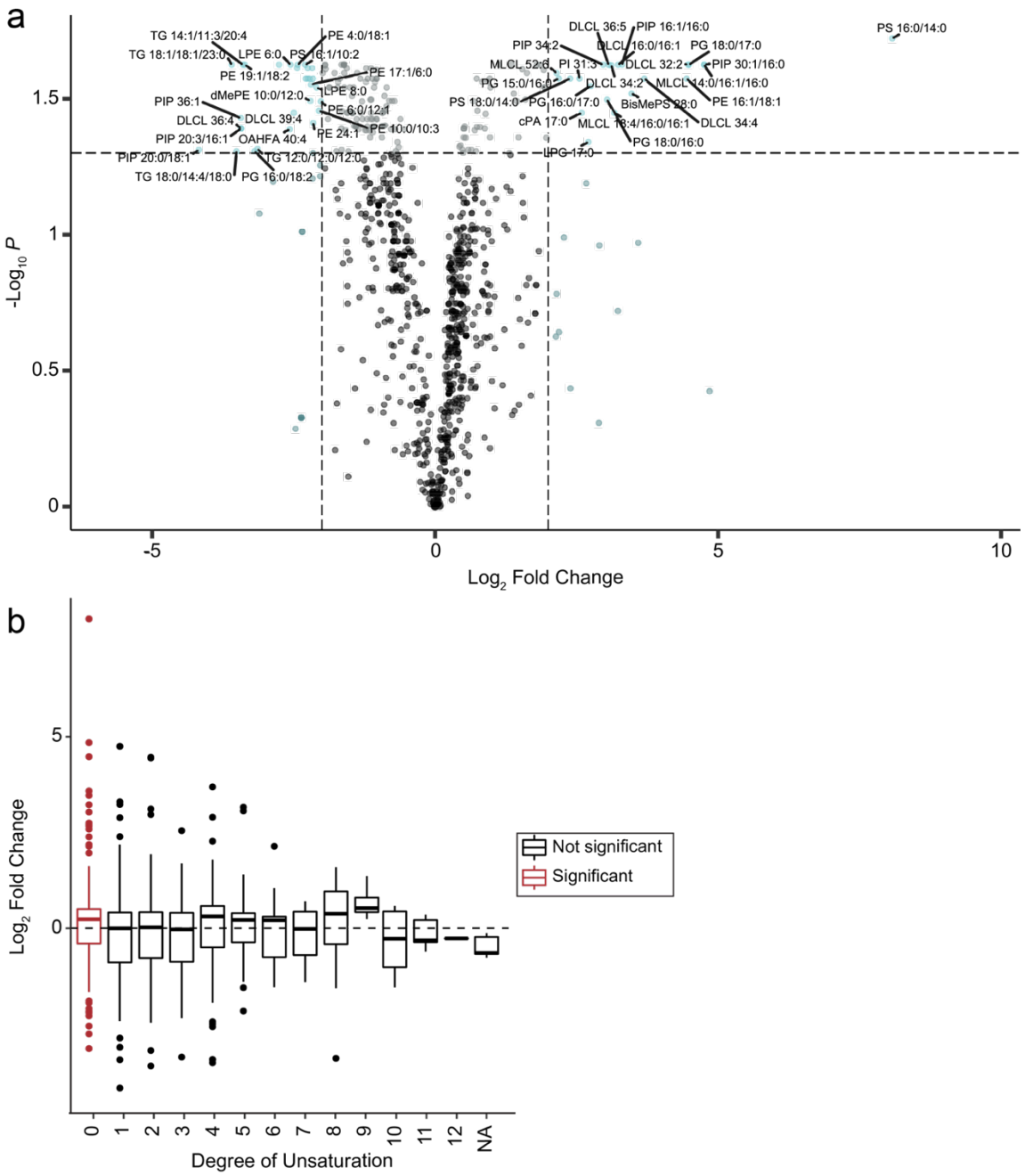

Figure S22. Lipid perturbations in response to MAC13772 treatment in *mcr-1* expressing *E. coli*. (a) Volcano plot comparing the *p-values* and fold change of MAC13772 treatment to the untreated control in *E. coli* expressing *mcr-1*. The horizontal dashed line indicates a $p = 0.05$ and the vertical dashed line a $\log_2$

fold-change = 2. **(b)** unsaturation enrichment for *E. coli* expressing *mcr-1* treated with MAC13772. Boxplot shows the mean and quartiles for each class. Lipid classes significantly enriched are in red. Lipid abbreviations are as follows: BisMePA, bismethyl phosphatidic acid; CL, cardiolipin; DG, diacylglycerol; LPE, lysophosphatidylethanolamine; LPG, lysophosphatidylglycerol; MG, monoacylglyderol; MGDG, glycosyldiacylglycerol; MGMG, glycosylmonoacylglycerol; PC, phosphatidylcholine; PE, phosphatidylethanolamine; PG, phosphatidylglycerol; PS, phosphatidylserine; TG, triacylglycerol.

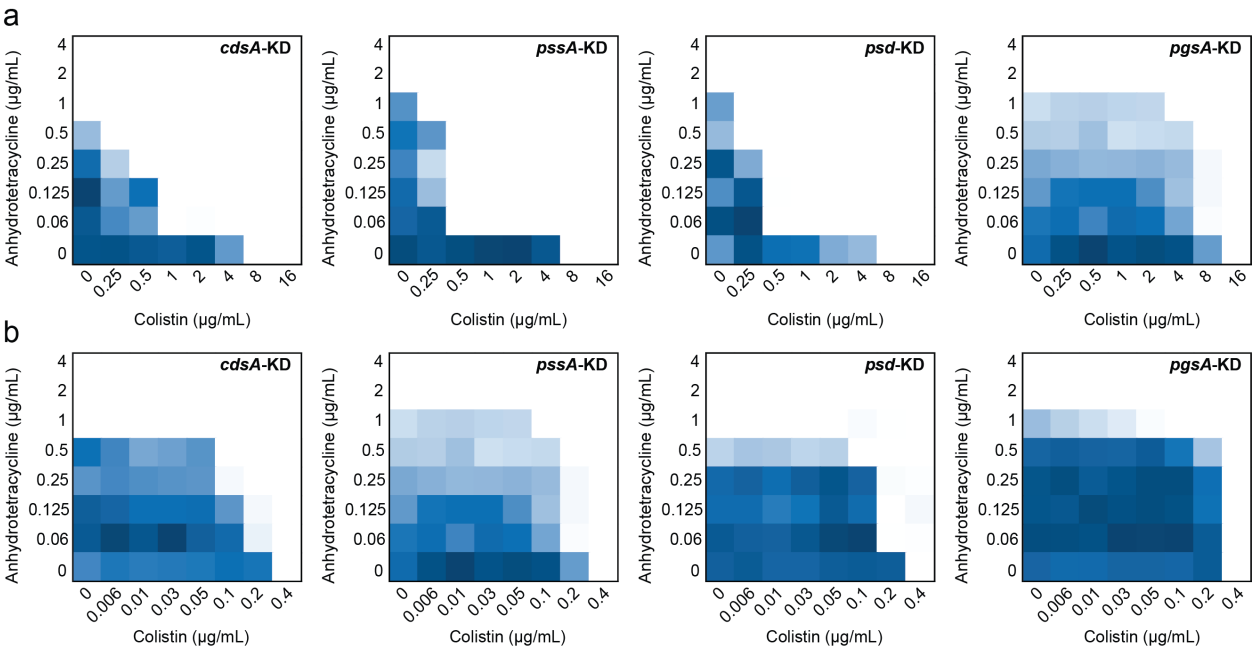

Figure S23. Depletion of phosphatidylethanolamine biosynthesis genes sensitize *mcr-1* expressing *E. coli* to colistin. Chequerboard assay of colistin and anhydrotetracycline against *E. coli* expressing **(a)** *mcr-1* or **(b)** empty vector and with a CRISPR knockdown of *cdsA, pssA, psd,* or *pgsA* (left to right). Dark regions represent higher cell density. Chequerboard data are representative of at least three biological replicates.

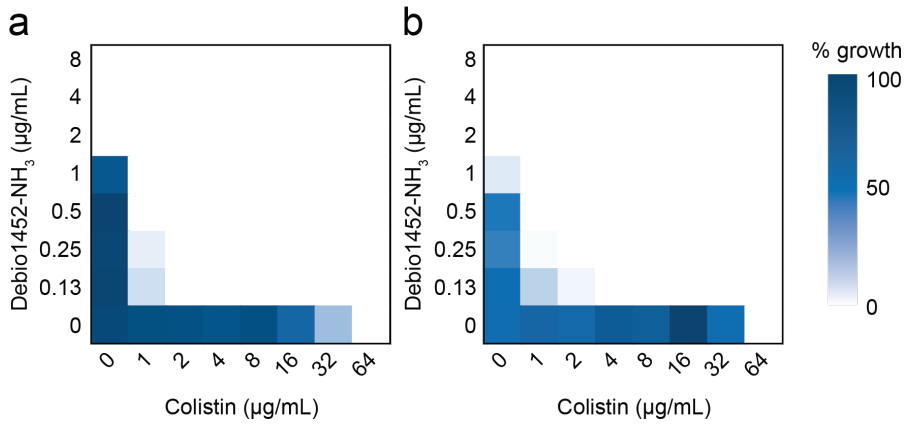

Figure S24. Debio1452-NH_3 synergizes with colistin against both *K. pneumoniae* expressing *mcr-1* and a colistin-resistant clinical isolate of *E. coli.* (a,b) Chequerboard broth microdilution assays between Debio1452-NH_3 and colistin against **(a)** *mcr-1* expressing *K. pneumoniae* or **(b)** colistin-resistant *E. coli.* Dark regions represent higher cell density. Chequerboard data are representative of at least 2 biological replicates.

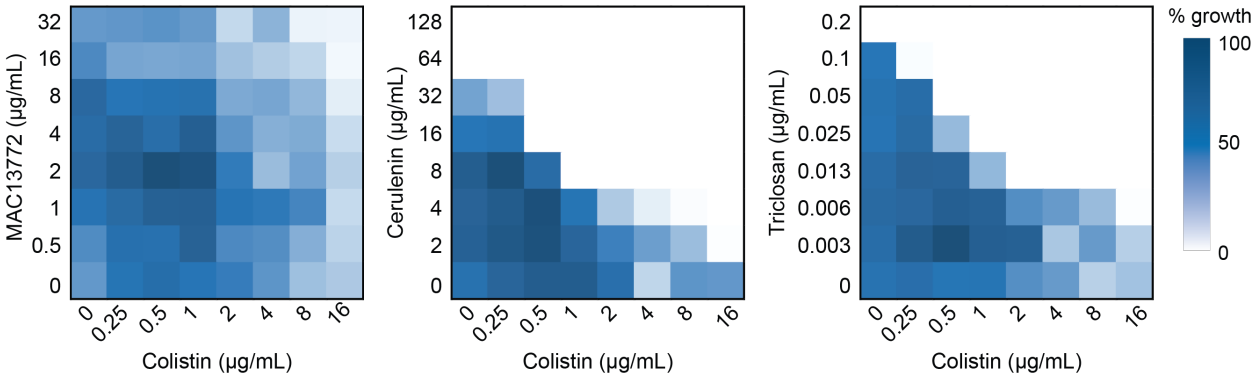

Figure S25. Resistance to the combination of MAC13772 and colistin does not induce cross-resistance to combinations of cerulenin or triclosan with colistin. Chequerboard broth microdilution assays between cerulenin, MAC13772, or triclosan and colistin against *E. coli* after 21 days of passaging in colistin and ¼ MIC MAC13772. Dark regions represent higher cell density. Chequerboard data are representative of at least 2 biological replicates.

Supplementary Information

For Supplementary Tables 1-10 see:

https://www.dropbox.com/sh/z41u6nj6jn8h1j0/AAAAuaO8rOHNo7ltrJ0a8xVGa?dl=0

References

1. Nation, R. L. & Li, J. Colistin in the 21st century. *Curr. Opin. Infect. Dis.* **22,** 535–543 (2009).

2. Liu, Y., Wang, Y., Walsh, T., Yi, L., Zhang, R., Spencer, J., Doi, Y., Tian, G., Dong, B., Huang, X., Yu, L., Gu, D., Ren, H., Chen, X., Lv, L., He, D., Zhou, H., Liang, Z., Liu, J. & Shen, J. Emergence of plasmid-mediated colistin resistance mechanism MCR-1 in animals and human beings in China: a microbiological and molecular biological study. *Lancet Infect. Dis.* **16,** 161–168 (2016).

3. Li, Z., Cao, Y., Yi, L., Liu, J. & Yang, Q. Emergent Polymyxin Resistance: End of an Era? *Open Forum Infect. Dis.* **6,** (2019).

4. Shafiq, M., Huang, J., Ur Rahman, S., Shah, J. M., Chen, L., Gao, Y., Wang, M. & Wang, L. High incidence of multidrug-resistant *Escherichia coli* coharboring *mcr-1* and *bla*CTX-M-15 recovered from pigs. *Infect. Drug Resist.* **12,** 2135–2149 (2019).

5. Zheng, B., Dong, H., Xu, H., Lv, J., Zhang, J., Jiang, X., Du, Y., Xiao, Y. & Li, L. Coexistence of MCR-1 and NDM-1 in clinical *Escherichia coli* isolates. *Clin. Infect. Dis.* **63,** 1393–1395 (2016).

6. Kara Ali, R., Surme, S., Balkan, I. I., Salihoglu, A., Sahin Ozdemir, M., Ozdemir, Y., Mete, B., Can, G., Ar, M. C., Tabak, F. & Saltoglu, N. An eleven-year cohort of bloodstream infections in 552 febrile neutropenic patients: resistance profiles of Gram-negative bacteria as a predictor of mortality. *Ann. Hematol.* **99,** 1925–1932 (2020).

7. Balkan, I. I., Alkan, M., Aygün, G., Kuşkucu, M., Ankaralı, H., Karagöz, A., Şen, S., Arsu, H. Y., Biçer, M., Kaya, S. Y., Karaali, R., Mete, B., Saltoğlu, N. & Tabak, F. Colistin resistance increases 28-day mortality in bloodstream infections due to carbapenem-resistant *Klebsiella pneumoniae*. *Eur. J. Clin. Microbiol. Infect. Dis.* **40,** 2161–2170 (2021).

8. Hancock, R. E. The bacterial outer membrane as a drug barrier. *Trends Microbiol.* **5,** 37–42 (1997).

9. Whitfield, C. & Trent, M. S. Biosynthesis and export of bacterial lipopolysaccharides. *Annu. Rev. Biochem.* **83,** 99–128 (2014).

10. Nikaido, H. Molecular basis of bacterial outer membrane permeability revisited. *Microbiol. Mol. Biol. Rev.* **67,** 593–656 (2003).

11. Poirel, L., Jayol, A. & Nordmann, P. Polymyxins: antibacterial activity, susceptibility testing, and resistance mechanisms encoded by plasmids or chromosomes. *Clin. Microbiol. Rev.* **30,** 557–596 (2017).

12. Needham, B. D. & Trent, M. S. Fortifying the barrier: the impact of lipid A remodelling on bacterial pathogenesis. *Nat. Rev. Microbiol.* **11,** 467–481 (2013).

13. Schindler, M. & Osborn, M. J. Interaction of divalent cations and polymyxin B with lipopolysaccharide. *Biochemistry* **18,** 4425–4430 (1979).

14. Sabnis, A., Hagart, K. L., Klöckner, A., Becce, M., Evans, L. E., Furniss, R. C. D., Mavridou, D. A., Murphy, R., Stevens, M. M., Davies, J. C., Larrouy-Maumus, G. J., Clarke, T. B. & Edwards, A. M. Colistin kills bacteria by targeting lipopolysaccharide in the cytoplasmic membrane. *Elife* **10,** (2021).

15. Simpson, B. W. & Trent, M. S. Pushing the envelope: LPS modifications and their consequences. *Nat. Rev. Microbiol.* **17,** 403–416 (2019).

16. Murata, T., Tseng, W., Guina, T., Miller, S. I. & Nikaido, H. PhoPQ-mediated regulation produces a more robust permeability barrier in the outer membrane of *Salmonella enterica* serovar Typhimurium. *J. Bacteriol.* **189,** 7213–7222 (2007).

17. Zhou, Z., Ribeiro, A. A., Lin, S., Cotter, R. J., Miller, S. I. & Raetz, C. R. Lipid A modifications in polymyxin-resistant *Salmonella* Typhimurium: PMRA-dependent 4-amino-4-deoxy-L-arabinose, and phosphoethanolamine incorporation. *J. Biol. Chem.* **276,** 43111–43121 (2001).

18. Raetz, C. R. H., Reynolds, C. M., Trent, M. S. & Bishop, R. E. Lipid A modification systems in Gram-negative bacteria. *Annu. Rev. Biochem.* **76,** 295–329 (2007).

19. Jeannot, K., Bolard, A. & Plésiat, P. Resistance to polymyxins in Gram-negative organisms. *Int. J. Antimicrob. Agents* **49,** 526–535 (2017).

20. Huang, J., Li, C., Song, J., Velkov, T., Wang, L., Zhu, Y. & Li, J. Regulating polymyxin resistance in Gram-negative bacteria: roles of two-component systems PhoPQ and PmrAB. *Future Microbiol.* **15,** 445–459 (2020).

21. MacNair, C. R., Stokes, J. M., Carfrae, L. A., Fiebig-Comyn, A. A., Coombes, B. K., Mulvey, M. R. & Brown, E. D. Overcoming *mcr-1* mediated colistin resistance with colistin in combination with other antibiotics. *Nat. Commun.* **9,** (2018).

22. Wang, Z., Koirala, B., Hernandez, Y., Zimmerman, M., Park, S., Perlin, D. S. & Brady, S. F. A naturally inspired antibiotic to target multidrug-resistant pathogens. *Nature* **601,** 606–611 (2022).

23. Roberts, K. D., Zhu, Y., Azad, M. A. K., Han, M.-L., Wang, J., *et al.* A synthetic lipopeptide targeting top-priority multidrug-resistant Gram-negative pathogens. *Nat. Commun.* **13,** 1625 (2022).

24. Farha, M. A., El-Halfawy, O. M., Gale, R. T., MacNair, C. R., Carfrae, L. A., Zhang, X., Jentsch, N. G., Magolan, J. & Brown, E. D. Uncovering the hidden antibiotic potential of cannabis. *ACS Infect. Dis.* **6,** 338–346 (2020).

25. Mohammadi, M., Khayat, H., Sayehmiri, K., Soroush, S., Sayehmiri, F., Delfani, S., Bogdanovic, L. & Taherikalani, M. Synergistic effect of colistin and rifampin against multidrug resistant *Acinetobacter baumannii*: a systematic review and meta-analysis. *Open Microbiol. J.* **11,** 63–71 (2017).

26. Nutman, A., Lellouche, J., Temkin, E., Daikos, G., Skiada, A., *et al.* Colistin plus meropenem for carbapenem-resistant Gram-negative infections: in vitro synergism is not associated with better clinical outcomes. *Clin. Microbiol. Infect.* **26,** 1185–1191 (2020).

27. Lin, L., Nonejuie, P., Munguia, J., Hollands, A., Olson, J., *et al.* Azithromycin synergizes with cationic antimicrobial peptides to exert bactericidal and therapeutic activity against highly multidrug-resistant Gram-negative bacterial pathogens. *EBioMedicine* **2,** 690–698 (2015).

28. Zhou, Y.-F., Liu, P., Zhang, C.-J., Liao, X.-P., Sun, J. & Liu, Y.-H. Colistin combined with tigecycline: a promising alternative strategy to combat *Escherichia coli* harboring *bla*NDM–5 and *mcr-1*. *Front. Microbiol.* **10,** 2957 (2020).

29. Gordon, N. C., Png, K. & Wareham, D. W. Potent synergy and sustained bactericidal activity of a vancomycin-colistin combination versus multidrug-resistant strains of *Acinetobacter baumannii*. *Antimicrob. Agents Chemother.* **54,** 5316–5322 (2010).

30. Domalaon, R., Silva, P. M. De, Kumar, A., Zhanel, G. G. & Schweizer, F. The anthelmintic drug niclosamide synergizes with colistin and reverses colistin resistance in Gram-negative bacilli. *Antimicrob. Agents Chemother.* **63,** (2019).

31. Minrovic, B. M., Jung, D., Melander, R. J. & Melander, C. New class of adjuvants enables lower dosing of colistin against *Acinetobacter baumannii*. *ACS Infect. Dis.* **4,** 1368–1376 (2018).

32. Tsai, C. N., MacNair, C. R., Cao, M. P. T., Perry, J. N., Magolan, J., Brown, E. D. & Coombes, B. K. Targeting two-component systems uncovers a small-molecule inhibitor of *Salmonella* virulence. *Cell Chem. Biol.* **27,** 793–805 (2020).

33. Zimmerman, S. M., Lafontaine, A. A. J., Herrera, C. M., Mclean, A. B. & Trent, M. S. A whole-cell screen identifies small bioactives that synergize with polymyxin and exhibit antimicrobial activities against multidrug-resistant bacteria. *Antimicrob. Agents Chemother.* **64,** (2020).

34. Mattingly, A. E., Cox, K. E., Smith, R., Melander, R. J., Ernst, R. K. & Melander, C. Screening an established natural product library identifies secondary metabolites that potentiate conventional antibiotics. *ACS Infect. Dis.* **6,** 2629–2640 (2020).

35. Baym, M., Stone, L. K. & Kishony, R. Multidrug evolutionary strategies to reverse antibiotic resistance. *Science.* **351,** (2016).

36. O'Rourke, A., Beyhan, S., Choi, Y., Morales, P., Chan, A. P., Espinoza, J. L., Dupont, C. L., Meyer, K. J., Spoering, A., Lewis, K., Nierman, W. C. & Nelson, K. E. Mechanism-of-action classification of antibiotics by global transcriptome profiling. *Antimicrob. Agents Chemother.* **64,** (2020).

37. Hood, M. I., Becker, K. W., Roux, C. M., Dunman, P. M. & Skaar, E. P. Genetic determinants of intrinsic colistin tolerance in *Acinetobacter baumannii*. *Infect. Immun.* **81,** 542–551 (2013).

38. The European Committee on Antimicrobial Susceptibility Testing. Breakpoint tables for interpretation of MICs and zone diameters. Version 11.0 (2021). at <http://www.eucast.org>

39. Clifton, L. A., Skoda, M. W. A., Le Brun, A. P., Ciesielski, F., Kuzmenko, I., Holt, S. A. & Lakey, J. H. Effect of divalent cation removal on the structure of Gram-negative bacterial outer membrane models. *Langmuir* **31,** 404–412 (2015).

40. Yang, Q., Li, M., Spiller, O. B., Andrey, D. O., Hinchliffe, P., Li, H., MacLean, C., Niumsup, P., Powell, L., Pritchard, M., Papkou, A., Shen, Y., Portal, E., Sands, K., Spencer, J., Tansawai, U., Thomas, D., Wang, S., Wang, Y., Shen, J. & Walsh, T. Balancing *mcr-1* expression and bacterial survival is a delicate equilibrium between essential cellular defence mechanisms. *Nat. Commun.* **8,** (2017).

41. Sun, Z. & Palzkill, T. Deep mutational scanning reveals the active-site sequence requirements for the colistin antibiotic resistance enzyme MCR-1. *mBio* **12,** (2021).

42. Carfrae, L. A., MacNair, C. R., Brown, C. M., Tsai, C. N., Weber, B. S., Zlitni, S., Rao, V. N., Chun, J., Junop, M. S., Coombes, B. K. & Brown, E. D. Mimicking the human environment in mice reveals that inhibiting biotin biosynthesis is effective against antibiotic-resistant pathogens. *Nat. Microbiol.* **5,** 93–101 (2020).

43. Zlitni, S., Ferruccio, L. F. & Brown, E. D. Metabolic suppression identifies new antibacterial inhibitors under nutrient limitation. *Nat. Chem. Biol.* **9,** 796–804 (2013).

44. Broussard, T. C., Price, A. E., Laborde, S. M. & Waldrop, G. L. Complex formation and regulation of *Escherichia coli* acetyl-CoA carboxylase. *Biochemistry* **52,** 3346–3357 (2013).

45. Tong, L. Structure and function of biotin-dependent carboxylases. *Cell. Mol. Life Sci.* **70,** 863–891 (2013).

46. Omura, S. The antibiotic cerulenin, a novel tool for biochemistry as an inhibitor of fatty acid synthesis. *Bacteriol. Rev.* **40,** 681–697 (1976).

47. Vance, D., Goldberg, I., Mitsuhashi, O. & Bloch, K. Inhibition of fatty acid synthetases by the antibiotic cerulenin. *Biochem. Biophys. Res. Commun.* **48,** 649–656 (1972).

48. Heath, R. J., Rubin, J. R., Holland, D. R., Zhang, E., Snow, M. E. & Rock, C. O. Mechanism of triclosan inhibition of bacterial fatty acid synthesis. *J. Biol. Chem.* **274,** 11110–11114 (1999).

49. Olaitan, A. O., Morand, S. & Rolain, J.-M. Mechanisms of polymyxin resistance: acquired and intrinsic resistance in bacteria. *Front. Microbiol.* **5,** (2014).

50. MacNair, C. R., Tsai, C. N. & Brown, E. D. Creative targeting of the Gram-negative outer membrane in antibiotic discovery. *Ann. N. Y. Acad. Sci.* **1459,** 69–85 (2020).

51. Stokes, J. M., MacNair, C. R., Ilyas, B., French, S., Côté, J.-P., Bouwman, C., Farha, M., Sieron, A. O., Whitfield, C., Coombes, B. K. & Brown, E. D. Pentamidine sensitizes Gram-negative pathogens to antibiotics and overcomes acquired colistin resistance. *Nat. Microbiol.* **2,** 17028 (2017).

52. Chen, C. C. & Feingold, D. S. Locus of divalent cation inhibition of the bactericidal action of polymyxin B. *Antimicrob. Agents Chemother.* **2,** 331–335 (1972).

53. Richter, M. F., Drown, B. S., Riley, A. P., Garcia, A., Shirai, T., Svec, R. L. & Hergenrother, P. J. Predictive compound accumulation rules yield a broad-spectrum antibiotic. *Nature* **545,** 299–304 (2017).

54. Farha, M. A., Verschoor, C. P., Bowdish, D. & Brown, E. D. Collapsing the proton motive force to identify synergistic combinations against *Staphylococcus aureus*. *Chem. Biol.* **20,** 1168–1178 (2013).

55. Sekyere, J. O. & Amoako, D. G. Carbonyl cyanide m-chlorophenylhydrazine (CCCP) reverses resistance to colistin, but not to carbapenems and tigecycline in multidrug-resistant Enterobacteriaceae. *Front. Microbiol.* **8,** (2017).

56. Bakker, E. P. & Mangerich, W. E. Interconversion of components of the bacterial proton motive force by electrogenic potassium transport. *J. Bacteriol.* **147,** 820–826 (1981).

57. Majdalani, N., Heck, M., Stout, V. & Gottesman, S. Role of RcsF in signaling to the Rcs phosphorelay pathway in *Escherichia coli*. *J. Bacteriol.* **187,** 6770–6778 (2005).

58. Parker, C. T., Kloser, A. W., Schnaitman, C. A., Stein, M. A., Gottesman, S. & Gibson, B. W. Role of the *rfaG* and *rfaP* genes in determining the lipopolysaccharide core structure and cell surface properties of *Escherichia coli* K-12. *J. Bacteriol.* **174,** 2525–2538 (1992).

59. Hagiwara, D., Sugiura, M., Oshima, T., Mori, H., Aiba, H., Yamashino, T. & Mizuno, T. Genome-wide analyses revealing a signaling network of the RcsC-YojN-RcsB phosphorelay system in *Escherichia coli*. *J. Bacteriol.* **185,** 5735–5746 (2003).

60. Sledjeski, D. D. & Gottesman, S. Osmotic shock induction of capsule synthesis in *Escherichia coli* K-12. *J. Bacteriol.* **178,** 1204–1206 (1996).

61. Lorenz, C., Dougherty, T. J. & Lory, S. Transcriptional responses of Escherichia coli to a small-molecule inhibitor of LolCDE, an essential component of the lipoprotein transport pathway. *J. Bacteriol.* **198,** 3162–3175 (2016).

62. Hews, C. L., Cho, T., Rowley, G. & Raivio, T. L. Maintaining integrity under stress: envelope stress response regulation of pathogenesis in Gram-negative bacteria. *Front. Cell. Infect. Microbiol.* **9,** (2019).

63. Price, N. L. & Raivio, T. L. Characterization of the Cpx regulon in *Escherichia coli* strain MC4100. *J. Bacteriol.* **191,** 1798–1815 (2009).

64. Niba, E. T. E., Naka, Y., Nagase, M., Mori, H. & Kitakawa, M. A genome-wide approach to identify the genes involved in biofilm formation in *E. coli*. *DNA Res.* **14,** 237–246 (2007).

65. Pratt, L. A. & Kolter, R. Genetic analysis of *Escherichia coli* biofilm formation: roles of flagella, motility, chemotaxis and type I pili. *Mol. Microbiol.* **30,** 285–293 (1998).

66. Dafopoulou, K., Xavier, B. B., Hotterbeekx, A., Janssens, L., Lammens, C., Dé, E., Goossens, H., Tsakris, A., Malhotra-Kumar, S. & Pournaras, S. Colistin-resistant *Acinetobacter baumannii* clinical strains with deficient biofilm formation. *Antimicrob. Agents Chemother.* **60,** 1892–1895 (2016).

67. Van Houdt, R. & Michiels, C. W. Role of bacterial cell surface structures in *Escherichia coli* biofilm formation. *Res. Microbiol.* **156,** 626–633 (2005).

68. Krishnamoorthy, G., Wolloscheck, D., Weeks, J. W., Croft, C., Rybenkov, V. V. & Zgurskaya, H. I. Breaking the permeability barrier of *Escherichia coli* by controlled hyperporination of the outer membrane. *Antimicrob. Agents Chemother.* **60,** 7372–7381 (2016).

69. Yao, J. & Rock, C. O. How bacterial pathogens eat host lipids: implications for the development of fatty acid synthesis therapeutics. *J. Biol. Chem.* **290,** 5940–5946 (2015).

70. Yao, J. & Rock, C. O. Exogenous fatty acid metabolism in bacteria. *Biochimie* **141,** 30–39 (2017).

71. Parsons, J. B. & Rock, C. O. Is bacterial fatty acid synthesis a valid target for antibacterial drug discovery? *Curr. Opin. Microbiol.* **14,** 544–549 (2011).

72. Magnuson, K., Jackowski, S., Rock, C. O. & Cronan, J. E. J. Regulation of fatty acid biosynthesis in *Escherichia coli*. *Microbiol. Rev.* **57,** 522–542 (1993).

73. Spapen, H., Jacobs, R., Gorp, V. Van, Troubleyn, J. & Honoré, P. M. Renal and neurological side effects of colistin in critically ill patients. *Ann. Intensive Care* **1,** 14 (2011).

74. Nair, A. B. & Jacob, S. A simple practice guide for dose conversion between animals and human. *J. Basic Clin. Pharm.* **7,** 27–31 (2016).

75. Parker, E. N., Drown, B. S., Geddes, E. J., Lee, H. Y., Ismail, N., Lau, G. W. & Hergenrother, P. J. Implementation of permeation rules leads to a FabI inhibitor with activity against Gram-negative pathogens. *Nat. Microbiol.* **5,** 67–75 (2020).

76. Li, B., Zhao, Y., Liu, C., Chen, Z. & Zhou, D. Molecular pathogenesis of *Klebsiella pneumoniae*. *Future Microbiol.* **9,** 1071–1081 (2014).

77. Feldman, M. F., Mayer Bridwell, A. E., Scott, N. E., Vinogradov, E., McKee, S. R., Chavez, S. M., Twentyman, J., Stallings, C. L., Rosen, D. A. & Harding, C. M. A promising bioconjugate vaccine against hypervirulent *Klebsiella pneumoniae*. *Proc. Natl. Acad. Sci. U. S. A.* **116,** 18655–18663 (2019).

78. MacNair, C. R. & Brown, E. D. Outer membrane disruption overcomes intrinsic, acquired, and spontaneous antibiotic resistance. *mBio* **11,** e01615-20 (2022).

79. Du, H., Chen, L., Tang, Y. W. & Kreiswirth, B. N. Emergence of the *mcr-1* colistin resistance gene in carbapenem-resistant Enterobacteriaceae. *Lancet Infect. Dis.* **16,** 287–288 (2016).

80. Li, Y., Sun, Q. L., Shen, Y., Zhang, Y., Yang, J. W., Shu, L. Bin, Zhou, H. W., Wang, Y., Wang, B., Zhang, R., Wang, S. & Shenc, Z. Rapid increase in prevalence of carbapenem-resistant enterobacteriaceae (CRE) and emergence of colistin resistance gene *mcr-1* in CRE in a hospital in Henan, China. *J. Clin. Microbiol.* **56,** e01932-17 (2018).

81. Wang, X., Wang, Y., Zhou, Y., Li, J., Yin, W., Wang, S., Zhang, S., Shen, J., Shen, Z. & Wang, Y. Emergence of a novel mobile colistin resistance gene, *mcr-8*, in NDM-producing *Klebsiella pneumoniae* article. *Emerg. Microbes Infect.* **7,** (2018).

82. CLSI. *Performance Standards for Antimicrobial Susceptibility Testing, 31st Edition*. (2021).

83. Mandler, M. D., Baidin, V., Lee, J., Pahil, K. S., Owens, T. W. & Kahne, D. Novobiocin enhances polymyxin activity by stimulating lipopolysaccharide transport. *J. Am. Chem. Soc.* **140,** 6749–6753 (2018).

84. Krishnamoorthy, G., Leus, I. V., Weeks, J. W., Wolloscheck, D., Rybenkov, V. V. & Zgurskaya, H. I. Synergy between active efflux and outer membrane diffusion defines rules of antibiotic permeation into Gram-negative bacteria. *mBio* **8,** e01172-17 (2017).

85. Mansilla, M. C., Cybulski, L. E., Albanesi, D. & De Mendoza, D. Control of membrane lipid fluidity by molecular thermosensors. *J. Bacteriol.* **186,** 6681–6688 (2004).

86. Purcell, A. B., Voss, B. J. & Trent, M. S. Diacylglycerol kinase A is essential for polymyxin resistance provided by EptA, MCR-1, and other lipid A phosphoethanolamine transferases. *J. Bacteriol.* **204,** e0049821 (2022).

87. Kobayashi, R., Suzuki, T. & Yoshida, M. *Escherichia coli* phage-shock protein A (PspA) binds to membrane phospholipids and repairs proton leakage of the damaged membranes. *Mol. Microbiol.* **66,** 100–109 (2007).

88. M. Buttke, T. & O'Neal Ingram, L. Inhibition of unsaturated fatty acid synthesis in *Escherichia coli* by the antibiotic cerulenin. *Biochemistry* **17,** 5282–5286 (2002).

89. Fu, L., Wan, M., Zhang, S., Gao, L. & Fang, W. Polymyxin B loosens lipopolysaccharide bilayer but stiffens phospholipid bilayer. *Biophys. J.* **118,** 138–150 (2020).

90. Cox, G., Sieron, A., King, A. M., De Pascale, G., Pawlowski, A. C., Koteva, K. & Wright, G. D. A common platform for antibiotic dereplication and adjuvant discovery. *Cell Chem. Biol.* **24,** 98–109 (2017).

91. Lambert, R. J. W. & Lambert, R. A model for the efficacy of combined inhibitors. *J. Appl. Microbiol.* **95,** 734–743 (2003).

92. Mangat, C. S., Bharat, A., Gehrke, S. S. & Brown, E. D. Rank ordering plate data facilitates data visualization and normalization in high-throughput screening. *J. Biomol. Screen.* **19,** 1314–1320 (2014).

93. Altschul, S. F., Gish, W., Miller, W., Myers, E. W. & Lipman, D. J. Basic local alignment search tool. *J. Mol. Biol.* **215,** 403–410 (1990).

94. Keseler, I. M., Mackie, A., Santos-Zavaleta, A., Billington, R., Bonavides-Martínez, C., *et al.* The EcoCyc database: reflecting new knowledge about Escherichia coli K-12. *Nucleic Acids Res.* **45,** 543–550 (2017).

95. Yan, A., Guan, Z. & Raetz, C. R. H. An undecaprenyl phosphate-aminoarabinose flippase required for polymyxin resistance in *Escherichia coli*. *J. Biol. Chem.* **282,** 36077–36089 (2007).

96. Galanos, C., Lüderitz, O. & Westphal, O. A new method for the extraction of R lipopolysaccharides. *Eur. J. Biochem.* **9,** 245–249 (1969).

97. Bligh, E. G. & Dyer, W. J. A rapid method of total lipid extraction and purification. *Can. J. Biochem. Physiol.* **37,** 911–917 (1959).

98. Caroff, M., Tacken, A. & Szabó, L. Detergent-accelerated hydrolysis of bacterial endotoxins and determination of the anomeric configuration of the glycosyl phosphate present in the 'Isolated lipid A' fragment of the Bordetella pertussis endotoxin. *Carbohydr. Res.* **175,** 273–282 (1988).

99. Chomczynski, P. & Sacchi, N. Single-step method of RNA isolation by acid guanidinium thiocyanate-phenol-chloroform extraction. *Anal. Biochem.* **162,** 156–159 (1987).

100. Martin, M. Cutadapt removes adapter sequences from high-throughput sequencing reads. *EMBnet.journal* **17,** (2011).

101. Li, H. & Durbin, R. Fast and accurate long-read alignment with Burrows-Wheeler transform. *Bioinformatics* **26,** 589–595 (2010).

102. Liao, Y., Smyth, G. K. & Shi, W. FeatureCounts: An efficient general purpose program for assigning sequence reads to genomic features. *Bioinformatics* **30,** 923–930 (2014).

103. Love, M. I., Huber, W. & Anders, S. Moderated estimation of fold change and dispersion for RNA-seq data with DESeq2. *Genome Biol.* **15,** (2014).

104. Karp, P. D., Midford, P. E., Billington, R., Kothari, A., Krummenacker, M., Latendresse, M., Ong, W. K., Subhraveti, P., Caspi, R., Fulcher, C., Keseler, I. M. & Paley, S. M. Pathway Tools version 23.0 update: Software for pathway/genome informatics and systems biology. *Brief. Bioinform.* **22,** 109–126 (2021).

105. Supek, F., Bošnjak, M., Škunca, N. & Šmuc, T. Revigo summarizes and visualizes long lists of gene ontology terms. *PLoS One* **6,** e21800 (2011).

106. Shinitzky, M. & Barenholz, Y. Fluidity parameters of lipid regions determined by fluorescence polarization. *Biochim Biophys Acta.* **515,** 367–394 (1978).

107. Mohamed, A., Molendijk, J. & Hill, M. M. Lipidr: a software tool for data mining and analysis of lipidomics datasets. *J. Proteome Res.* **19,** 2890–2897 (2020).

108. Calvo-Villamañán, A., Ng, J. W., Planel, R., Ménager, H., Chen, A., Cui, L. & Bikard, D. On-target activity predictions enable improved CRISPR-dCas9 screens in bacteria. *Nucleic Acids Res.* **48,** (2020).

109. Depardieu, F. & Bikard, D. Gene silencing with CRISPRi in bacteria and optimization of dCas9 expression levels. *Methods* **172,** 61–75 (2020).

Chapter IV – Conclusions

Summary

The work presented in this thesis highlights the promise of targeting biotin biosynthesis to treat Gram-negative bacterial infections. Chapter 2 validates biotin biosynthesis as an overlooked target in Gram-negative pathogens using an innovative mouse model to mimic the human nutrient environment. This work highlights the importance of relevant infection models in determining and validating antibiotic targets. We investigate the potential of targeting biotin biosynthesis in a combination therapy approach in chapter 3, identifying a synergistic interaction between colistin and biotin biosynthesis inhibitor, MAC13772, specific to colistin-resistant pathogens. This study reveals a connection between biotin biosynthesis and phospholipid composition that can be exploited to resensitize bacteria to colistin. Together, these studies emphasize the potential applications of nutrient biosynthesis inhibitors. Furthermore, raise several questions on validating nutrient biosynthesis pathways and the link between biosynthesis pathways and antimicrobial resistance.

Overlooked nutrient stress targets

Mouse infection models are the gold standard for evaluating preclinical antibiotic efficacy and establishing fitness determinants during infection. For essential targets, this has proved to be a relatively reliable model capable of predicting efficacy in human infections[1]. However, in non-canonical targets, a

more comprehensive approach may be required to ensure the applicability of infection conditions. Biotin biosynthesis has previously been viewed as a non-essential fitness determinant during *A. baumannii, K. pneumoniae,* and *P. aeruginosa* murine infections[2–4]. Chapter 2 reports that biotin levels in mouse plasma exceed those present in human plasma by 40-fold. We propose that the increased biotin levels account for the discordance between biotin biosynthesis requirements during human and murine infections. While progress has been made towards humanizing the murine immune system[5], considerations for the nutritional environment have been overlooked. Understanding how mouse disease models recapitulate human physiology is integral in identifying targets and testing antimicrobial leads.

Recently advances in RNA-Seq technology have enabled the study of pathogen's transcriptional response during human infection[6,7]. For example, RNA-Seq studies show biotin biosynthesis genes are upregulated during Enterotoxigenic *E. coli* gastrointestinal infections[8] and *Salmonella enterica* serotype Typhi bloodstream infections in humans[9]. In Chapter 2, we show that biotin biosynthesis is essential in human mimicking infection conditions, suggesting that RNA-Seq data may predict nutrient requirements in the host. Despite this example, the applicability of gene expression profiles to predicting fitness determinants remains unclear. In *P. aeruginosa* acute burn wound and chronic wound murine infections, there was no correlation between gene

expression and mutant fitness, except for metabolic genes[10]. Indeed, studies exploring bacterial gene expression in the human environment may be uniquely positioned to predict the role of metabolic pathways between human and murine hosts.

The comparison of transcriptomic profiles in humans and mice can be used to validate mouse models of infection. For example, there is a strong correlation between the transcriptomic profile of a *P. aeruginosa* surgical wound infection in mice and human infections, suggesting the mouse disease model successfully replicates the host environment[6]. However, the transcriptional profiles of *P. aeruginosa* lung and burn wound models do not correlate to gene expression in human infection[6]. Performing RNA-Seq on clinical infection samples is limited by the genetic variability in bacteria; however, accounting for the inherent variability will assist in designing robust models to mimic the human environment. We anticipate that these types of studies can identify variations between the human and mouse environment, leading to the development of superior animal infection models.

Comparing bacterial fitness in biological fluids such as plasma, sputum, and urine from humans and mice may unveil overlooked nutrient stress pathways. We demonstrate biotin biosynthesis is dispensable in mouse plasma, yet critical in human plasma. Similarly, arginine biosynthesis is essential for *P. aeruginosa* for growth in human and fetal bovine serum but dispensable in mouse

serum[11]. In vivo susceptibility testing with the pantothenate antimetabolite, pantoyltaurine, demonstrated efficacy in a rat infection model but not a mouse model. Increased pantothenate levels in mouse plasma are predicted to have suppressed the activity of pantoyltaurine in the mouse model[12]. Pantothenate biosynthesis is critical for *K. pneumoniae* in human serum; however, dispensable in murine infection models[13]. Future work exploring the importance of pantothenate biosynthesis in rat bloodstream infection models is of interest. Comprehensive studies comparing gene essentiality in human and mouse plasma would help unveil the extent of nutritional variation between the in vivo environments. Alternative animal infection models should be identified to evaluate the dispensability of nutrient biosynthesis genes in conditions mimicking humans.

Although biological fluids are beneficial in validating nutrient stress targets, they are limited in understanding the holistic dynamics of nutrient limitation during infection. The intracellular concentrations of several metabolites, including arginine, histidine, and tryptophan, are modulated by the host immune response[14–16]. Host arginine is converted to NO as part of the innate immune response. NO exerts an antimicrobial effect against pathogens while altering arginine availability[14,17]. Additionally, INF-γ modulates the intracellular concentration of histidine and tryptophan by upregulating histidine and tryptophan degrading enzymes[15,16]. This is particularly relevant for *M. tuberculosis* as histidine and tryptophan auxotrophs are unable to replicate during infection. Host-

mediated nutrient deprivation plays a more prominent role in chronic infections than acute infection. The importance of host nutrient modulation to extracellular infections has not been established.

Bacterial infection alters nutrient availability for extracellular pathogens in the lung[18]. For example, aspartate and glutamine concentrations are decreased, and glutamate and lysine concentrations increased in murine lungs during *A. baumannii* infection[19]. Changes to glutamate and glutamine are known to modulate of macrophage activity[20]. The implications of altered nutrient levels on gene essentiality have not been fully explored. By contrast, another study found no changes in amino acid availability in the extracellular milieu of lungs infected with *K. pneumoniae*[21]. Likewise, *K. pneumoniae* had minimal differences in biosynthetic requirements during infection of neutropenic or wild-type mice[21,22]. These findings suggest in vitro growth in representative nutrient conditions could predict essentiality during infection. Importantly, bronchoalveolar fluid in humans is similar in amino acid content to mice, allowing essential nutrient biosynthetic pathways to translate to the clinic[22]. Future studies should use several techniques to identify differences in the nutritional environment during infection between humans and mice.

Inhibiting nutrient stress is a viable antibiotic approach

The acquisition and biosynthesis of nutrients are critical to bacterial pathogenesis, and inhibiting these processes has incredible potential as an antibiotic approach. As reported in chapters 1, 2, and 3, targeting nutrient stress pathways has been successfully exploited using a wide range of inhibitors, a subset of which demonstrate efficacy in animal infection models[15,23]. Furthermore, sulfonamides establish a precedent for the clinical success of an inhibitor of bacterial nutrient biosynthesis[24]. Almost 100 years have passed since the discovery of sulfonamides, and no new inhibitors of nutrient biosynthesis have entered clinical development[25]. However, the reliance on nutrient-rich media for antimicrobial discovery and susceptibility testing largely accounts for the lack of promising inhibitors[26].

Chapter 2 validates biotin biosynthesis as an overlooked antibacterial target for Gram-negative pathogens, *A. baumannii*, *K. pneumoniae*, and *P. aeruginosa*. Specifically, we found biotin biosynthesis is critical for the replication of pathogens in human plasma, yet dispensable in mouse plasma. The importance of biotin for *K. pneumoniae* growth in human serum was confirmed[13]. Despite our finding that biotin biosynthesis was dispensable for *S.* Typhimurium, several articles have demonstrated that biotin biosynthesis is important for intracellular replication of *Salmonella* species[27–29]. Furthermore, MAC13772 can reduce intracellular replication of *S.* Typhimurium in macrophages[30]. The biotin

concentration within *Salmonella* containing vacuoles is estimated to be less than 200 μM; nevertheless, this is still above the predicted biotin requirements of *S.* Typhimurium[31]. The impact of streptavidin treatment on the intracellular biotin concentration in mice has not been determined and may not directly replicate the intracellular environment within humans. Although, we anticipate it makes the biotin concentration more comparable to humans. Further study of the intracellular domain in humans will be integral to validating biotin biosynthesis as a target for *Salmonella* species.

Nutrient availability can vary widely between different sites of infection and microenvironments in the host[32]. Exploring the heterogeneity of metabolite concentrations and the nutritional capabilities of various pathogens is essential to a comprehensive understanding of the host during infection. Biotin concentrations have been reported for several biological fluids, including cerebrospinal fluid, saliva, and urine[32]. Additionally, biotin levels have been estimated in the small and large intestines. Chapter 2 identifies the biotin requirements of *A. baumannii* and *P. aeruginosa* as 4.7 ng/mL and 5.5 ng/mL, respectively. Notably, the biotin concentration in cerebrospinal fluid is predicted to be insufficient to support the replication of either pathogen. Biotin concentrations in the gastrointestinal tract are expected to be significantly higher than in other sites in the body, with 110-170 ng/mL in the ileum and 7-11 ng/ml in the colon[33]. While this likely precludes biotin biosynthesis as an antibiotic target for GI infections, it suggests sufficient

exogenous biotin to support the growth of the microbiome. Treatment with broad-spectrum antibiotics disrupts a patient's gut microbiome and can select for resistance in off-target bacteria. Further studies exploring the impact of treatment with an inhibitor of biotin biosynthesis such as MAC13772 on the diversity of the gut microbiome are of interest. That said, we predict that biotin concentrations in the intestines, particularly the ileum, are sufficient to support the growth of the microbiome and that an inhibitor of biotin biosynthesis will have minimal impact on the host microbiome.

Developing narrow-spectrum antibiotics is another potential strategy to reduce the impact of antibiotic treatment on the host microbiome. In chapter 2, we found biotin requirements were pathogen-specific. Pathogens with a predicted high-affinity biotin transporter, such as *E. coli* and *S.* Typhimurium, had a biotin requirement approximately 50-times lower than pathogens lacking a biotin transporter. The variation in the dispensability of biotin biosynthesis genes suggests the ability to develop narrow-spectrum antibiotics. Exploring the array of nutritional capabilities of various pathogens is essential to a comprehensive understanding of the spectrum of activity during infection. Recently, the discovery of hygromycin A as a selective antibiotic against the causative agent of Lyme disease, *B. burgdorferi,* highlighted the potential for narrow-spectrum antibiotics[34].

Nutrient biosynthesis inhibitors hold promise for antibiotic development. Many nutrient biosynthesis pathways are unique to bacteria reducing the potential for mechanism-based toxicity. Furthermore, antibiotics targeting nutrient biosynthesis can potentially spare commensal bacteria by targeting pathogenic bacteria or site-specific activity. Biotin biosynthesis is a pathway of particular interest as it has been validated for priority pathogens. We suggest revisiting previously dismissed inhibitors of biotin biosynthesis in mouse models mimicking human conditions. The ability to treat bacterial infections in the post-antibiotic era will depend on identifying and exploiting conditionally essential targets like biotin biosynthesis to develop novel antibiotics.

Future efforts in validating nutrient biosynthesis targets

Discovering new exploitable bacterial processes susceptible to chemical inhibition is critical to combatting antibiotic resistance. A recent focus on understanding gene essentiality during infection and the adoption of in vitro conditions mimicking the in vivo environment looks to expand the target base for antimicrobial screening efforts[35–37]. The uncertain vulnerability of metabolic and biosynthetic processes has primarily resulted in their dismissal as viable antibiotic targets. Tn-Seq has proved to be a helpful tool in identifying nutrient biosynthesis as a promising target in many pathogens[10,15,22]. TnSeq screens in *K. pneumoniae* and *M. tuberculosis* have explored the role of the host immune response on bacterial pathogenesis[15,21]. In *M. tuberculosis,* $CD4^+$ T-cells play an important

role in mediating intracellular nutrient availability[15]. Polymicrobial environments are common in many infection environments, including cystic fibrosis and chronic wounds[38,39]. Novel community-dependent essential genes have been identified for *S. aureus* and *P. aeruginosa* during co-infection[40]. Future efforts should look to apply Tn-Seq screens to understand the role of the host immune response, co-infection, or chemical perturbants in mediating the nutritional environment during infection. Furthermore, the easy, efficient, and rapid construction of Tn-libraries provides future opportunities to explore if there is any strain specificity in metabolic fitness determinants.

Our current knowledge of the microenvironments within humans and mice is still incomplete. The dynamics of the environment over the course of infection are even less understood. Auxotrophic bacterial strains are essential for identifying nutrient stress targets required during infection and probing the host environment for specific metabolites. However, understanding the evolving host environment can be difficult if auxotrophs fail to establish infection. Competitive infections and Tn-Seq screens can be limited in differentiating between lethality, growth inhibition, and slow growth phenotypes. The vulnerability of nutrient biosynthesis pathways during bacterial persistence has not been thoroughly investigated. Studies have been limited to *M. tuberculosis,* where conditional knockdowns of enzymes in several key biosynthetic pathways have been evaluated, including homoserine biosynthesis[41] and biotin biosynthesis[42]. *M.*

tuberculosis results in long-term infections in both humans and mice, facilitating the study of persistence. Additionally, conditional knockdown systems compatible with infection models have been developed to study gene essentiality in *M. tuberculosis* but do not exist for other pathogens[43]. In vitro studies of lethality have been assessed for essential genes in *E. coli* using Tn-Seq to follow the loss of mutants in a population[44]. Significant technological developments are still required prior to applying similar systems in vivo.

The impact of colistin resistance on bacterial nutrient stress

Colistin is a last-resort therapeutic increasingly used to treat multidrug-resistant Gram-negative infections. However, resistance and treatment failure are growing concerns. Combination therapy approaches have proved to be productive in addressing the emergence of antibiotic resistance and efficacy[45]. Antibiotic resistance exerts a fitness cost changing the expression of metabolic pathways[46]. Exploiting altered metabolic pathways may represent an untapped target space for developing innovative therapies specifically against drug-resistant bacteria. Our findings in chapter 3 strongly support that targeting nutrient biosynthesis pathways is a promising strategy to contain multidrug-resistant infections. We report that inhibiting biotin biosynthesis can resensitize *mcr-1* expressing bacteria to colistin. This research found that by indirectly inhibiting fatty acid biosynthesis, MAC13772 altered bacterial phospholipid composition, leading to colistin sensitivity. However, how changes to

phospholipid composition alter colistin's interaction with the inner membrane, specifically in resistant bacteria, remains unclear. A deeper understanding is hindered by incomplete knowledge of the mechanistic details of *mcr-1* mediated resistance and colistin's lytic activity.

Expression of *mcr-1* confers polymyxin resistance by adding PEtN to a phosphate of lipid A[47]. The cationic nature is proposed to reduce the electrostatic interaction between colistin and LPS[48]. However, MCR-1 mediated modification of lipid A prevents colistin's lytic abilities but not outer membrane perturbation[49,50]. The literature offers several hypotheses to explain this phenomenon. Several groups predict that the modification of lipid A alters outer membrane properties, including strengthening LPS packing[49,51–53]. The altered structure of the outer membrane is theorized to modify the penetration of colistin beyond the outer membrane[21]. Exploring colistin localization using florescent labelled colistin molecules and measurement of outer membrane properties, such as curvature, composition, and rigidity, could aid in supporting these assertions. However, an alternative hypothesis where modified LPS in the inner membrane prevents colistin's lytic action was recently proposed[50].

High levels of *mcr-1* expression are associated with a severe fitness cost in the absence of colistin[54]. Bacterial growth is impaired both through the high protein levels in the inner membrane and the modification of lipid A[54]. Analogously, the tight regulation of LPS decoration by the PhoPQ and PmrAB

two-component systems suggests constant modification is detrimental to fitness in some environments[55]. It is projected that *mcr-1* is expressed at low to moderate levels where no impact on bacterial growth is observed to mediate the fitness cost. Accordingly, several groups report that *mcr-1* expression results in the incomplete decoration of LPS in the outer membrane[50,54,56]. Colistin can interact with the unmodified LPS to permeabilize the outer membrane.

Work by Sabnis *et al.* reveals that the outer leaflet of the inner membrane contains a small amount of LPS that interacts with colistin leading to inner membrane disruption. This counters the traditional model where colistin interacts with phospholipids to perturb the inner membrane and lyse bacteria[57]. The group further found that in *mcr-1* expressing bacteria, most LPS in the inner membrane is modified by PEtN reducing lysis[50]. Chapter 3 finds that adding a pore in the outer membrane has no impact on colistin resistance, further supporting the assertion that changes to the inner membrane mediate colistin resistance. Direct evidence of colistin using the pore to traverse the outer membrane would further support this assertion. Additionally, we find that changes to phospholipid composition alter colistin susceptibility in *mcr-1* expressing bacteria suggesting the model presented by Sabnis *et al.* may be oversimplified. The role of inner membrane fluidity, phospholipid composition, and fatty acid saturation on colistin resistance should be explored independently.

MAC13772 treatment had no impact on LPS modification but reduced PE. PE acts as the PEtN donor for lipid A modification[58]. Accordingly, reductions in PE may lead to changes in LPS modification, specifically in the inner membrane. The impact of inhibiting biotin or fatty acid biosynthesis on LPS modification with PEtN should be measured separately in the inner and outer membrane fractions. PE is the major phospholipid in *E. coli*, the reduction in PE leads to increased PG in *mcr-1* expressing *E. coli*[59]. Changes to phospholipid charge may also play a role in colistin's interaction with the inner membrane, PE is a zwitterionic phospholipid, and PG is anionic. The increase in anionic character may support colistin's disruption of the inner membrane. Inhibition of biotin biosynthesis also altered the degree of fatty acid saturation by reducing unsaturated fatty acids. Similarly, cerulenin inhibits unsaturated fatty acid synthesis, completely modifying the saturation of membrane lipids[60]. Changes to fatty acid saturation could also mediate colistin sensitivity by changing packing density and membrane fluidity.

Recent literature suggests that inhibiting fatty acid biosynthesis may play a broader role in resensitizing resistant bacteria[61,62]. Ciprofloxacin-resistant strains of *P. aeruginosa* were found to have elevated expression of unsaturated fatty acid biosynthesis genes[61]. Inhibition of fatty acid biosynthesis with triclosan potentiated ciprofloxacin against resistant bacteria. Notably, we found that the treatment of *mcr-1* expressing *E. coli* with MAC13772 decreased fatty acid unsaturation, suggesting a connection between inhibition of fatty acid

biosynthesis and unsaturation. In chapter 3, we did not observe any synergistic interactions between a panel of 10 antibiotics and triclosan in *mcr-1* expressing *E. coli.* However, ciprofloxacin was not tested, and our *E. coli* strain is sensitive to fluoroquinolones. Furthermore, triclosan has pleiotropic effects and can permeabilize the bacterial membranes at high concentrations altering the proton motive force[63]. Genetic approaches studying the impact of inhibiting fatty acid biosynthesis will help uncover if a similar mechanism is mediating changes in antibiotic susceptibility.

Identifying potential combinations between inhibitors of nutrient biosynthesis and antibiotics is of interest to combat the antibiotic-resistance crisis. Previous work in the laboratory revealed several interactions between probes of nutrient stress and antibiotics against *E. coli*[64]. Identifying the impact of other antibiotic-resistance elements on metabolic processes could detect vulnerable pathways for future combination therapies. Ongoing work in our group is exploring the fitness cost for carbapenem-resistance in host mimicking conditions. Specifically, finding *E. coli* expressing VIM-2 has impaired growth in nutrient-limited media. We are currently working to better understand this cost's underlying mechanism and identify potential targets for combination therapy approaches.

Targeting nutrient stress to prevent the development of resistance

Traditionally, combinations of antibiotics require the efficacy of both components to inhibit bacterial growth[46,65]. As such, resistance may develop more rapidly than in monotherapy approaches. The acquisition of resistance to monotherapy can alter the interactions between two drugs to induce synergy in resistant mutants or increase sensitivity to another drug[46]. In chapter 3, we found that the presence of subinhibitory concentrations of a biotin or fatty acid biosynthesis inhibitor prevented the development of colistin resistance. The ability of biotin and fatty acid biosynthesis inhibitors to prevent the development of colistin resistance in vitro raises prospects for the use of such a combination prophylactically in colistin-sensitive infections. Testing the potential of fatty acid biosynthesis inhibitors to prevent the development of colistin resistance in chronic infection models is of interest. Notably, a similar strategy has been applied against the parasite *Plasmodium chabaudi*[66]*.* Parasites resistant to the drug pyrimethamine require more PABA than drug-susceptible parasites. Wale *et al.* prevented the development of pyrimethamine resistance during murine infection by restricting PABA.

Concluding remarks

Increasing rates of antibiotic resistance coupled with failures in antibiotic development threaten a post-antibiotic era. Identifying and validating novel

targets and discovering potent inhibitors of these processes are essential to overcome this formidable challenge. Targeting nutrient stress is one of many promising strategies to counter the antibiotic resistance crisis. Encouraging improvements to the regulatory and economic environment gives hope for developing and successfully launching the next generation of antibiotic therapies.

.

References

1. Tängdén, T., Lundberg, C. V., Friberg, L. E. & Huttner, A. How preclinical infection models help define antibiotic doses in the clinic. *Int. J. Antimicrob. Agents* **56**, (2020).

2. Subashchandrabose, S. *et al. Acinetobacter baumannii* genes required for bacterial survival during bloodstream infection. *mSphere* **1**, e00013-15 (2016).

3. Bachman, M. A. *et al.* Genome-wide identification of Klebsiella pneumoniae fitness genes during lung infection. *mBio* **6**, e00775-15 (2015).

4. Skurnik, D. *et al.* A comprehensive analysis of in vitro and in vivo genetic fitness of Pseudomonas aeruginosa using high-throughput sequencing of transposon libraries. *PLoS Pathog.* **9**, e1003582 (2013).

5. Legrand, N. *et al.* Humanized mice for modeling human infectious disease: challenges, progress, and outlook. *Cell Host Microbe* **6**, 5–9 (2009).

6. Cornforth, D. M. *et al. Pseudomonas aeruginosa* transcriptome during human infection. *Proc. Natl. Acad. Sci. U. S. A.* **115**, 5125–5134 (2018).

7. Bjarnsholt, T. *et al.* The importance of understanding the infectious microenvironment. *Lancet Infect. Dis.* **22,** 88-92 (2022).

8. Crofts, A. A. *et al.* Enterotoxigenic *E. coli* virulence gene regulation in human infections. *Proc. Natl. Acad. Sci. U. S. A.* **115**, 8968–8976 (2018).

9. Sheikh, A. *et al.* In vivo expression of *Salmonella enterica* serotype Typhi genes in the blood of patients with typhoid fever in Bangladesh. *PLoS Negl. Trop. Dis.* **5**, e1419 (2011).

10. Turner, K. H., Everett, J., Trivedi, U., Rumbaugh, K. P. & Whiteley, M. Requirements for *Pseudomonas aeruginosa* acute burn and chronic surgical wound infection. *PLoS Genet.* **10**, e1004518 (2014).

11. Poulsen, B. E. *et al.* Defining the core essential genome of *Pseudomonas aeruginosa*. *Proc. Natl. Acad. Sci. U. S. A.* **116**, 10072-10080 (2019)

12. Spry, C., Kirk, K. & Saliba, K. J. Coenzyme A biosynthesis: an antimicrobial drug target. *FEMS Microbiol. Rev.* **32**, 56-106 (2008).

13. Weber, B. S. *et al.* Genetic and chemical screening in human blood serum reveals unique antibacterial targets and compounds against *Klebsiella pneumoniae*. *Cell Rep.* **32**, (2020).

14. Gogoi, M., Datey, A., Wilson, K. T. & Chakravortty, D. Dual role of arginine metabolism in establishing pathogenesis. *Curr. Opin. Microbiol.* **29**, 43-48 (2016).

15. Zhang, Y. J. *et al.* Tryptophan biosynthesis protects mycobacteria from CD4 T-cell-mediated killing. *Cell* **155**, 1296–1308 (2013).

16. Dwivedy, A. *et al.* De novo histidine biosynthesis protects *Mycobacterium tuberculosis* from host IFN-γ mediated histidine starvation. *Commun. Biol.* **4**, (2021).

17. Chen, X., Qin, S., Zhao, X. & Zhou, S. L-Proline protects mice challenged by *Klebsiella pneumoniae* bacteremia. *J. Microbiol. Immunol. Infect.* **54**, 213-220 (2021).

18. Xu, Y. *et al.* In vivo gene expression in a *Staphylococcus aureus* prosthetic joint infection characterized by RNA sequencing and metabolomics: A pilot study. *BMC Microbiol.* **16**, (2016).

19. Lonergan, Z. R., Palmer, L. D. & Skaar, E. P. Histidine utilization is a critical determinant of *Acinetobacter* pathogenesis. *Infect. Immun.* **88,** e00118-20 (2020)

20. Gras, G., Porcheray, F., Samah, B. & Leone, C. The glutamate-glutamine cycle as an inducible, protective face of macrophage activation. *J. Leukoc. Biol.* **80**, 1067-1075 (2006).

21. Paczosa, M. K. *et al.* Transposon mutagenesis screen of *Klebsiella pneumoniae* identifies multiple genes important for resisting antimicrobial activities of neutrophils in mice. *Infect. Immun.* **88**, e00034-20 (2020).

22. Silver, R. J. *et al.* Amino acid biosynthetic pathways are required for *Klebsiella pneumoniae* growth in immunocompromised lungs and are druggable targets during infection. *Antimicrob. Agents Chemother.* **63**, e02674-18 (2019).

23. Wellington, S. *et al.* A small-molecule allosteric inhibitor of *Mycobacterium tuberculosis* tryptophan synthase. *Nat. Chem. Biol.* **13**, 943–950 (2017).

24. Bourne, C. R. Utility of the biosynthetic folate pathway for targets in antimicrobial discovery. *Antibiotics*. **3**, 1-28 (2014).

25. Theuretzbacher, U. *et al.* Critical analysis of antibacterial agents in clinical development. *Nat. Rev. Microbiol.* **18**, 286–298 (2020).

26. Brown, E. D. & Wright, G. D. Antibacterial drug discovery in the resistance era. *Nature* **529**, 336–343 (2016).

27. Cohen, H. *et al.* Intracellular *Salmonella* Paratyphi A is motile and differs in the expression of flagella-chemotaxis, SPI-1 and carbon utilization pathways in comparison to intracellular *S*. Typhimurium. *PLoS Pathog.* **18**, e1010425 (2022).

28. Fowler, C. C. & Galán, J. E. Decoding a *Salmonella* Typhi regulatory network that controls typhoid toxin expression within human cells. *Cell Host Microbe.* **23**, 65-76 (2018).

29. Shi, L. *et al.* Proteome of *Salmonella enterica* serotype Typhimurium grown in a low Mg2+/pH medium. *J. Proteomics Bioinforma.* **2**, 388-397 (2009).

30. McLaughlin, C. The de novo biosynthesis of biotin is required for the optimal growth of *Salmonella enterica* serovar Typhimurium in the intracellular environment. (Rhodes University, 2021).

31. Röder, J., Felgner, P. & Hensel, M. Comprehensive single cell analyses of the nutritional environment of intracellular *Salmonella enterica*. *Front. Cell. Infect. Microbiol.* **11**, (2021).

32. Wishart, D. S. *et al.* HMDB 4.0: the human metabolome database for 2018. *Nucleic Acids Res.* **46**, 608–617 (2018).

33. Yang, B., Feng, L., Wang, F. & Wang, L. Enterohemorrhagic *Escherichia coli* senses low biotin status in the large intestine for colonization and infection. *Nat. Commun.* **6**, 6592 (2015).

34. Leimer, N. *et al.* A selective antibiotic for Lyme disease. *Cell.* **184**, 5405-5418 (2021).

35. Turner, K. H., Wessel, A. K., Palmer, G. C., Murray, J. L. & Whiteley, M. Essential genome of *Pseudomonas aeruginosa* in cystic fibrosis sputum. *Proc. Natl. Acad. Sci. U. S. A.* **112**, 4110–4115 (2015).

36. Krismer, B. *et al.* Nutrient limitation governs *Staphylococcus aureus* metabolism and niche adaptation in the human nose. *PLoS Pathog.* **10**, e1003862 (2014).

37. Zlitni, S., Ferruccio, L. F. & Brown, E. D. Metabolic suppression identifies new antibacterial inhibitors under nutrient limitation. *Nat. Chem. Biol.* **9**, 796–804 (2013).

38. Gjødsbøl, K. *et al.* Multiple bacterial species reside in chronic wounds: A longitudinal study. *Int. Wound J.* **3**, 225-231 (2006).

39. Filkins, L. M. & O'Toole, G. A. Cystic fibrosis lung infections: polymicrobial, complex, and hard to treat. *PLoS Pathog.* **11**, e1005258 (2015).

40. Ibberson, C. B. *et al.* Co-infecting microorganisms dramatically alter pathogen gene essentiality during polymicrobial infection. *Nat. Microbiol.* **2**, 17079 (2017).

41. Hasenoehrl, E. J. *et al.* Derailing the aspartate pathway of *Mycobacterium tuberculosis* to eradicate persistent infection. *Nat. Commun.* **10**, 4215 (2019).

42. Park, S. W. *et al.* Evaluating the sensitivity of *Mycobacterium tuberculosis* to biotin deprivation using regulated gene expression. *PLoS Pathog.* **7**, e1002264 (2011).

43. Schnappinger, D., O'Brien, K. M. & Ehrt, S. Construction of conditional knockdown mutants in mycobacteria. *Methods Mol. Biol.* **1285**, 151-175 (2015).

44. Gallagher, L. A., Bailey, J. & Manoil, C. Ranking essential bacterial processes by speed of mutant death. **117**, 18010-18017 (2020)

45. Tyers, M. & Wright, G. D. Drug combinations: a strategy to extend the life of antibiotics in the 21st century. *Nat. Rev. Microbiol.* **17**, 141–155 (2019).

46. Baym, M., Stone, L. K. & Kishony, R. Multidrug evolutionary strategies to reverse antibiotic resistance. *Science.* **351**, (2016).

47. Liu, Y. *et al.* Emergence of plasmid-mediated colistin resistance mechanism MCR-1 in animals and human beings in China: a microbiological and molecular biological study. *Lancet Infect. Dis.* **16**, 161–168 (2016).

48. Nikaido, H. Molecular basis of bacterial outer membrane permeability revisited. *Microbiol. Mol. Biol. Rev.* **67**, 593–656 (2003).

49. MacNair, C. R. *et al.* Overcoming *mcr-1* mediated colistin resistance with colistin in combination with other antibiotics. *Nat. Commun.* **9**, 458 (2018).

50. Sabnis, A. *et al.* Colistin kills bacteria by targeting lipopolysaccharide in the cytoplasmic membrane. *Elife* **10**, e65836 (2021).

51. Stokes, J. M. *et al.* Pentamidine sensitizes Gram-negative pathogens to antibiotics and overcomes acquired colistin resistance. *Nat. Microbiol.* **2**, 17028 (2017).

52. Ma, W. *et al.* Biophysical impact of lipid A modification caused by mobile colistin resistance gene on bacterial outer membranes. *J. Phys. Chem. Lett.* **12**, 11629-11635 (2021).

53. Jiang, X. *et al.* Outer membranes of polymyxin-resistant *Acinetobacter baumannii* with phosphoethanolamine-modified lipid A and lipopolysaccharide loss display different atomic-scale interactions with polymyxins. *ACS Infect. Dis.* **6**, 2698-2708 (2020).

54. Yang, Q. *et al.* Balancing *mcr-1* expression and bacterial survival is a delicate equilibrium between essential cellular defence mechanisms. *Nat. Commun.* **8**, 2054 (2017).

55. Band, V. I. & Weiss, D. S. Mechanisms of antimicrobial peptide resistance in Gram-negative bacteria. *Antibiot.* **4**, 18–41 (2015).

56. Liu, Y. Y. *et al.* Structural modification of lipopolysaccharide conferred by *mcr-1* in gram-negative ESKAPE pathogens. *Antimicrob. Agents Chemother.* **61**, e00580-17 (2017).

57. Poirel, L., Jayol, A. & Nordmann, P. Polymyxins: antibacterial activity, susceptibility testing, and resistance mechanisms encoded by plasmids or chromosomes. *Clin. Microbiol. Rev.* **30**, 557–596 (2017).

58. Suardíaz, R. *et al.* Catalytic mechanism of the colistin resistance protein MCR-1. *Org. Biomol. Chem.* **19**, 3813-3819 (2021)

59. Sohlenkamp, C. & Geiger, O. Bacterial membrane lipids: diversity in structures and pathways. *FEMS Microbiol. Rev.* **40,** 133-159 (2015).

60. M. Buttke, T. & O'Neal Ingram, L. Inhibition of unsaturated fatty acid synthesis in *Escherichia coli* by the antibiotic cerulenin. *Biochemistry* **17**, 5282–5286 (1998).

61. Su, Y. *et al.* Enhanced biosynthesis of fatty acids contributes to ciprofloxacin resistance in *Pseudomonas aeruginosa*. *Front. Microbiol.* **13**, (2022).

62. Yu-bin, S. *et al.* Enhanced biosynthesis of fatty acids Is associated with the acquisition of ciprofloxacin resistance in *Edwardsiella tarda*. *mSystems* **6**, e00694-21 (2022).

63. Maiden, M. M. & Waters, C. M. Triclosan depletes the membrane potential in *Pseudomonas aeruginosa* biofilms inhibiting aminoglycoside induced adaptive resistance. *PLoS Pathog.* **16**, e1008529 (2020).

64. El Zahed, S. S. & Brown, E. D. Chemical-chemical combinations map uncharted interactions in *Escherichia coli* under nutrient stress. *iScience* **2**, 168–181 (2018).

65. MacNair, C. R. & Brown, E. D. Outer membrane disruption overcomes intrinsic, acquired, and spontaneous antibiotic resistance. *mBio* **11**, e01615-20 (2022).

66. Wale, N. *et al.* Resource limitation prevents the emergence of drug resistance by intensifying within-host competition. *Proc. Natl. Acad. Sci. U. S. A.* **114**, 13774-13779 (2017).